5

777

SECURITY CLASSIFICATION OF THIS PAGE (When Data Entered)

REPORT DOCUMENTATION PAGE	READ INSTRUCTIONS BEFORE COMPLETING FORM

1. REPORT NUMBER	2. GOVT ACCESSION NO.	3. RECIPIENT'S CATALOG NUMBER
RADC-TR-77-401 Vol II (of two)		

4. TITLE (and Subtitle)	5. TYPE OF REPORT & PERIOD COVERED
UNATTENDED/MINIMALLY ATTENDED RADAR STUDY. Volume II.	Final Technical Report.
	6. PERFORMING ORG. REPORT NUMBER
	ER 77-4109-VOL-2

7. AUTHOR(s)	8. CONTRACT OR GRANT NUMBER(s)
French, A.W.	F30602-76-C-0389
Berube, J.L.	

9. PERFORMING ORGANIZATION NAME AND ADDRESS	10. PROGRAM ELEMENT, PROJECT, TASK AREA & WORK UNIT NUMBERS
Raytheon Company Wayland MA 01778	P.E. 63101F J.O. E2330103

11. CONTROLLING OFFICE NAME AND ADDRESS	12. REPORT DATE
Rome Air Development Center (OCDE) Griffiss AFB NY 13441	December 1977
	13. NUMBER OF PAGES
	410

14. MONITORING AGENCY NAME & ADDRESS(if different from Controlling Office)	15. SECURITY CLASS. (of this report)
Same 375p.	UNCLASSIFIED
	15a. DECLASSIFICATION/DOWNGRADING SCHEDULE N/A

16. DISTRIBUTION STATEMENT (of this Report)

Approved for public release; distribution unlimited.

17. DISTRIBUTION STATEMENT (of the abstract entered in Block 20, if different from Report)

Same

18. SUPPLEMENTARY NOTES

RADC Project Engineer: Adrian S. Briggs (OCDE)

The effort reported here was sponsored by the Electronic Systems Division/XR, Hanscom AFB MA 01731.

19. KEY WORDS (Continue on reverse side if necessary and identify by block number)

UAR - Unattended Radar
MAR - Minimally Attended Radar
DEW Line
Life Cycle Cost
Surveillance
Reliability

20. ABSTRACT (Continue on reverse side if necessary and identify by block number)

This report presents results of a study of alternative radar design approaches that could be developed to optimally satisfy requirements for unattended and minimally attended radar operations. The requirements, detailed in the study statement of work, consist of two sets of nominal radar performance parameter goals; one set for the unattended radar (Type A) and a second for the minimally attended radar (Type B). Based on these requirements, alternative radar design approaches were synthesized for the Type A and evaluated for →

next page

DD FORM 1473 EDITION OF 1 NOV 65 IS OBSOLETE
1 JAN 73

298359

reliability, life cycle cost (LCC) and performance. A preferred design approach for a Type B radar is presented along with rationale by which the preferred choice evolved.

TABLE OF CONTENTS

iii

TABLE OF CONTENTS (Continued)

TABLE OF CONTENTS (Continued)

LIST OF ILLUSTRATIONS

LIST OF ILLUSTRATIONS (Continued)

LIST OF ILLUSTRATIONS (Continued)

LIST OF ILLUSTRATIONS (Continued)

EVALUATION

The effort reported is one of three parallel study contracts performed under Project E233 by direction of ESD/XR. These reports identify alternative concepts and activity necessary to support the development of a short-range, unattended radar and a long-range minimally attended radar. The short-range radar is being viewed for application in DEW Line to replace the AN/FPS-19 and the long-range radar is being viewed for application by the Alaskan Air Command to replace the AN/FPS-93. These studies provide the assurance that current technology can support the development of unattended/minimally attended radars that offer improved performance and can significantly reduce operating and maintenance costs.

These efforts were performed in accordance with 1978-1982 TPO III, Thrust C Advanced Sensor Technology. The results will be used by ESD to develop system acquisition strategy for SEEK FROST (Project 2448), PE 12412F. It also provides supplemental data supporting SEEK IGLOO (Project 968H), PE 12325F.

Adrian S. Briggs

ADRIAN S. BRIGGS
RADC Project Engineer

SECTION 1

INTRODUCTION AND SUMMARY

This report summarizes the results of a study into the technical demands
and related cost impacts of a new generation of unattended radar systems. The
primary emphasis of the study addresses the requirements for a 2 dimensional
60 nautical mile (NMI) radar system for operation on the DEWLINE. A secondary
aspect of the study considers the technological demand of minimal to unattended
operation for 3 dimensional 200 NMI air defense radars. The 2D/60 NMI and
3D/200 NMI radars have been designated Type A and Type B respectively.

There are certain well defined differences between the new generation of
unattended radars and radars previously developed. While these differences are
clearly visible, the reason why older designs did not incorporate such features
is more complicated and not dependent on technology considerations alone.

The question that this study most usefully addresses is why radars are
practical that have an order of magnitude improvement in reliability over the
most modern operational systems.

1.1 TYPE A PRIMARY RADAR KEY CONSIDERATIONS

The requirement for unattended operation introduces two previously
minimized issues:

1. Absolute minimum prime power consumption (500 watts goal). Very low
    power is considered fundamental to the ultimate realization of unattended
    radar systems for the following reasons:

    * An unattended radar cannot function without an unattended power
      source. The lower the power demanded, the more viable the
      realization of a highly reliable power source.

    * Minimum power dissipation in the radar is consistent with maxi-
      mum reliability. The more internal heat generated by a com-
      ponent the higher the failure rate.

1-1

2. All maintenance repairs to be completed with a 3 hour site visit.

It will be shown that these two basic issues lead to a highly parallel (redundant) architecture at RF with very graceful degradation properties and full remote switching capability for non-redundant sub-system elements.

The concepts of highly parallel architectures are not new. What is new is the realization of low cost air dielectric stripline and solid-state RF power generation at ultra high frequencies. These two technology advances have led to the cost-effective realization of highly distributed phased array transmitter/receiver configurations. It will be shown that with present in-hand technology, a highly parallel system and hardware architecture with very graceful degradation properties can be realized for the Type A radar. This highly parallel architecture permits failures at the system and hardware level to be apportioned in range, azimuth and elevation such that the total randomized detection volume lost in a given time interval never exceeds that resulting from an equivalent 2 dB loss in transmit power.

This study assumes that for the Type A radar as directed at the "tripwire" type operation of a contiguous network protecting a boundry (DEWLINE), the reliability model herein will be acceptable with minor variations. Given this assumption, the technological risks for the Type A radar are relatively small, while problems of demonstrating system mean-time-between-failures an order of magnitude greater than previously demanded, are within management comprehension.

1.2 TYPE A SIF/IFF KEY CONSIDERATIONS

The IFF system for use with unattended radars is also shown to be readily attainable with proven techniques. Because of a proposed mode of on-demand IFF operation for Type A radars which requires IFF interrogations only for new or dropped tracks and the predicted low aircraft populations at DEWLINE sites, a 30:1 improvement in equipment failure rates over continuous operation has been conservatively estimated, greatly simplifying IFF reliability and power consumption demands.

1.3 TYPE B SYSTEM KEY CONSIDERATIONS *

In the case of the Type B radar the nearly four-fold increase in detection range creates power generation requirements that presently prohibit a similar architecture as for the Type A radar. This in turn, leads to a system with less graceful degradation and more cumbersome redundancy. The IFF for Type B operation was denied the advantage of low duty cycle operation; however unlike the primary radar the very small and compact nature of IFF hardware make redundancy at high levels a simple and cost-effective solution to meeting reliability demands. The basic difference between the Type A and B IFF configuration is the autonomous electronically scanned ring array and the planar array piggybacked on the primary radar antenna respectively.

1.4 BASIC RELIABILITY ISSUE

The greatest unknown, and therefore risk identified in the study is the acceptability of the reliability model assumptions. These assumptions in turn impact the redundancy requirements and hence the cost and viability of radars for extended periods of unattended operation.

---

*In accordance with the Statement-of-Work directions the major effort under this study was concentrated on the Type A radar. Section 3.0 contains rationale for the selection of the preferred configuration for Type B. It has not been possible within the time constraints of this study to conclude the type of rigorous trade-offs for the selected Type B configuration needed to produce the same overall cost/performance visibility as for the Type A radar.

SECTION 2
TYPE A DESIGN STUDY

The study was conducted as shown in Figure 2.1-1. The initial task was to determine which of the performance goals stated in the contract statement-of-work should drive the generalized system design. The rationale that developed is shown in Figure 2.1-2. It can be seen that the two prime influences are low power consumption and 3 hour visit for repair.

2.1 GENERALIZED DESIGN GUIDELINES

2.1.1 PRIMARY RADAR

Low power consumption dictated minimum losses particularly at RF. This required all RF amplifying circuits to be mounted in close proximity to the radiating elements of the antenna. Need to eliminate friction, wind resistance and inertia determined an electronic scan in azimuth. A basic guideline that the antenna must be suitable for mounting on a 100 ft tower to enable contiguous coverage at all elevations for sites spaced at approximately 40 nmi intervals lead to the need to constrain the radiating aperture. The low power requirement dictated maximizing the radiating aperture. The antenna configuration selected for both UHF and L-Band is a 44 ft diameter by 7 ft high ring array. The limit on the azimuth aperture was practical considerations of mounting 100 ft high in 180 knot winds. The elevation aperture was determined by the number of beams needed to cover 0 to 40° degrees on the assumption the full aperture would be used for each beam. A 7 ft high elevation aperture provides 6 beams at L-Band and 2 at UHF. A larger elevation aperture would give an excessive number of beams to be processed at L-Band and more beams at UHF would take an undesirably large aperture.

The ring array was preferred over other candidates because of the invariant beam shape characteristics over 360°. The ring array is the nearest electronic equivalent to a mechanically rotated antenna. The diameter was basically determined by element spacing for sidelobe control coupled with judgemental factors on problems of mounting meaningful larger diameters 100 ft in the air. The

Figure 2.1-1. Study Model
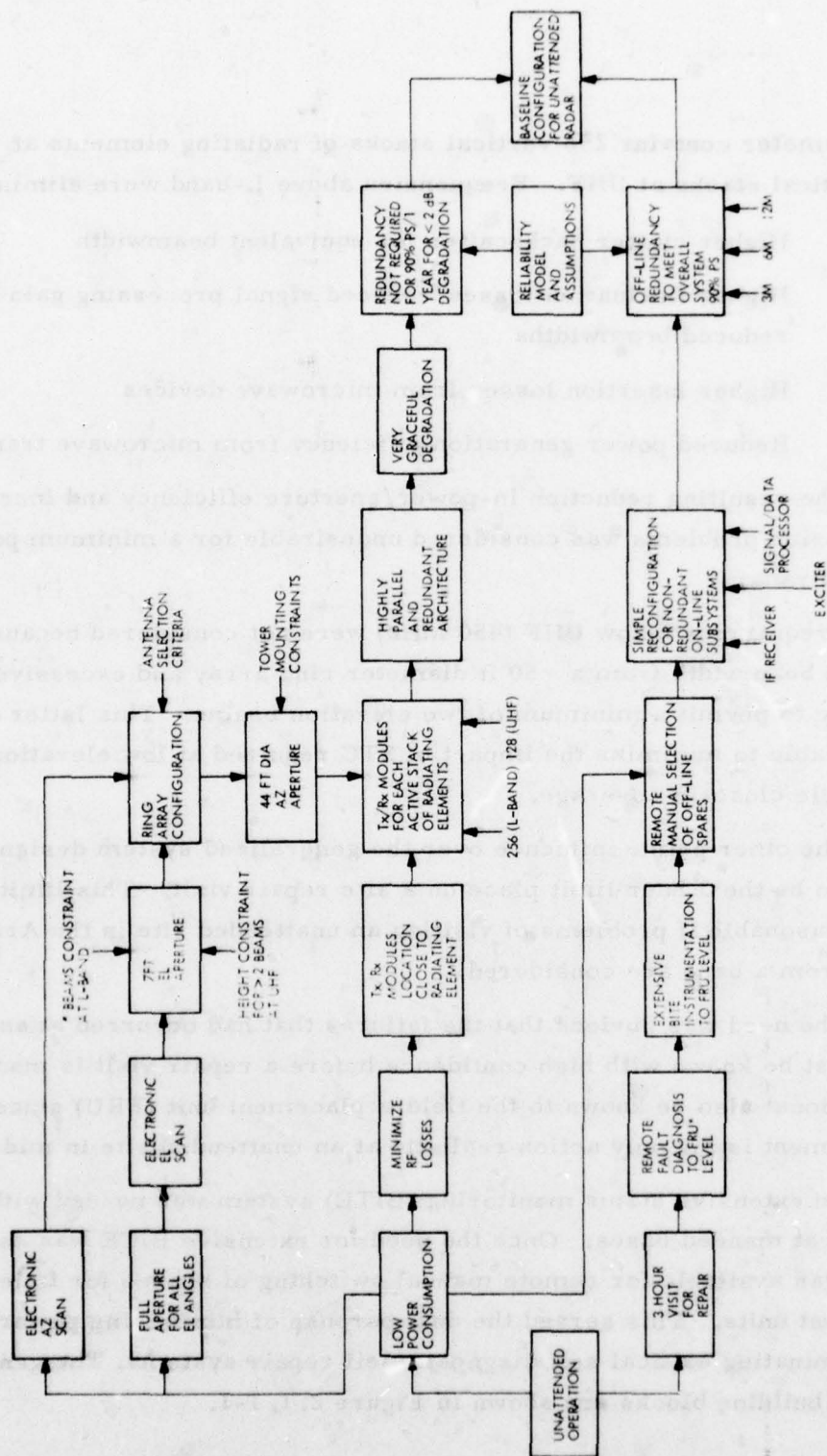
Figure 2.1-2. Generalized System Design Guidelines for Unattended Radar

Flowchart boxes:

- BASELINE CONFIGURATION FOR UNATTENDED RADAR
- REDUNDANCY NOT REQUIRED FOR <2 dB / 1 YEAR FOR 90% PS / DEGRADATION
- RELIABILITY MODEL AND ASSUMPTIONS
- OFF-LINE REDUNDANCY TO MEET OVERALL SYSTEM 90% PS
- VERY GRACEFUL DEGRADATION
- HIGHLY PARALLEL AND REDUNDANT ARCHITECTURE
- SIMPLE RECONFIGURATION FOR NON-REDUNDANT ON-LINE SUBSYSTEMS
- 3M 6M 12M
- SIGNAL DATA PROCESSOR
- EXCITER
- IF RECEIVER

- ANTENNA SELECTION CRITERIA
- RING ARRAY CONFIGURATION
- TOWER MOUNTING CONSTRAINTS
- 44 FT DIA AZ APERTURE
- Tx/Rx MODULES FOR EACH ACTIVE STACK OF RADIATING ELEMENTS
- 256 (L-BAND) 128 (UHF)
- ELECTRONIC EL SCAN
- 7 FT EL APERTURE
- * BEAMS CONSTRAINT (AT L-BAND)
- HEIGHT CONSTRAINT FOR > 2 BEAMS AT UHF
- Tx Rx MODULES LOCATION CLOSE TO RADIATING ELEMENT
- ELECTRONIC AZ SCAN
- FULL APERTURE FOR ALL EL ANGLES
- MINIMIZE RF LOSSES
- REMOTE MANUAL SELECTION OF OFF-LINE SPARES
- EXTENSIVE BITE INSTRUMENTATION TO FRU LEVEL
- REMOTE FAULT DIAGNOSIS TO FRU* LEVEL
- LOW POWER CONSUMPTION
- 3 HOUR VISIT FOR REPAIR
- UNATTENDED OPERATION

44 ft diameter contains 256 vertical stacks of radiating elements at L-band and 128 vertical stacks at UHF. Frequencies above L-band were eliminated because:

- Higher clutter backscatter for equivalent beamwidth

- Higher fluctuation losses/reduced signal processing gain for reduced beamwidths

- Higher insertion losses from microwave devices

- Reduced power generation efficiency from microwave transistors

The resulting reduction in-power/aperture efficiency and increased clutter suppression problems was considered undesirable for a minimum power unattended radar.

Frequencies below UHF (450 MHz) were not considered because of excessive azimuth beamwidth from a ~50 ft diameter ring array and excessive elevation aperture to permit a minimum of two elevation beams. This latter configuration is desirable to minimize the impact of STC required at low elevation angles on high angle close-in coverage.

The other prime influence over the generalized system design was determined to be the 3 hour limit place on a site repair visit. This limit was judged to be reasonable if problems of visiting an unattended site in the Arctic up to 200 miles from a base are considered.

The need was obvious that the failures that had occurred at an unattended site must be known with high confidence before a repair visit is made. This failure must also be known to the field replacement unit (FRU) since simple replacement is the only action realistic at an unattended site in mid-winter.

An extensive status monitoring (BITE) system was needed with remote readout at manned bases. Once the need for extensive BITE was established a tool was available for remote manual switching of spares for failed non-redundant units. This served the dual purpose of minimizing power consumption and eliminating critical self diagnosis/self repair systems. The generalized system building blocks are shown in Figure 2.1.1-1.
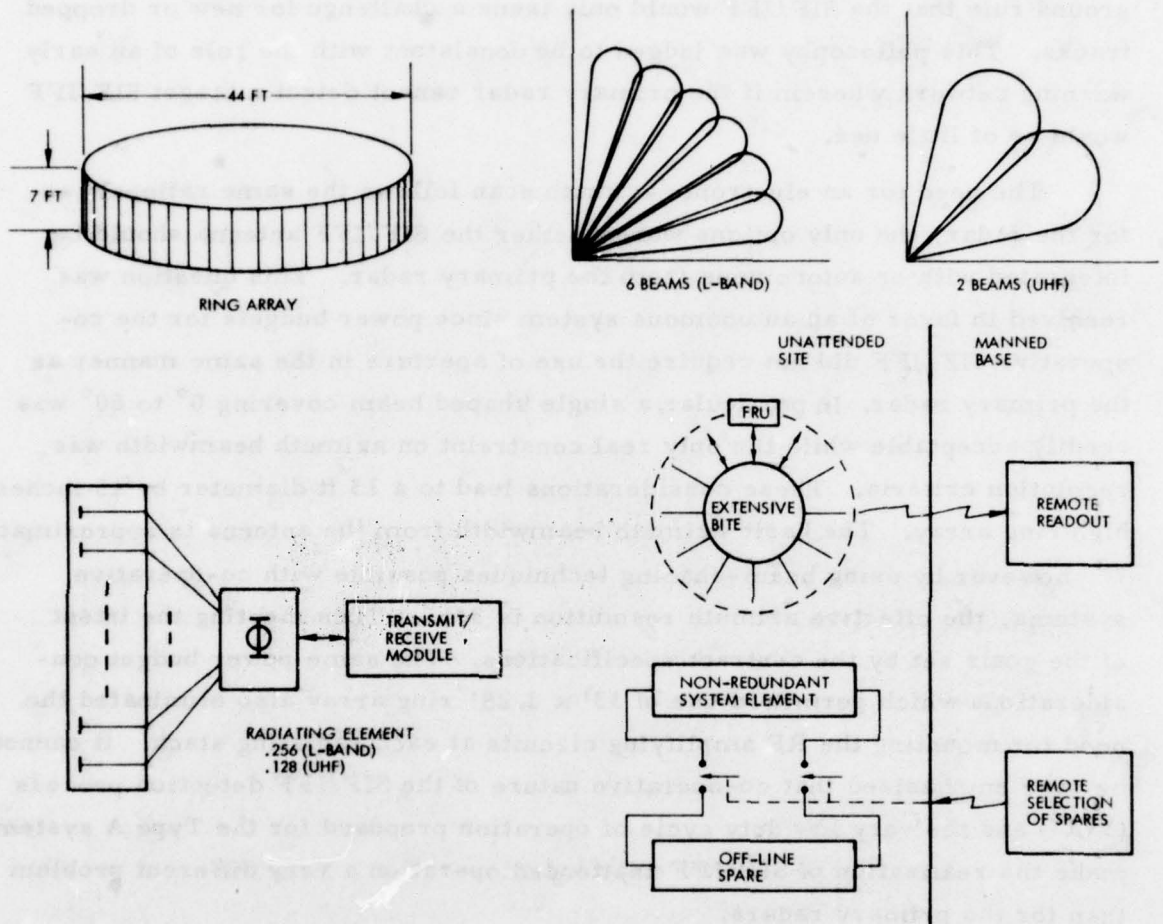
Figure 2.1.1-1. Generalized System Building Blocks

Labels within the figure:

44 FT

7 FT

RING ARRAY

6 BEAMS (L-BAND)

2 BEAMS (UHF)

UNATTENDED SITE

MANNED BASE

FRU

EXTENSIVE BITE

REMOTE READOUT

TRANSMIT/ RECEIVE MODULE

RADIATING ELEMENT
.256 (L-BAND)
.128 (UHF)

NON-REDUNDANT SYSTEM ELEMENT

OFF-LINE SPARE

REMOTE SELECTION OF SPARES

2.1.2 SIF/IFF

The generalized system design guidelines for the SIF/IFF emerged from similar philosophies as for the primary radar. The basic difference being the ground rule that the SIF/IFF would only issue a challenge for new or dropped tracks. This philosophy was judged to be consistent with the role of an early warning network wherein if the primary radar cannot detect a target SIF/IFF would be of little use.

The need for an electronic azimuth scan follows the same rationale as for the radar, the only options were whether the SIF/IFF antenna should be integrated with or autonomous from the primary radar. This question was resolved in favor of an autonomous system since power budgets for the co-operative SIF/IFF did not require the use of aperture in the same manner as the primary radar. In particular, a single shaped beam covering 0° to 50° was readily acceptable while the only real constraint on azimuth beamwidth was resolution criteria. These considerations lead to a 13 ft diameter by 15 inches high ring array. The basic azimuth beamwidth from the antenna is approximately 7°, however by using beam-shaping techniques possible with co-operative systems, the effective azimuth resolution is 3.5°. Thus meeting the intent of the goals set by the contract specifications. The same power budget considerations which permitted use of 13' x 1.25' ring array also eliminated the need for mounting the RF amplifying circuits at each radiating stack. It cannot be over emphasized that co-operative nature of the SIF/IFF detection process $(1/R^2)$ and the very low duty cycle of operation proposed for the Type A system make the realization of SIF/IFF unattended operation a very different problem than for the primary radars.

Having established the basic rationale for the hardware autonomy of the SIF/IFF and the differences in the problem of unattended operation, the remainder of the study did not attempt to draw parallels between the primary radar and the SIF/IFF configurations.

2.2 PRIMARY RADAR SYSTEM DESIGN

2.2.1 GENERALIZED SYSTEM BLOCK DIAGRAM

The basic system architecture options evolved primarily from minimum prime power considerations, the remaining key performance requirements for Type A operation were classified as shown in Figure 2.2.1-1.

Using the above guidelines a generalized system block diagram as shown in Figure 2.2.1-2 was developed.

The 44 ft diameter by 7 ft high ring array contains 256 stacks of radiating elements at L-band and 128 at UHF. The stacks are constructed of an etched teflon-glass substrate supported between two ground planes by a nylon honeycomb. Each stack contains an integral elevation network which is excited by a transmit/receive solid-state module (TRSSM). The TRSSM is coupled to the azimuth steering network, an array of switches which control the input/output signals to of a circular dielectric lens. The lens was selected as the basic signal phasing medium because of the highly reliable nature of this passive element coupled with proven performance in other Raytheon systems. A single receiver/exciter subsystem is used, however, the receiver may have from one to six channels as shown in Table 2.2.2-1. Coherent pulsed doppler processing was selected because of superior false alarm control and ability to achieve full volume subweather visibility and protection against chaff. The signal/data processor is a highly parallel system designed around a "common element", i.e., a parallel microprocessor architecture that handles a subset of the total processing tasks on a nearly-independent basis.

The generalized system block diagram establishes a basic set of parameters as shown in Table 2.2.1-1 which remain constant for any specific UHF or L-Band configuration.

Table 2.2.1-1

Array Diameter	44 ft.
Array Height	7 ft.
Maximum Range	60 NM
Receiver Noise Figure	1.4 dB

PARAMETER	GOAL	ASSUMED TOLERANCE
• COVERAGE	60 NM RNG, 100 K FT ALT FOR 16 M² TGT	MUST BE MET AS SPECIFIED
	30 NM RNG, 100 K FT ALT FOR 1 M² TGT	REDUCED ALTITUDE COVERAGE MAY BE ACCEPTABLE
• DETECTION	0.95 P_D IN 3/4 SCANS	DIFFERENT DETECTION RULES
• TARGET VELOCITY	±2400 KNOTS	AS SPECIFIED
• TRACK INITIATION	16 SEC	+50%
• FRAME TIME	4 SEC	$\begin{Bmatrix} -50 \\ +100 \end{Bmatrix}$ %
• ACCURACY	0.25 NM (R) 0.5° (AZ)	AS SPECIFIED
• RESOLUTION	0.5 NM (R) 3° (AZ)	SOME FLEXIBILITY IN AZIMUTH
• SIDELOBES	30 dB EACH WAY	SOME FLEXIBILITY
• RAM	3, 6 AND 12 MON. AT 90% CONF	AS SPECIFIED
• PRIME POWER	500 WATTS	AS CLOSE AS POSSIBLE

Figure 2.2.1-1. Type A Key Requirements
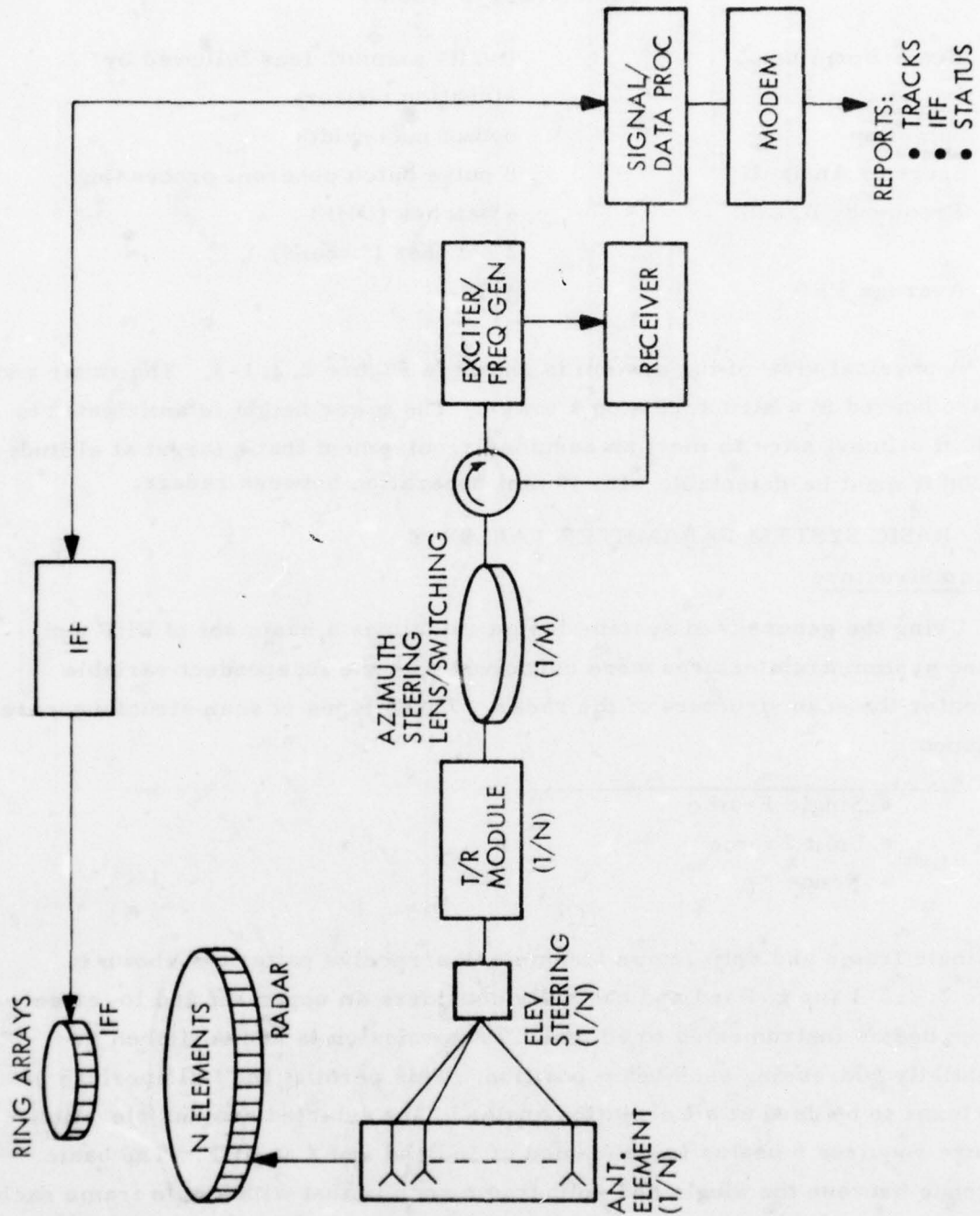
Figure 2.2.1-2. Generalized Type A Radar

Table 2.2.1-1 (Cont)

Beam Forming:	R-2R* azimuth lens followed by elevation network
Sampling	0.8 of pulsewidth
Spectral Analysis	8 pulse batch coherent processing
Frequency Agility	4 batches (UHF)
	2 batches (L-band)
Average PRF	1150

A physical view of the system is shown in Figure 2.2.1-3. The radar and
IFF are housed in a structure atop a tower. The tower height is anticipated to
be 100 ft at most sites to meet an assumed requirement that a target at altitudes
100-200 ft must be detectable with 40 nmi separation between radars.

2.2.2 BASIC SYSTEM PARAMETER VARIANTS

a) Scan Structure

Using the generalized system design guidelines a basic set of UHF and
L-Band system architectures were conceived with the independent variable
parameter the scan structure of the radar. Three types of scan structure were
developed:

- Single Frame
- Split Frame
- Fence

The single frame and split frame transmission/receive pattern is shown in
Figure 2.2.2-1 for L-Band and basically considers an upper set and lower set
of three beams instrumented to 60 nmi. Transmission is accomplished by
sequentially addressing each beam position. This permits the full aperture of
the antenna to be used at all evelation angles. The selected antenna elevation
aperture requires 6 beams to be formed at L-Band and 2 at UHF. The basic
difference between the single and split frame scan is that with single frame each

---

* The theory of the R-2R lens is described in Section 2.3.3. The name is
  derived from the fact that for a lens of radius R, the array has a radius 2R.
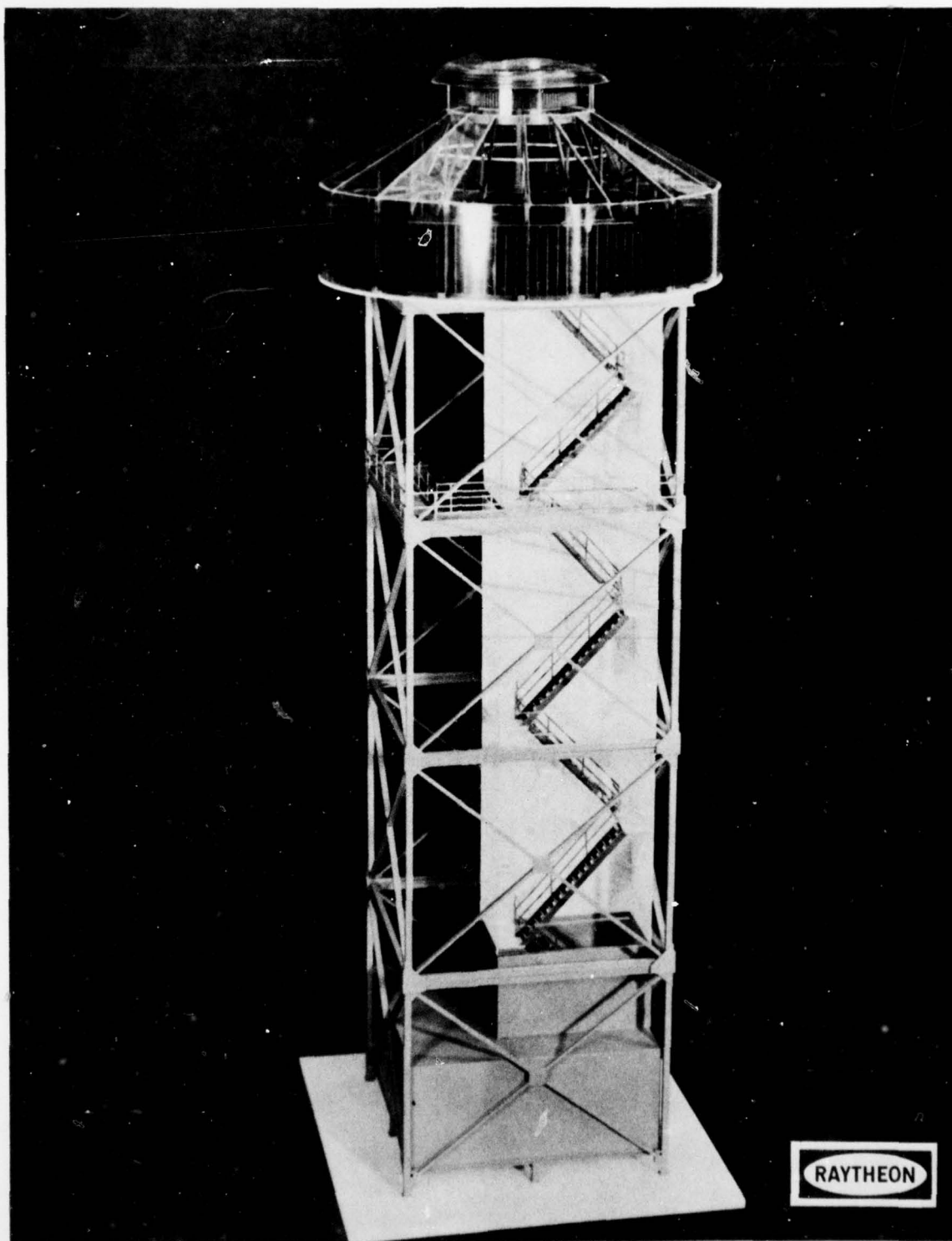
Figure 2.2.1-3. Type A Radar Configuration
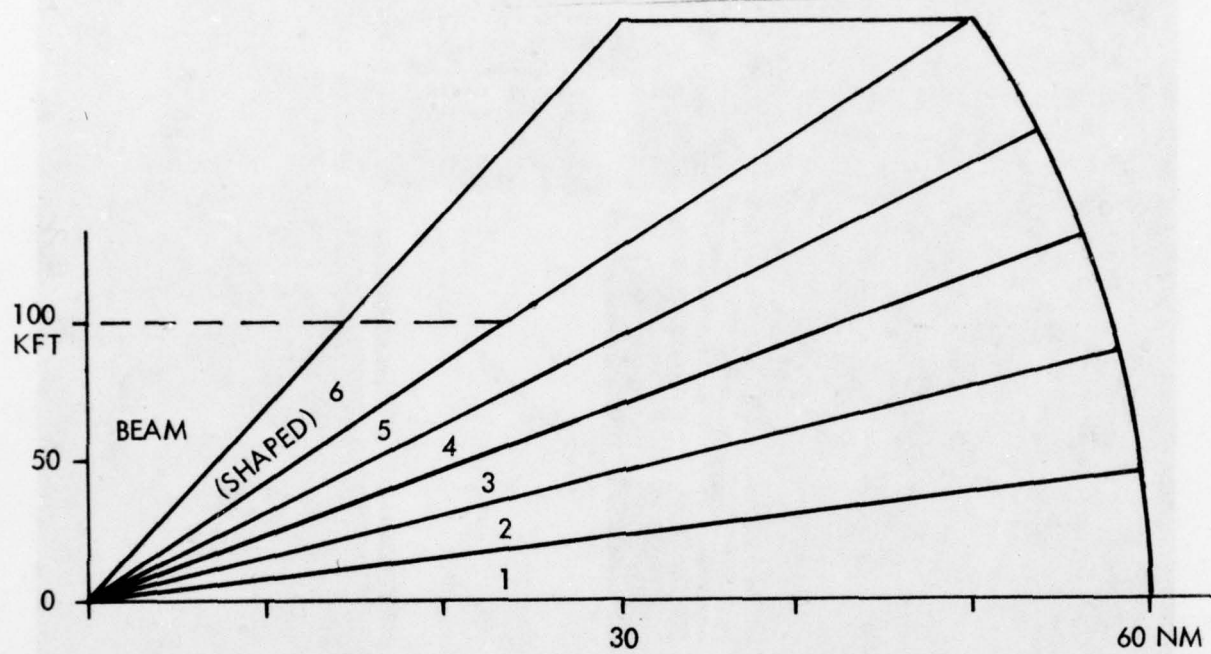
Figure 2.2.2-1.   Single/Split Frame Scan Structure

beam position is addressed each scan while for the split frame the upper and lower set of 3 beams are addressed sequentially. The dependent variables of these two scan structures are:

- Frame Time
- Number of receivers per total complement of beams

The Fence type of scan structure is intended to minimize the number of receivers required by programming the detection volume so that one or two receivers are time shared between a set of beams. The net result is that a detection fence is established. Figure 2.2.2-2 shows the relative timing of transmission and reception for each beam at L-band.

From the above basic variables the following candidates emerged:

Table 2.2.2-1

Freq	Scan Type	No Beams	No Receivers	Frame Time (Secs)
L	Split	6	3	7.2
L	Single	6	6	3.6
L	Single	6	3	7.2
L	Fence	6	2	3.4
L	Fence	6	1	6.8
UHF	Split	2	1	7.2
UHF	Single	2	2	3.6
UHF	Single	2	1	7.2
UHF	Single	1	1	3.6
UHF	Fence	2	1	3.6

b) Transmitter Configurations

The transmitter pulse length is another variable with significant impact. As stated previously each beam is sequentially addressed by the transmitter module. A basic pulse width per beam of 6 microseconds was assumed. Range gate width is 80% of the pulse width to achieve some oversampling. However, based on emperical data from Lincoln Labs experiment with the moving target
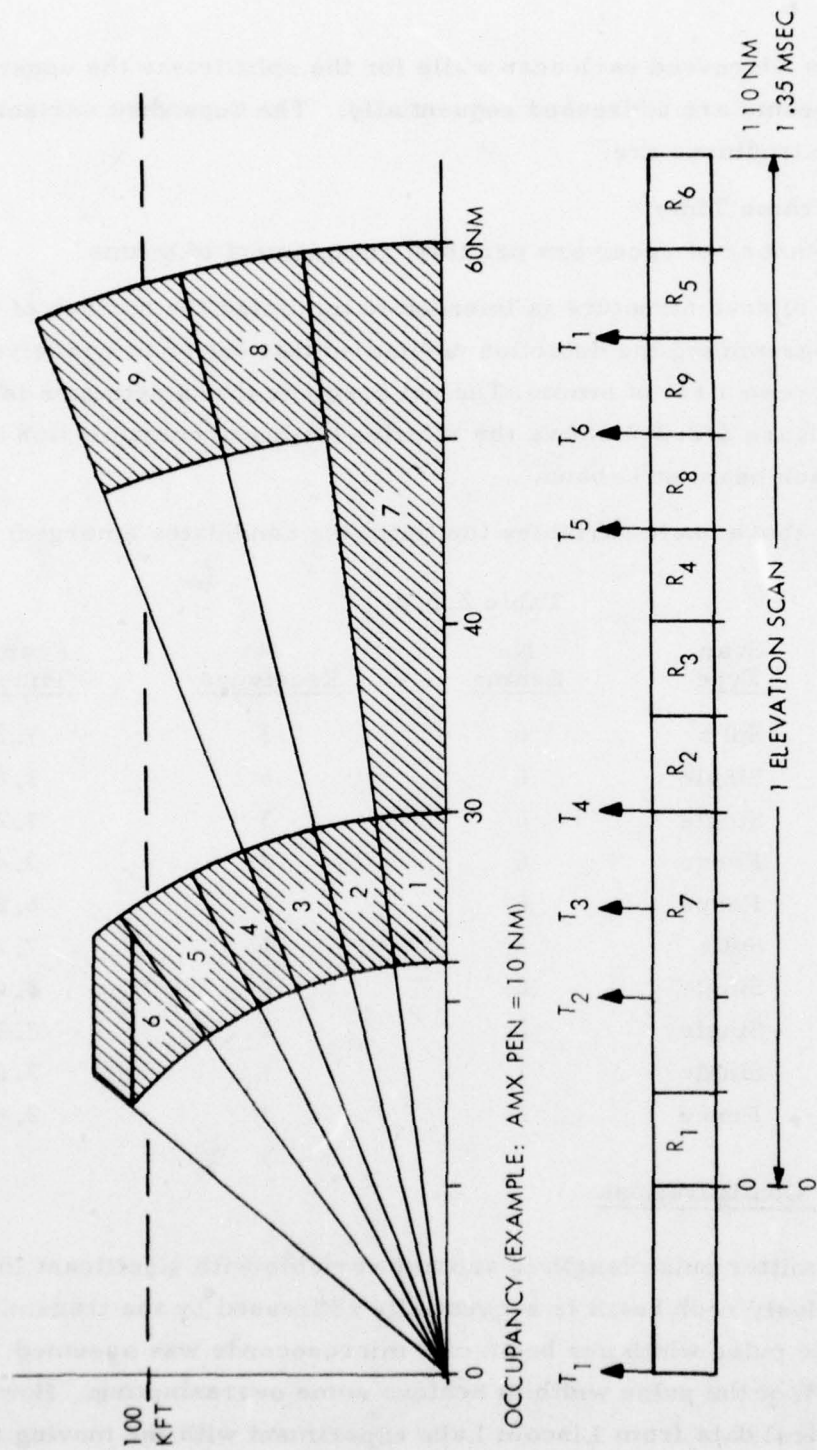
Figure 2.2.2-2. Fence/Tracker Configuration

detector (MTD) it may be desirable to reduce transmitter pulse lengths to 1.5 microseconds at L-band. This parameter is one of the most significant differences between UHF and L-band. At L-band it is estimated that for a constant 10^{-5} P_{fa} the signal processor CFAR threshold must be 10 dB higher if only 3 as opposed to 15 samples of weather data are available. The question as to how many samples are available is a function of the size of the weather cell and the transmitter pulse length. If weather cells are approximately 1 NMI in depth a 6 microsecond pulse would require a 10 dB increase in CFAR threshold as apposed to a 1.5 microsecond pulse. The prime impact of the smaller pulse width is the cost of the signal processor which must now accommodate a four-fold increase in range/azimuth cells to be processed. The present experimentation being carried out on the FPS-20 search radar should define the advantages of 1.5 vs 6 microsecond radar pulses at L-band. In order to evaluate the cost impact of 1.5 vs 6 microsecond pulses both pulse lengths will be evaluated for each L-band system configuration. At UHF 6 microsecond pulses are satisfactory due to much reduced backscatter from weather.

Although minimum prime power considerations dictate a TRSSM for each radiating stack (256 L-band, 128 UHF) the azimuth beam steering network will permit this number to be reduced by one fourth if the modules are located behind a quadrant switch. In this case a set of 64 modules is "walked" around the 256 stacks under the control of the switching network. The trade-off here is cost of TRSSM's vs higher power to overcome increased insertion losses (~3 dB two way at L-band). A secondary consideration here is the reduced graceful degradation properties of the RF subsystem particularly for unattended periods of 12 months.

c) System Parameter Summary

Other variations possible in system parameters are, Frame time, detection rule, and track initiation time. Frame time basically trades hardware for data rate. A 2 out of 3 detection rule can save about 0.4 dB in power compared to 3 out of 4 but results in less time to uncover blind speeds, resolve velocity ambiguity and reject multiple time around targets. Track initiation time is the dependent variable and is determined by the detection rule and scan structure.

2-15

As can be seen from the previous paragraphs a wide range of implementation of the generalized system block diagram are possible. Table 2.2.2-2 summarizes 72 candidate system configurations. The next step was to select a set of parameters and establish a baseline design. This baseline was developed and costed in great detail.

The assumptions were that (1) the baseline is one of the more attractive alternatives, (2) contains essentially similar subsystems as in most other candidates, and (3) subsystem design and cost can be extended to other candidates designs by simple extrapolation.

2.2.3 BASELINE SYSTEM DESCRIPTION

The selected baseline is an L-Band split-frame system with 6 beams, 3 lens and receiver channels. The pulse width is 6 microseconds and the TRSSM's are located at the radiating stack. The baseline design parameters are shown in Table 2.2.3-1. The split-frame type of scan is generated by searching the lower three beams on one azimuth scan and then the upper three beams on the next scan. An intermediate search alarm is made on the basis of one scan detection. Subsequent searches at this azimuth are made at the same elevation (high-low) for three more scans to satisfy the track initiation requirement. On one group of three beams, the transmitted pulse is "machine-gunned", i.e., different segments of the total pulse are rapidly switched into different beams. Reception occurs simultaneously on all three beams.

The Baseline System block diagram is shown in Figure 2.2.3-1. Top level details for each subsystem are shown and the major interfaces are defined. The general definition of the subsystems are summarized in the paragraphs below.

a) Antenna Subsystem

Figure 2.2.3-2 shows the concept for one of the radiating stacks. Each stack contains 20 radiating elements. Integrated into the stripline forming the stack are:

- Radiation elements
- Elevation feed network
- RF connections
- BITE pilot pulse input network

2-16

Table 2.2.2-2 Type A Alternative System Configurations.

No.	Freq.	Scan Type	No. Beams	No. Lenses	No. Rcvrs	ΔT Trans. (us)	ΔT Pulse (us)	TRSSM Loc	Det Rule TRSSM	No. TRSSM	Pwr Mod (w)	R.G. CPI	Frame Time (sec)	T.I. Time (sec)	Comment
1.	L	Split	6	3	3	18	6	ANT	3/4	256	40	450	7.2[1]	16.2[1]	Baseline
2.	L	Split	6	6	3	18	6	ANT	3/4	256	40	450	7.2[1]	16.2[1]	Imp. high el. coverage
3.	L	Split	6	3	3	4.5	1.5	ANT	3/4	256	160	1800	7.2[1]	16.2[1]	Imp. high el. coverage
4.	L	Split	6	6	3	4.5	1.5	ANT	3/4	256	160	1800	7.2[1]	16.2[1]	Imp. high el. coverage
5.	L	Split	6	3	3	18	6	Q.SW.	3/4	64	80	450	7.2[1]	16.2[1]	Reduced control comp.
6.	L	Split	6	6	3	18	6	Q.SW.	3/4	64	80	450	7.2[1]	16.2[1]	Imp high el. coverage
7.	L	Split	6	3	3	4.5	1.5	Q.SW.	3/4	64	320	1800	7.2[1]	16.2[1]	
8.	L	Split	6	6	3	4.5	1.5	Q.SW.	3/4	64	320	1800	7.2[1]	16.2[1]	
9.	L	Single	6	6	6	36[2]	6	ANT	3/4	256	40	900	3.6	14.4	Inc. rad. pwr. & comp.
10.	L	Single	6	6	3	18	6	ANT	3/4	256	40	450	7.2[1]	28.8[1]	Excess. frame time
11.	L	Single	6	3	3	18	6	ANT	3/4	256	40	450	7.2[1]	28.8[1]	Above + red. el. cov.
12.	L	Single	3	3	3	18	6	ANT	3/4	256	40	450	7.2[1]	14.4	Loss of hi. el. coverage
13.	L	Single	6	6	6	9	1.5	ANT	3/4	256	160	3600	3.6	14.4	Inc. rad pwr & comp.
14.	L	Single	6	6	3	4.5	1.5	ANT	3/4	256	160	1800	7.2[1]	28.8[1]	
15.	L	Single	6	3	3	4.5	1.5	ANT	3/4	256	160	1800	7.2[1]	28.8[1]	Reduced hi. el. coverage
16.	L	Single	3	3	3	4.5	1.5	ANT	3/4	256	160	1800	7.2[1]	14.4	Loss of hi. el. coverage
17-20		Same as 9 - 12						Q.SW.	3/4	64	80	Same as 9 - 12			Mod. pos. trade-off
21-24		Same as 13 - 16						Q.SW.	3/4	64	320	Same as 13 - 16			
25	L	Fence	6	6	2	36	6	ANT	3/4	256	40	280	3.4	13.7	10 nm "thick" fence
26	L	Fence	6	6	1	36	6	ANT	2/3	256	40	280	6.8	20.5	Won't handle max speed tgt.
27	L	Fence	6	3	2	36	6	ANT	3/4	256	40	280	3.4	13.7	Reduced hi. el. coverage
28	L	Fence	6	3	1	36	6	ANT	2/3	256	40	280	6.8	20.5	Reduced hi. el. coverage

Notes: (1) Track initiation time and average frame time can be reduced by one-fourth if top 3 beams instrumented only to 30 NM with corresponding "hole" in coverage.

(2) Transmitter radiation time in one effective pulse repetition interval (one-eighth of CPI).

Table 2.2.2-2 (Continued) Type A Alternative System Configurations.

No.	Freq.	Scan Type	No. Beams	No. Lenses	No. Rcvrs	ΔT Trans. (μs)	ΔT Pulse. (μs)	TRSSM Loc	Det Rule	No. TRSSM	Pwr Mod (w)	R.G. CPT	Frame Time (sec)	T.I. Time (sec)	Comment
29-32		Same as 25 - 28				9	1.5		Same		160		Same	Same	Pulsewidth trade
33-36		Same as 25 - 28						Q.SW.	Same	64	80		Same	Same	Mod. pos. trade
37-40		Same as 25 - 28				9	1.5	Q.SW.	Same		320		Same	Same	Pw + Mod. pos. trade
41	UHF	Single	2	2	2	12	0	ANT	3/4	128	150	300	3.6	14.4	
42	UHF	Single	2	2	1	6	6	ANT	3/4	128	150	150	7.2[1]	28.8[1]	Excessive frame time
43	UHF	Single	2	1	1	6	6	ANT	3/4	128	150	150	7.2[1]	28.8[1]	Above + red. el. cov.
44	UHF	Single	1	1	1	6	6	ANT	3/4	128	150	150	3.6[1]	14.4[1]	Loss of elev. cov.
45	UHF	Single	2	2	2	3	1.5	ANT	3/4	128	600	1200	3.6	14.4	
46	UHF	Single	2	2	1	1.5	1.5	ANT	3/4	128	600	600	7.2[1]	28.8[1]	
47	UHF	Single	2	1	1	1.5	1.5	ANT	3/4	128	600	600	7.2[1]	28.8[1]	
48	UHF	Single	1	1	1	1.5	1.5	ANT	3/4	128	600	600	3.6[1]	14.4[1]	
49-52		Same as 41 - 44						Q.SW.	Same	32	200		Same		
53-56		Same as 45 - 48						Q.SW.	Same	32	800		Same		
57	UHF	Split	2	1		6	6	ANT	3/4	128	150	150	7.2	16.2	
58	UHF	Split	2	1		6	6	ANT	3/4	128	150	150	7.2	16.2	Red. in el. coverage
59-60		Same as 57 - 58				1.5	1.5	ANT	3/4	128	600	600	7.2	16.2	Pulsewidth trade
61-62		Same as 57 - 58						Q.SW.	3/4	32	200	150	7.2	16.2	Mod. Pos trade
63-64		Same as 57 - 58				1.5	1.5	Q.SW.	3/4	32	800	600	7.2	16.2	Pw/Mod pos. trade
65	UHF	Fence	2	1		12	6	ANT	3/4	128	150	150	3.6	14.4	15 nm "thick" fence
66	UHF	Fence	2	1		12	6	ANT	3/4	128	150	150	3.6	14.4	Red. hi. el. cov.
67-68		Same as 65 - 66				3	1.5		Same		600	600	3.6	14.4	Pulsewidth trade
69-70		Same as 65 - 66				12	6	Q.SW.	3/4	32	200	150	3.6	14.4	Mod. pos. trade
71-72		Same as 65 - 66				3	1.5	Q.SW.	3/4	32	800	600	3.6	14.4	Pw/pos. trade

The purpose of the pilot pulse network is to inject a pulse into each beam receiving channel to constantly monitor system operation.

Table 2.2.3-1
Baseline System Specification

Frequency	1200 - 1400 MHz
Scan Structure	Split Frame
Polarization	Vertical
Azimuth Coverage	360°
Elevation Coverage	0° - 45°
Antenna Description	Ring Array
Dimensions	44' Diam. 7' Ht
Azimuth Beamwidth	1.4°
Elevation Beamwidth	6°
Number of TRSSM's	256
TRSSM Peak Power	40 watts
Average PRF	1150 Hz
Pulsewidth	6 us
Number of Azimuth Lenses	3
Number of Receive Channels	3
Receiver Noise Figure	1.4 dB
Frame Time	7.2 Sec
Track Initiation Time	16.0 Sec

b) Transmit/Receive Solid-State Modules (TRSSM)

The baseline TRSSM is located at the radiating stack and contains 1 transmitter and 3 receiver modules. The low power requirement that dictated the location of TRSSM also forces use of class C final amplifier operation for efficient amplification. This creates some difficulty in achieving low transmit sidelobes as the illumination function to the antenna is essentially uniform. The Baseline TRSSM has a peak power output of 40 watts at L-band. Three separate receive channels are provided with a 1.4 dB noise figure.

2-19
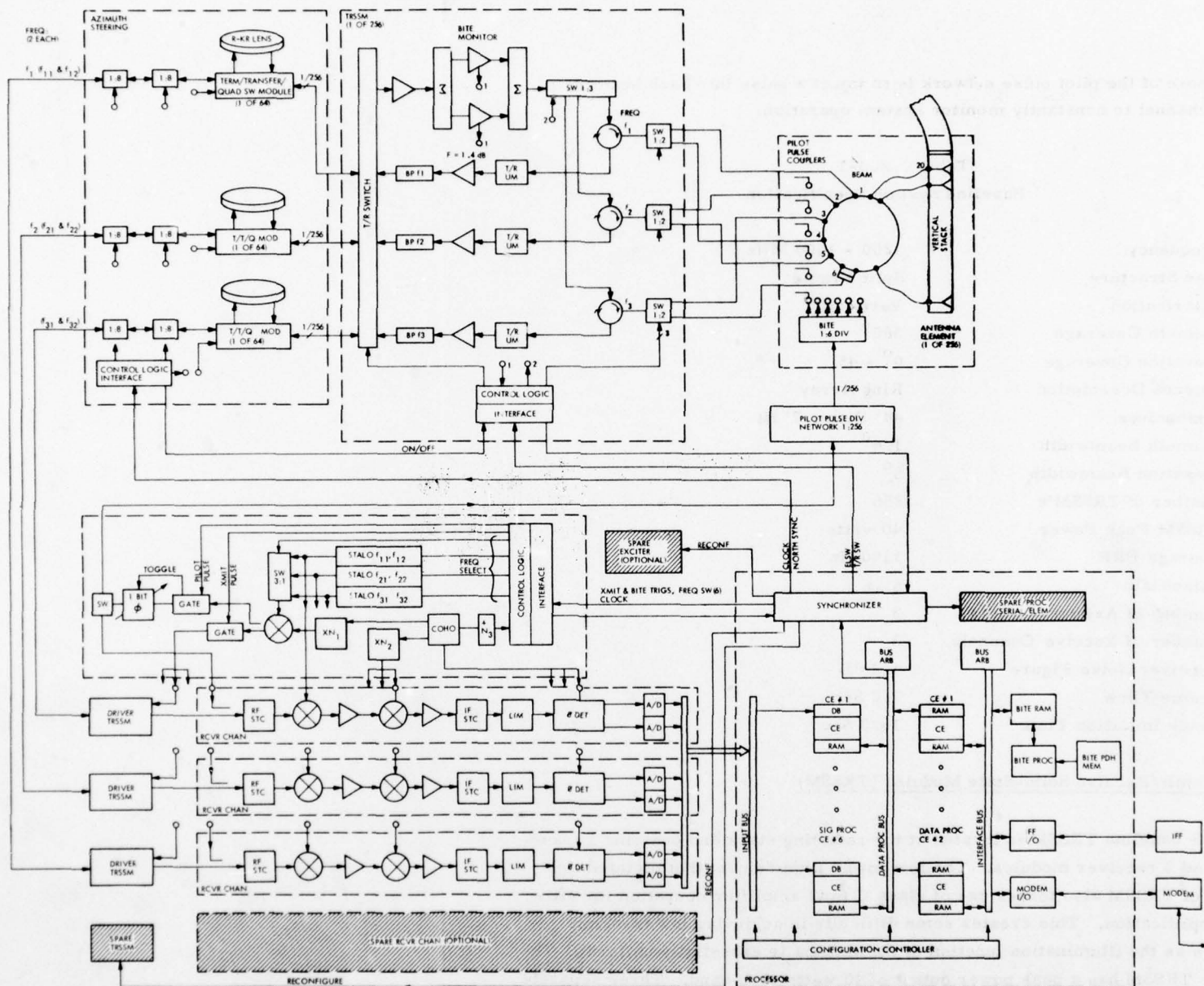
Figure 2.2.3-1

Baseline System
Block Diagram

Implementation of a controllable taper within the TRSSM to achieve low antenna sidelobes on receive was considered as a side variable. The complexity of implementing such a controllable precise taper into each module proved to be quite expensive. As the primary purpose of low sidelobes, in what is essentially a trip-wire, air defense system function, is to protect against ECM degradation, it was decided to include the taper design option into a baseline variant configured for ECCM.

Three azimuth steering lens inputs drive the transmitter portion and complete the receive paths. The three lenses are focused to cover beams 1 and 2, 3 and 4, and 5 and 6. Three separate frequencies are used (f_1, f_2, and f_3) to maximize isolation between adjacent beams and provide some additional frequency agility fill-in between beams.

On one half-frame (one scan around covering one half of the elevation), beams 1, 2, and 3 are radiated with frequencies f_1, f_2, and f_3, respectively. On the succeeding half frame, beams 4, 5 and 6 are radiated with f_1, f_2, and f_3.

Beams 1 and 2 inputs are handled by one lens and are separable by means of time on transmit and frequency on receive. This separation is made clearer by the sketch shown in Figure 2.2.3-3 for the transmission and reception on the lower 3 beams. The T/R switch and 1:3 elevation switch in the TRSSM, route the three subpulses through a common amplifier chain and then into the appropriate three output duplexers. A 1:2 switch provides High-Low elevation switching on a scan-by-scan basis.

The receiver front-ends employ a low noise figure (1.4 dB) preamplifier and a bandpass filter. Each receiver front end would be designed to cover one third of the band (≈ 50 MHz). Frequency agility would occur within each band such that one frequency from each band is always used. This assumes that 25 MHz frequency separation is sufficient to achieve independent sampling on aircraft size targets. The receiver front end outputs are then routed to the appropriate lens for summing into one output per beam. The T/R switch must effectively sum two of the received signals as, for example, beams 1 and 2 share a common lens. Signal-to-noise degradation does not occur as the two signals are effectively diplexed.
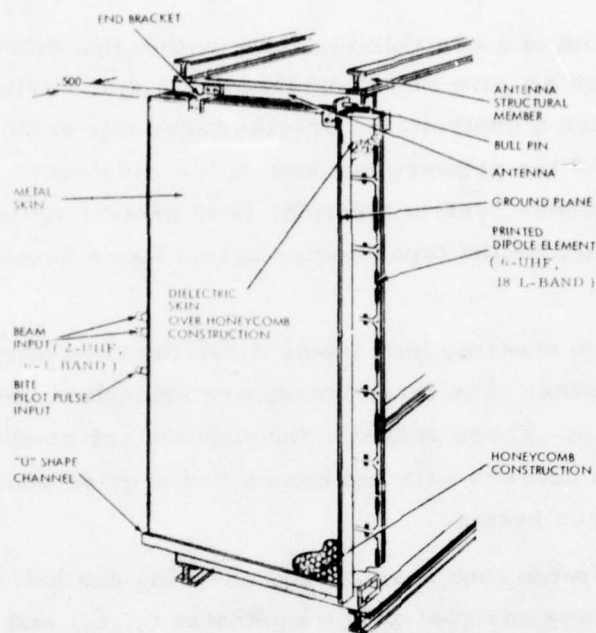
Figure 2.2.3-2 Antenna Radiating Stack
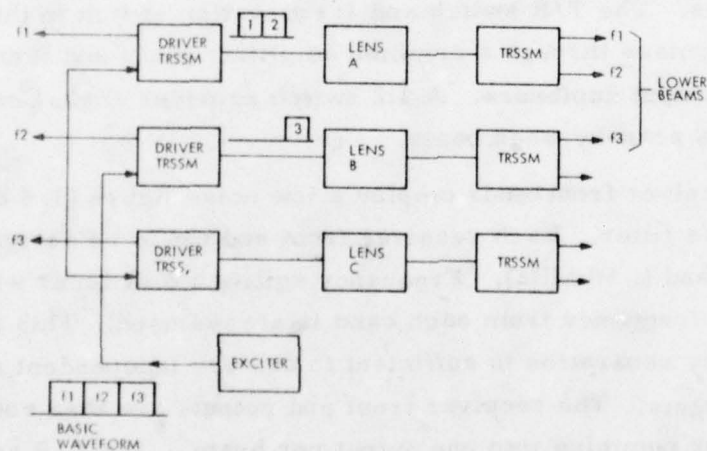
Figure 2.2.3-3 Beam Separation

The TRSSM's also receive control signals from the azimuth steering subsystem which turns each module off when not in use to conserve power. The on-off command is also used to drive internal TRSSM logic to determine position in the active scan cycle in order to determine the correct receiver taper attenuation to insert.

c) Azimuth Steering

Three R-2R lens are employed for the Baseline Azimuth Steering subsystem. One lens is used for two adjacent beams (1 and 2, 3 and 4, 5 and 6). The lens efficiently takes one of 256 different inputs and distributes the energy with correct phasing to 64 different outputs. The lens itself has 128 equally spaced ports around the circumference. By injecting a signal at one port a correctly phased wavefront can be picked off the 64 ports which cover a 180° arc directly opposite the input port. Quadrant switches (part of the T/T/Q module in Figure 2.2.3-1) are employed to further distribute these 64 active outputs to 64 out of 256 possible antenna elements. Because a 180° arc of the lens feeds a 90° arc of the antenna array, it is necessary to complete 2 scans of the lens for one scan of the antenna. For this purpose a transfer switch is incorporated in the switching matrix to sequentially connnect diametrically opposed antenna elements to each lens port. The number of beam positions is doubled by dividing energy equally between adjacent input ports to achieve mid-beam positions. This reduces the effect of the azimuth cross-over nulls.

Various numbers of lenses were considered as alternatives (6 and 3 at L-band and 2 and 1 at UHF). The larger number of lenses (one per beam) reduces defocussing loss at higher elevation angles at the cost of more hardware.

d) Receiver/Exciter

The Baseline system employs a single exciter with three STALO's to generate the separate frequencies used on each beam. Each STALO is capable of generating two frequencies for frequency diversity. The transmitter drive pulse is achieved by sequentially switching each STALO into a mixer at the appropriate time to form the three frequency triplet pulse. A portion of the Exciter signal is gated to form the BITE pilot pulse which is then phase shifted in a one-bit phase shifter to form a PRF/2 doppler offset and distributed to all 256 antenna units. Three separate dual conversion, coherent detection, receiver

2-23

channels are used. Dual conversion was selected to allow the first IF to be at a high frequency as an ECCM aid. The A/D converters (in-phase and quadrature) are packaged with each channel.

Alternatives at L-band are for 1, 2, 3 and 6 receiver channels. At UHF, a single conversion system was examined with 1 and 2 receiver channels and an exciter with two STALO's.

e) Signal/Data Processor

The processor concept has a parallel architecture using multiple "common elements (CE)". A common element is a self contained microprocessor consisting of an arithmetic logic unit (ALU), program memory and data memories.

A top level block diagram of the processor or is shown in Figure 2.2.3-4. The digitized inputs from the receiver channels are distributed directly to the signal processing CE's by means of the input bus. CFAR data is transferred between signal processing CE's via the data processing bus which also serves to route signal processing alarms to the data processor and provide control signals to the radar processor. The data processor also consists of a number of CE's with some minor differences to optimize the CE for data processing functions. Interfaces with the IFF, BITE processor and communication system are made via the interface bus.

Six CE's are used in the Baseline System to process approximately 75 range gates each. The functions performed are:

- Double buffer input

- Spectral analysis

- Magnitude

- Weighting

- Sliding (16 gate) range average

- Clutter map

- Interference detector

- ECM strobe detection

Figure 2.2.3-4 Signal Processor Common Element Architecture

Spare signal processing CE's can be switched in by an address change command from the configuration controller.

Two CE's are used for the data processing to perform the functions:

- Command same-elevation (High/Low) for detected target azimuth on next three scans

- Multiple time around rejection

- Velocity ambiguity resolution

- Uncover blind speeds (accomplished by PRF stagger between batches)

- Track initiation (3/4 correlation)

- Track

- Target designation and interface to IFF

- Interface with communication channel

- Interface with BITE processor

The processor alternatives considered are in the number of CE's required to process the number range gates dictated by the system configuration. The Baseline processor has 6 signal processor CE's, 2 data processor CE's and 2 spare CE's. If the pulsewidth is reduced to 1.5 μsec versus the 6 μsec assumed for the Baseline, then the number of signal processor CE's increases by a factor of 4. It also varies directly as the number of required receiver channels.

The synchronizer provides triggers and control signals as follows:
- To exciter:
    - Trigger triplet plus bite pulse trigger
    - Frequency select (set 1 or set 2 alternately with batches)
    - BITE test select - switches pilot pulse into receiver front-end or directly into receiver channel input.
- To azimuth steering
    - Clock
    - North sync pulse
- From receiver
    - Clock(s)

2-26

- From BITE
  - BITE test changes
- From data processor CE
  - High/Low elevation switch command
- To TRSSM
  - High/Low elevation switch command
  - Elevation beam switching pre-trigger and BITE gate switching pre-trigger
- Reconfigure spare LRU's
  - Driver TRSSM's
  - Receiver channels
  - Exciter

f) <u>Built-in Test Equipment (B.I.T.E.)</u>

As can be seen from Figure 2.1-2 the BITE concept is driven by the need for a 3 hour repair visit. This requires apriori knowledged at a permanently manned site which field replaceable units (FRU's) has failed. Given the availability of this failure data at the manned sites and the technological risk of designing a self-diagnosis/self repair fault correcting system the concept of manual reconfiguration of failed non-redundant (inherently) subsystems has been selected. This permits human judgement to enter the failure modes analysis problem posed by identified failure readouts.

The BITE system utilizes the following tests:

TRSSM power monitor

Pilot pulse* injection at antenna element

*BITE pilot pulse is 10 range gates long.

Pilot pulse injection at receiver first mixer input

Digital test input into signal processor input bus.

Test (1) samples the final amplifier bias current to determine that radiation occurred at the appropriate times. The pattern of failures detected, when analyzed, is sufficient to determine -

- Exciter failure
- Azimuth steering failure (down to LRU)
- TRSSM failure in Xmtr chain

Test (2) when performed, for two cycles with and without inputs tests:

- Receiver front-ends
- Receiver channels and diplexer TRSSM's
- Signal processor

Tests (3) and (4) are ordered when (2) uncovers a problem to isolate between receiver and processor.

All CE's perform the BITE pilot pulse processing and report the result in order to isolate to failed CE level.

The BITE processor has an independent control system which interfaces with all TRSSM's and:

- Addresses TRSSM
- Senses GO/NO GO on power monitor
- Switch all but one TRSSM off during pilot pulse.

A list of field replaceable units (FRU) is shown as Table 2.2.3-2. The BITE system isolates failures down to the FRU level and reports the FRU failure and type to the attended Logistic Node for Maintenance action. Upon detection of a failed FRU for which an unused spare exists, the BITE processor will identify that the spare should be switched in. This will be implemented by manual control at the permanently manned site.

g) Tower/Shelter

An outline drawing of the tower/shelter design is shown as Figure 2.2.3-5. The radar/IFF shelter is depicted atop a 100 foot tower. The radar/IFF shelter is a self-supporting steel building with radome curtain walls for the radar (lower) and IFF array. The tower would be produced in equal twenty-five foot high sections and could then be assembled in heights ranging from twenty-five to one hundred feet. A minimum height of twenty-five feet is recommended to accommodate the life support building and to allow for snow buildup. An enclosed stairwell is recommended for easy access under all weather conditions. Suggested positioning of the communication antennas are shown.

Table 2.2.3-2

Field Replaceable Units (FRU's)

	LRU	No. *
1.	Antenna Element	256
	(includes antenna stack, bootlace lens,	
	1:6 power divider and cables).	
2.	TRSSM	256
3.	Terminating/Transfer/Quadrant Switches	64
4.	Input Switch Dividers (2nd Tier)	24
5.	Input Switch Dividers (1st Tier)	3
6.	Driver TRSSM	3
7.	Receiver Channel	3
8.	Exciter	1
9.	Signal Processor CE	6
10.	Data Processor CE	2
11.	Synchronizer	1
12.	Other Signal Proc. LRU's	≈3
13.	BITE Processor	1
14.	Pilot Pulse Divider Network	
15.	IFF	≈6

*Excluding Standby Spares
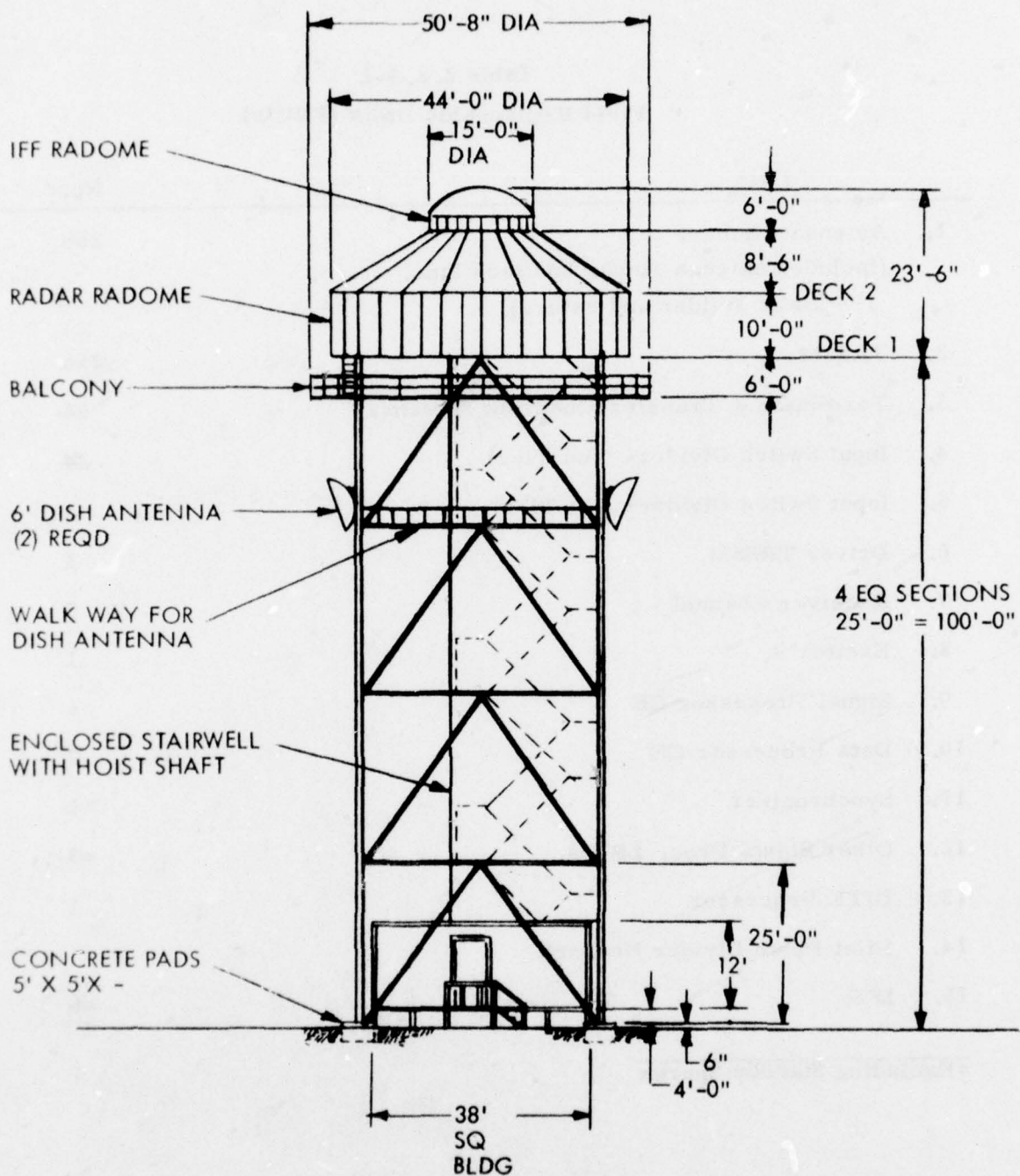
Figure 2.2.3-5. Unattended Radar Tower and Radome

A list of radar/site interface criteria for the baseline system is given in Table 2.2.3-3.

Table 2.2.3-3

Radar/Site Interface Criteria

Weight

Radar System	20
IFF System	1
Radome and Structure	75
Tower/Stairway	155
	251 K Lbs

2.2.4 SUBSYSTEM DESIGN VARIATIONS

The variations in design by subsystem are summarized in Table 2.2.4-1. Although 72 system configurations have been identified, it can be seen that subsystem perturbations are few in number.

The change to the Baseline block diagram of Figure 2.2.3-1 to bring the TRSSM back behind the quadrant switch is shown in Figure 2.2.4-1.

The top level system block diagram for UHF is shown in Figure 2.2.4-2 for a single lens, split-frame, TRSSM at antenna configuration.

The changes to the TRSSM to achieve various numbers of channel capability are described in Section 2.3.2.

Table 2.2.4-1

Subsystem Alternatives

A. ANTENNA:
1) L-band/3 beam
2) L-band/6 beam
3) UHF/1 beam
4) UHF/2 beam

B. TRSSM

	Freq	Location	No. Rcvrs	P_T	Total Pulsewidth
1)	L	Antenna	3	40W	18 μs
2)	L	Antenna	6	40W	36
3)	L	Antenna	3	160	4.5
4)	L	Antenna	6	160	9
5)	L	Quadrant Switch	3	80	18
6)	L	Quadrant Switch	6	80	36
7)	L	Quadrant Switch	3	320	4.5
8)	L	Quadrant Switch	6	320	9
9)	UHF	Antenna	1	150	6 μs
10)	UHF	Antenna	2	150	12
11)	UHF	Antenna	1	600	1.5
12)	UHF	Antenna	2	600	3
13)	UHF	Quadrant Switch	1	200	6
14)	UHF	Quadrant Switch	2	200	12
15)	UHF	Quadrant Switch	1	800	1.5
16)	UHF	Quadrant Switch	2	800	3

Table 2.2.4-1. (Cont)

C. AZIMUTH STEERING

      L-band/TRSSM at antenna

      L-band/TRSSM at Quadrant switch

      UHF/TRSSM at antenna

      UHF/TRSSM at Quadrant switch

D. RECEIVER/EXCITER

      L-band/3 channel

      L-band/6 channel

      UHF/1 channel

      UHF/2 channel

E. SIGNAL PROCESSOR

      Common Element Design (one configuration)

F. BITE/MAINTENANCE

      FRU Failure reporting

      Repair on demand   } one configuration

G. POWER DISTRIBUTION

      Assumes that DC voltages (regulated) are GFE.

Figure 2.2.4-1. TRSSM At Quadrant Switch

2-34

Figure 2.2.4-2. UHF Baseline Block Diagram

2.3 PRIMARY RADAR DETAIL DESIGN

2.3.1 ANTENNA DESIGN

a) Configuration Considerations

As stated previously in discussing generalized system design guidelines an electrically scanned antenna is a necessary part of a low power consumption unattended radar. The candidate antenna configurations are basically the multifaced array, the Dome antenna, the Hourglass antenna and the cylindrical array.

The multiface array is not economic for a 360° scan requirement. It generates essentially cone shaped beams when scanned off boresight and as such has difficulty achieving the goal of 0.5 degree azimuth accuracy on all targets.

The Dome antenna provides an alternate approach to improve the cost-effectiveness of hemispheric coverage. It uses a single active planar array to illuminate a passive dome lens, which forms a pencil beam in space. This antenna however suffers from gain degradation at low elevation angles and has difficult polarization problems in certain directions, and thus is not a good candidate.

The Hourglass antenna, using a concave cylindrical reflector (shaped like an hourglass) and a ring array feed, represents an excellent antenna geometry for the 360° azimuth coverage. However, due to the requirement of an exterior feed array, the horizontal dimension of the antenna tends to be large. For example, if a 44' diameter cylindrical reflector is used, the feed array diameter is approximately 60'. Furthermore, to achieve the desired elevation pattern shaping, the antenna also requires an oversized aperture. This configuration is not desirable given the tower mounting constraints and radome problems.

The cylindrical array offers the best solution to the tower/radome constraints, (44 ft. diameter with integral low loss radome) and possesses a number of other distinct advantages; the beam steerability, the pattern invariance, the effective usage of the radiating aperture and the ease of protection for weather. The first advantage is due to the existence of the microwave lens device for the azimuth beam steering, as will be discussed later. The pattern invariance is a property realizable with all circularly symmetric arrays, such that the azimuth beam is electronically steered without scanning loss.

2-36

b) Baseline Antenna Design

The Type A baseline antenna configuration is a circular array of 256 vertical element stacks, equally spaced around a 44-foot diameter circle. This diameter was selected as the largest allowable (for this number of elements) to prevent excessive grating sidelobes. The aperture height is approximately 7 feet for the baseline configuration. The relationship between the antenna components and other subsystems is generally illustrated in Figure 2.2.1-2.

The elevation plane RF-feed network is a multiple beam feed network where the number of array elements is 20 with an array aperture spacing of 4.8 inches ($\approx 0.5287\lambda$). The number of simultaneous elevation plane beams is taken at a minimum of 6 (feed input ports) such that the highest angle beam could be a shaped RF-combination of two or more beams and the 5 lower beams are of pencil-beam nature. Several different feed techniques have been examined including a bootlace lens, a Blass-Lopez, and a Butler Matrix structure. The azimuth plane RF-feed network is to be a switching matrix associated with an R-lens whose radius R is taken such that the array elements along any arc of essentially 90° are azimuthally co-phased at a specified elevation angle. Three R-lenses are utilized in the baseline configuration. Each lens is to be associated with two adjacent beams and co-phased at the elevation angle halfway between the beam peak angles of the two beams.

A transmit-receive solid state module (TRSSM) is located at each antenna element stack.

c) Cylindrical Array Pattern Analysis

The radiation patterns of the cylindrical array have been analyzed with the aid of a computer program formulated for this purpose. The analytical details are given in Appendix A. The results are summarized in the following.

The geometric variables of the cylindrical array are given in Figure 2.3.1-1. The cylindrical array consists of M vertical stacks with each stack containing N stripline dipole radiators. At each step-scanned beam position, only 90° of the array is excited. Cylindrical array patterns can be analyzed in terms of two separable amplitude patterns: (i) the elevation pattern $G_E(\theta)$ held constant, and (ii) the elevation dependent azimuth pattern $G_A(\phi, \theta)$. The azimuth beamwidth is also a function of the number of R-2R lenses employed, as the beam tends to defocus out of the elevation plane for which the lens was optimized. The use of three lenses in the baseline configuration permits approximate focussing for each adjacent pair of the 6 beams. A greater or lesser number of lenses determines a greater or lesser amount of defocussing, respectively.

The derived amplitude distribution over the 20-element vertical aperture array is taken as given in Table 2.3.1-1.

Since Class C TR-modules are employed at the circular array elements within the (active) 90° arc, the amplitude distribution over the 63 element horizontal aperture array is taken as unity.

For an antenna array of this type, the element pattern contribution of the array elements is of considerable importance. A cosine-squared element pattern behavior was assumed in both the azimuth and elevation principal planes for the baseline system.

It was also assumed that the elevation feed network was designed such that the elevation plane beams are essentially orthogonal and the first sidelobe levels are 23 dB down.
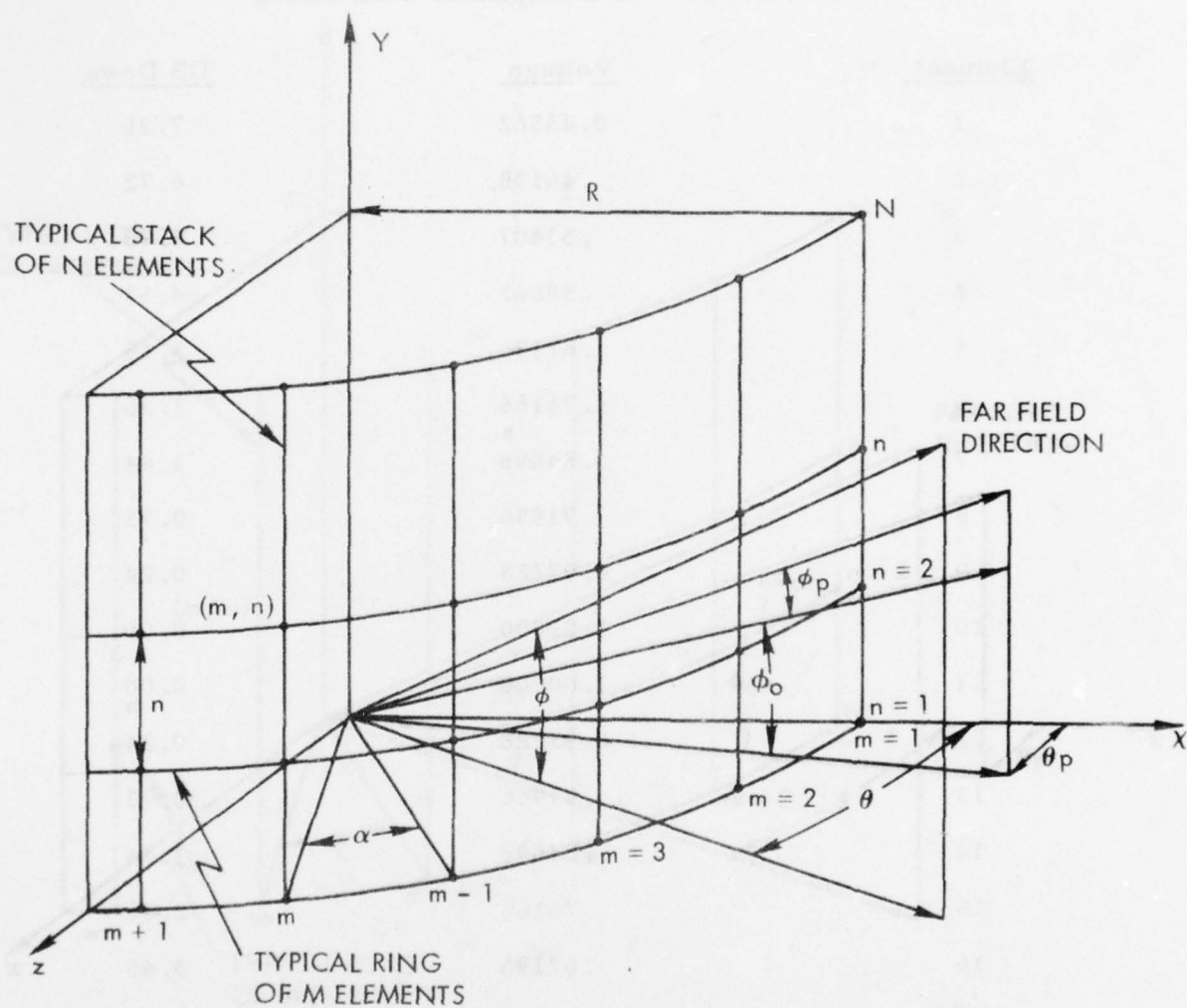
Figure 2.3.1-1 Circular Cylindrical Array
Geometry

Table 2.3.1-1

Baseline Elevation Amplitude Distribution

Element	Voltage	DB Down
1	0.43362	7.26
2	.46133	6.72
3	.51407	5.78
4	.58663	4.63
5	.67196	3.45
6	.76166	2.36
7	.84698	1.44
8	.91956	0.73
9	0.97228	0.24
10	1.00000	0.00
11	1.00000	0.00
12	0.97228	0.24
13	.91956	0.73
14	.84698	1.44
15	.76166	2.36
16	.67196	3.45
17	.58663	4.63
18	.51407	5.78
19	.46133	6.72
20	0.43362	7.26

The orthogonal requirement can be satisfied by positioning the beam peak directions at elevation angles θ_n where,

$$\sin \theta_n = \left[Z_o + (1.3) n \right] / \left[(20) \ (0.5287) \right]$$

where n is an index counting the beam number above the horizon and Z_o is established by the desired underside horizon point of the lowest beam.

Figure 2.3.1-2 contains plots of the calculated pattern peak regions of the 6 elevation plane beams for the baseline configuration. The R-lenses were co-phased at $6.3°$, $20.8°$, and $37.5°$ for these calculations. The crossover levels vary between 5 and 8 dB while the beams are orthogonal.

The gain fall-off at the higher elevation angles is due to two factors: - (1) the cosine-squared element pattern and (2) the azimuth plane defocusing associated with the R-lens co-phasal angles. A broader elevation element pattern could be designed and larger number of lens could be used to reduce the gain fall-off. The use of more lenses is discussed in the next section as an alternate configuration.

A plot of the Baseline two-way, free-space, elevation plane coverage is shown as Figure 2.7.1-1 in Section 2.7, Type A Performance Evaluation.

Holes in the desired coverage are evident and are due to the crossover levels associated with the use of orthogonal multiple beams. The depth of these coverage holes can be reduced by using elevation beams with a shallower crossover. This option is also discussed in the next section on alternative designs.

Figure 2.3.1-3 contains plots of the near-in azimuth plane patterns as calculated at the elevation angle of each beam peak. The nominal half-power beamwidth is approximately 1.4. The gain fall-off and azimuth defocusing effects are evident.
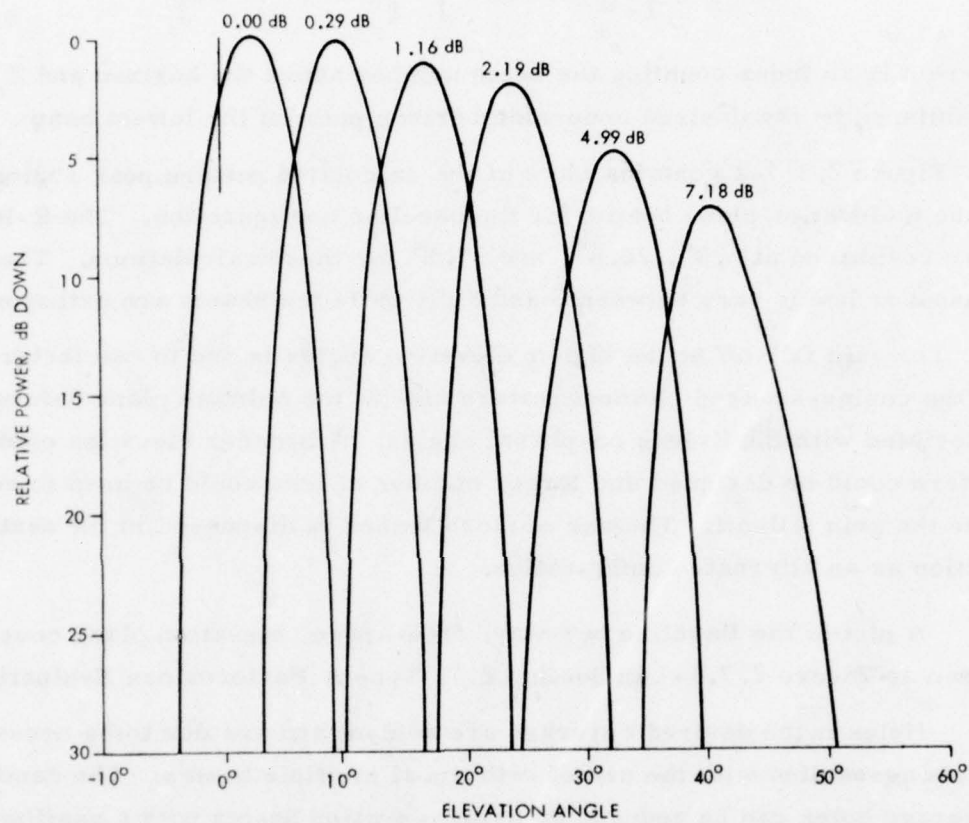
Figure 2. 3. 1-2.   Calculated Baseline Elevation Plane
Beam Patterns

ELEVATION BEAMS

———	#1 at 2.7°
— — —	#2 at 9.7°
·········	#3 at 17.0°
—·—·—	#4 at 24.6°
—··—··—	#5 at 32.6°
—···—···—	#6 at 41.5°

RELATIVE POWER, dB DOWN

AZIMUTH ANGLE
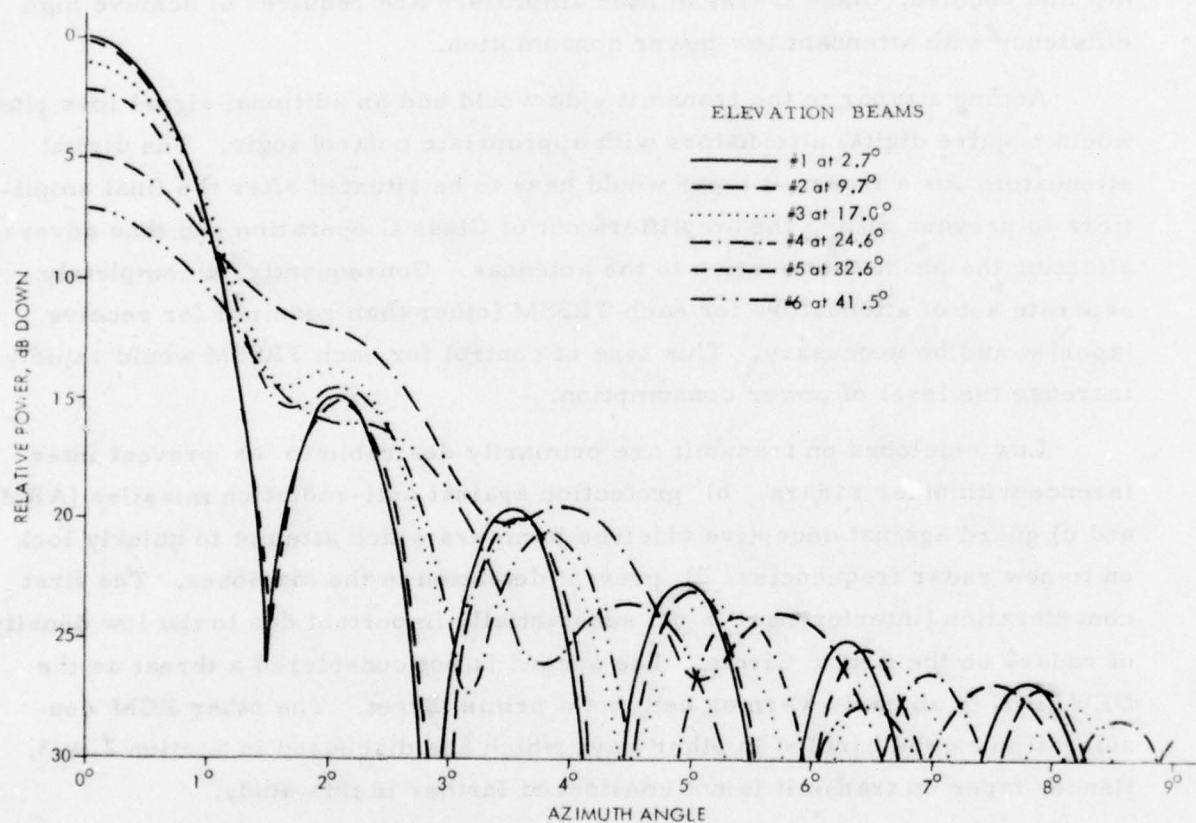
Figure 2. 3. 1-3.   Calculated Baseline Azimuth Plane
Pattern Cuts

d) Azimuth Sidelobe Control

The goal established for sidelobes is 30 dB (1-way). The use of Class C amplifiers at each element makes it difficult to achieve this goal for both transmit and receive. Class C transmitter amplifiers are required to achieve high efficiency with attendant low power consumption.

Adding a taper to the transmit side would add an aditional signal loss plus would require digital attenuators with appropriate control logic. The digital attenuators for a transmit taper would have to be situated after the final amplifiers to prevent pulling the amplifiers out of Class C operation and thus adversely affecting the phase distribution to the antennas. Consequently, a completely separate set of attenuators for each TRSSM (other than required for receive taper) would be necessary. This type of control for each TRSSM would rapidly increase the level of power consumption.

Low sidelobes on transmit are primarily desirable to a) prevent interference with other radars, b) protection against anti-radiation missiles (ARM), and c) guard against deceptive sidelobe jammers which attempt to quickly lock on to new radar frequencies, d) prevent detection in the sidelobes. The first consideration (interference) is not substantially important due to the low density of radars on the Arctic Circle. The second is not considered a threat as the DEW LINE is an early warning net, not a prime target. The other ECM consideration can be handled in other ways which are discussed in Section 2.4.3. Hence, taper on transmit is not considered further in this study.

While the receive taper involves the same type of taper loss, it has a substantial benefit for ECCM purposes (see Section 2.7.3). It can be achieved with one set of controllable attenuators located at the azimuth steering subsystem. Consequently receive taper is assumed for the ECCM configurations.

Figure 2.3.1-4 shows calculated far-field azimuth plane patterns for 63 active elements for several values of taper. The case of uniform taper (the expected transmit excitation) is shown as a solid line; it can be seen that the near-in sidelobes fall off essentially at 15, 20, 23, 25, 35 dB levels. Although not shown, the worst case far-out sidelobe level (for the low elevation beams) has been calculated as approximately 22 dB down at $\pm 90^\circ$ away from the main beam direction.

2-44
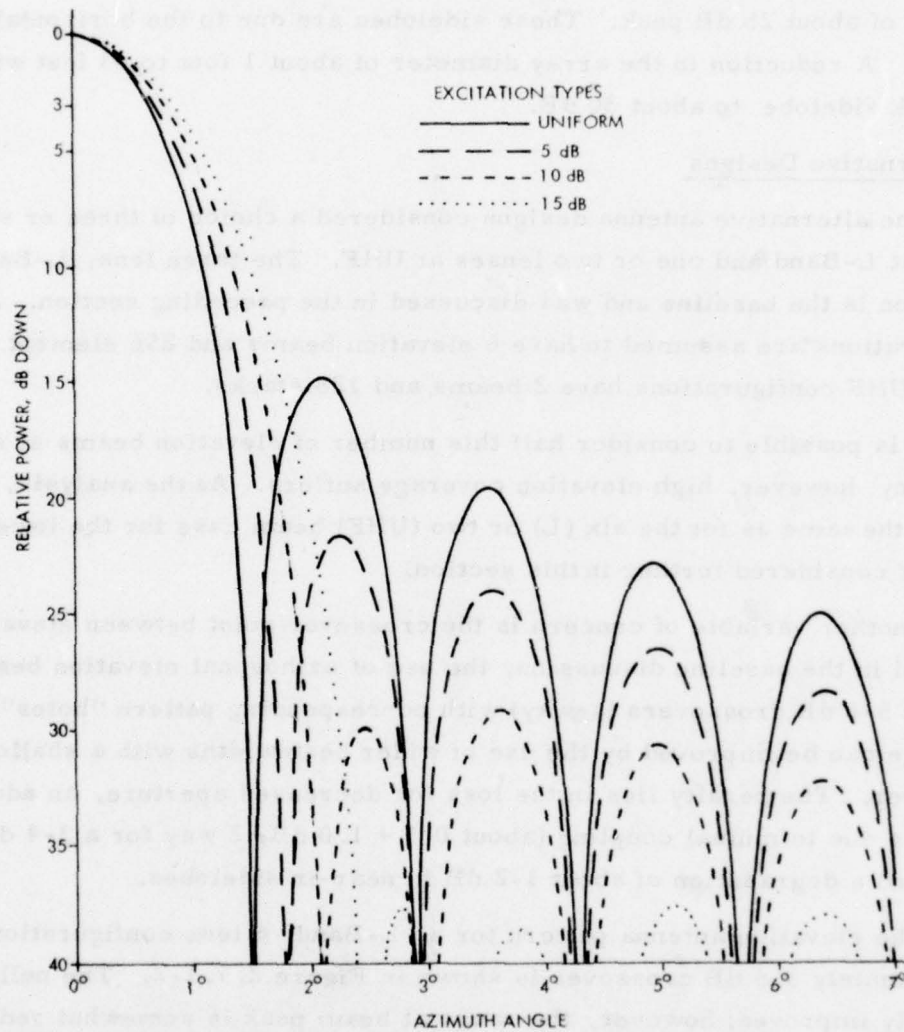
Figure 2. 3. 1-. 4 Calculated Azimuth Plane Patterns

In receive, the R-2R lens has a natural 5 dB taper; this reduces the near-in receive sidelobes by about 4-6 dB. An additional 5 dB of taper (10 dB total) places essentially all sidelobes below 30 dB. The exception are lobes at $\pm 90^{\circ}$ azimuth of about 25 dB peak. These sidelobes are due to the horizontal element spacing. A reduction in the array diameter of about 1 foot to 43 feet will reduce this peak sidelobe to about 30 dB.

e) Alternative Designs

The alternative antenna designs considered a choice of three or six R-2R lenses at L-Band and one or two lenses at UHF. The three lens, L-Band configuration is the baseline and was discussed in the preceding section. All L-Band configurations are assumed to have 6 elevation beams and 256 element stacks and all UHF configurations have 2 beams and 128 stacks.

It is possible to consider half this number of elevation beams at either frequency; however, high elevation coverage suffers. As the analysis, for this case is the same as for the six (L) or two (UHF) beam case for the lower beams, it is not considered further in this section.

Another variable of concern is the crossover point between elevation beams. As noted in the baseline discussion, the use of orthogonal elevation beams results in about 5-6 dB crossovers (1-way) with corresponding pattern "holes". The coverage can be improved by the use of wider beamwidths with a shallower crossover. The penalty lies in the loss for decreased aperture, an additional feed loss due to mutual coupling (about 0.5 + 1.0 dB, 2 way for a 3-4 dB crossover, and a degradation of about 1-2 dB in near-in sidelobes.

The elevation antenna pattern for an L-Band, 6 lens configuration with an approximately 3.5 dB crossover is shown in Figure 2.7.1-2. The nulls are considerably improved; however, the range at beam peak is somewhat reduced due to the losses described above.

The UHF antennas are configured with 6 radiating elements per stack spaced at 14 inches for each vertical stack. An elevation feed network with two input beam ports generates two elevation plan beams with crossover points of approximately 4.5 dB.

The 2 lens two-way elevation coverage for UHF is shown as Figure 2.7.1-3 in Section 2.7. The lower beam is pointed at 9° elevation, and the upper at 32°. The elevation coverage for the one-lens UHF system would be substantially similar.

The advantage of a two lens configuration can be seen by comparing Figures 2.3.1-5 and 2.3.1-6 Figure 2.3.1-5 shows calculated azimuth plane pattern cuts through the elevation angles at which the two beams were focused. Deep nulls are evident. Figure 2.3.1-6 shows calculated azimuth plane pattern cuts through the same elevation angles when a single R-2R lens is focused at 25° elevation. Filling of the pattern nulls is now evident along with a general raising of near-in sidelobes. The peak gain would also be somewhat less.

f) Low Cost Antenna Technology

The detailed structure of the antenna including the vertical element stacks, the elevation feed network and the various interconnections were extensively investigated to determine the lowest-cost solution. The original designs employed a Bootlace lens (space constrained) type of feed as other types of feed networks such as a Butler Matrix appeared to involve too many interconnections to be cost competitive. Subsequent investigation into air-stripline techniques of construction proved that such was not the case.

A typical vertical stack using a "component" type Bootlace lens feed network is shown in Figure 2.3.1-7. The array of elements themselves were fabricated in conventional stripline using Duroid dielectric. This type of stack is similar to that developed at Raytheon for the Transportable Surveillance Radar (TSR). A TSR element stack is shown in Figure 2.3.1-8.

Three types of feed networks were studied - a Bootlace lens, a Butler Matrix, and a Blass-Lopez feed. Each was examined in both a component and an integrated version. The component version utilized the appropriate
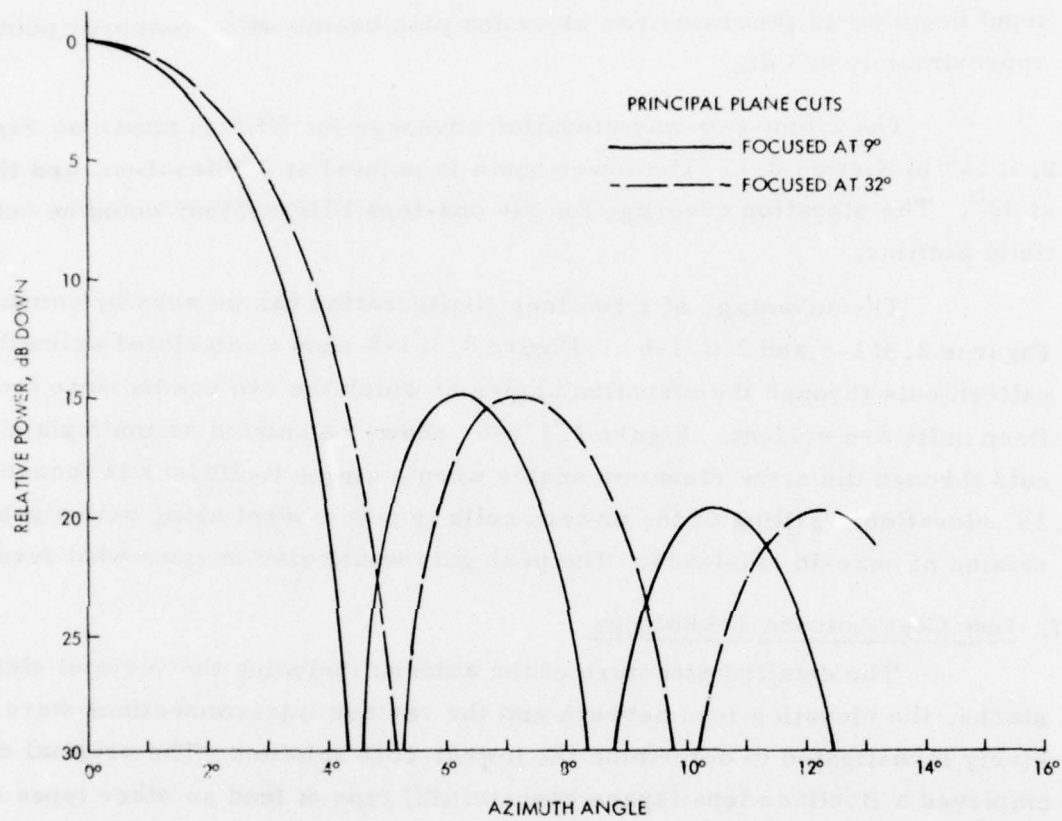
Figure 2. 3. 1-5.   Calculated Azimuth Plane Patterns
(Two-Lens Configuration)

2-48
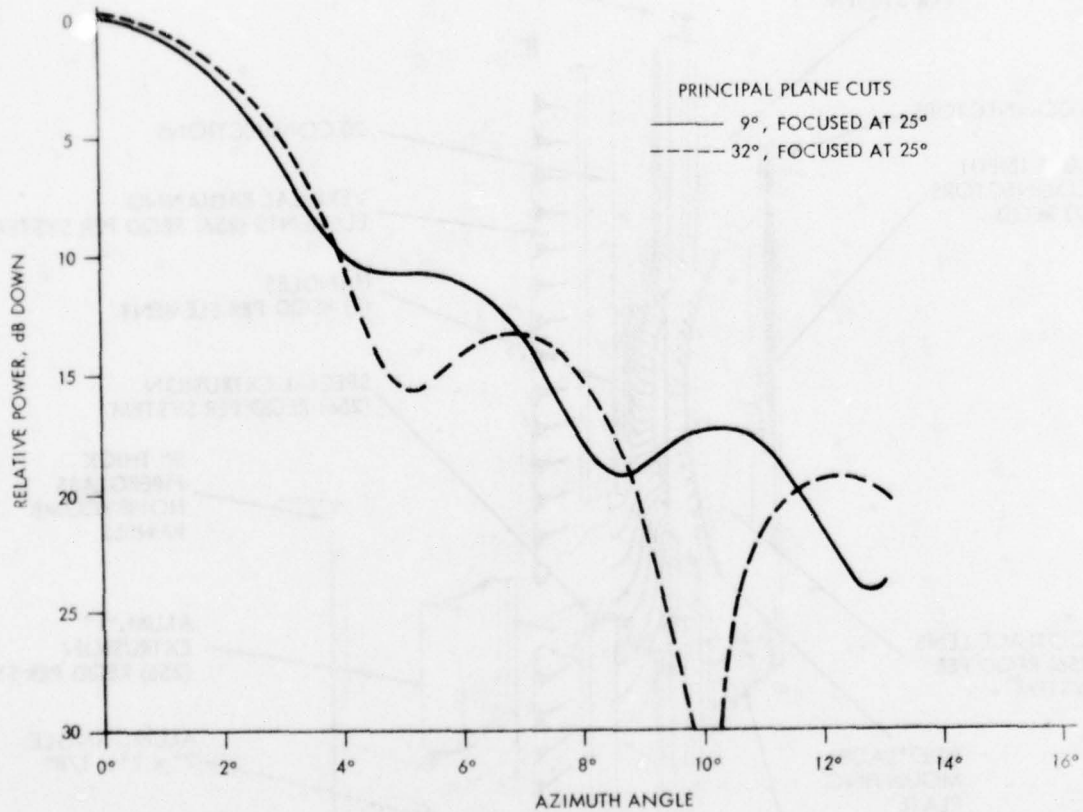
Figure 2. 3. 1-6. Calculated Azimuth Plane Patterns
(One-Lens UHF Configuration)

2-49

T/R MODULE (256) REQD PER SYSTEM

4" WIDE FLANGE BEAM

6 CONNECTORS

LENS INPUT CONNECTORS (7) REQD

20 CONNECTIONS

VERTICAL RADIATING ELEMENTS (256) REQD PER SYSTEM

HANDLES (2) REQD PER ELEMENT

SPECIAL EXTRUSION (256) REQD PER SYSTEM

3" THICK FIBERGLASS HONEYCOMB PANELS

BOOTLACE LENS (256) REQD PER SYSTEM

ALUM. "T" EXTRUSION (256) REQD PER SYSTEM

BOOTLACE MOUNTING PLATE

ALUM. ANGLE 2" x 2" x 1/8"

POWER SUPPLIES

STEEL ANGLE

Figure 2. 3. 1-7.   Typical Vertical Stack - Bootlace
Lens Feed (Cutaway View)

2-50
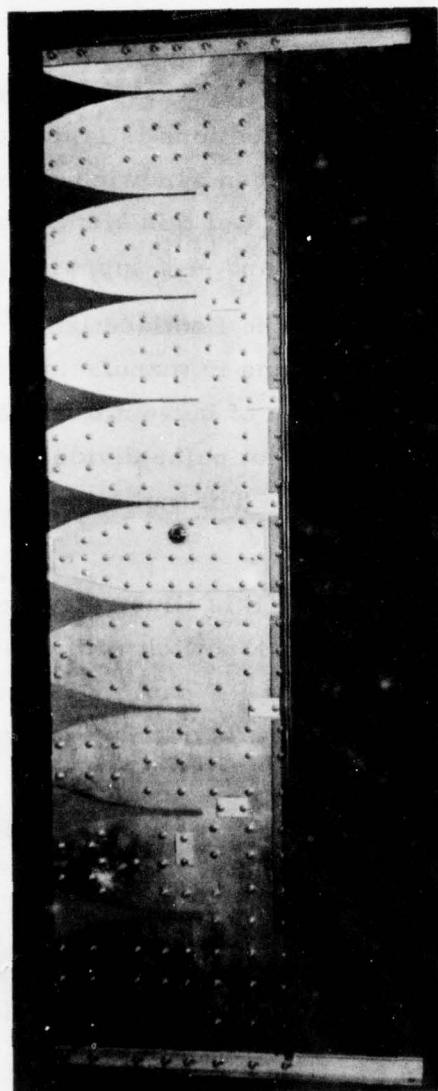
Figure 2. 3. 1-8.   TSR Vertical Sta

components (lens, hybrids, couplers, radiators, etc.), supplied interconnecting cables, and designed a suitable structure to support the pieces. In this type of construction, the Blass-Lopez and Butler Matrix became very costly for the baseline version.

The integrated version use an air-stripline technique where the entry microwave circuit including interconnections is laid out and etched on a thin dielectric substrate. The circuit is then sandwiched between two layers of nylon honeycomb and finally two layers of thin aluminum stock. The complete assembly is light weight, rigid and self supporting.

The integrated version of the Bootlace lens feed for L-band is shown in Figure 2.3.1-9. The Bootlace lens is manufactured separately and "dropped" into the stripline assembly. Because of lay-out difficulties in minimizing the number of crossing RF lines - the pilot pulse divider network - used for BITE - is included as a separate component. The radiating dipole elements are etched on the dielectric substrate.

A Blass-Lopez feed for UHF is illustrated in Figure 2.3.1-10. The entire structure is now a honeycomb sandwich with dimension 4 ft. by 8 ft. and 1/2-inch thick. Eight interconnecting RF semi-rigid cables are required for crossing RF lines dictated by the Blass-Lopez structure. The pilot pulse divider network can now also be etched on the same substrate. For UHF, the only interconnections are the two beam inputs and a single pilot pulse input. The Butler Matrix feed structure would look the same except that seven external RF cables are required.

The schematic representations of the Blass-Lopez and Butler networks are shown in Figure 2.3.1-11 and 2.3.1-12 respectively.

The relative costs of producing vertical element stacks for several different feed network/fabrication technique combinations is shown in Table 2.3.1-2. It is apparent from Table 2.3.1-2 that - using the integrated air-stripline technique - either the Blass or Butler feeds results in a lower cost antenna solution.
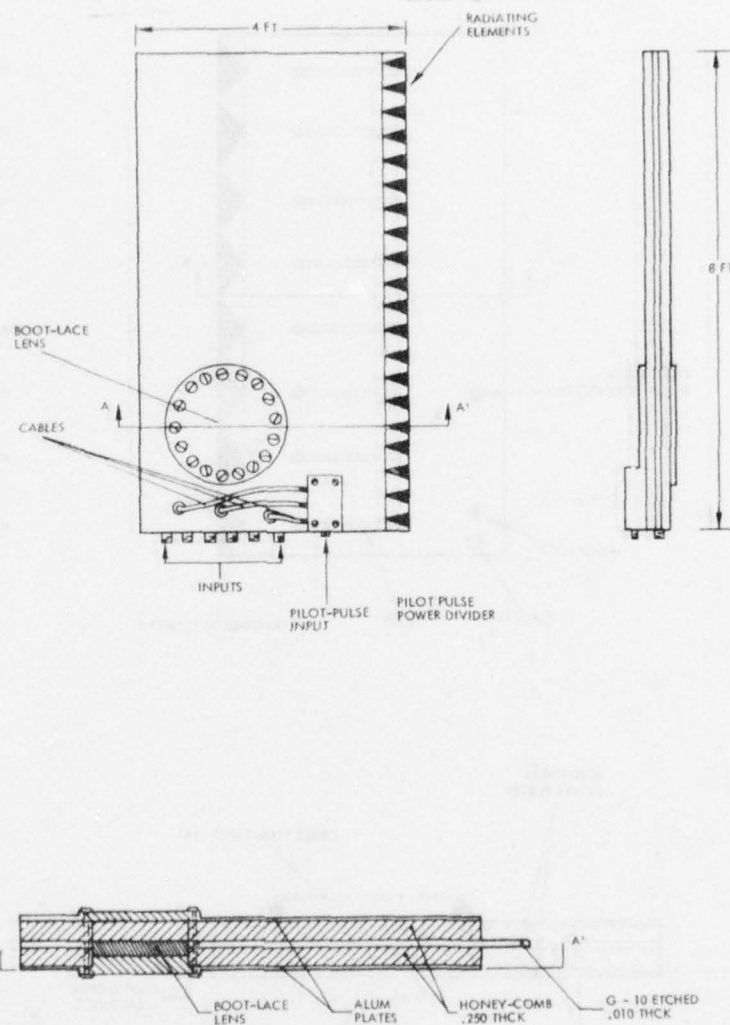
Figure 2. 3. 1-9.   L-Band Antenna Stack Bootlace   Lens; Integrated

PILOT PULSE
INPUT CONNECTOR

INPUT I

INPUT II   CABLE   RADIATING ELEMENT

ALUMINUM
COVER PLATES

CABLE SEMI-RIGID .141

G-10 ETCHED
0.010 THICK

HONEYCOMB MAT'L
0.250 THICK
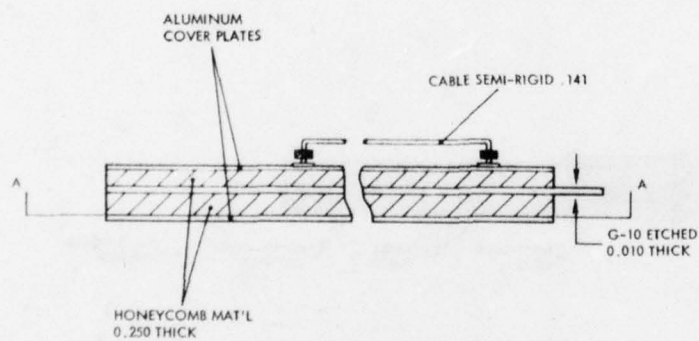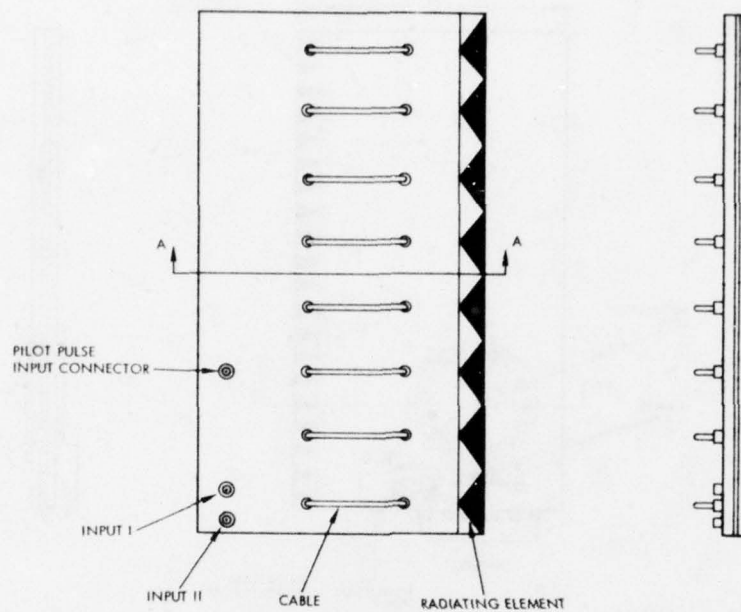
Figure 2. 3. 1-10.   UHF Antenna Stack (Blass-Feed)

2-54
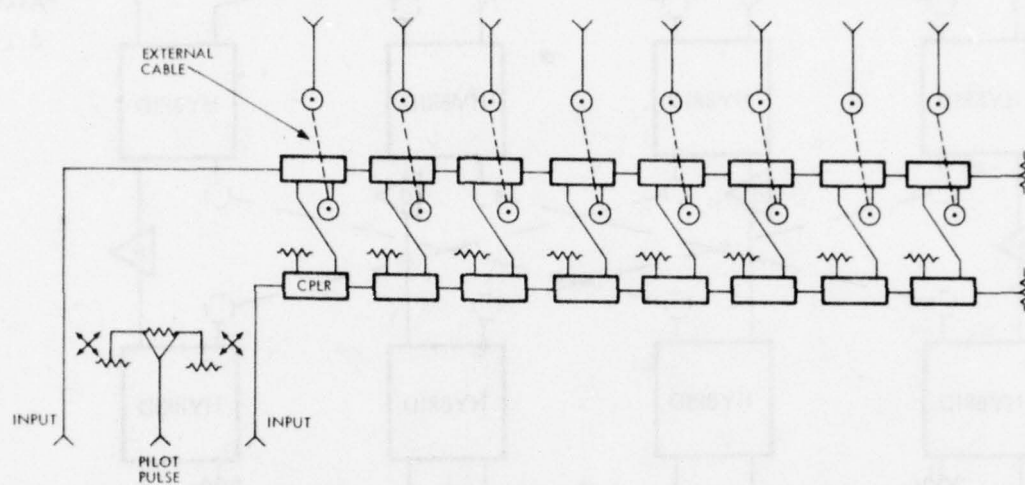
Figure 2.3.1-11 Schematic Antenna Element for "Blass" Transmission
Line Feed U.H.F. Type-A Radar

2-55
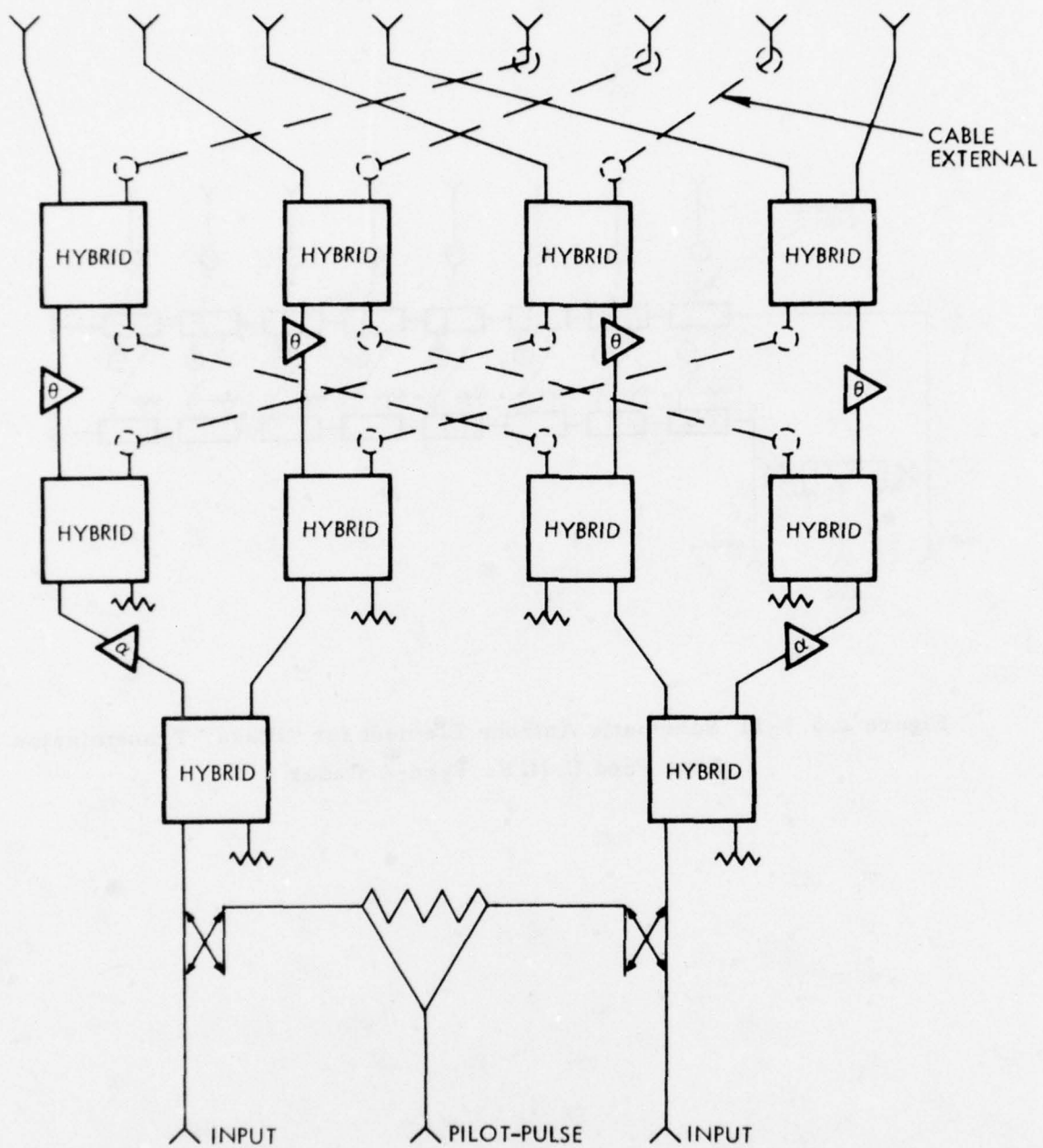
Figure 2.3.1-12 Schematic Antenna Element for Butler Matrix
U.H.F. Type-A Radar

Table 2.3.1-2

Relative Antenna Production Costs

Frequency	Feed	Fabrication	Relative Cost
L	Bootlace Lens	Component	1.0
	Bootlace Lens	Integrated	0.95
	Blass or Butler	Integrated	0.55
UHF	Bootlace Lens	Component	1.0
	Bootlace Lens	Integrated	0.85
	Blass or Butler	Integrated	0.45

A concept drawing of the UHF Blass/Butler antenna stack is shown in Figure 2.2.3-2. The support structure and method of installation is also illustrated. The antenna stack (a 4' x 8' sheet) is slid into position between a bottom "O" channel and two top end brackets. A ball pin is used to secure and align the stack and permits quick release. The support structure consists of two top and two bottom structural elements which go around the entire array.

An enlarged detail of the UHF integrated antenna is shown in Figure 2.3.1-13 with various cut-a-ways to illustrate the important construction details.
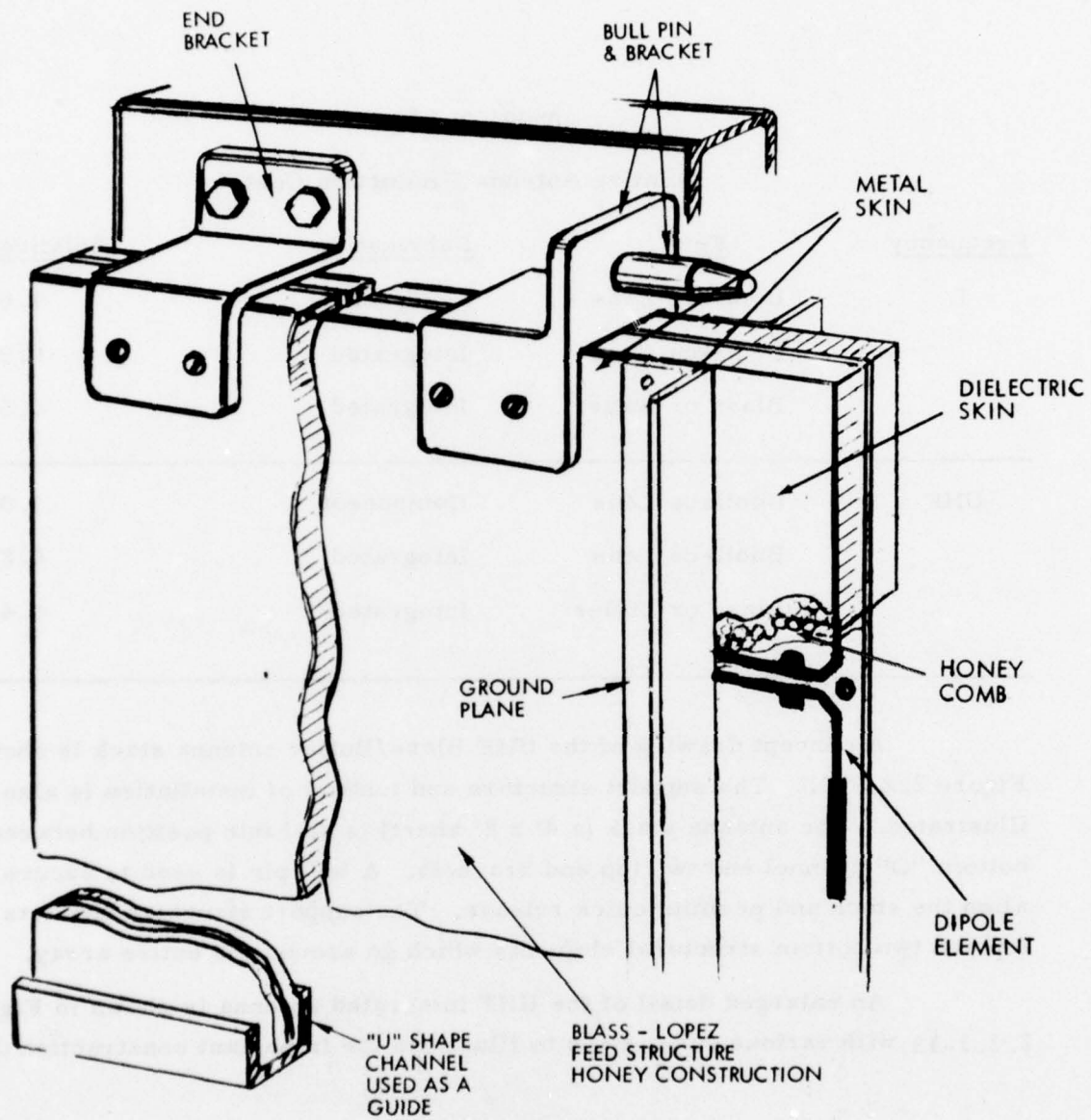
Figure 2. 3. 1-13.   UHF Integrated Antenna Enlarged
Detail Section of the Antenna

2.3.2 TRANSMIT/RECEIVE SOLID STATE MODULE (TRSSM)

a) TRSSM Design - State-Of-The-Art

The current design state-of-the-art in solid state TR combined transmit and receive solid state modules (TRSSM) is such that microwave integrated circuit (MIC) modules can be produced inexpensively and reliably in high production volumes. Many of the techniques which would be used are currently being put into practice on modules for the L-Band Transportable Surveillance Radar (TSR) and the UHF PAVE PAWS phased array radar system. These techniques include mounting Teflon-Glass or ceramic microwave integrated circuit boards in cast aluminum housings designed to optimize the electrical, mechanical and thermal interfaces of the module to the outside world. A bank of TSR modules is shown in Figure 2.3.2-1. A PAVE PAWS module is shown in Figure 2.3.2-2.

The module components required are well within the present state-of-the-art for most of the configurations studied. The usual pacing item is the transmitter output transistor. The requirements for the output transistor in the baseline system is 24 watts output, 6.5 dB gain and 45% collector efficiency at L-band. Currently, L-band devices are being evaluated at Raytheon which have over 100 watts peak output, 8.0 dB gain and 55% collector efficiency.

The device required for the baseline module represents a very conservative derating from the highest power devices currently available. A lower power device represents an advantage in semiconductor yields, broadband matching and device-to-device parameter variations over a high power device in a given frequency range. Other components within the module such as circulators, switches, hybrids and low noise amplifiers have been in production for several years and have well developed histories. The baseline module is a relatively low risk item well within the current state-of-the-art.

The baseline TRSSM design block diagram is shown in Figure 2.3.2-3. The baseline TRSSM has a single channel transmitter and a three channel low noise receiver front end. This configuration with the appropriate switching as shown in Figure 2.3.2-3 is capable of rapidly 'machine gunning' the transmitted pulse waveform into either the lower three or upper three beams. The receive portion is capable of receiving three simultaneous signals. The theory of operation of the Baseline System is given in Section 2.2.3.
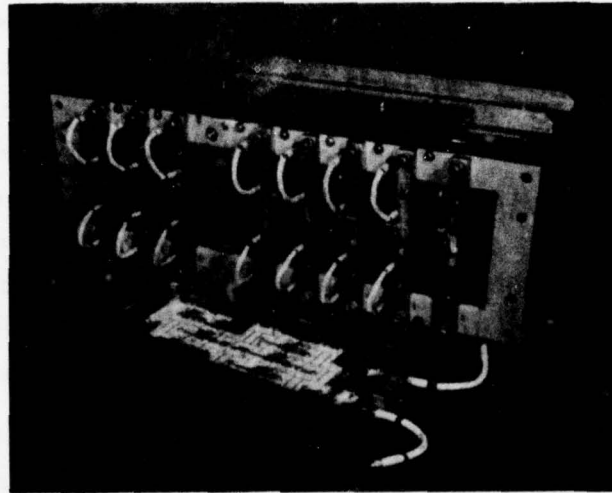
Figure 2.3.2-1. "L" Transmitter Module Bank (TSR)
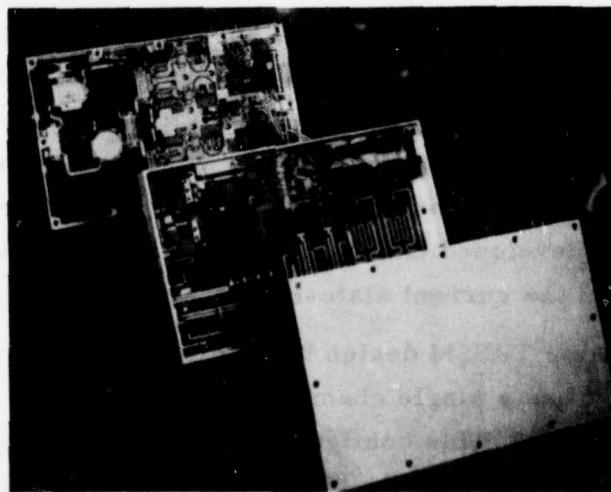
Figure 2.3.2-2. UHF Transceiver Module (PAVE PAWS)
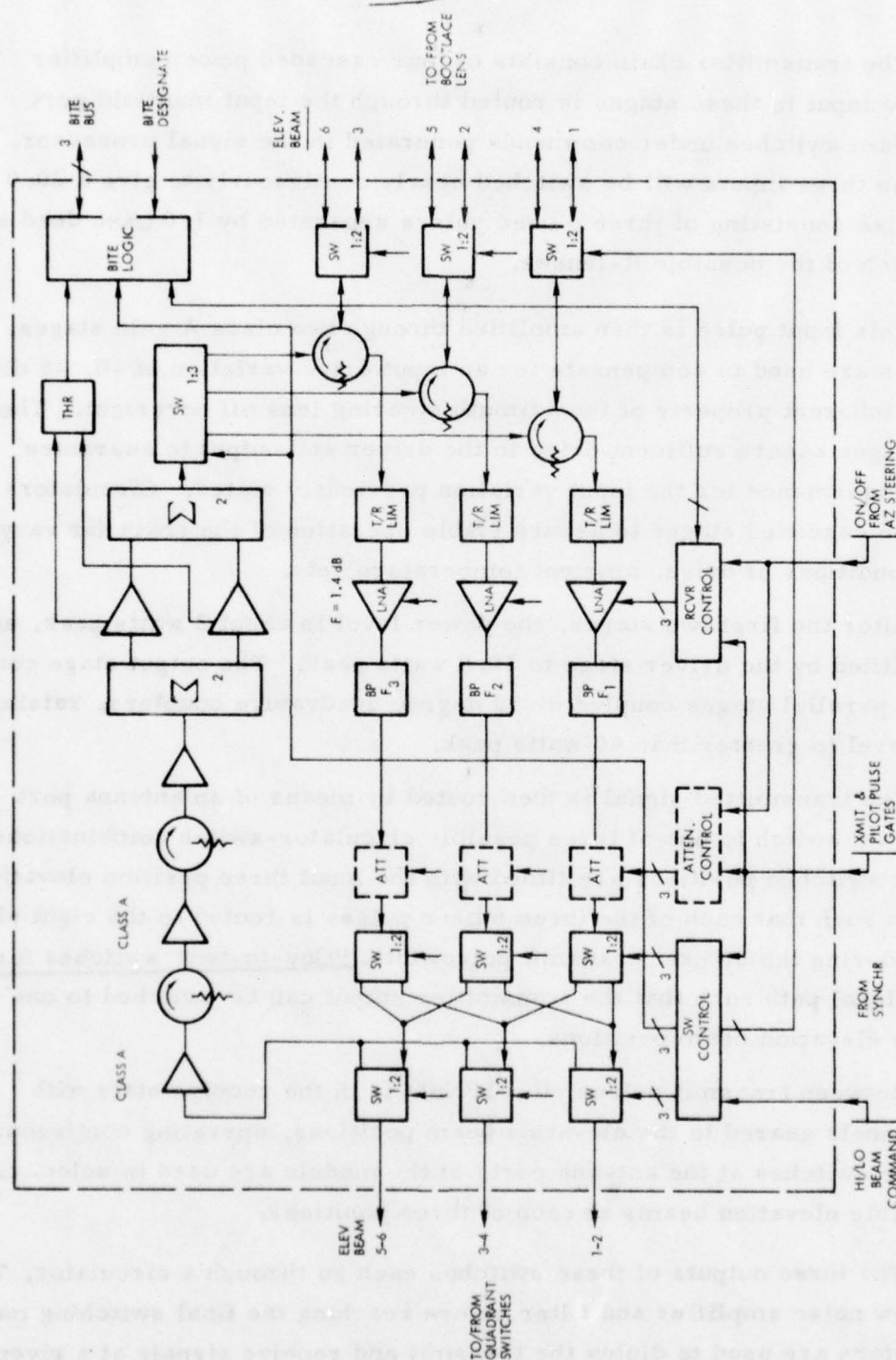
Figure 2.3.2-3. T/R Module (3 Channel)

The transmitter chain consists of four cascaded power amplifier stages. The input to these stages is routed through the input manifold port elevation beam switches under commands generated in the signal processor. In practice, the three inputs will be switched nearly contiguously to give a 20.0 μsec transmit pulse consisting of three 6 μsec pulses separated by 1.0 μsec dead spaces, one from each of the possible R-lenses.

This input pulse is then amplified through two class A gain stages. These stages are used to compensate for an input drive variation of +0, -5 dB which is an inherent property of the azimuth steering lens off boresight. The two input stages assure sufficent drive to the driver and output to guarantee saturated performance for the input variation previously stated. Circulators are used between cascaded stages to assure stable operation of the chain for varying operating conditions of drive, ambient temperature, etc.

After the first two stages, the power level is about 2 watts peak, and this is amplified by the driver stage to 10.0 watts peak. The output stage consists of two parallel stages coupled by 90 degree quadrature couplers, raising the signal level to greater than 40 watts peak.

The transmitted signal is then routed by means of an antenna port elevation beam switch to one of three possible circulator-switch combinations. These three switched positions are timed with the input three position elevation beam switch such that each of the three 6 μsec pulses is routed to the right elevation lens during the 20 μsec transmit pulsewidth. "One-to-two" switches further select the signal path such that the transmitter output can be switched to one of six possible elevation beam positions.

Between transmit pulses, the TRSSM is in the receive state with several channels geared to the elevation beam positions, operating continuously. The two-way switches at the antenna ports of the module are used to select one of two possible elevation beams at each of three positions.

The three outputs of these switches each go through a circulator, T/R Limiter, low noise amplifier and filter before reaching the final switching matrix. The circulators are used to diplex the transmit and receive signals at a given elevation beam port. The T/R Limiter serves a dual function, first to place a

2-62

good termination on the circulator during the transmit period and second to protect the Low Noise Amplifier (LNA) from transmitter leakage and high level signals from other radars or close-in targets. The LNA consists of solid state amplifier stages designed for minimum possible noise figure. These stages have sufficient gain to establish the noise figure of the system along with losses in their input paths. The receive noise figure looking into the LNA is estimated to be 1.4 dB.

Bandpass filters are used to separate the module bandpass into three contiguous frequency ranges such that each amplifier output corresponds to a particular elevation beam and frequency range. This is done so that the noise contributions of each beam position do not add up in the manifold port multiplexers in such a way as to diminish the signal-to-noise ratio of the system. The bandwidth of each bandpass filter is matched to the signal instantaneous bandwidth thereby avoiding a mismatch loss.

The baseline system includes provisions for sidelobe suppression through amplitude taper. The figure shows attenuators and control elements to perform this function. There is no taper attempted in transmit for the baseline as the complexity involved in making a linear Class C amplifier is not warranted. The receive taper is recommended in any ECCM configuration. There is an inherent amplitude taper in the R-lens of down to -5.0 dB, but for the same reasons, it is difficult to try to take advantage of this in the transmitter amplifiers.

This natural amplitude taper can be utilized in receive, however, along with the taper added by the controllable attenuators. The attenuators which are after the bandpass filters are used to introduce amplitude taper as a function of module position in the array quadrant. As the azimuth beam is stepped through its beam positions, logic in the module keeps track of when it was activated (by command from the azimuth steering subsystem) and how many modules have been activated since it was turned on. From this information, the logic generates a word which sets the attenuator for a particular value of attenuation.

A set of two-way switches and reactive combiners next multiplex the outputs of the receive channels such that each of the three R-lenses will see the output of two channels. These combined signals then go through the manifold port elevation beam switches.

All of the beam switching as well as the BITE logic and taper attenuator control will use CMOS integrated circuits except for the logic functions where speed is important such as T/R switching which will use a TTL line receiver. The use of low power logic elements in combination with the switching off of LNAs when not in use and the use of active bias in the LNAs themselves all conserve prime power.

The TRSSM will be built using well-proven hybrid electronic techniques. MIC boards will be mass produced using photolighographic techniques to assure unit-to-unit repeatability. The total baseline module package can be built within outline dimensions of 12" L x 8" W x 2-1/2" high, including connectors and heat sink fins.

The electrical specifications for the TRSSM are given in Table 2.3.2-1.

Table 2.3.2-1

Baseline TRSSM Specifications

Peak Power Output	40W pk
Transmit Gain	26 dB
Input Power Varition for Rated P_{out}	$\pm {}^{0}_{5}$ dB
Instantaneous Bandwidth	200 MHz
Receiver Noise Figure (looking into LNA)	1.4 dB
Receiver Gain	12 dB
Receiver Channel Width at -3 dB	66.6 MHz
at -60 dB	120 MHz
Taper Attenuator Bits	8
Taper Attenuator Range	9-18 dB
T/R Switching Speed	0.5 μ sec
Elevation Beam Switching Speed	0.5 μ sec
T/R Limiter Protect Level	20W pk
LNA 1.0 dB Compression Point	+13 dBm

b) Alternative Designs

Several variations on the baseline module have been considered at both L-band and UHF. A list of these alternatives is given in Table 2.2.4-1 with their key requirements.

The 6-channel L-band module assembly is shown in Figure 2.3.2.4. This module is virtually identical to the 3-channel version except for its elevation beam manifold port switch. Each of the 6 elevation beam manifold ports has a circulator for isolating transmit and receive signals, the transmit signals all going to a 6:1 switch which selects the correct path to be amplified by the transmitter. The outputs of the three receive amplifier/attenuator chains are split 1:2 such that six possible receiver paths exist at the manifold ports of the module. This allows the processing of the various frequency/elevation beam signals in another section of the radar.

This module is somewhat more expensive than the 3-channel in that more circulators are used and the manifold port switching is more complex. In addition, the size of the assembly would have to be increased by a small amount to accept the six extra circulators.

At UHF, several conceptual differences exist with the L-band modules. A two-channel UHF design is shown in Figure 2.3.2-5 and a one-channel design in Figure 2.3.2-6. Because of the less extensive elevation beam switching, less receiver channels are required at UHF than L-band.

Basically, the UHF transmitter uses the same concept as the L-band unit. After an input switch and circulator, two gain stages coupled through an isolator provide drive to the driver stage and a parallel output stage. Again, the two-input stages provide sufficient gain to drive the chain into saturation even though the input level can drop as much as 5.0 dB as a function of module position around the circular array. The other major difference is in the power level of the transmitter which at 150 watts peak output for the baseline UHF (TRSSM's located at the antennas) is higher than the level at L-band. Location of the TRSSM behind the azimuth steering quadrant switches raises the power requirement to 200 watts (additional 1.5 dB 2-way loss). This is still well within conservative design margins at UHF (two 125 watt output transistors).

- 6 microsecond pulse
- Output transistors 50 watts each (TRSSM behind Q switch)
- Output transistors 25 watts each (TRSSM at antenna)
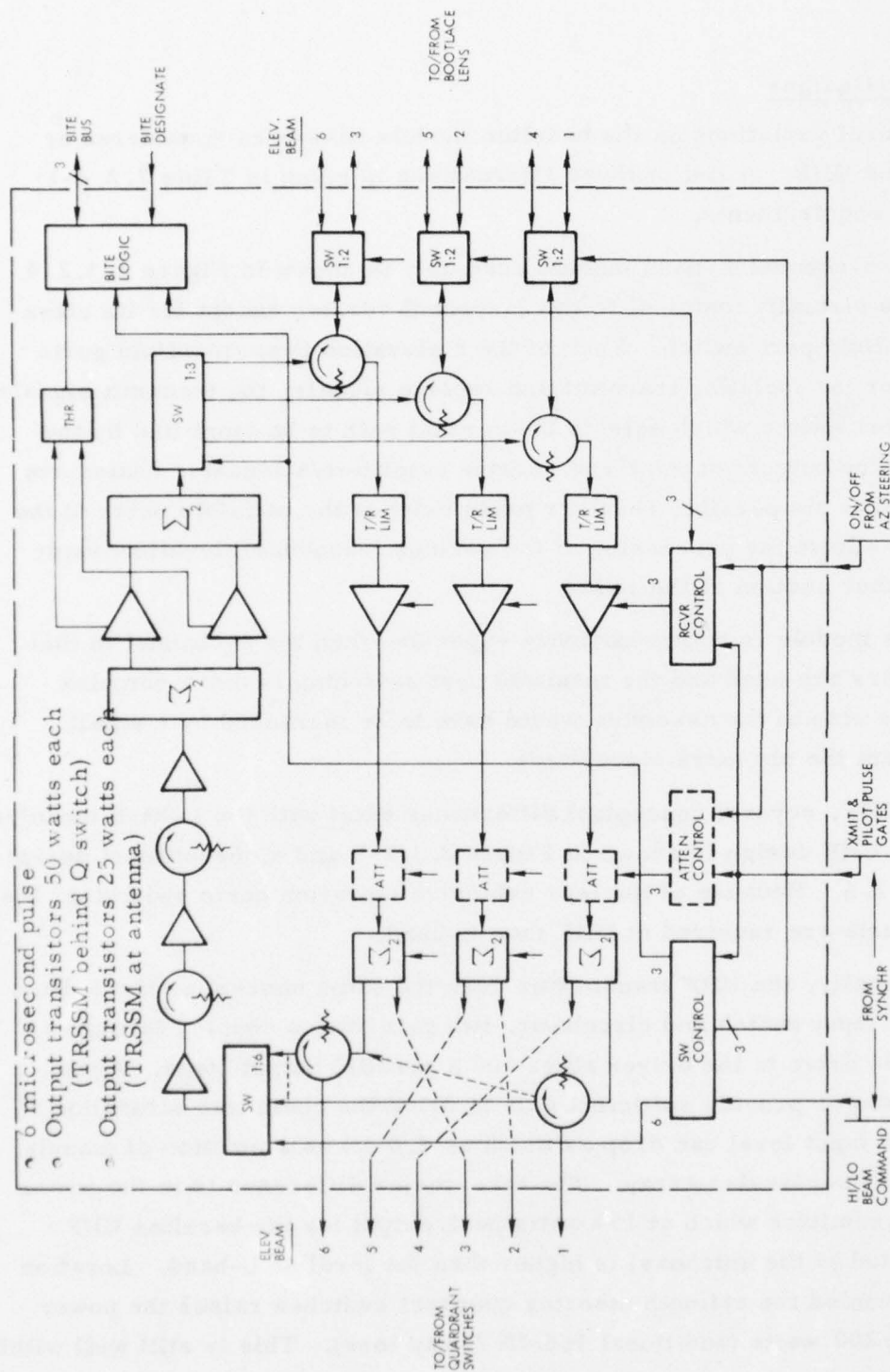
Figure 2.3.2-4 T/R Module (L-Band, 6 Channel)
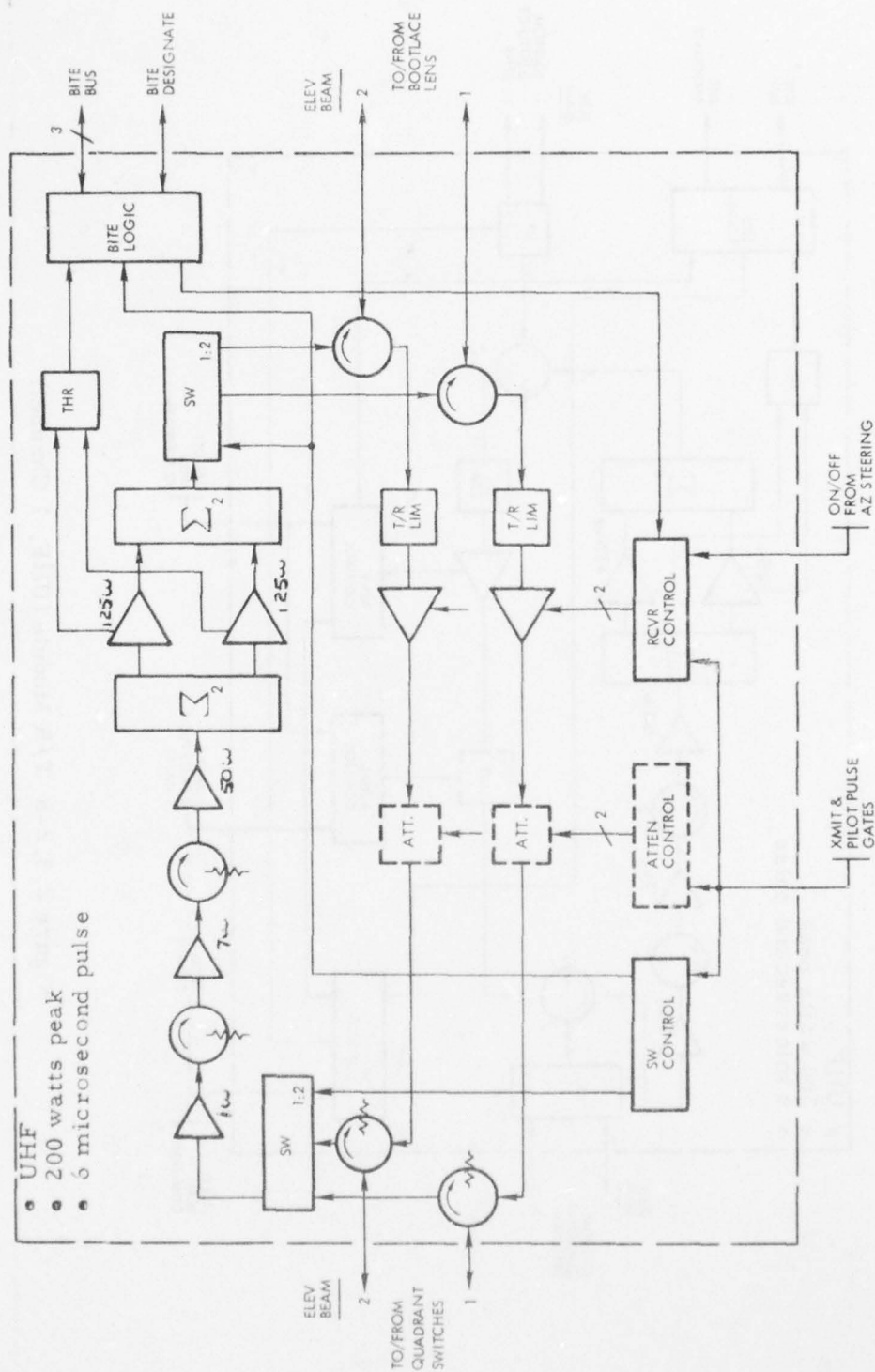
Figure 2.3.2-5. T/R Module (UHF, 2 Channel)

2-67

Figure 2.3.2-6 T/R Module (UHF, 1 Channel)

Again, a circulator is used at the antenna port end of the module to diplex and isolate the receive and transmit signals. An elevation beam switch is then used to switch to the appropriate input port on the bootlace lens to give two elevation beams for the two channel version. The only difference in the single channel version would be the deletion of the elevation beam switches from the manifold and antenna port ends of the module respectively.

In receive, the signal comes through the elevation beam switch at the antenna port through a circulator to a T/R limiter which provides a termination to the circulator during transmit and protection to the LNA for overloads at all times. The LNA then raises the signal level establishing the noise figure of the system at that point. The noise figure of the LNA stage will be about 1.4 dB which is well within the state-of-the-art for presently available devices. A digital attenuator and control circuit is used to achieve amplitude taper on receiver as a function of module position.

As with the possible L-band modules, the components used at UHF will be derated sufficiently from the state-of-the-art that the module represents a low risk production item. Construction will again be using hybrid electronic techniques particularly suited to the building of large quantities of low cost modular assemblies. Final size of a typical UHF module of either type would be about 8" W x 28" L x 4" High including connectors and heat sink elements. A typical UHF TRSSM is shown in Figure 2.3.2-7.

Collector efficiency and gain are slightly better on a per stage basis at UHF than L-band. In production quantities, there is little difference in performance of the receiver front ends for L and UHF frequency bands. Noise figure of LNA transistors is several tenths of a dB lower at UHF, but this is largely lost in input circuit losses such as circulators and the T/R Limiter. In large quantities, there will be no large cost differences between UHF and L-band on the receiver side of the module. The major cost differences will occur in the configuration of the Receiver (three versus six channel version).

Major variables which drive the TRSSM design, in addition to frequency choice, are:

TOP COVER

PRINTED CIRCUIT
BOARD

INSERTS

4"

28"

8"

CONNECTORS
QTY 256 PER SYSTEM
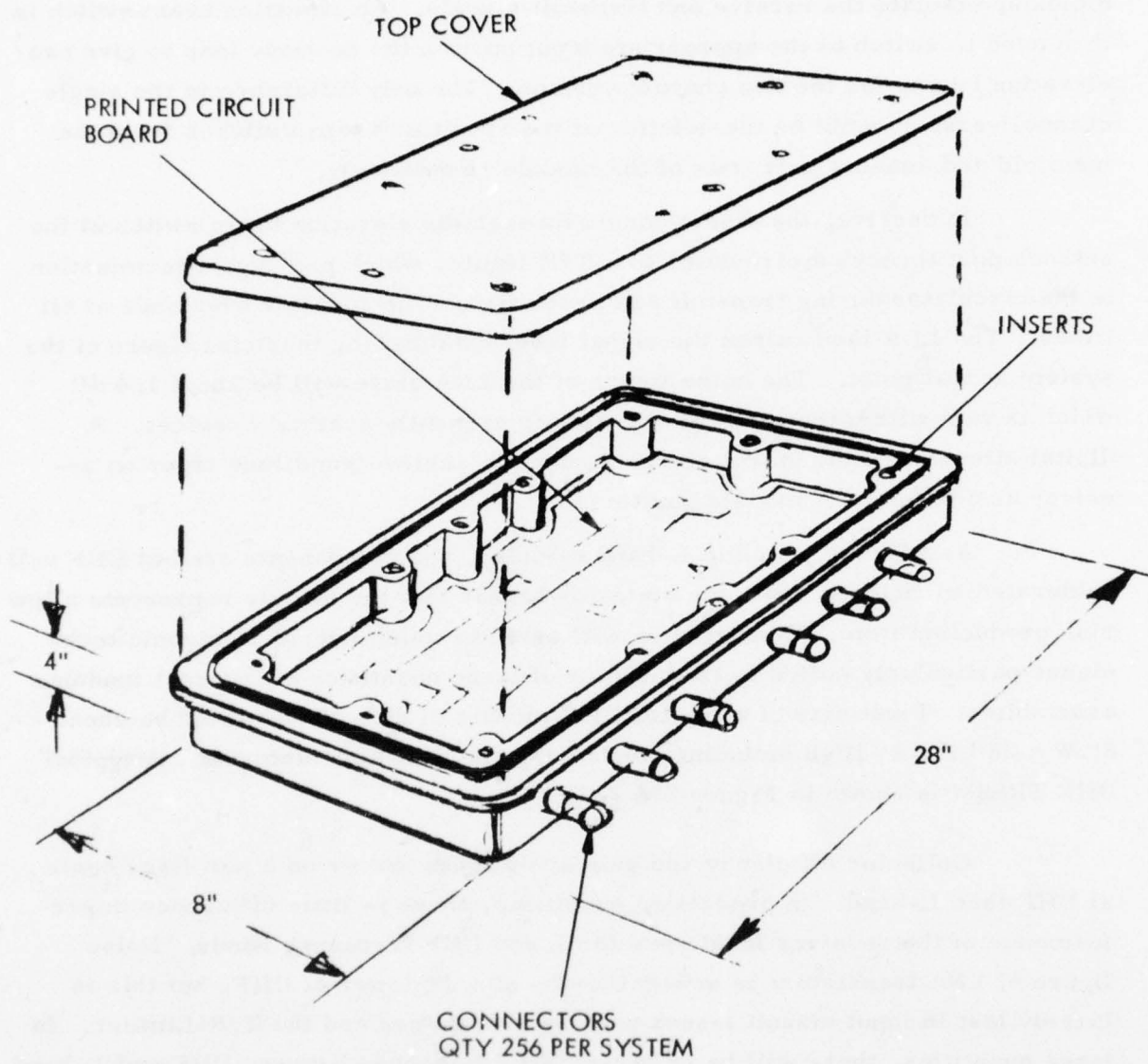
Figure 2. 3. 2-7.   T/R Module Type A

- TRSSM location:
  - At antenna stack
  - Behind quadrant switch
- Transmitted pulsewidth:
  - 6 μsec pulse
  - 1.5 μsec pulse

These alternatives have been discussed in Section 2.2.4. Both of these variables drive the peak power requirements of the TRSSM and thus have a very substantial impact on its design, cost, power consumption and failure rate. For example, the baseline configuration requires only 40 watts peak at L-Band which is easily satisfied by a 1:1:1:2 transistor configuration as shown in Figure 2.3.2-3 with a minimum number of components. An L-Band configuration with a 1.5 μsecond pulsewidth and located behind the quadrant switch (No. 39 Table 2.2.2-2) must deliver 320 watts for the same system performance. This necessitates a 1:1:1:4 transistor configuration with a resulting increase in failure rates and cost. This latter configuration is shown as Figure 2.3.2-8.

A comparison between several typical configurations is made in Table 2.3.2-2. Each TRSSM configuration is identified by its important parameters as well as the number assigned to the appropriate system configuration during the study. The variables shown include module failure rates, production cost per radar and the number of production cost per expected module failures per radar in a 20 year Operations and Support Phase. These values are used to estimate the repair cost and spares consumption cost per radar for 20 years. The reader is referred to Section 2.8, Cost Sensitive Analysis, for the assumptions and equations used in making these calculations.

The impact of the system complexity (number of TRSSM's and receiver channels) and the TRSSM complexity itself (measured in peak power effect on design) can be readily seen in the cost values shown in Table 2.3.2-2. The repair costs vary from 301K per radar down to 10K and the spares consumption shows the same variation. Neglected in this comparison is the effect on requirement for maintenance visits which tends to be reflected by the number of module failures.
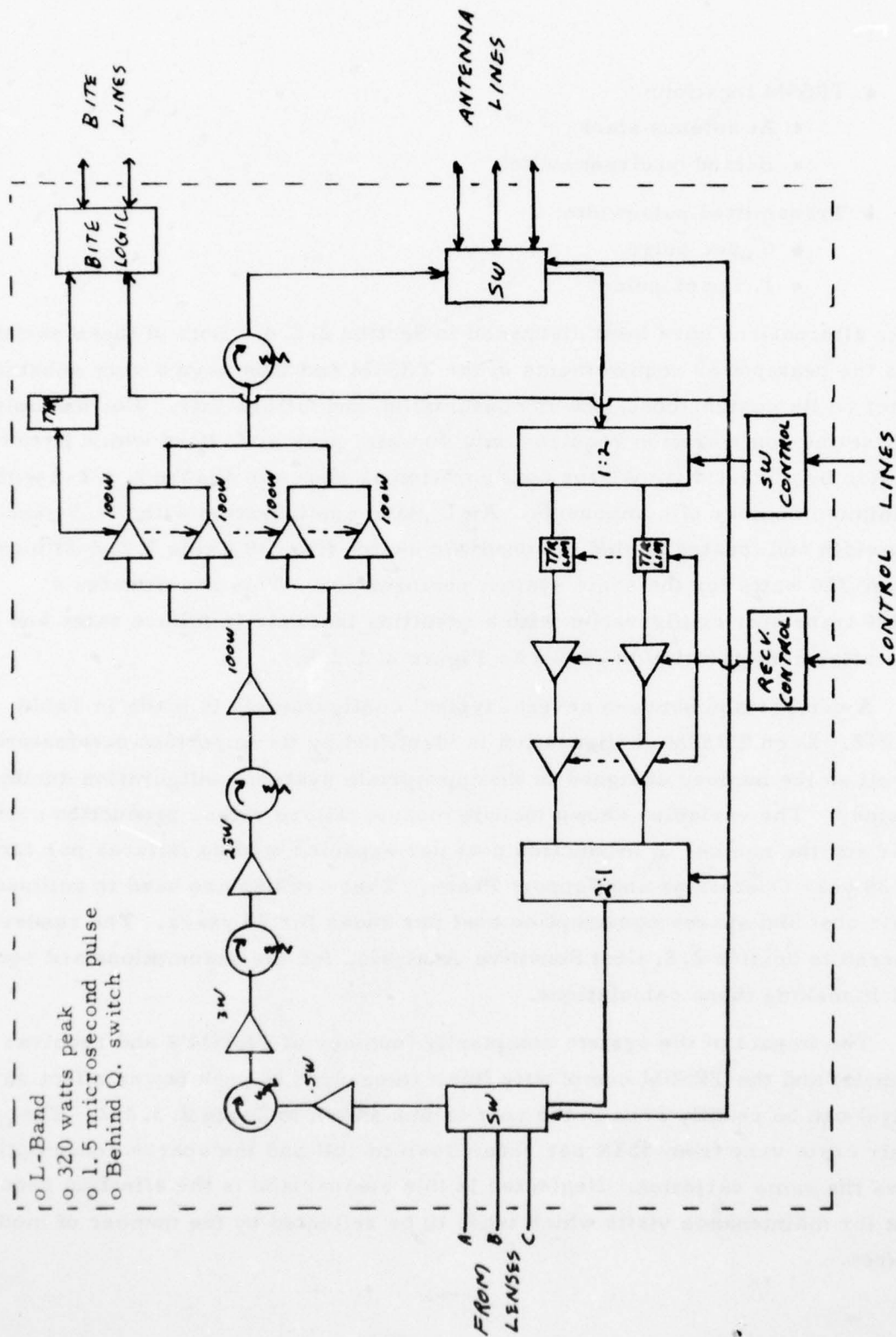
Configuration No. 39 TRSSM

Figure 2.3.2-8

o L-Band
o 320 watts peak
o 1.5 microsecond pulse
o Behind Q. switch

Table 2.3.2-2

	Configuration Definition								TRSSM Trade Variables			
Conf	Freq	Scan Type	TRSSM Location	Peak Power (w)	PW (μsec)	No Rcvr Chan	Failure Rate* (10⁶ Hrs Per Mod)	No TRSSM	No. Mod Failures Per Radar (20 Yrs.)	Product Cost Per Radar ($K PCL)	Repair Cost Per Radar (20 Yrs.) ($K PCL)	Spares Consumption Cost (20 Yrs.) ($K PCL)
1	L	Split	Ant.	40	6	3	11.3	260	514			
36	L	Fence	Q. SW	80	6	1	9.6	65	109			
39	L	Fence	Q. SW	320	1.5	2	12.0	66	139			
41	UHF	Split	Ant.	150	6	1	8.6	128	194			
49	UHF	Single	Q. SW	200	6	2	9.2	35	56			
62	UHF	Split	Q. SW	200	6	1	6.3	34	37			

*As stated in Section 2.6.1 the failure rates are double the actual 217B predictions.

2.3.3 AZIMUTH STEERING

a) General Theory

The azimuth plane pattern for each elevation beam formed by the verti-
cal element stack is quite broad (i.e., essentially that of the dipole radiator) and
requires the excitation of many adjacent stacks to produce a desired narrow
azimuth beam. The baseline antenna system achieves its azimuth plane beam-
width by properly phasing the signal energy from an array of vertical stacks
within a sector of $\pm 45^{\circ}$ about the desired azimuthal pointing direction. This
phasing is accomplished through the use of a modified circular R-2R parallel plate
lenses[3,4], one for each of the three elevation beams. The lenses are modified
in the sense of being cophased for focusing at specified elevation plane angles
for each elevation beam. The modification is merely a slight adjustment of the
R-lens diameter.

Figure 2.3.3-1 shows the classical R-2R lens geometry that assures
a plane wave is generated by feeding the R-lens at an excitation point diametri-
cally opposite to the desired pointing direction of the 2R-array. Note that using
the R-lens ports along $\pm 90^{\circ}$ of arc opposite the excitation point causes a $\pm 45^{\circ}$
arc along the array circumference to be driven. This means that for the L-band
system, since the baseline array has 64 elements on a 90° arc, the R-lens will
have 64 elements on a 180° arc and 128 elements on its circumference. Similar
considerations apply to UHF.

The R-lens design is also proposed as using material with a dielectric
constant $K = 38$. Figure 2.3.3-2 shows a 100-port lens of a similar design by
Raytheon. At L-Band the diameters of the R-lenses involved are approximately
50'' depending upon a precise determination of the elevation plane cophasing
requirements. The 128 output ports are spaced 0.38'' apart around the lens
circumference. At UHF, however, the number of array elements is 128 and

[3] Rotman, W. and Turner, R.F., "Wide-Angle Microwave Lens for Line Source
Application," IRE Trans. On Antennas and Propagation, November 1963, pp.
623-632.

[4] Boyns, J.E., et al., "A Lens Feed for a Ring Array," IRE Trans. on Antenna
and Propagation, March 1968, pp. 264-267.
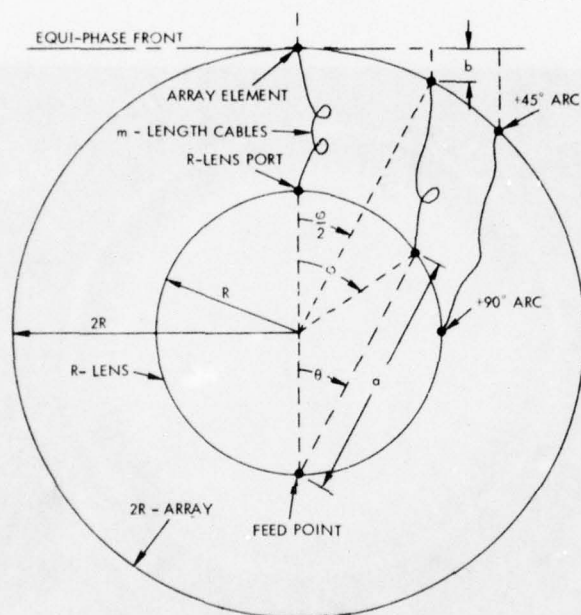
Figure 2.3.3-1. Classical R-2R Lens Geometry
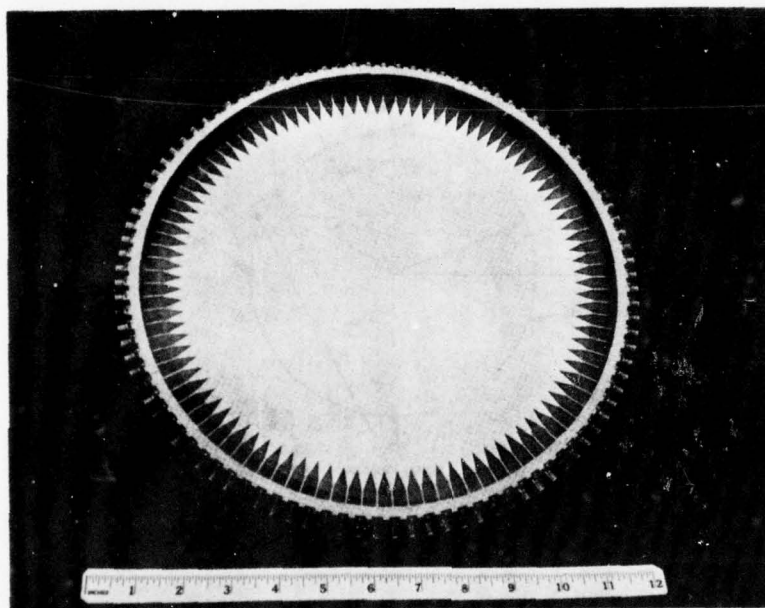
Figure 2.3.3-2. 100 - Port R-KR Lens

only one or two simultaneous elevation plane beams are configured. The number of R-lens ports is 64.

The baseline antenna system does not use the amplitude tapering property inherent in the R-lens for azimuth plane sidelobe control in transmit, since the TR-modules operate in a Class C equal output power mode. The lens amplitude tapering is used in receive along with additional taper as described in Section 2.7.3.

A single thread path diagram for the baseline configuration is shown in Figure 2.3.3-3. This figure illustrates the azimuth signal distribution in a functional way. The distribution of the exciter and receiver signals is indicated. As explained in Section 2.3.4, these functions are performed by additional TRSSM modules for the sake of commonality. A Bootlace lens is shown as the antenna elevation feed network; as discussed in Section 2.3.1, other types of feeds have been considered.

In the azimuth steering subsystem, a set of quadrant switches connecting each R-lens port to four vertical stacks around the array and a set of transfer switches interconnecting diametrically opposed R-lens ports serve to index sequentially the R-lens feed point twice around its circumference while the driven ports on the 2R-array are indexed for one pass around its circumference. Beam pointing directions throughout 360° in azimuth are thus provided.

The function of the Beam Steering Switch Assembly is to connect the Exciter and the T-R modules to the correct ports of the R-lens and to properly terminate the non-used ports on the lens. Figure 2.3.3-4 shows a schematic of the complete assembly. In order to minimize connectors on the R-lens, every other beam position is obtained by exciting two adjacent ports on the Lens thus creating a virtual port in between the two exciter ports. This approach requires the switch to connect the exciter to two ports on the lens every other beam (i.e., excite J1; excite J1 and J2; excite J2, etc.). For this reason the switch assembly feeding the lens is split with one part feeding the ODD numbered ports and a second part feeding the EVEN numbered ports. The ODD/EVEN switch controls this alternate one-two port excitation process.

2-77

VERTICAL STACK
256

NOTCH RADIATOR
20 × 256 = 5120

TRANSMISSION LINE
20 × 256 = 5120

BOOTLACE LENS
256

TR-MODULE
256

TRANSMISSION LINE
256 × 3 = 768

QUADRANT SWITCH
64 × 3 = 192

TRANSFER SWITCH
64 × 3 = 192

R-LENS
1 × 3 = 3

TERMINATING PORT SWITCH
64 × 3 = 192

FEEDING PORT SWITCH
2 × 3 = 6

ODD   EVEN

BEAM EXCITER SWITCH
1 × 3 = 3

ASSORTED INTERCONNECTIONS

DUPLEXER
1 × 3 = 3

TRANSMIT BEAM SWITCH
1

RECEIVER
3

EXCITER
1

Figure 2.3.3-3.   Single Thread Path Diagram

2-78
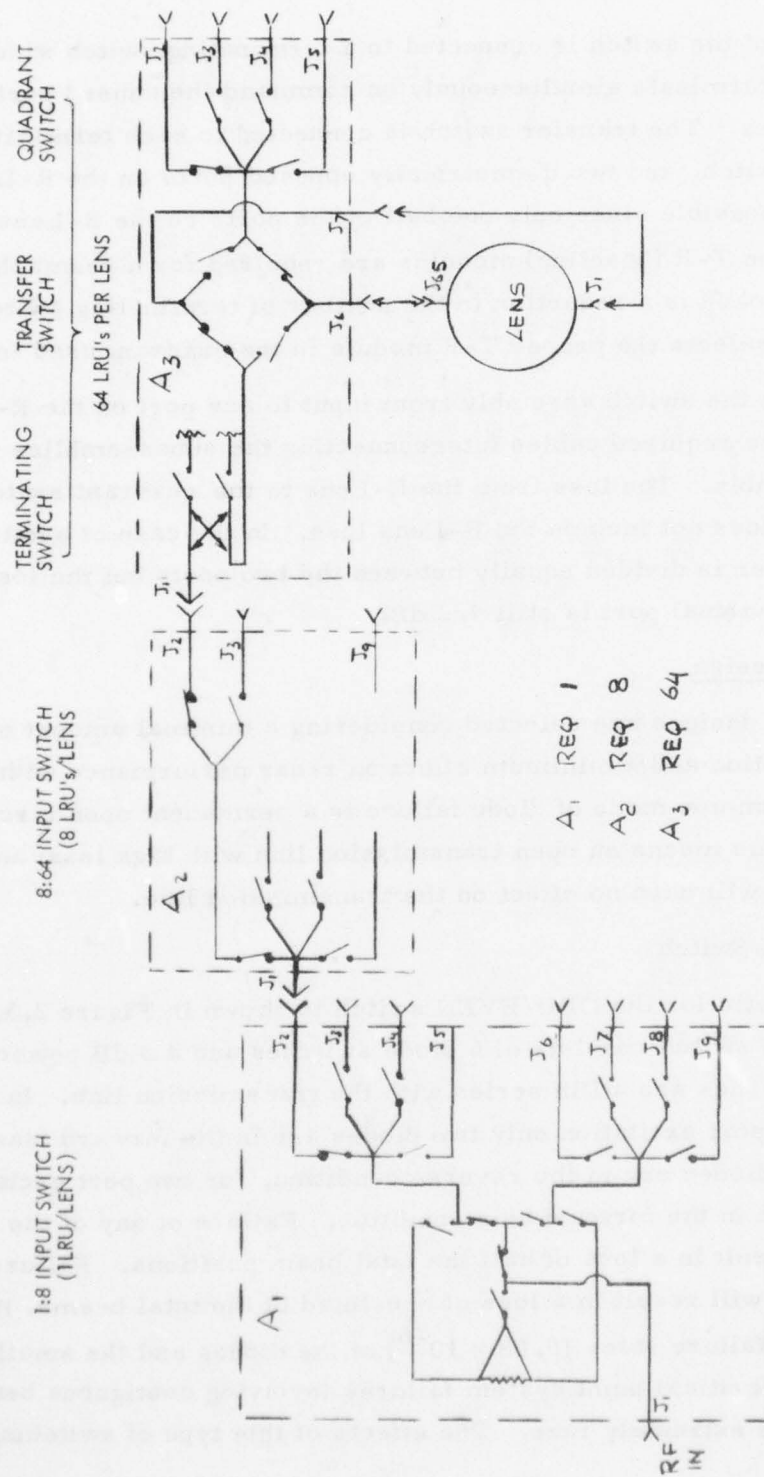
Figure 2.3.3-4. Azimuth Steering Subsystem

Each port of the switch is connected to a terminating switch which makes it possible to terminate simultaneously on command the unused ports of the switch and the lens. The transfer switch is connected to each terminating switch, a quadrant switch, and two diametrically opposed ports on the R-Lens. This combination is possible since only one half of the ports on the R-Lens and only one quarter of the T-R (baseline) modules are required for a beam; the advantage of the approach is a reduction in the number of terminating switches. The quadrant switch selects the proper T-R module in the quadrant used in the array.

The loss in the switch assembly from input to any port on the R-Lens is 4.2 dB including the required cables interconnecting the subassemblies in the Beam Steering Assembly. The loss from the R-Lens to the quadrant switch outputs is 1.2 dB, this does not include the R-Lens loss. In the case of excitation of two ports, the power is divided equally between the two ports but the loss from the input to the virtual port is still 4.2 dB.

b) Baseline Design

The switch designs are selected considering a minimal amount of control power dissipation and a minimum effect on radar performance with diode failure. The most common mode of diode failure is a permanent open circuit. With a series diode this means an open transmission line with high loss; an open circuit parallel diode will have no effect on the transmission line.

ODD/EVEN Switch

The schematic for the ODD/EVEN switch is shown in Figure 2.3.3-5. The ODD/EVEN switch consists of 6 diode switches and a 3 dB power divider. The diodes are all in series with the transmission line. In this case for single port excitation only two diodes are in the forward bias condition and four diodes are in the reverse condition, for two port excitation three diodes are in the forward bias condition. Failure of any of the diodes a_1 or a_2 will result in a loss of half the total beam positions. Failure of diodes a_3 or a_4 will result in a loss of one-third of the total beams. Because of the very low failure rates (0.08×10^{-6}) of the diodes and the small number involved at this critical point system failures involving contiguous beam positions will be extremely rare. The effects of this type of switching have

2-80
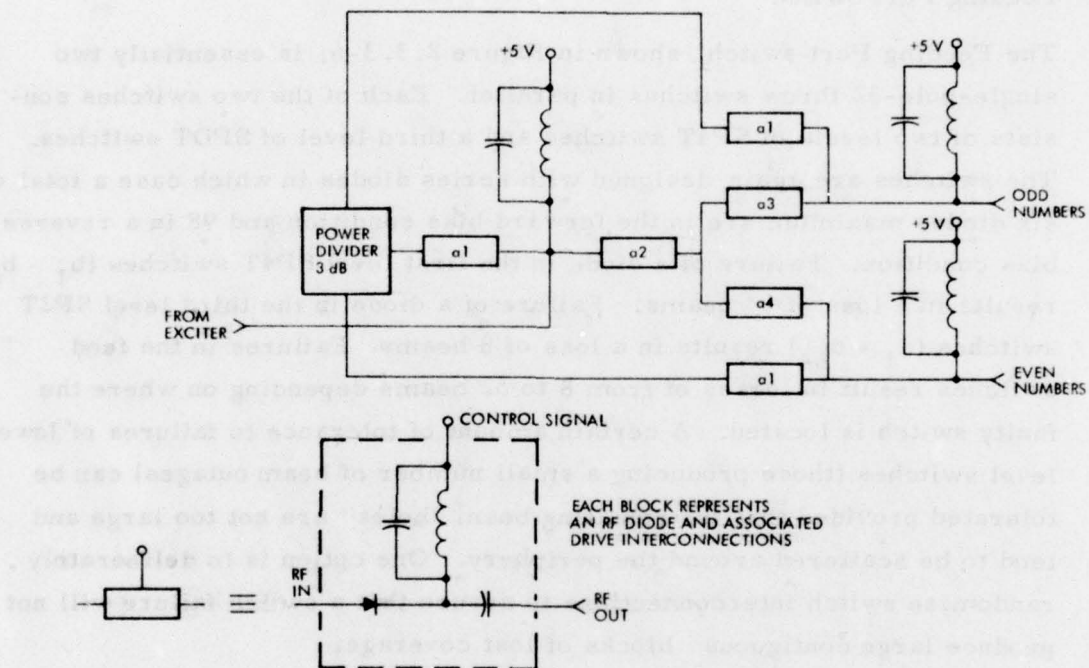
Figure 2.3.3-5. Schematic For Odd/Even Switch

been carefully modeled and the results are presented in the section on reliability (Section 2.6). Because of the unacceptable degradation which would result from a failure in this switch, no system failure tolerance has been assumed for this type of fault.

Feeding Port Switch

The Feeding Port switch, shown in Figure 2.3.3-6, is essentially two single-pole-32 throw switches in parallel. Each of the two switches consists of two levels of SP4T switches and a third level of SPDT switches. The switches are again designed with series diodes in which case a total of six diodes maximum are in the forward bias condition and 98 in a reverse bias condition. Failure of a diode in the first level SP4T switches (b_1 - b_8) results in a loss of 64 beams. Failure of a diode in the third level SP2T switches (d_1 - d_{64}) results in a loss of 8 beams. Failures in the feed switches result in losses of from 8 to 32 beams depending on where the faulty switch is located. A certain amount of tolerance to failures of lower level switches (those producing a small number of beam outages) can be tolerated provided that the resulting beam "holes" are not too large and tend to be scattered around the periphery. One option is to deliberately randomize switch interconnections to assure that a switch failure will not produce large contiguous blocks of lost coverage.

Terminating Switch

The Terminating Switch, shown in Figure 2.3.3-7, consists of a 90°, 3 dB coupler with two parallel diodes for switches. With the diodes in the forward bias condition, the R.F. power will be reflected to the output port and will only be subject to the insertion loss of the coupler. If the diodes are in the reverse bias condition, both ports of the coupler are terminated. With this approach, a maximum of four diodes are in the forward bias condition and 60 in the reverse bias condition for any Beam position. Failure of one diode will make proper termination of two ports on the R-Lens impossible. The actual effect on radar performance is difficult to predict but will not be substantial.

NOTE: SWITCH FOR EVEN NUMBERED PORTS IS SAME
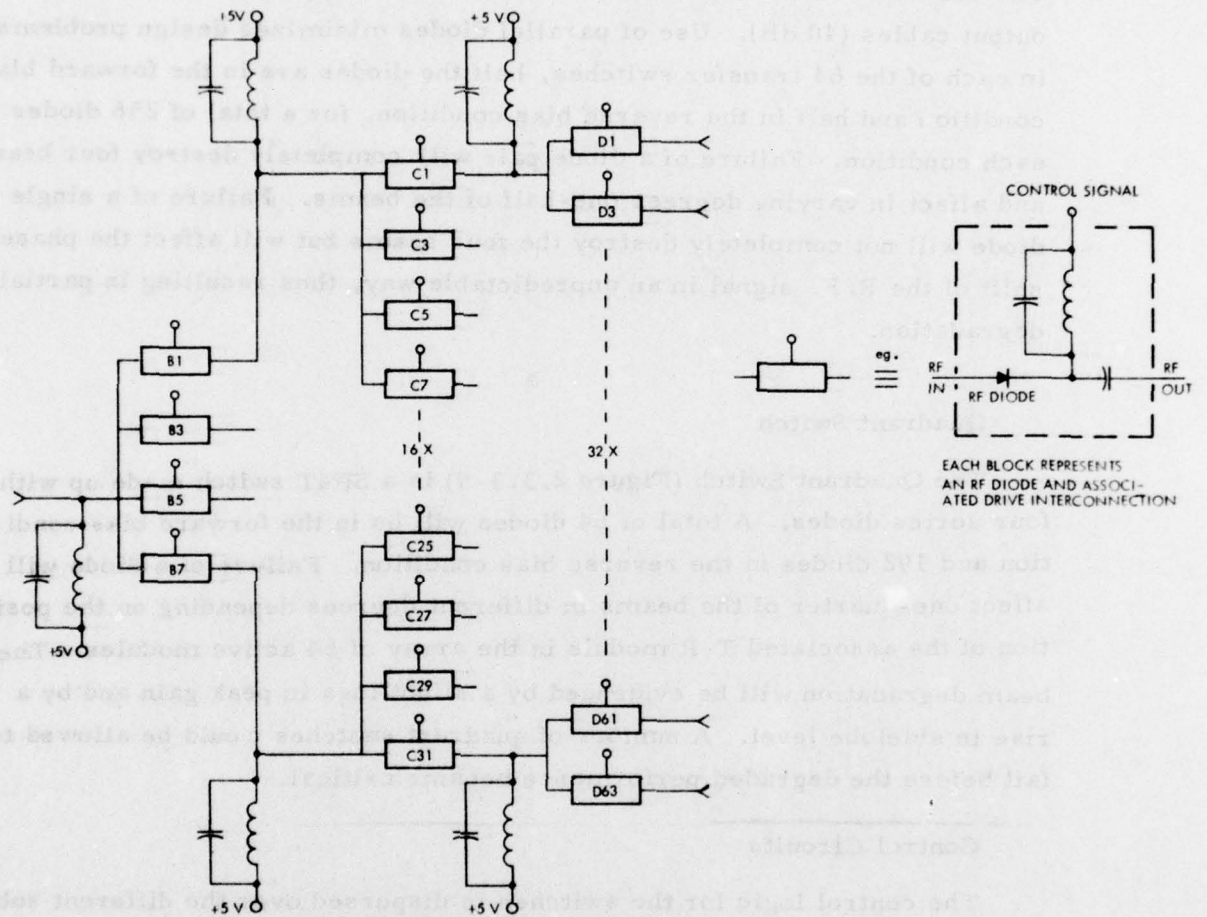
Figure 2.3.3-6 Feeding Port Switch

Transfer Switch

The Transfer Switch (Figure 2.3.3-8) is essentially a bridge consisting of four SPST switches. The switches are formed using two parallel diodes. The use of two diodes quarantees sufficient isolation between the input and output cables (40 dB). Use of parallel diodes minimizes design problems. In each of the 64 transfer switches, half the diodes are in the forward bias condition and half in the reverse bias condition, for a total of 256 diodes in each condition. Failure of a diode pair will completely destroy four beams and affect in varying degrees one-half of the beams. Failure of a single diode will not completely destroy the four beams but will affect the phase shift of the R.F. signal in an unpredictable way, thus resulting in partial degradation.

Quadrant Switch

The Quadrant Switch (Figure 2.3.3-9) is a SP4T switch made up with four series diodes. A total of 64 diodes will be in the forward bias condition and 192 diodes in the reverse bias condition. Failure of a diode will affect one-quarter of the beams in different degrees depending on the position of the associated T-R module in the array of 64 active modules. The beam degradation will be evidenced by a slight loss in peak gain and by a rise in sidelobe level. A number of quadrant switches could be allowed to fail before the degraded performance became critical.

Control Circuits

The control logic for the switches is dispersed over the different sub-assemblies with the advantage of making each assembly simple to test during production and also to keep interconnecting cables to a minimum. All logic will be CMOS with negligible power dissipation (less than 500 mw for all the logic). Because of the slow switching rates of the switches (10 - 30 μsec), a simple low dissipation switch driver is used and the only dissipation will be in the switches in the forward bias condition. The total power dissipation for a single R-Lens assembly will be 21 watts including logic and diode driver dissipation. (There are 205 diodes in the forward bias condition with 100 mw per driver dissipation plus 500 mw for the logic).

It should be noted that with the switching matrix fan-out proposed, there is complete symmetry in the R.F. signal path and the control path. In this case, an R.F. signal path is not influenced by any control signal from a different R.F. path. This concept has also permitted the switching network to be grouped in multiple switch modules where switch and control functions are hardwired over very short distances. This dramatically increases the reliability of the azimuth steering network.

EACH BLOCK REPRESENTS
AN RF DIODE AND ASSOCIATED
DRIVE INTERCONNECTION
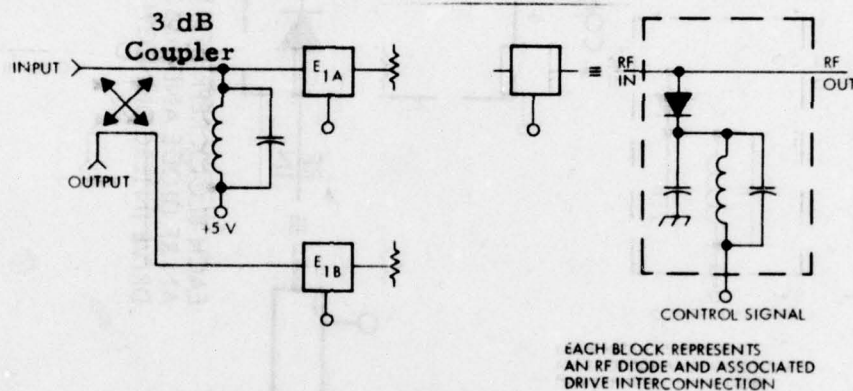
Figure 2.3.3-7. Schematic For Terminating Switch

EACH BLOCK REPRESENTS
A PAIR OF RF DIODES AND
ASSOCIATED DRIVE
INTERCONNECTIONS
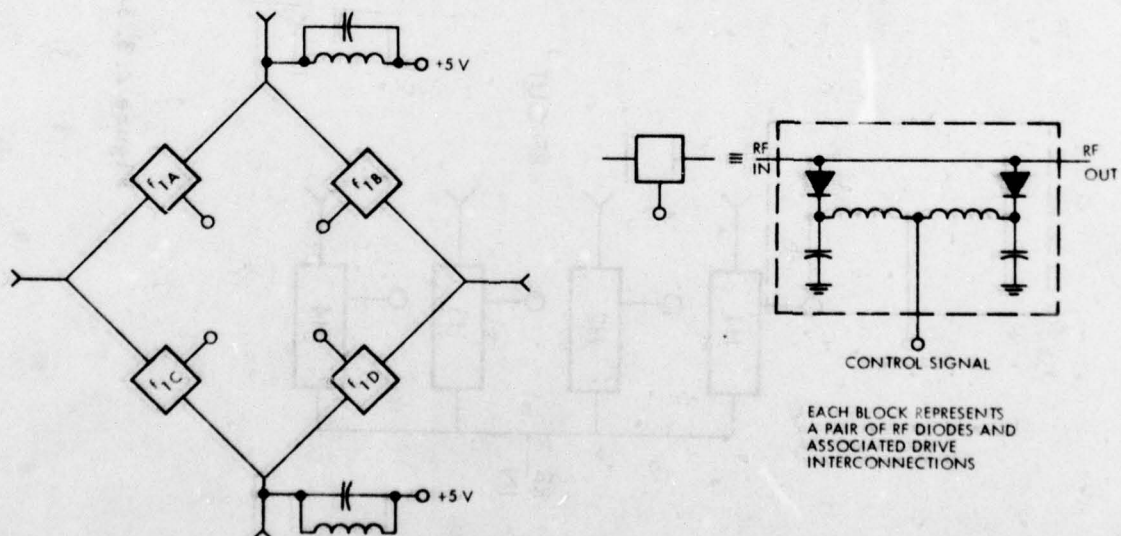
Figure 2.3.3-8. Schematic For Transfer Switch
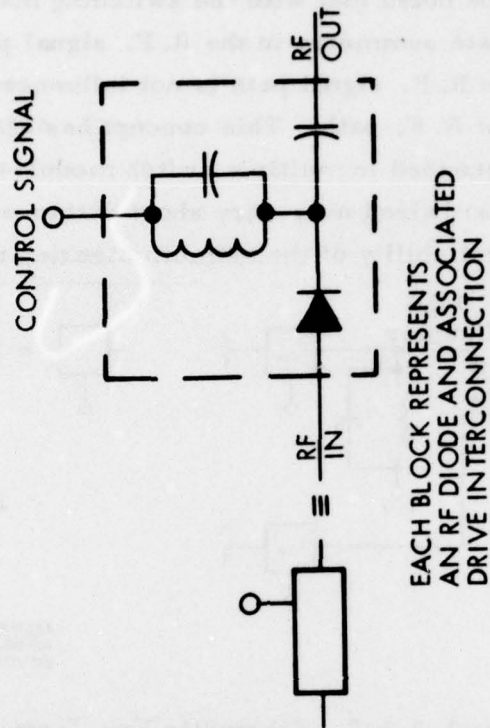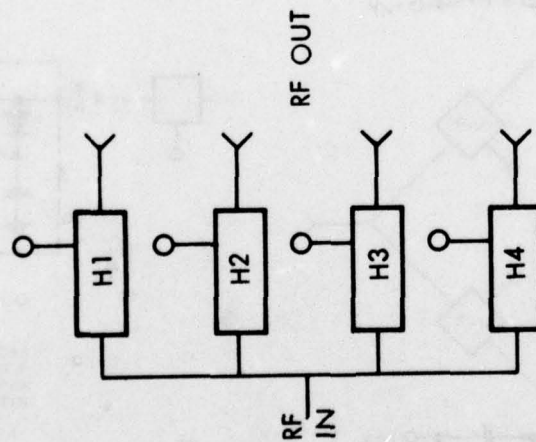
Figure 2.3.3-9.   Schematic For A Quadrant Switch

c) Mechanical Design

Each switch assembly has been broken up into Field Replaceable Units (FRU) considering replacement and fault isolation. No FRU has more than ten connectors and the largest size is 27" x 12" x 2". Table 2.3.3-1 shows the FRU breakdown for the L-band assembly.

Table 2.3.3-1

L-Band Assembly

FRU	Description	Qty. Req'd/R-Lens
A1	Contains ODD/EVEN Switch and first level feeding switches (a and b switches)	1
A2 - A9	Contains second and third level feeding switches (c and d switches)	8
A10 - A63	Contains terminating, transfer and quadrant switches (e, f, and h switches)	64

The construction of a typical module is shown in Figure 2.3.3-10. All R.F. circuits will be made using Teflon-Fiberglass as medium; the diodes are inexpensive glass P.I.N. diodes which will operate in a temperature range from -65°C to +150°C (-85°F to +300°F). The interconnecting cables will be made of 141 semi-rigid cable and SMA connectors (temperature range: -65°C to +200°C).

d) Alternative Designs

The schematic for a UHF lens azimuth distribution system is shown in Figure 2.3.3-11. The number of terminating, transfer and quadrant switches is reduced to 32 due to the fewer number of antenna elements to be fed (128 versus 256 for the Baseline). However, the same number of serial switches is involved between the lens output and the radiating stacks at UHF and L-Band. The number of serial switches in the feeding port switch is reduced by one (32 inputs per lens instead of 64).

The module FRU breakdown assumed for UHF is shown in Table 2.3.3-2. Although the UHF subsystem is simpler, the number of FRU's assumed is about the same per lens structure. This was done to facilitate placing the TRSSM's between the terminating/transfer switches and quadrant switches. Positioning the TRSSMs at this point reduces their number by a factor of four.

STRIPLINE

BIAS & CONTROL CONNECTOR
ON OPPOSITE SIDE

CONTROL & DRIVERS

ODD-EVEN SWITCH ASSEMBLY

2"

12"

27"

3"

J_1 J_2 J_3 J_4 J_5 J_6 J_7 J_8 J_9
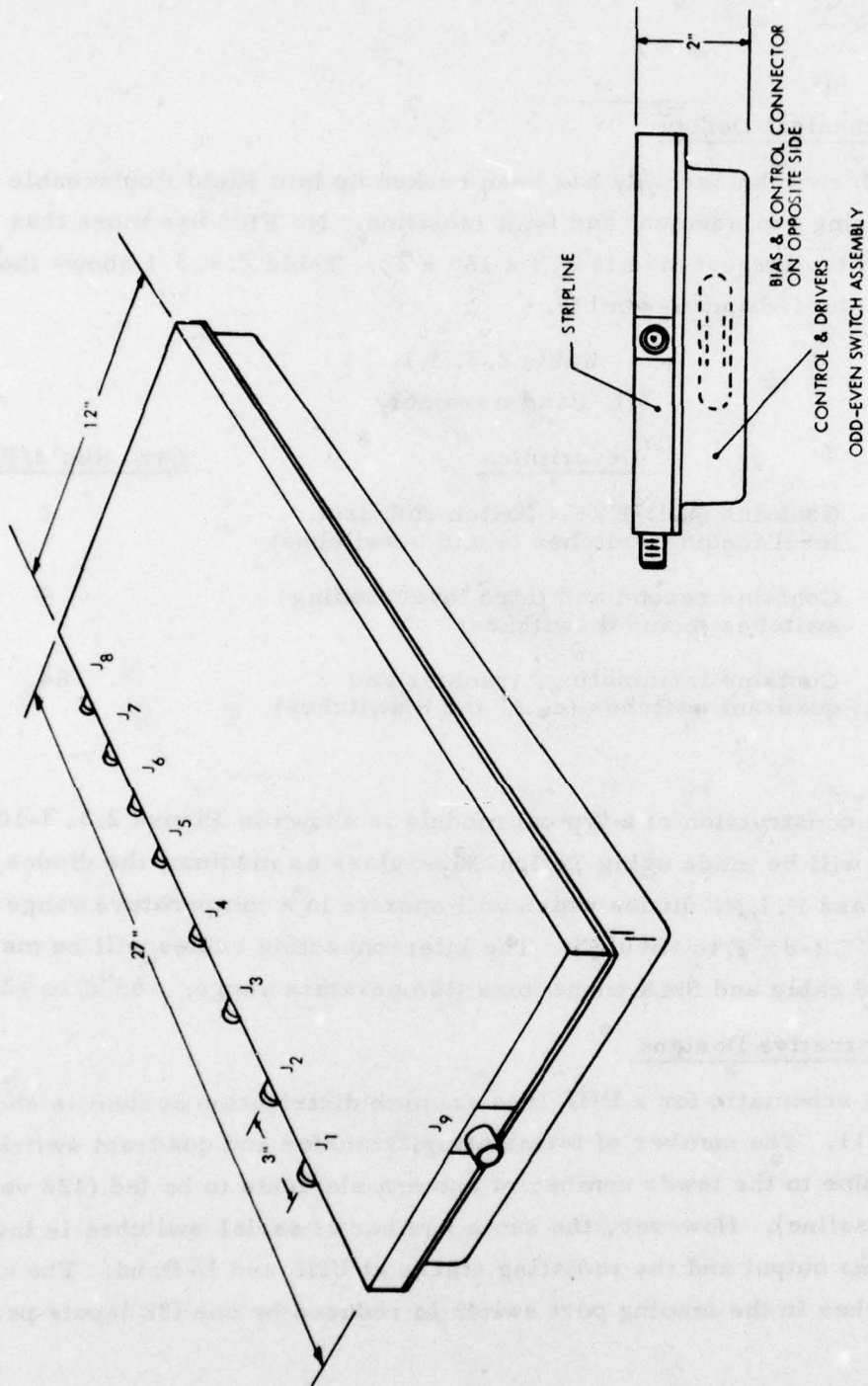
Figure 2.3.3-10. Typical Module Construction
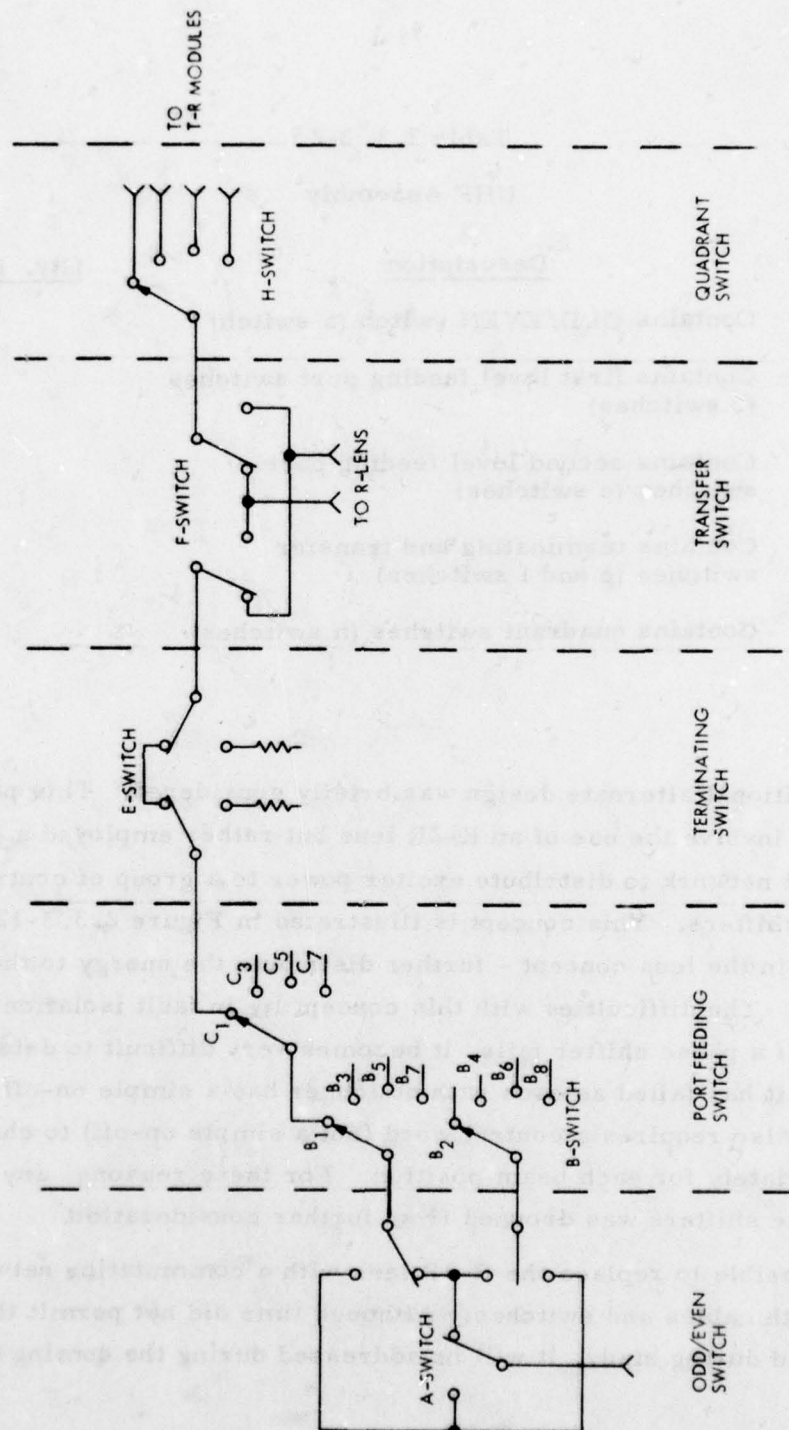
Figure 2.3.3-11. UHF Switch Assembly Schematic

Table 2.3.3-2

UHF Assembly

FRU	Description	Qty. Req'd/Lens
A1	Contains ODD/EVEN switch (a switch)	1
A2 - A3	Contains first level feeding port switches (b switches)	2
A4 - A11	Contains second level feeding port switches (c switches)	8
A12 - A43	Contains terminating and transfer switches (e and f switches)	32
A44 - A75	Contains quadrant switches (h switches)	32

One additional alternate design was briefly considered. This particular design did not involve the use of an R-2R lens but rather employed a passive corporate feed network to distribute exciter power to a group of controllable digital phase shifters. This concept is illustrated in Figure 2.3.3-12. Quadrant switches - as in the lens concept - further distribute the energy to the 256 Baseline TRSSM's. The difficulties with this concept lie in fault isolation and control complexity. If a phase shifter fails, it becomes very difficult to determine remotely that it has failed as each path no longer has a simple on-off state. Each phase shifter also requires a control word (not a simple on-off) to change its phase appropriately for each beam position. For these reasons, any alternative involving phase shifters was dropped from further consideration.

It is possible to replace the R-2R lens with a commutating network of differential length cables and switches. Although time did not permit this approach to be evaluated during study, it will be addressed during the coming year.
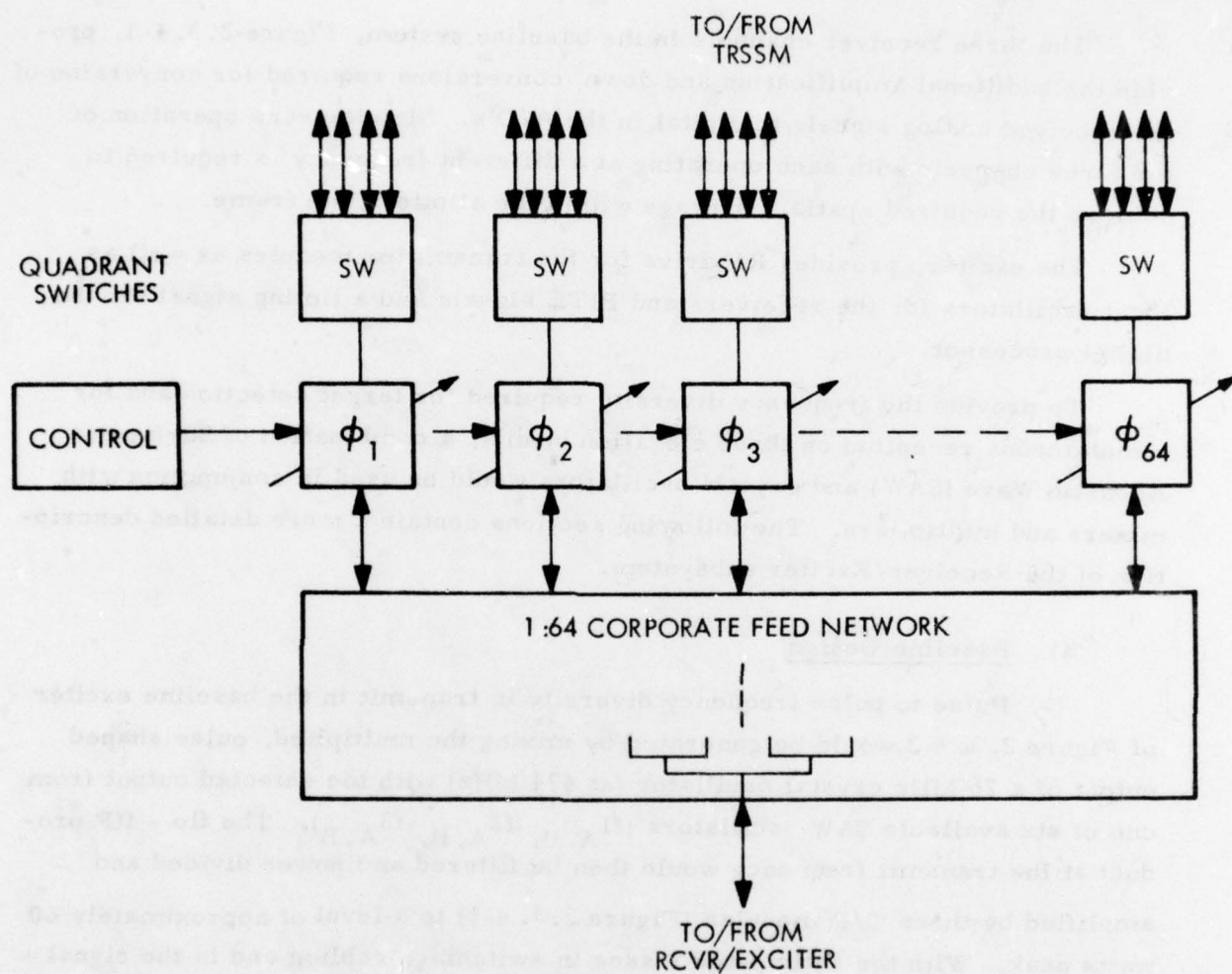
Figure 2. 3. 3-12.   Corporate Feed/Phase Shifter Azimuth Distribution Network

2.3.4 RECEIVER/EXCITER

The three receiver channels in the baseline system, Figure 2.3.4-1, provide the additional amplification and down conversions required for conversion of the received analog signals to digital in the A/D's. Simultaneous operation of the three channels with each operating at a different frequency is required to achieve the required spatial coverage within the allotted time frame.

The exciter, provides RF drive for the transmitter modules as well as local oscillators for the receivers and BITE signals and a timing signal for the digital processor.

To provide the frequency diversity required for target detection and for simultaneous reception on three elevation beams, a combination of Surface Acoustic Wave (SAW) and crystal oscillators would be used in conjunction with mixers and multipliers. The following sections contain a more detailed description of the Receiver/Exciter subsystem.

a) <u>Baseline Design</u>

Pulse to pulse frequency diversity in transmit in the baseline exciter of Figure 2.3.4-2 would be generated by mixing the multiplied, pulse shaped output of a 76 MHz crystal oscillator (at 494 MHz) with the selected output from one of six available SAW oscillators ($f1_{A,B}$, $f2_{A,B}$, $f3_{A,B}$). The $flo - fIF$ product at the transmit frequency would then be filtered and power divided and amplified by three T/R modules (Figure 2.3.4-1) to a level of approximately 60 watts peak. With the anticipated losses in switching, cabling and in the signal distribution of the azimuth lens system, this level would insure adequate RF drive for the 64 activated T/R modules in the array.

The six SAW oscillators operating at a frequency of approximately 580 MHz would also function as the first local oscillators (≈ 1745 MHz) in the receive down conversion process. The oscillators would be arranged in a group of three (f1, f2, and f3) to provide sequential transmission through three elevation beams at different frequencies and the simultaneous reception of all three through the receivers that are individually tuned to receive one of these three frequency bands.
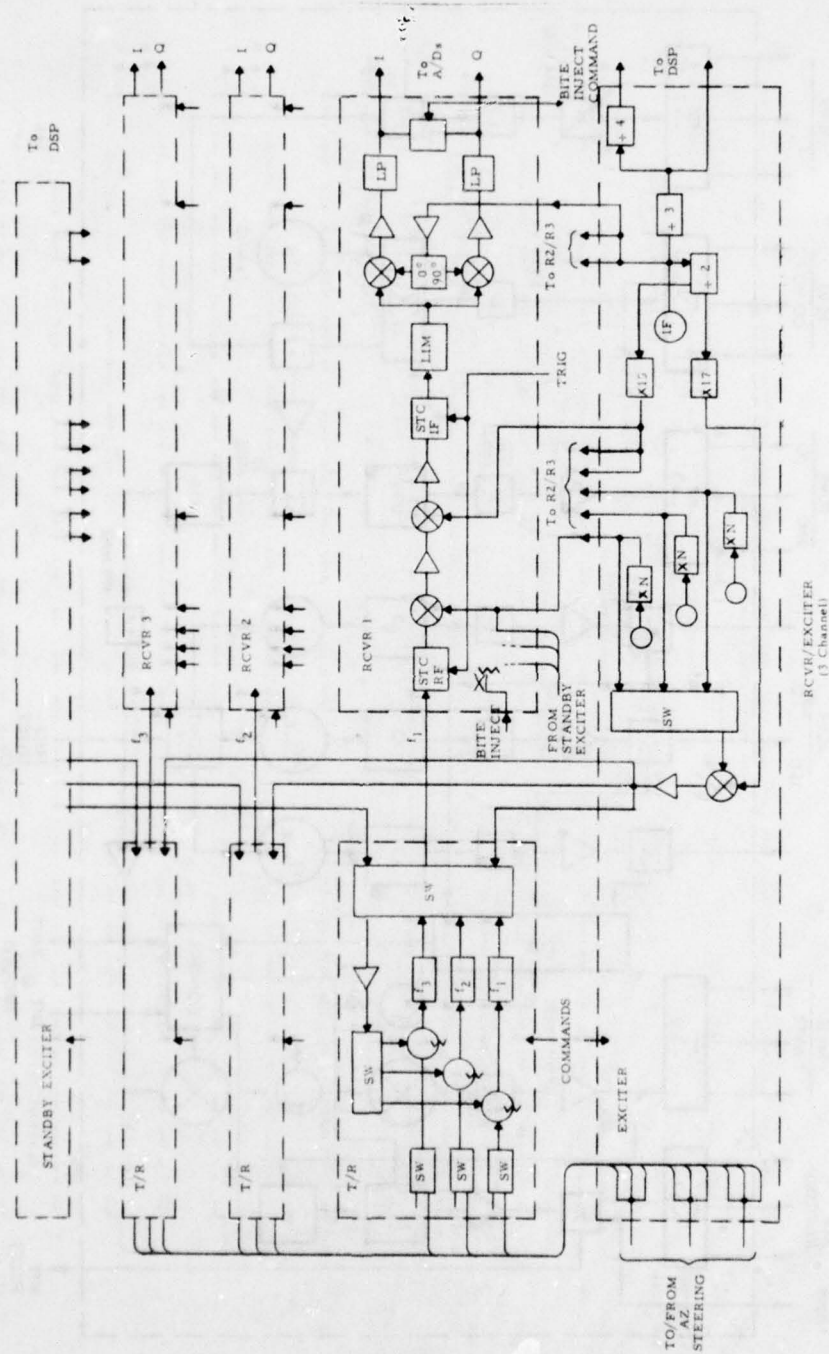
Figure 2.3.4-1. RCVR/Exciter (3 Channel)

2-93
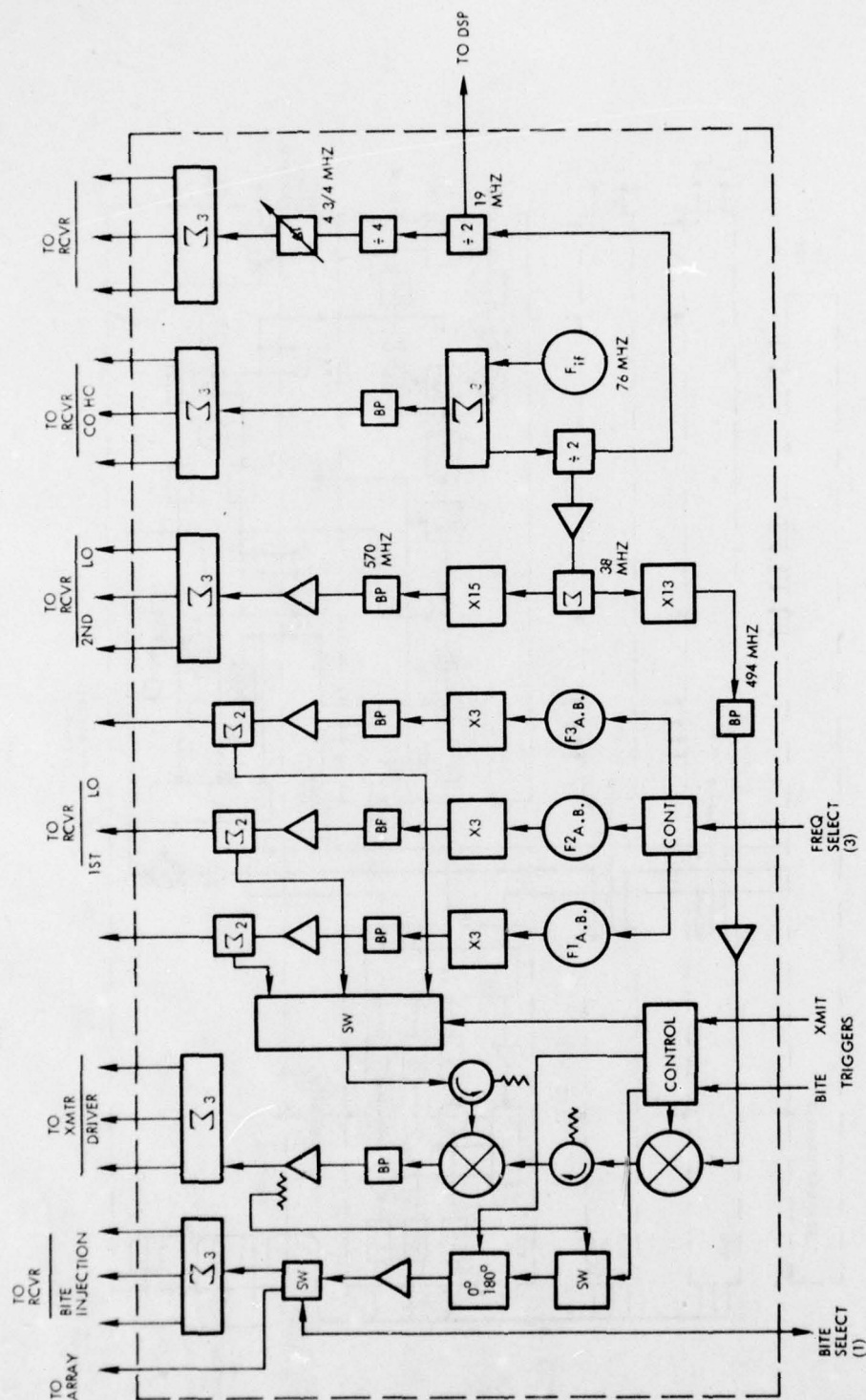
Figure 2.3.4-2. Exciter Module

Down conversion from the first IF of 494 MHz in the receive path to a
76 MHz second IF would be accomplished by mixing the receive signal with a
570 MHz LO signal from the exciter. This 570 MHz LO would be generated by
dividing and multiplying the 76 MHz crystal oscillator. The 76 MHz oscillator
would also provide the reference signal for the quadrature detectors and (after
division to 4.75 MHz) for the A/D's. BITE signals for testing the receiver
channels would also be made available by coupling off a portion of the signal for
the transmitter driver.

Three of the baseline dual conversion receivers configured in Figure
2.3.4-3 would be arranged in parallel to provide for the simultaneous reception
of the three elevation beam frequencies. Sensitivity time control (STC) at both
the 1250 MHz RF frequency and at the 76 MHz 2nd IF frequency would be utilized
to reduce the dynamic range required in the A/D converters. Bandpass filters
insure that each receiver processes only returns in the frequency band it has
been assigned.

Following the STC at the 2nd IF, quadrature detectors will supply
video outputs for the eight bit A/D converters. The STC's will operate with an
R4 law with a runout time that would be experimentally optimized

Based on reliability analysis (Section 2.6), the baseline exciter
requires various levels of redundant protection for the 3, 6 and 12 month main-
tenance interval. Some redundancy is provided by having dual SAW oscillators
for each of the three frequency bands. The approach chosen with its use of
multiple frequencies and of multiple channel receiver has the advantage of grace-
ful degradation. To further enhance the reliability, off-line standby redundancy
would be provided in both the receiver and exciter. This would take the form of
parallel receiver and exciter paths which would be manually switched from manned
sites into service in the event of a failure in these chains. Since these parallel
units are normally off, the only increase in power drain is that created by switch-
ing. The method of switching in a spare exciter module is indicated in Figure
2.3.4-1.

With each receiver requiring between 25 and 35 watts of DC power and the
exciter requiring between 40 and 50 watts range, the total DC power consumption
for the three receivers and the one exciter would be in the 115 to 155 watt range.

Figure 2.3.4-3. RCVR Module (L-Band)

b) Alternative Designs

The Receiver/Exciter for the UHF version would be similar in concept to the L-band version previously described. However, since the operating frequency at UHF is close to the first IF frequency for the L-band receivers, a single conversion receiver can be used for the UHF requirement. There the incoming RF signals at UHF would be converted directly down to a 76 MHz IF. Quadrature detection and the subsequent A/D conversion would be as before. A UHF receiver channel block diagram is shown in Figure 2.3.4-4.

Since only two elevation beams are necessary to satisfy the specified detection and frame time criteria, only one or two receive channels will have to be carried through A/D conversion.

Although a receiver employing R.F. amplification only would be easier to implement and would have an advantage in reliability over the proposed double and single conversion receivers at L-band and at UHF, its failure to provide adequate rejection for undesired signals seriously limits its usefulness in a minimal ECM environment. Based on this consideration, the TRF receiver does not appear to be an attractive solution.

The field replaceable unit (FRU) in the baseline receiver/exciter system would be a complete exciter module or one of three receiver modules. Typical module construction of either the receiver or exciter is illustrated in Figure 2.3.4-5. These modules would be stored in a single cabinet along with the signal/data processor (see Section 2.3.5, Figures 2.3.5-8 and 2.3.5-9).

The design concepts chosen for the receiver/exciters can be implemented with either conventional components or with MHIC (Microwave Hybrid Integrated Circuit) components. With the MHIC approach to design, size is reduced and coaxial connectors for individual components are not used internal to the overall subsystem modules. For purposes of this study, a conservative approach has been followed in that space has been allowed for conventional components, although part of Raytheon's approach to realizing high reliability has been to avoid connectors internal to modules, and to integrate components into subsystem modules to minimize connectors.
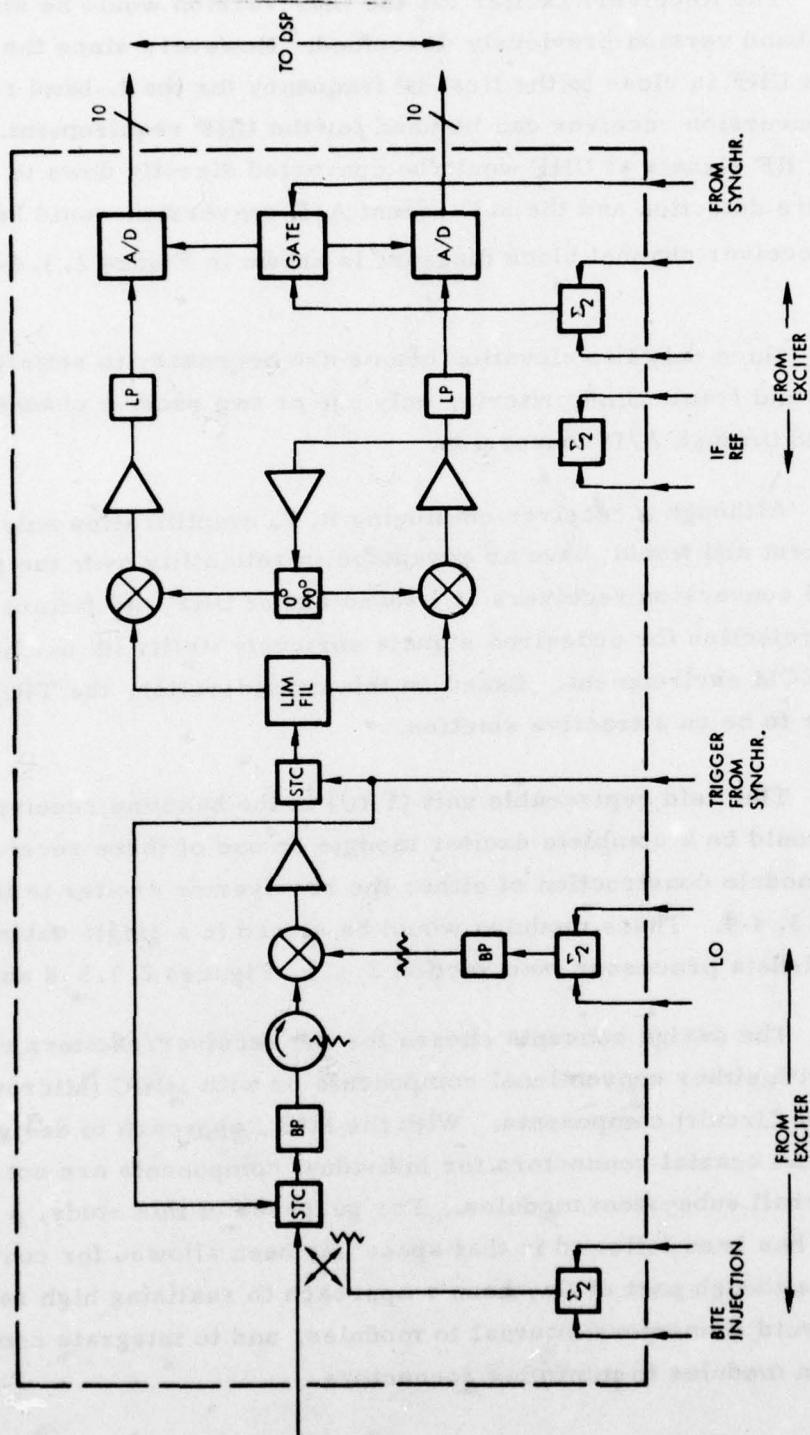
Figure 2. 3. 4-4. Rcvr Module (UHF)

PC CARD
28 PER
MODULE

BOTTOM
COVER

TOP COVER

2"

20"

30"

QTY PER SYSTEM
3 RCVR
1 EXCITER
1 STANDBY EXCITER
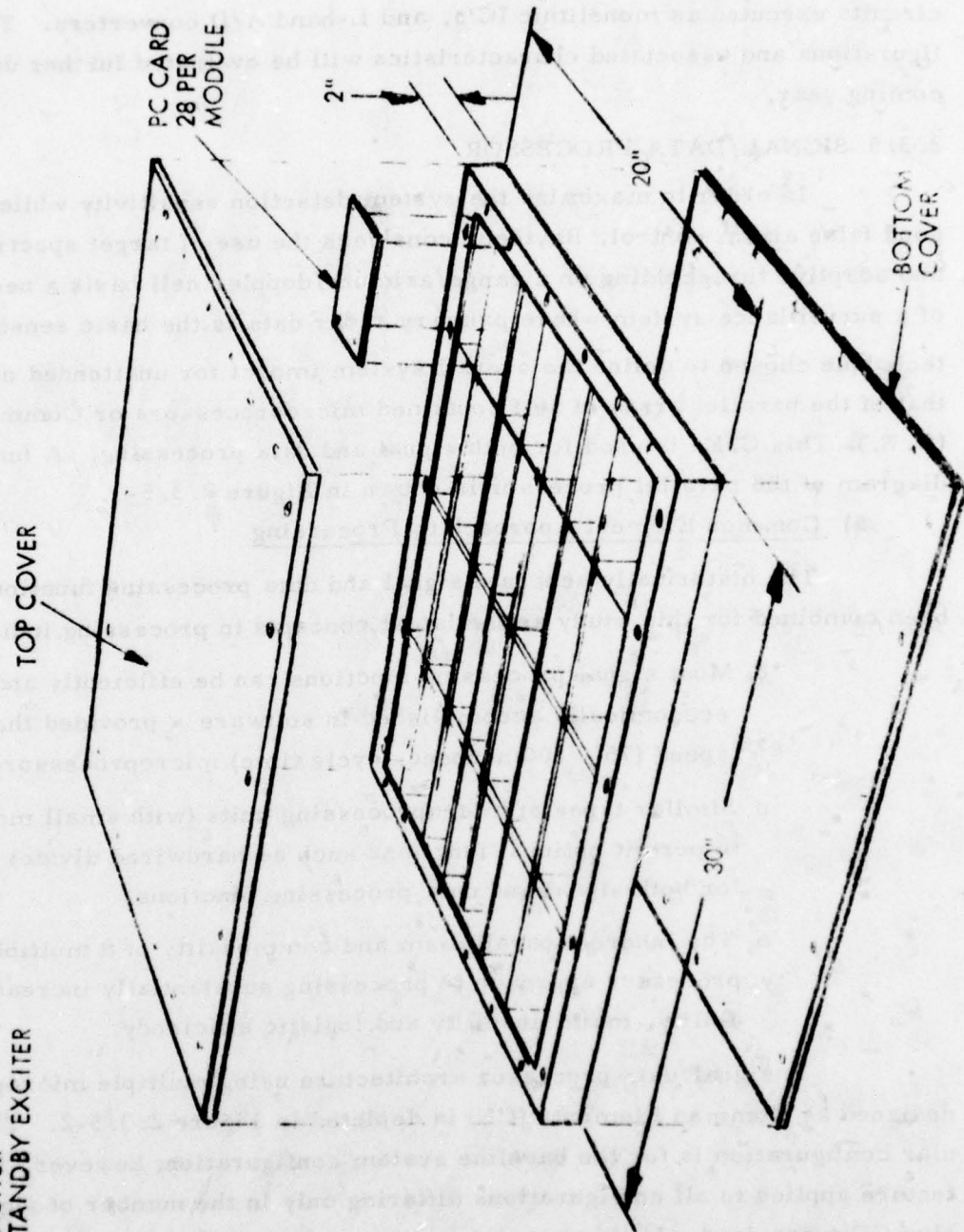
Figure 2.3.4-5. Rcvr and Exciter Module Type A

Anticipated in the near future are configurations that utilize microwave circuits executed as monolithic IC's, and L-band A/D converters. These configurations and associated characteristics will be evaluated further during the coming year.

2.3.5 SIGNAL/DATA PROCESSOR

In order to maximize the system detection sensitivity while providing good false alarm control, Raytheon considers the use of target spectral analysis and adaptive thresholding on a range/azimuth/doppler cell basis a necessary part of a surveillance system where primary radar data is the basic sensor data. The technique chosen to define the overall system impact for unattended operation is that of the parallel array of self contained microprocessors or Common Elements (C.E.). This C.E. is used for both signal and data processing. A functional diagram of the parallel processor is shown in Figure 2.3.5-1.

a) <u>Common Element Approach to Processing</u>

The historically separate signal and data processing functions have been combined for this study as the latest concepts in processing indicate that:

o Most signal processing functions can be efficiently and economically accomplished in software - provided that high speed (75 - 100 nanosec. cycle time) microprocessors are used.

o Similar types of microprocessing units (with small modifications to permit optional functions such as hardwired divide) can be used for both signal and data processing functions.

o The inherent parallelism and commonality of a multiple microprocessor approach to processing substantially increases reliability, maintainability and logistic efficiency.

A signal/data processor architecture using multiple microprocessors designed as Common Elements (CE) is depicted in Figure 2.3.5-2. This particular configuration is for the baseline system configuration; however, the architecture applies to all configurations differing only in the number of signal processing CE's required. In this concept, a group of parallel CE's are used to accomplish the traditional signal processing functions. A second parallel CE set performs the data processing algorithms.

2-100
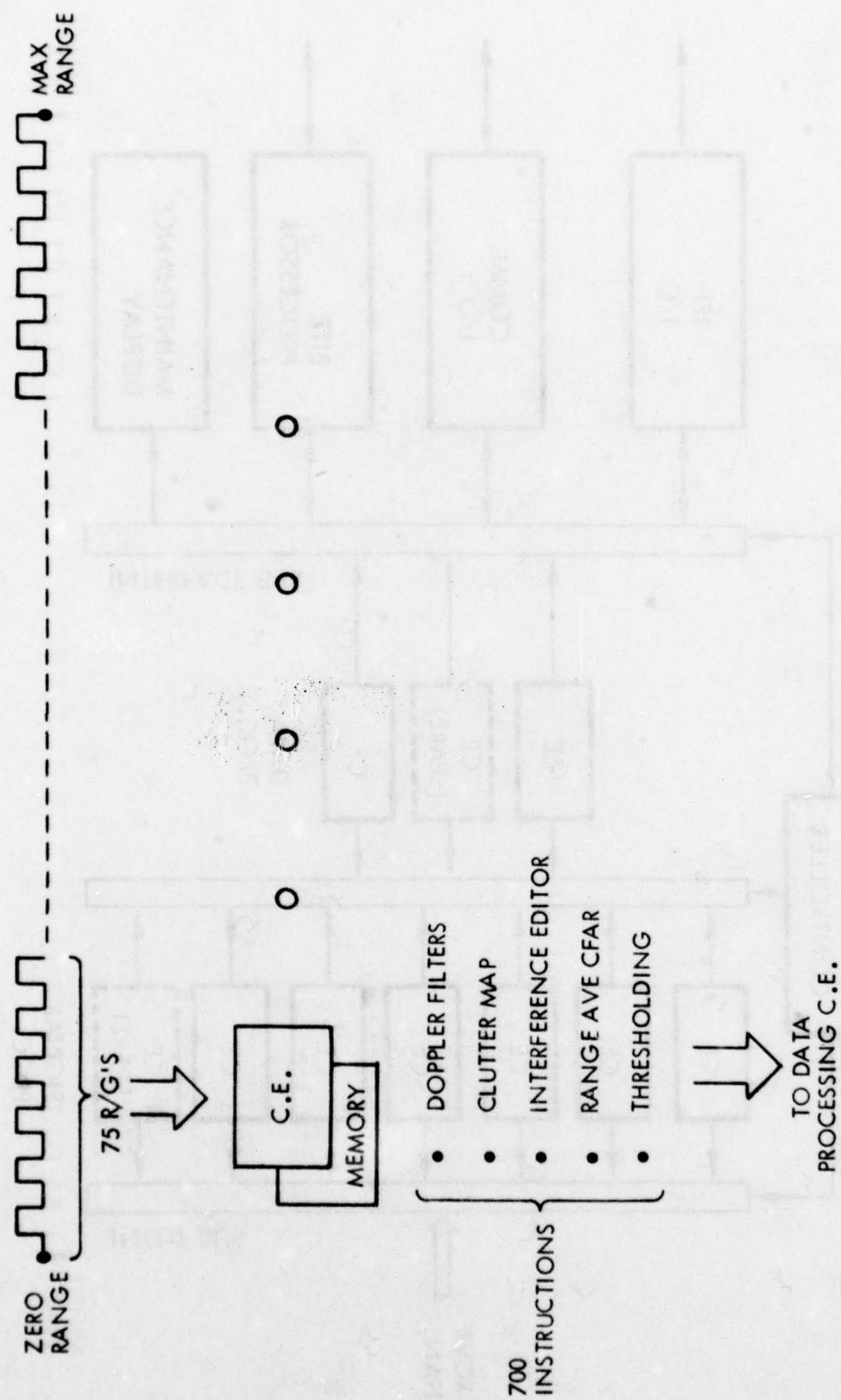
Figure 2.3.5-1. Parallel Processing

ZERO RANGE

MAX RANGE

75 R/G'S

C.E.

MEMORY

DOPPLER FILTERS
CLUTTER MAP
INTERFERENCE EDITOR
RANGE AVE CFAR
THRESHOLDING

700 INSTRUCTIONS

TO DATA PROCESSING C.E.
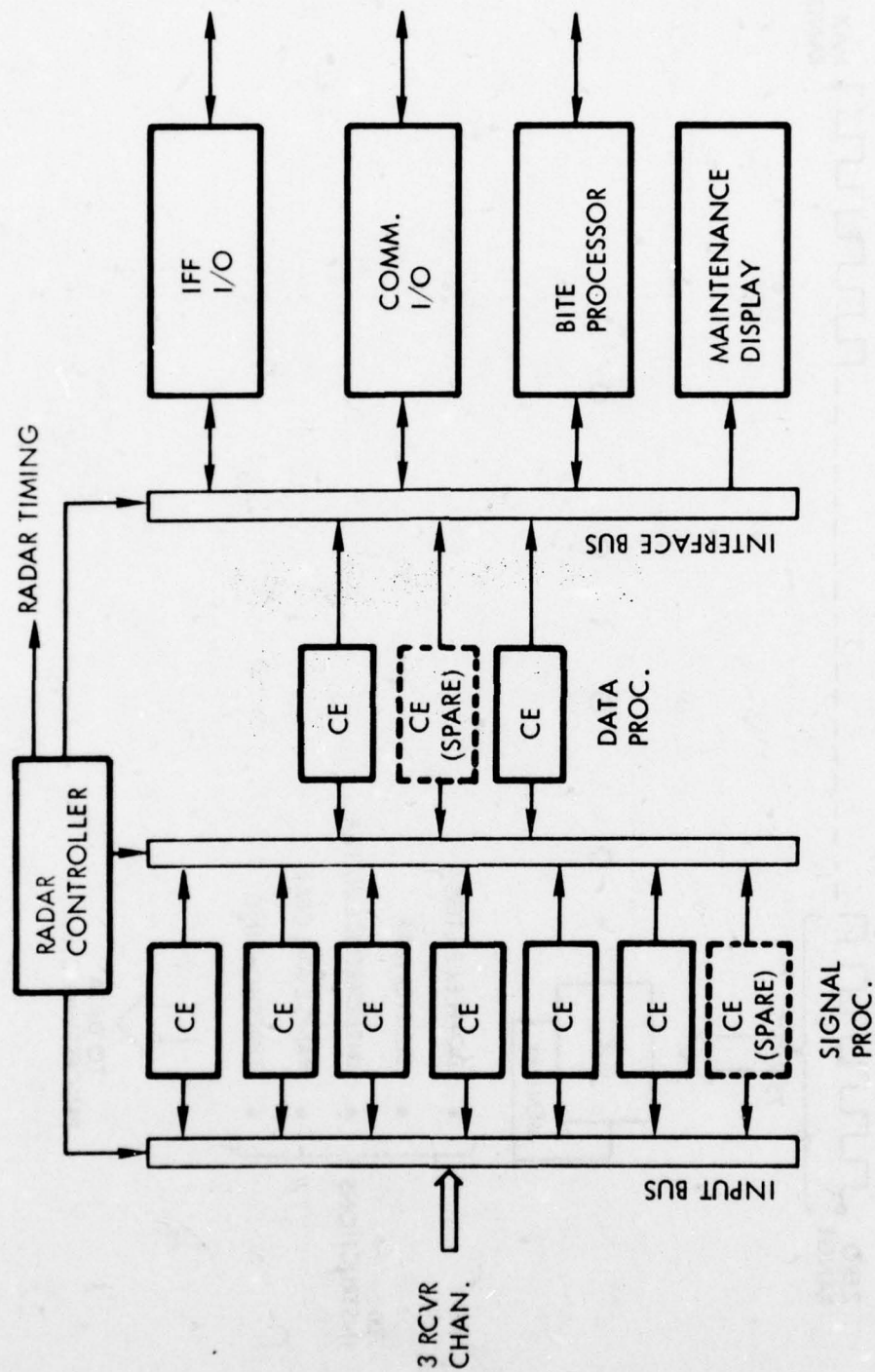
Figure 2.3.5-2 Baseline Processor Configuration Type A CE Configuration

The signal processor CE's perform identical functions for different sequential groups of input range gates. The number of range gates that a single CE can handle is determined by the time available for processing, the complexity of the algorithms and the speed of the processor.

The data processor CE's divide the total processing load by sectors. These sectors can be adaptively changed to equalize track handling loads between the CE's.

For both types, a spare CE can be rapidly activated by changing the logical address of the spare to that of the failed unit. A spare CE is shown in both the signal and data processing set in Figure 2.3.5-2. The number of spares required varies with the system configuration (number of range gates per unit time) and the unattended design time (3, 6 or 12 months).

A radar controller performs the functions of system synchronization and system reconfiguration. Data bus structures with built-in redundancy are used to interface with the receivers, IFF, Built-In-Test Equipment (BITE), a small maintenance display (for checking a repaired system), and between the CE's themselves.

b) Processing Requirements

The basic processor functions are listed in Table 2.3.5-1. The functional requirement is also shown as well as the recommended technique to implement the function.

One of the key advantages of the CE approach lies in its ability to be easily adapted (by reprogramming) to different techniques as they become available.

The processing functions are shown in block diagram form in Figure 2.3.5-3 to show their relationships. The A/D converter, a function usually associated with signal processing, is not shown. The A/D converters are packaged with the receiver channel modules to reduce sampling jitter. A 10 bit (9 bit data plus sign) A/D is used with each in phase (I) and quadrature (Q) channel. For various system configurations, the number of simultaneous receiver inputs ranges from 1 to 6 (2 to 12 I & Q channels). The clutter improvement factor limitation with this number of bits, assuming a noise level higher than the least significant bit, is about 60 dB.

Table 2.3.5-1

Signal/Data Processor Functions

Function	Baseline Requirement	Technique
• Signal visibility	$V_0 = 7$ dB (per pulse)	Spectral filtering, freq. agility, incoh. integration
• Ground clutter rejection	$I_G = 45$ dB (95 percentile clutter)	Spectral filtering
• Weather clutter rejection	$I_W = 20$ dB	Spectral filtering
• CFAR	Noise: Clutter: $\Big\}$ $P_{FA} = 10^{-3}$ Saturation:	Range average Clutter map Interference editor
• Target Estimation	Range: 0.25 NM Azimuth: 0.5° Range rate: 1 filter	Range centroid Monodwell Filter, multiple PRF
• Target tracking	TI Time = 16 sec False TI rate = 1/hr. Track Drop = 12 sec	3/4 scan correlation CFAR 0/3 scan correlation
• ECCM	Strobe reporting Jamming suppression	CFAR threshold variation Sidelobe blanking Spectral Filtering Frequency diversity CFAR
• Radar Control/BITE	-	Radar controller
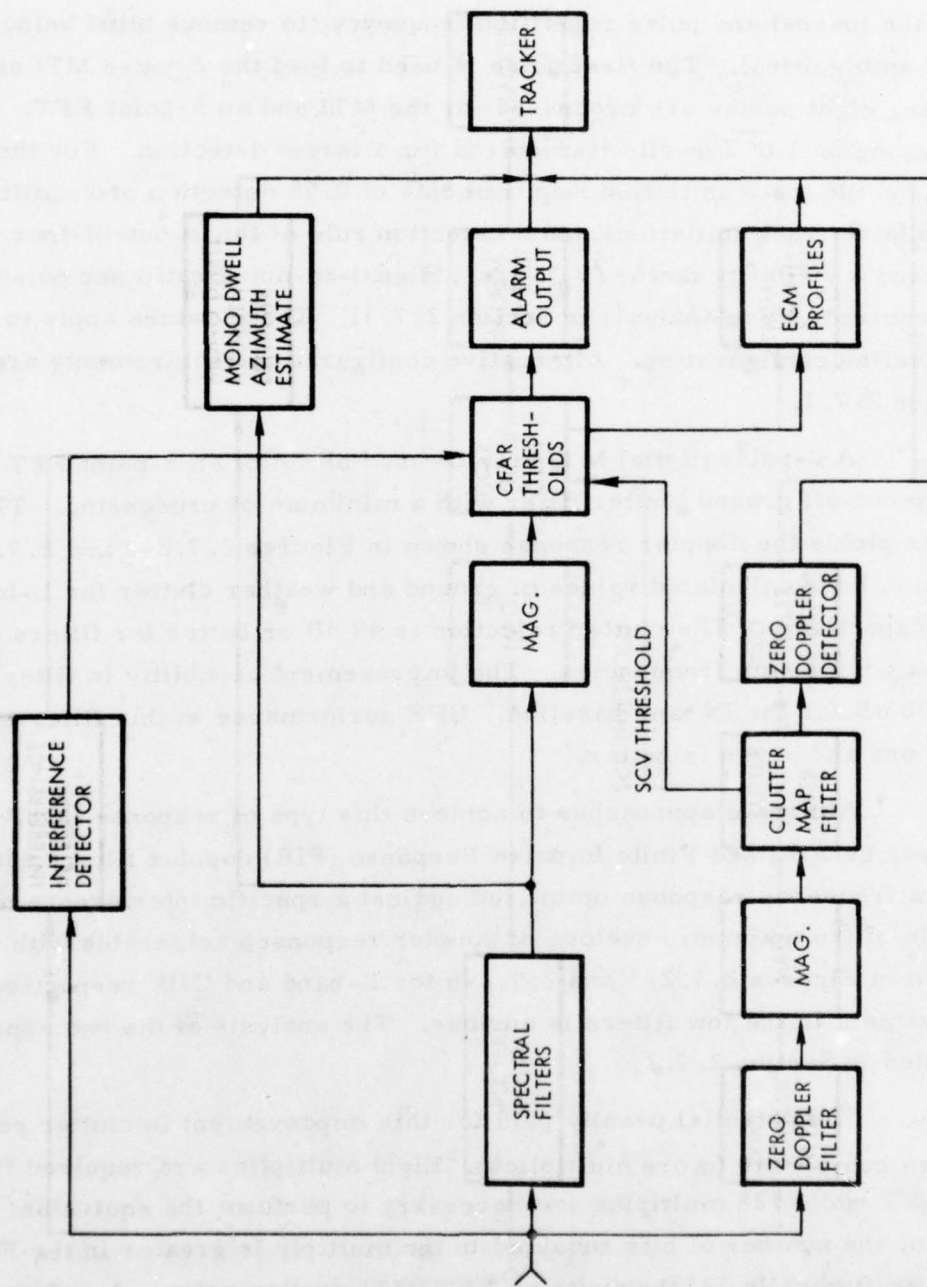
Figure 2.3.5-3. Functional Processing Block Diagram

The Baseline radar transmits two batches of 8 pulses each on the target in one beam position. Each is at a different RF frequency (to reduce target fluctuation losses) and pulse repetition frequency (to remove blind velocities and resolve ambiguities). The first pulse is used to load the 2-pulse MTI and the remaining eight pulses are processed by the MTI and an 8-point FFT. A threshold crossing on 1 of 2 dwells is required for a target detection. For these conditions and the track initiation requirements of 0.95 detection probability, 1 hour between false track initiations and a detection rule of three-out-of-four (3/4) scans, and a visibility factor (V_0), i.e., signal-to-noise ratio per pulse of 12.7 dB is required. (See analysis in Section 2.7.1). These values apply to the L-band baseline configuration. Alternative configuration requirements are given in Section 2.7.1.

A 2-pulse digital MTI may be used ahead of an 8-point FFT to achieve a sharp cut-off ground clutter filter with a minimum of processing. This combination yields the doppler response shown in Figures 2.7.2-3 and 2.7.2-4 in Section 2.7 for calculated values of ground and weather clutter for L-band and UHF respectively. The clutter rejection is 48 dB or better for filters three through six for both frequencies. The improvement capability in filter two is about 30 dB for the L-band baseline. UHF performance in this filter and in filters one and seven is better.

Alternate approaches to achieve this type of response involve the design or generalized Finite Impulse Response (FIR) doppler filters with non-uniform frequency response optimized against a specific interference model. An example of the optimum envelope of doppler responses achievable with this approach is given in Figures 2.7.2-5 and 2.7.2-6 for L-band and UHF respectively. The improvement in the low filters is obvious. The analysis of the two approaches is presented in Section 2.7.2.

The potential penalty paid for this improvement in clutter rejection is software complexity (more multiplies). Eight multiplies are required to an eight-point FFT while 128 multiples are necessary to perform the equivalent FIR. In addition, the number of bits required in the multiply is greater in the FIR implementation (typically 12) than with an FFT/MTI configuration. A software multiply

(Booth algorithm) thus would require substantially greater machine time with a FIR implementation. Another alternative is to use an MTI ahead of a generalized FIR network. This approach reduces the number of bits required per multiply in the FIR to about 4 bits. The relative complexity and performance of these filters will be examined versus the MTI/FFT approach during the coming year.

Range average CFAR logic is used to set the threshold on each filter adaptively to reject weather, ECM, impulse interference, and changes in the noise background. The 16 range gate average consists of 8 range gates on either side of the cells that are examined for a target ($\approx \pm 3.2$ NM for 4.8 μsec range samples or ± 0.8 NM for 1.2 μsec samples).

A clutter map accumulates history of the zero-doppler clutter returns from the zero-doppler filter to control the target threshold of the zero-doppler channel. Targets larger than the clutter in any range/azimuth clutter map cell are detected and merged with detections from the other filters. Because of the inability of the clutter map to control single false alarms a track is not initiated from the clutter map.

An interference editor is used to suppress large point clutter which exceeds the dynamic range of the A/D converter. If the average value of the nine pulses at the output of either the I or Q A/D converter is within a pre-determined value of the maximum A/D level, then that range gate is suppressed.

Target parameter estimation is accomplished conventionally by centroid techniques.

ECM profiles (strobe reports) can be determined by monitoring the average CFAR threshold in a coherent processing interval (CPI) level. These will be the greatest when the mainlobe is pointed at the jammer. Sidelobe blanking also eliminates jamming inputs except at the mainlobe, thus pointing out the jammer azimuth. The signal processor has inherent capabilities to suppress ECM, both brute force noise and deception. See Section 2.7.3 for an analysis of ECCM techniques.

2-107

Table 2.3.5-2

Data Processing Functions

Type	Function	Peak Rate
Alarm Inputs	Accept alarms	20/cpi
Single-scan detections	Alarm correlation (1/2)	10/cpi
Track initiation	Detection correlation (3/4)	40/scan
Track	Continued detections (1/3)	40/scan
Drop Track	No detections (0/3)	40/scan
IFF correlation	Designate to IFF, compare response	40/scan
Communication output	Send track/IFF/BITE report	40/scan

The signal processing alarms are passed to the data processor CE's for each CPI. The primary data processing functions are track initiation, track and interface (IFF, BITE, communications, radar) control. The definition of the data processing variables and the estimated frequency is given in Table 2.3.5-2.

The software requirements to handle the functions described for the signal processor have been analyzed. The most efficient algorithm to implement any given function has been sought; however, it is evident that considerable work has yet to be done in this area. The estimates for the number of signal processing instructions is shown in Table 2.3.5-3. The instructions are the number executed in any coherent processing interval by each C.E.

The data processing instruction estimate is given in Table 2.3.5-4. These estimates are based upon implementation of similar algorithms in previous developed systems and the rates given in Table 2.3.5-2.

Table 2.3.5-3

Signal Processing Algorithms

Algorithm	Instructions
Spectral Filtering (optimum)	300
Magnitude	92
CFAR	98
Alarm Output	14
Interference Detector	100
Zero Doppler Filter	24
Clutter Map	50
ECM Profiles	(50) ECCM configuration
Total	(728) Instructions per CPI

c) Common Element Design

Basic Architecture

The baseline common element architecture is shown in Figure 2.3.5-4.
The leading edge of a single phase clock is used to synchronously clock the
micro-instruction, the A, B and F registers. The new ALU output is valid
at the end of the clock cycle. The micro-instructions are overlapped to
give an instruction thru put rate equal to one cycle as shown in Table
2.3.5-5.

Table 2.3.5-4
Data Processing Requirements

Computer Instructions	Number of Computer 16 Bits Instructions
Target Estimation	3000
• Azimuth	
• Range	
• Range Rate	
• Reject Multiple-Time	
Scan-to-Scan Correlation	1000
Target Tracking	2000
• Track Prediction	
• Track Maintenance	
Overhead (X2 of Above)	6000
• Executive	
• I/O	
• Interfacing (IFF, ETC)	
	12,000
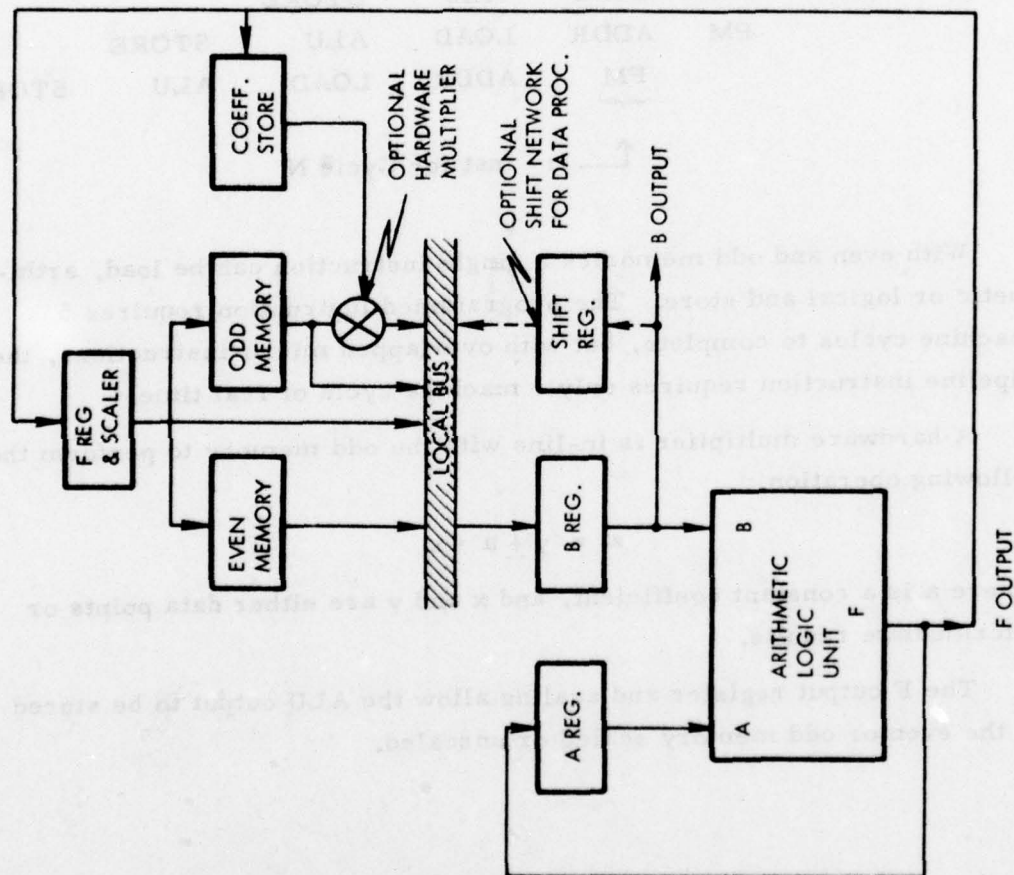
Figure 2.3.5-4. Common Element Architecture

Table 2.3.5-5

Overlapped Instructions

									Inst. #
PM	ADDR	LOAD	ALU	STORE					1
	PM	ADDR	LOAD	ALU	STORE				2
		PM	ADDR	LOAD	ALU	STORE			3
			PM	ADDR	LOAD	ALU	STORE		4
			PM	ADDR	LOAD	ALU	STORE	5

⌐ μ - inst for Cycle N

With even and odd memories a single instruction can be load, arithmetic or logical and store. The programmed instruction requires 5 machine cycles to complete, but with overlapped micro-instructions, the pipeline instruction requires only 1 machine cycle of real time.

A hardware multiplier is in-line with the odd memory to perform the following operation.

$$z = y \pm a \cdot x$$

Where a is a constant coefficient, and x and y are either data points or intermediate results.

The F output register and scaling allow the ALU output to be stored in the even or odd memory scaled or unscaled.

The F output scaling allows the FFT to be left justified and use divide by two scaling. This maximizes dynamic range and minimizes the effect of arithmetic noise due to multiply truncation and coefficient quantization due to finite register lengths.

The signal processing CE interfaces and memories are shown in Figure 2.3.5-5. The interchange of CFAR alarm data, program loading, inspect and change of data and programs is via the data processor two-port RAM interface with the common bus. This same loading technique was first used on TSR. The operational programs will be stored in PROMS and, therefore, will not have to be loaded. The distributed memories for input storage and clutter map memories are also shown on Figure 2.3.5-6.

The CE architecture shown in Figure 2.3.5-4 utilizes a low power Schottky 181 MSI arithmetic logic unit (ALU). This ALU is a generally available device with a cycle time of about 100 nsec. An alternate design currently being pursued at Raytheon incorporates a low power Schottky 2901 ALU with a somewhat longer cycle time (150 - 200 nsec), but with several integrated features which might make certain types of algorithms more efficient. One of these devices shall be selected for design and development of the CE processor.
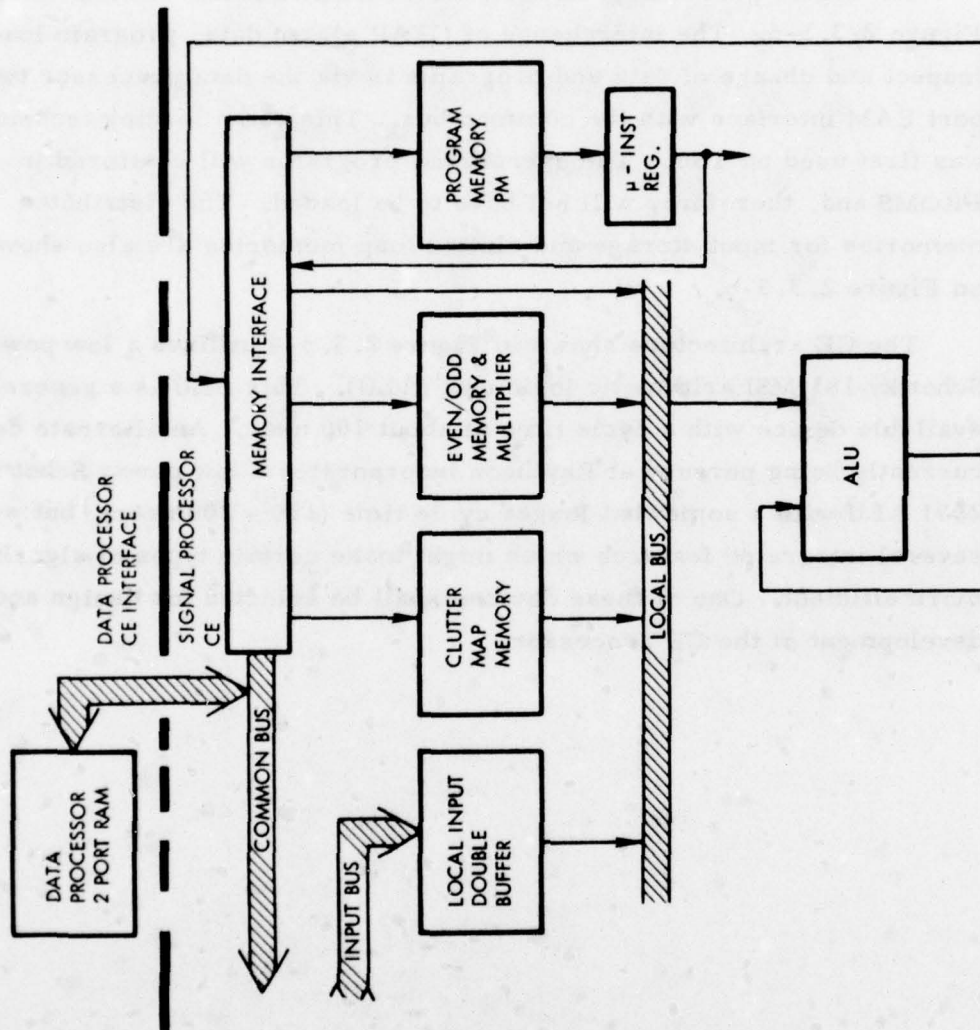
Figure 2.3.5-5. Common Element Block Diagram
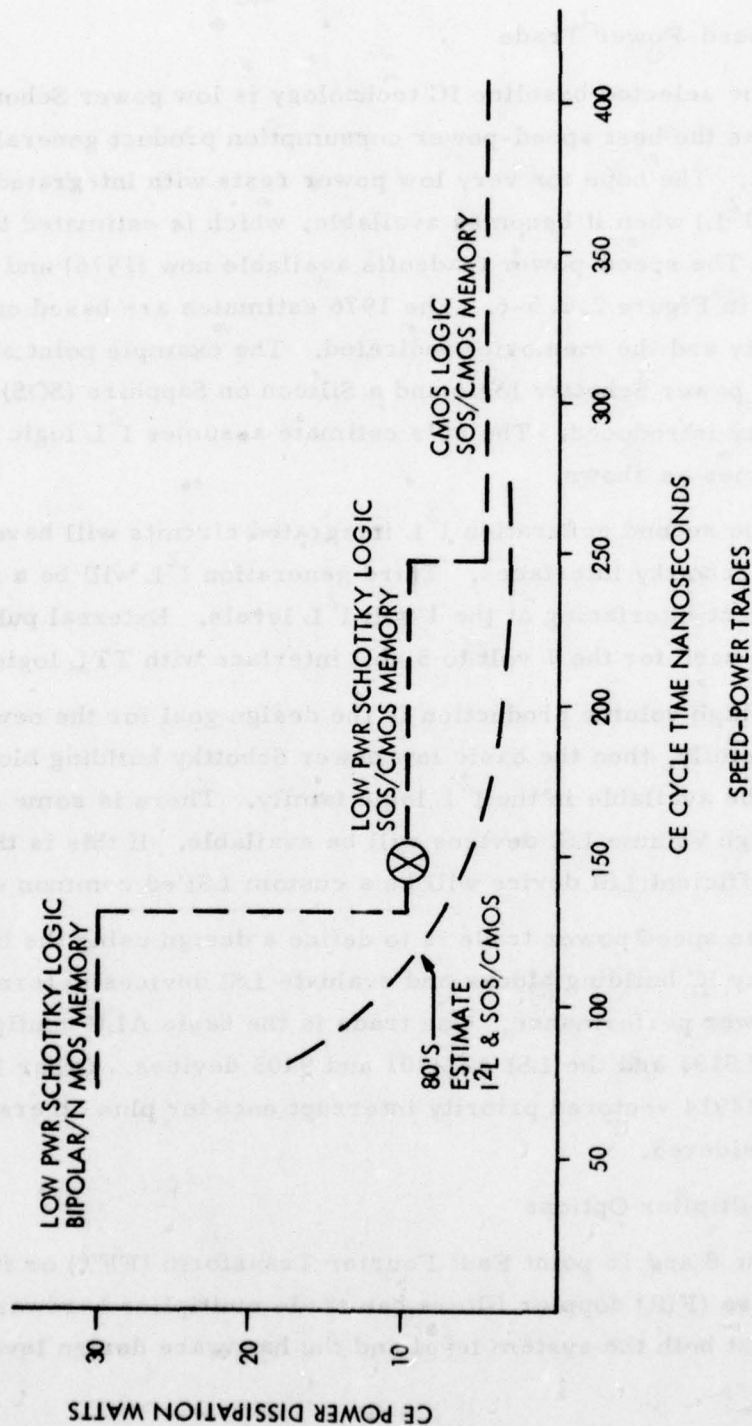
Figure 2.3.5-6. CE Speed Power Trades

Speed-Power Trade

The selected baseline IC technology is low power Schottky as this type has the best speed-power consumption product generally available to date. The hope for very low power rests with integrated-injection logic (I^2L) when it becomes available, which is estimated to be about 1980. The speed-power tradeoffs available now (1976) and by 1980 are shown in Figure 2.3.5-6. The 1976 estimates are based on low power Schottky and the memories indicated. The example point shown is based on low power Schottky logic and a Silicon on Sapphire (SOS) memory recently introduced. The 80's estimate assumes I^2L logic plus the memories as shown.

The second generation I^2L integrated circuits will have on-chip low power Schottky interfaces. Third generation I^2L will be a family of IC's for direct interfacing at the 1 volt I^2L levels. External pull-up resistors will be used for the 1 volt to 5 volt interface with TTL logic.

If high volume production is the design goal for the new one volt I^2L logic family, then the basic low power Schottky building blocks will most likely be available in the I^2L logic family. There is some concern that only high volume LSI devices will be available. If this is the case, the most efficient LSI device will be a custom LSI'ed common element.

The speed power trade is to define a design using the basic low power Schottky IC building blocks and evaluate LSI devices in terms of speed and power performance. One trade is the basic ALU configuration using the 54LS181 and the LSI AM2901 and 9405 devices. Other LSI devices are the AM2914 vectored priority interrupt encoder plus others that need to be considered.

Multiplier Options

The 8 and 16 point Fast Fourier Transform (FFT) or finite impulse response (FIR) doppler filters can trade multiplier hardware speed and power at both the system level and the hardware design level.

The system trade is whether to use the optional in-line hardware multiplier or an optional shift register for the modified Booth multiply algorithm. The 8 point FFT requires only 8 real multiplies by $1/\sqrt{2}$. The all zero's FIR or transversal doppler filters require 8 or 9 bit coefficients without an MTI clutter notch and only 4 bit coefficients with an MTI clutter notch. With 4 bit coefficients the programmed Booth algorithm is approximately the same speed as the in-line hardware multiplies. The programmed multiply time depends on the number of bits in the constant coefficient set equal to 1.

The 16 point transform requires 32 two point transforms to translate signals from the time domain to the frequency domain. A programmed FFT can take advantage of the fact that most of the multiplies are by 0, 90 and 45 degrees as shown in Table 2.3.5-6.

Table 2.3.5 6

16 Point FFT Multiplies

Complex Multiplies	Real Multiplies
22 by 1 (0 or 90°)	0
6 by $\sqrt{2}$ (45°)	12
4 by cos N22.5° + sin N22.5°	16
N = 1, 3, 5 or 7	
Total 32 Complex	28 Real

In general purpose hardware, 32 complex multiplies require 128 real multiplies. A special purpose FFT program for a 16 point transform can reduce the number of real multiplies by approximately a factor of 5.

The in-line hardware multiplier has the advantage for 32 and larger point FFT transforms.

The hardware design trade will be to evaluate in-line hardware multiplier designs in terms of speed, power, cost, operating temperature range and mechanical mounting constraints. The TI 54284, 54285 and AMD's

25S05 MSI multiplier IC's can be used to evaluate LSI devices like the TRW MPY-16AJ 16 x 16 array multiplier or other LSI multipliers such as the Monolithic Memory 6755 device.

The signal processing functions are distributed among the CE's in range with each CE processing a batch of range gates. The bulk memories for input storage and clutter maps are also distributed. The number of signal processing common elements can be estimated as,

$$N_{CE_{SP}} = \frac{(N_R)(N_C) T_{SP}}{CPI}$$

where CPI = coherent processing interval

T_{SP} = time to execute complete signal processing instruction set for one range gate

N_R = number of range gates

N_C = number of receiver channel inputs

For an average PRF of 1150 Hertz and a nine pulse dwell, the CPI is 7.83 msec. If the instruction set shown in Table 2.3.5-3 were all simple instructions such as adds, then each instruction would take one cycle as illustrated in Table 2.3.5-5. Multiplication, however, either hardwired or programmed, takes longer. To account for the added time for a mix of simple instructions with multiplies, a total signal processing time T_{SP} equal to about 1000 cycles is assumed. Figure 2.3.5-7 shows the number of signal processing CE's required as a function of cycle time for several range gate sampling times. For a 100 nsec device, that number is about 6.

In signal processing the multipliers are all by constant coefficients and are required to have a high thruput rate. In data processing the multiplies and divides are by variables for interpolation algorithms. With a slower thruput rate requirement, the multiplies and divides can be done with a modified Booth algorithm. For data processing CE's, the optional shift network between the B output and local bus shown in Figure 2.3.5-4 would be required for multiplies and devides.

2-118
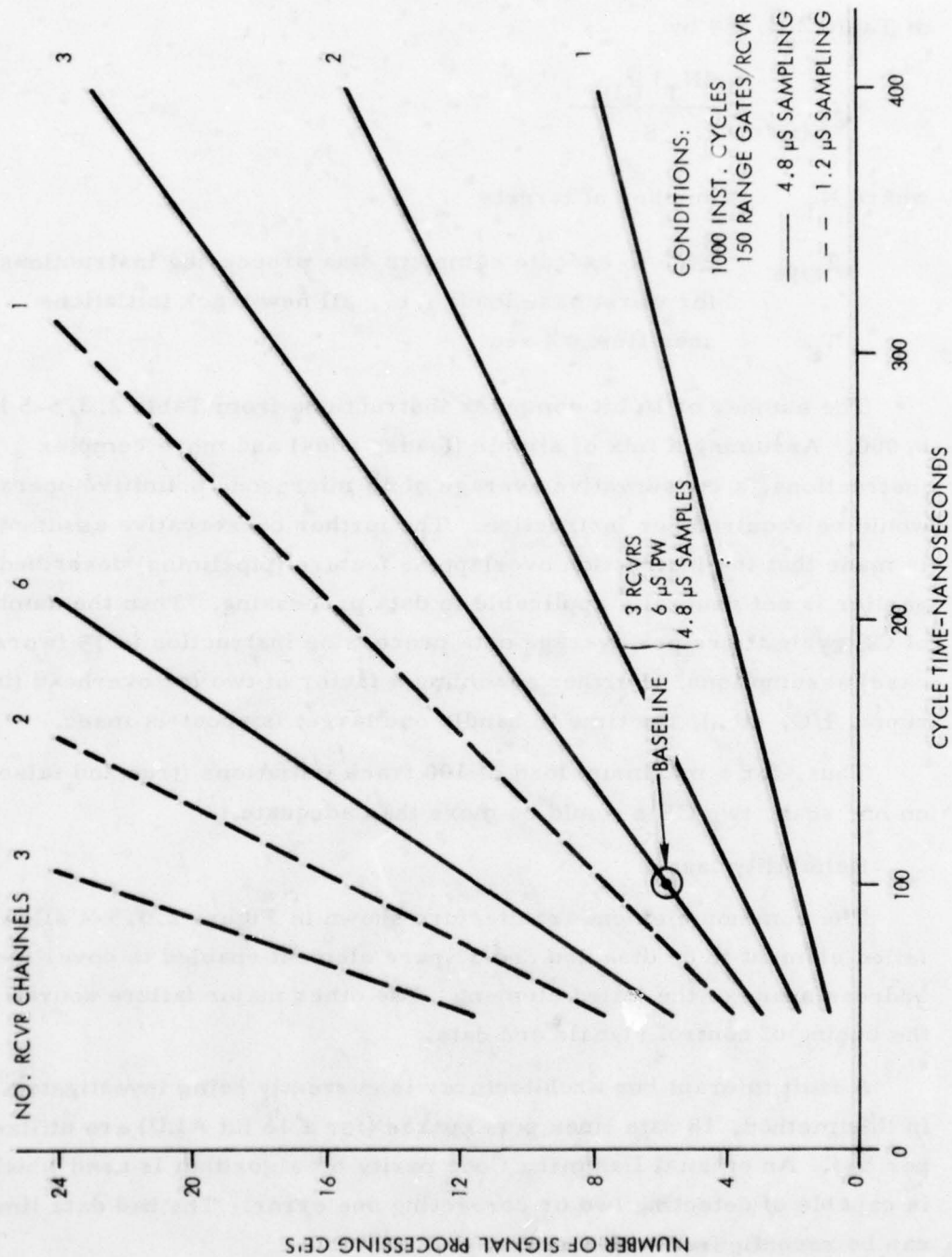
Figure 2. 3. 5-7. Signal Processing CE's Required

The number of data processing CE's can be evaluated with the aid of of Table 2.3.5-4 by

$$N_{CE_{DP}} = \frac{(N_T)\,T_{DP}}{T_S}$$

where N_T = number of targets

T_{DP} = time to execute complete data processing instructions for worst case load, i.e., all new track initiations

T_S = scan time $\cong 4$ sec

The number of 16 bit computer instructions from Table 2.3.5-5 is 6,000. Assuming a mix of simple (loads, adds) and more complex instructions, a conservative average of 15 microcode primitive operations would be required per instruction. The further conservative assumption is made that the instruction overlapping feature (pipelining) described earlier is not generally applicable to data processing. Then the number of CE cycle times per average data processing instruction is 15 (worst case) assumptions. Further assuming a factor of two for overhead (interrupts, I/O, etc.), the time to handle one target is about 18 msec.

Thus, for a maximum load of 100 track initiations (true and false) on one scan, two CE's would be more than adequate.

Reliability Issues

The common element architecture shown in Figure 2.3.5-4 allows a failed element to be disabled and a spare element enabled to cover the address space of the failed element. The other major failure source is the busing of control signals and data.

A fault tolerant bus architectures is currently being investigated. In this method, 18 data lines plus spares (for a 16 bit ALU) are utilized per bus. An optimal Hamming Code parity bit algorithm is used which is capable of detecting two or correcting one error. The bad data line can be reconfigured with a spare.

2-120

Mechanical Construction

The signal/data processing functions would be designed and fabricated for standard sized Augat 8200 series cards with a capability of 180 integrated circuits. These cards would be mounted in a drawer of a cabinet along with the receiver exciter modules. The cabinet construction is illustrated in Figure 2.3.5-8 (front view) and 2.3.5-9 (rear view). Space for 60 Augut cards would be available which should be sufficient to handle most configurations.

LIFTING EYES

RCVR MODULES
EXCITER MODULES

RFI COMBO
GASKETS
ON ALL DOOR
& PANELS

PROCESSOR
DRAWER

5-ROWS OF 12
AUGAT 8200
SERIES PANEL
CARD BOARD
SIZE 16.175
(180 PATTERN)
X 7.475

HANDLE

CONTROL PANEL
HINGED

CAPTIVE
HARDWARE

POWER
SUPPLIES

SLIDES

24"

72"

24"
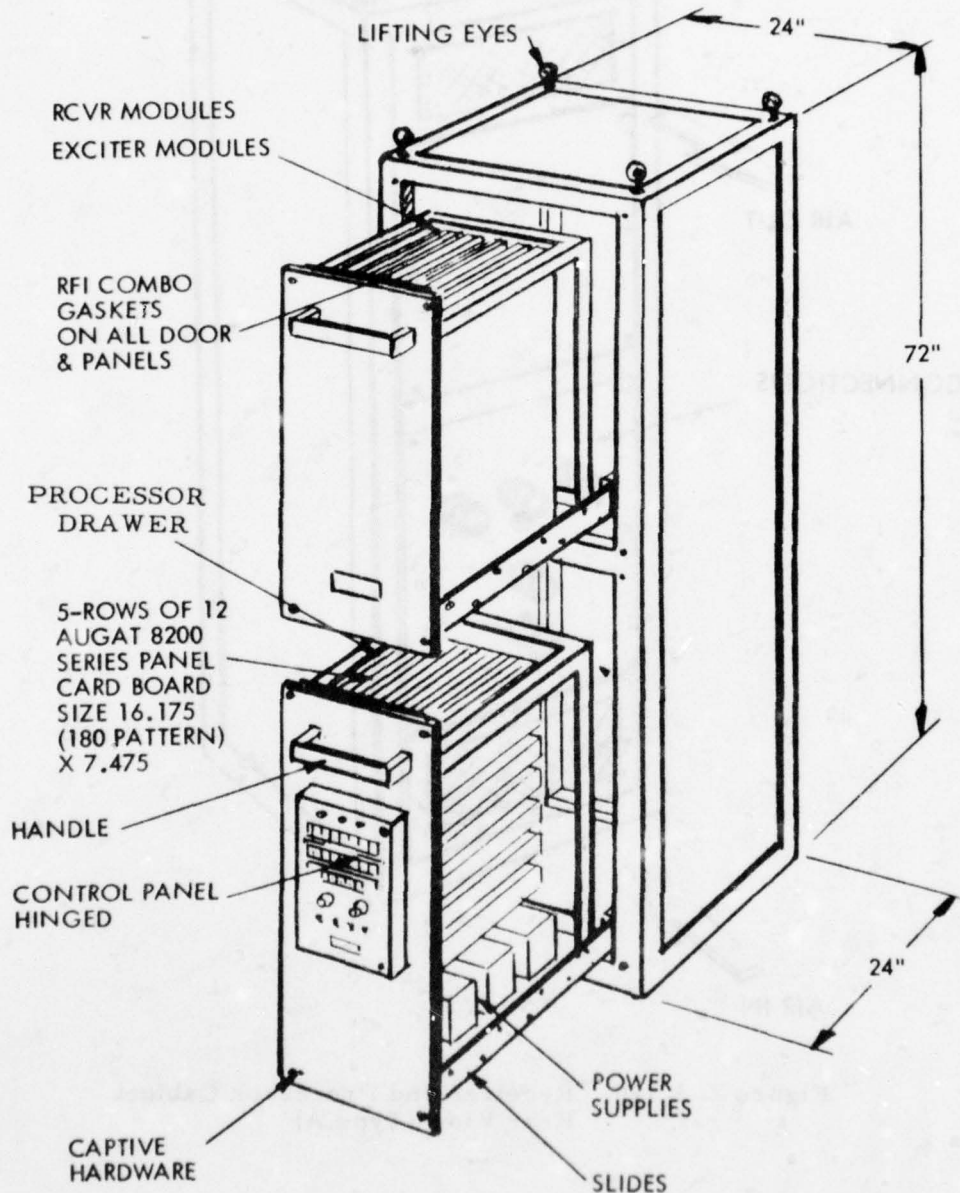
Figure 2.3.5-8.   Receiver and Processor Cabinet
Unattended Radar System, Front
View (Type A)

AIR OUT

INTERCONNECTIONS
PANEL

AIR IN
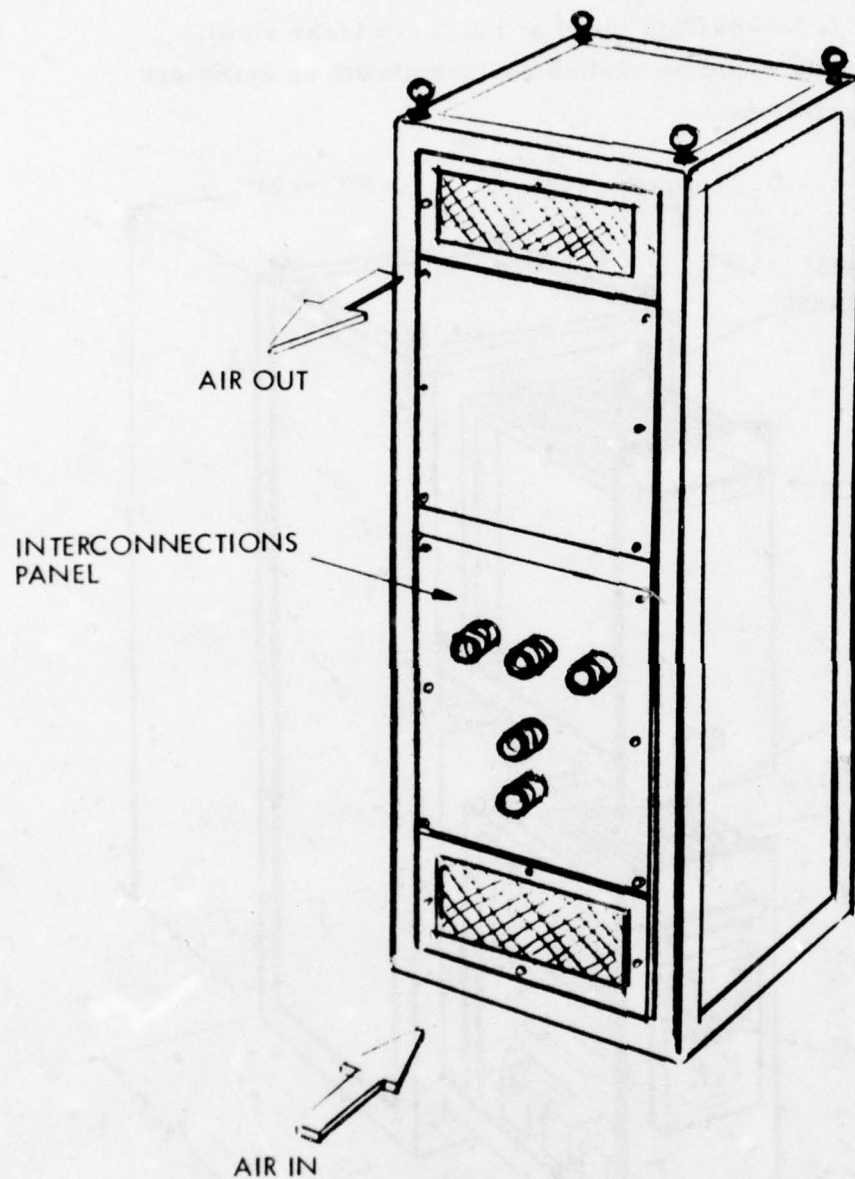
Figure 2.3.5-9. Receiver and Processor Cabinet
Rear View (Type A)

Possible Alternative

An alternative option which requires further investigation is the emerging technology of charge coupled devices (CCD).

CCD technology promises devices with excellent speed-power products and very high functional density per integrated circuit.

CCD may be implemented as either analog or digital devices. Analog CCD's possess the advantage of very low power consumption. The use of digital CCD implies several distinct advantages over analog. These include the inherent noise immunity of digital circuits and the flexibility of digital functions. A fully programmable function can be created with CCD's.

An inherent disadvantage of analog CCD's is their limited memory retention time ($\sim$ 1 second). This is overcome in digital CCD's by refreshing the data on a periodic basis. The power required for data refresh, however, places digital CCD memory at a disadvantage with regard to CMOS/505 memory now available.

A possible hybrid signal processing configuration could employ analog CCD's for the spectral filtering and associated functions while either digital CCD's or bipolar elements could be used for those functions requiring considerable memory such as the clutter map and CFAR.

CCD technology is being pursured in a number of laboratories, including Raytheon, at the current time. Some devices have been produced which show great progress. However, digital CCD devices are not generally available, and it appears that their commercially introduction is several years away. Some analogue CCD devices are currently available.

For the purpose of this study, CCD technology was not considered as reliable cost and failure rate data was not available. However, the potential of CCD devices to greatly reduce the requirement for processing power is a powerful agreement not to overlook this new technology. The use of CCD's will be examined in greater detail in the coming year.

2-123

2.4 BITE SUBSYSTEM

As shown previously one of the driving requirements for unattended operation is the 3 hour visit for repair. This in turn dicated the need for a priori knowledge of which FRU has failed before the site is visited. An extensive BITE concept has been developed for the system which continually excersizes the system FRU's for a good/bad indication. This excersizing of the system is performed at a reasonably slow rate ($\approx$ one/hour) which permits a single microprocessor chip such as the 8080 to control all BITE functions. It should be noted that if a "godhead" of the system operation is to be identified it is the BITE microprocessor and as such must be nearly foolproof. This fool-proofing is accomplished by voting amongst a number of 8080 chips to determine the likelihood of the data being valid. The small size and cost of the 8080 make this form of reliability feature very attractive.

2.4.1 BITE PLAN

The Type A radar network is assumed to be divided into groups of 12 unattended sites associated with a single manned Logistics Node (LN). Each unattended site reports periodically to the Logistics Node. The periodic report contains radar, IFF and BITE status data.

A general block diagram of the BITE concept is shown in Figure
2.4.1-1. The remote (unattended) site major subsystem is shown along with
the essential BITE elements for both the unattended site and the Logistics Node.
Under the direction of the remote BITE Processor, periodic testing by signal
injection or sampling techniques permits the detection of equipment faults and
the isolation of these faults to the nearest field replaceable unit (FRU). This
fault data is then set to the Logistics Node BITE subsystem.

At the Node, data from all remote sites is evaluated and stored. A
failed FRU for which an unused spare is available can be switched out of the
system and the spare activated under remote command from the Node operator.

The fault evaluation at the Node also determines if a radar perfor-
mance at a given remote site is the minimum needed to postpone a repair trip
or whether repairs are required immediately. If immediate repair is war-
ranted, then the Node BITE processor can be commanded to print-out a detailed
list of required FRU's to be replaced.

2.4.2 FAULT ISOLATION

The primary technique of achieving fault isolation to the nearest
FRU is by signal injection and sampling. These two techniques determine if
a fault exists anywhere in the unattended system. In several specific instances,
subsequent BITE testing is required to further isolate faults. Provision is also
made to transmit back to the Node, upon command, certain types of raw data to
permit refined analysis of the system's performance under marginal conditions.
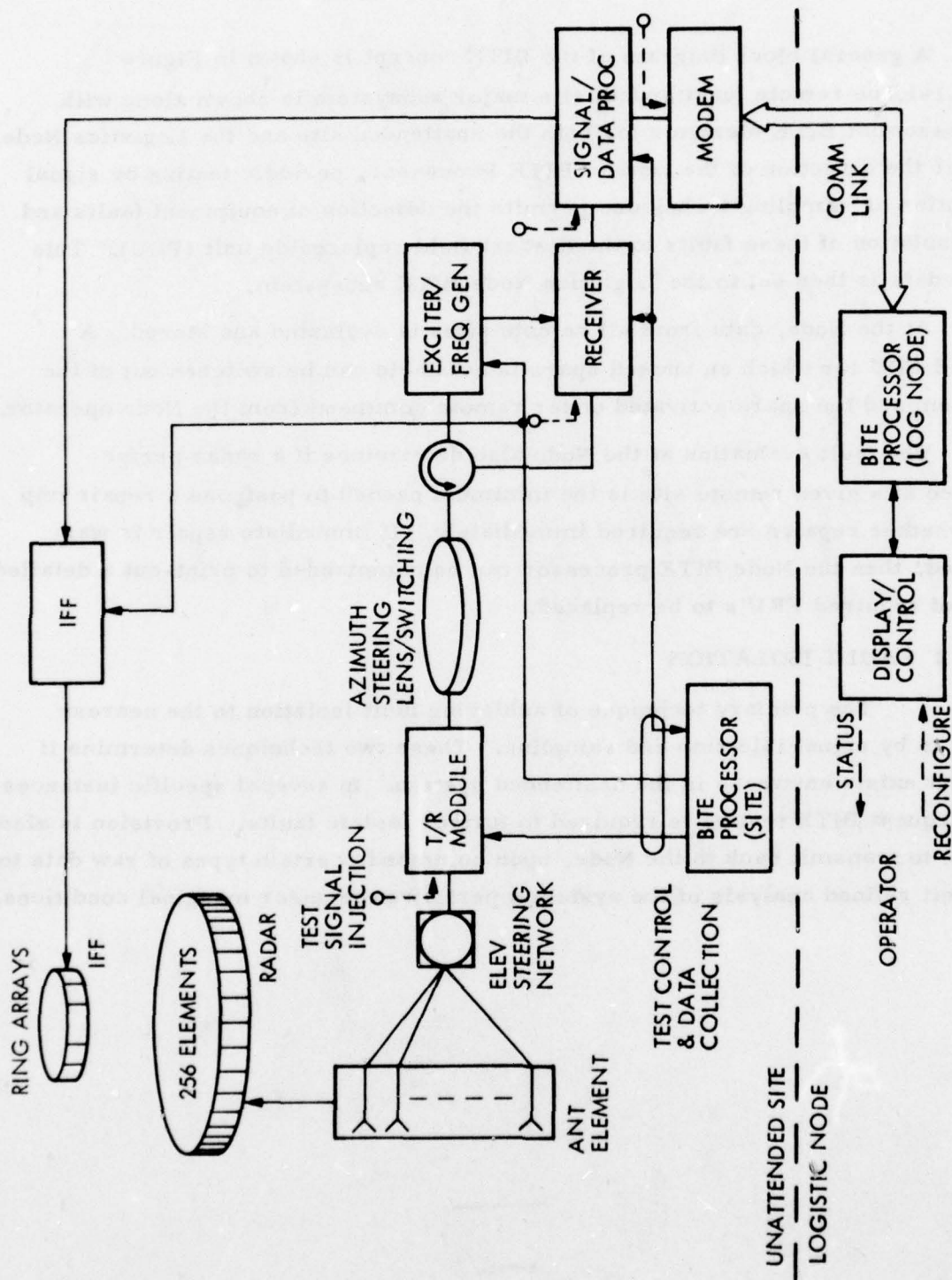
Figure 2.4.1-1 Type A BITE Concept

The number and type of FRU's are shown in Table 2.4.1-1. All of these units, with the exception of the processor, are self-contained modules. These module limits were established to yield a small number of external connection points which must be broken for removal. An additional constraint was to keep a single module's cost reasonably low to reduce the number of expensive units required in the logistics pipeline. The processor FRU's are printed circuit cards (PCB) and consist of common element (CE) processors and several other units such as the radar controller and input/output circuits. It is not clear at this time whether or not an FRU can readily be broken down to a single card. Much depends on the size of the card (Augut or standard size printed circuit) and a more detailed design of the processor itself. In any case, the maximum number of cards per FRU appears to be about two. This investigation will be pursued during the coming year.

The generalized signal injection and sampling points are shown in Figure 2.4.1-1.

The two basic tests which are performed periodically are the transmit-receive solid state module (TRSSM) sampling test and the pilot pulse signal injection test. Both of these tests are performed sequentially (on a TRSSM or antenna element) as the beam scans around the ring array. This relatively low rate of change of sampling position conserves power consumption as the switching logic can be relatively slow speed CMOS.

The following paragraphs describe the tests for the Baseline Configuration. For a detailed description of the Baseline subsystems the reader is referred to the appropriate preceding Sections (2.3.1 through 2.3.5).

a)   Transmitter/Azimuth Lens Test

The transmitter and azimuth lens tests are combined because the operation of the azimuth lens and its switching network is determined entirely through observing each transmitter performance over the 360° scan interval. The first time a transmitter is activated, its operating condition is determined. The subsequent observations of that unit (255) are made for the sole purpose of determining that the lens switch is operating properly for that transmitter unit.

Table 2.4.1-1 Baseline Radar Field
Replaceable Units (FRUs)

FRU	NO.*
1. ANTENNA ELEMENT (INCLUDES RADIATING ELEMENTS, FEED NETWORK, BITE INJECTION AND INTER-CONNECTIONS	256
2. TRSSM	256
3. TERMINATING/TRANSFER/QUADRANT SWITCHES	192
4. INPUT SWITCH DIVIDERS (2ND TIER)	24
5. INPUT SWITCH DIVIDERS (1ST TIER)	3
6. DRIVER TRSSM	3
7. RECEIVER CHANNEL	3
8. EXCITER	1
9. SIGNAL PROCESSOR CE	6
10. DATA PROCESSOR CE	2
11. RADAR CONTROLLER	1
12. OTHER SIGNAL PROC. LRUs	4
13. BITE PROCESSOR	1

*EXCLUDING STANDBY SPARES

The transmitter test determines that the power amplifier is operational and the antenna is being properly loaded. The presence of the three frequency components indicates that the exciter is functioning correctly. This information is obtainable by monitoring the power amplifier bias for the three intervals of the transmitter pulse.

As the monitoring of that unit continues for a total of 256 pulse groups, an operational profile is obtained. Proper operation of the azimuth lens and switch position is indicated when the transmitter is activated for 64 consecutive times and quiescent for 192 consecutive times. Should there be a break in the series of "ons" or an "on" during the period the unit should be quiescent, a problem in azimuth lens/switch system is indicated. The rules which are applied to diagnose the problem to the faulty FRU are shown in Table 2.4.2-1.

Sometimes the data acquired during one azimuth position profile are sufficient to isolate a problem. In other instances more data from related azimuth positions are required. If the additional data have not been received yet, the discrepancies of the current profile (rather than the entire profile), are stored for later use. By reducing the data stored to essentials the total memory storage required diminishes by two orders of magnitude.

The maximum time to detect all fault in the transmitter or azimuth steering is about one-half hour. This maximum would occur if a relatively minor failure (one that essentially degraded one element on one beam) occurred for the last position tester. The large majority of faults would be detected within a few frames, particularly if some type of optimized search such as a "binary" search were used. This search implies testing elements at opposite (180°) ends first then at 90°, then 45°, etc. Thus, failures in input port switch positions (see Section 2.2.4) would be detected early.

Table 2.4.2-1

Azimuth Switch Diagnostic Logic

Observation	Problem
No pulse on single azimuth position for given amplifier, half way through its excitation interval (64), PA's on 31 left and 32 right positions also inoperative during that interval.	Transfer switch input node open.
No pulse for one azimuth position only.	Transfer switch input node shorted.
No pulse on single TRSSM position all other beam unaffected.	Faulty 2nd stage switch FRU. Since eight 2nd stages exist per lens, isolation accomplished by noting which of eight octal groupings contains fault.
No pulse on alternate time intervals during "on" cycle.	Faulty 2nd stage switch FRU. Octal group containing fault determines which of eight 2nd stages is faulty.
No pulse on alternate 4 time intervals.	Faulty 2nd stage switch FRU. Octal group containing fault determines which of eight 2nd stages is faulty.
No pulse on full octal group out of 64.	Faulty 1st stage switch FRU
No pulse for 360°.	Faulty TRSSM or exciter. Receiver test or subsequent TRSSM test needed for further isolation.
Stationary pulse (always there)	Switch counter inoperative (First stage switch FRU).

b)   Pilot Pulse Test

There are three basic receiver channels in the Baseline Configuration each used for a different frequency.   Each receiver channel has 256 front ends residing in the T/R modules.   The receiver front ends feed the main channels via the azimuth steering switch, the azimuth lens and the driver modules.   Since the receiver test is the second basic test, the condition of azimuth lens and switch are known at the start.   Therefore, the elements of interest are the front ends, the TRSSM units and the main channels themselves.

The first step in the test is to check the entire receiver system as a whole by use of a pilot pulse generated at the antenna and observe the characteristics of the signal as received, processed and stored by the signal processor.   The contents of the processors memory are examined and compared with stored correct pattern.   The measured pattern may differ from the stored pattern by degrees ranging from loss of sensitivity to catastrophic failure.

The front ends would indicate problems existing at various azimuth positions whereas, problems uniform over azimuth angle would suggest TRSSM, IF receiver channel, exciter or signal processor.   A signal injected at the input of the receiver main channel allows determination of channel sensitivity and channel operation.   For example, an indication of normal operation at the receiver main channel in an otherwise inoperative channel, independent of azimuth angle, would implicate the appropriate driver TRSSM module.   No response to the injected signal on the other hand would suggest problems in the receiver or signal processor.   The exciter would have been isolated during the transmitter test.   The resolution of the problem at this point requires a processor test.

A successful pilot pulse test over all antenna elements will, in conjunction with the transmitter/azimuth steering test, validate that all FRU's are operative (with respect to a threshold) with the exception of the antenna stacks and BITE processor. The antenna stack are completely passive and should not fail unless damaged by outside sources. It should be noted (from Section 2.3.1) that the pilot pulse is injected at the antenna stack. Thus all of the connectors (which are the most likely source of failure) are included in the test.

The BITE processor is the final arbiter of the system and as such should have the greatest reliability triple on-line redundancy with voting is planned for this function. One malfunction in the BITE would then be quickly detected.

c) Processor Test

On alternate scans, the BITE pilot pulse is not injected. This permits the signal processor output functions to be compared both with and without signal input. The test with a pilot pulse is a signal level in a particular doppler filter and range gate and above a specified threshold. In the presence of noise alone, the measured CFAR thresholds should not exceed preset values.

The processor is a unit that is able to test itself. Its test consists of several steps.

1. It exercises its instruction repertoire
2. It exercises its I/O
3. It executes a sample problem

Failure of any of these tests causes the processor to indicate its difficulty to the BITE processor.

A fault isolated to either the receiver or processor is isolated by injecting a digital test word onto the processor input bus to all CE's. (The A/D converters are located with the receivers). If all CE's process the simulated input correctly, then the fault lies with the receiver channel. If not, then the fault may lie with a CE (assuming one incorrect response), the bus structure, the radar controller or one of the I/O's.

2-132

The I/O's (IFF, BITE and Modem) are checked periodically by exchange of test messages. The buses are continually checked by a requirement for a double error detecting, single error correcting, Hamming data code (see Section 2.3.5). The radar controller is checked by a more detailed exercise under command from the BITE processor.

There may occur certain marginal conditions which defy the capability of simple go-no go testing to detect them. Examples might be an increase in the noise level in certain selective portions of the doppler band or sudden spike-like transients.

To allow for the eventuality of these and other unforseen degradations, the capability to remotely place an operator in the BITE loop has been planned. Upon request from the Node operator, certain types of processor data will be transmitted to the node. The types of data selectible at several range azimuth points shall include:

- FFT spectrum
- CFAR thresholds
- Clutter map
- Alarm output
- Data processor files

d) IFF Test

The IFF subsystem is self checking (see Section 2.5). The IFF performs its own test after every target designation from the radar or every half-hour, whichever occurs first. The IFF BITE status is then inserted into a register accessible for inspection by the BITE processor.

e) Communication Link Test

On a periodic basis (at least once per half-hour), tests messages shall be exchanged between the BITE processors at the unattended and node sites. The successful exchange shall confirm that both the communication link and the BITE processors are operational.

2-133

f) Fault Message

The fault detection and isolation described thus far, provides a performance profile of the radar. This performance data must be deposited in signal processor memory reserved for messages to be sent to the logistics unit. One of the common elements of the signal processor has the task of sending a radar target message train back to the logistics unit periodically. A space in this data train is made available to the BITE processor to deposit its current performance assessment. The BITE data is separated at the logistics node and diverted to the logistics BITE system.

The BITE data is also retained in current form within the BITE memory. This version is made available to a simple CRT display standard at all remote units. The purpose of the display is to provide the repair technician with a means of checking his repair prior to returning to his home base. The display at the remote site is powered off normally to conserve power. The repair technician only turns it on briefly to confirm that his repair was effective.

2.4.3 BITE HARDWARE DESIGN

The requirement to minimize prime power at the unattended site demands that power economy be practiced in the design of the BITE System. Fortunately the availability of a substantial selection of complementary MOS (CMOS) digital logic building blocks drawing on the order of microamperes of current is available. These units have reasonable switching speeds and draw current only during the switching transition, thereby accounting for their low power consumptions. In their static position they present little input loading so that a given CMOS gate may condition many others. The processor is the AMD 9080 militarized microprocessor, chosen for its reliability, low power requirement and adequacy to perform the BITE task.

Figure 2.4.3-1 shows the block diagram of the BITE processing system. The major parts are:

1. Central Processor (3)
2. BITE Program Memory (3)
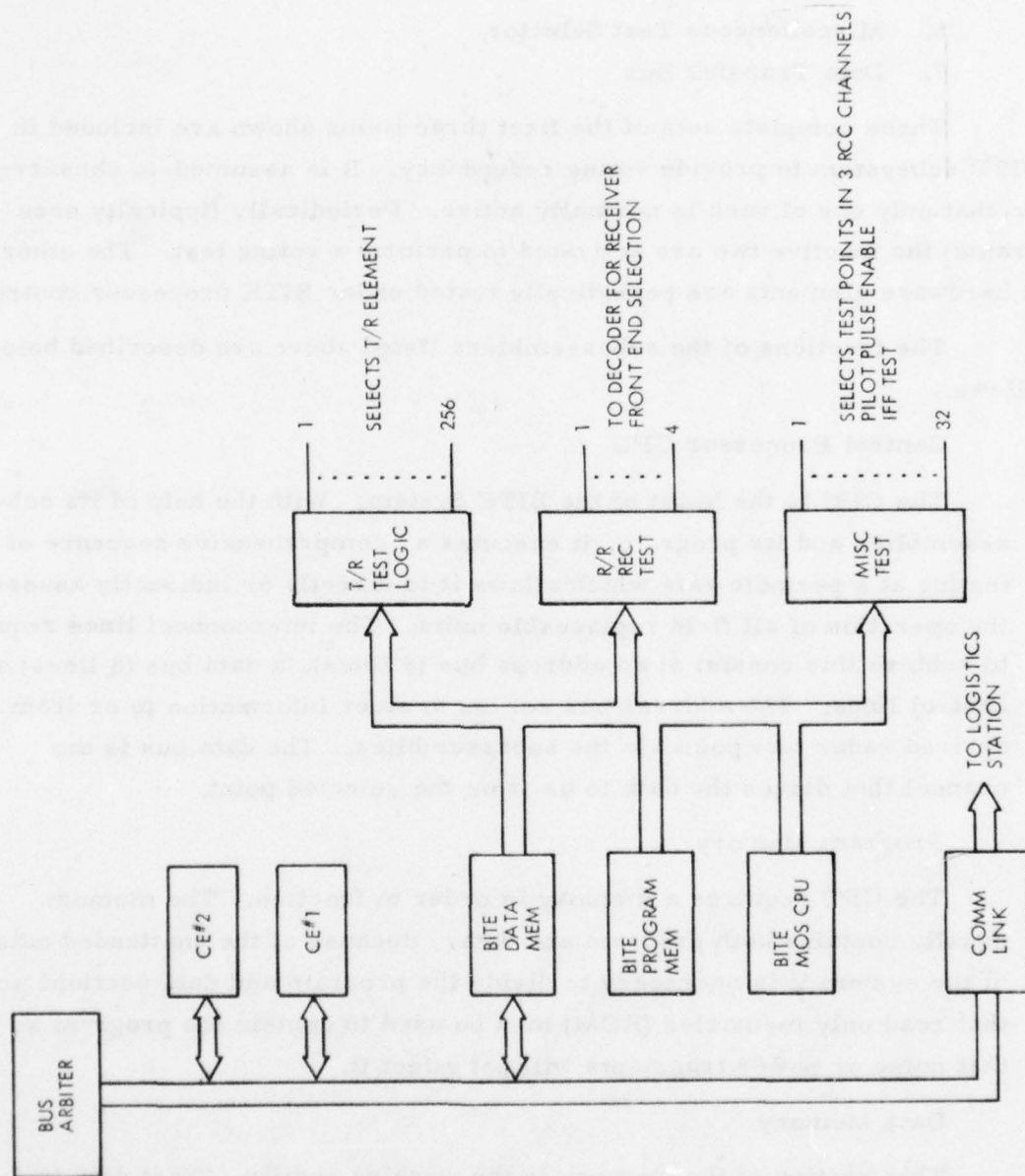
Figure 2.4.3-1 BITE System Hardware General Block Diagram

3.   BITE Data Memory (3)

4.   TR Selector Logic

5.   TR Test Selector

6.   Miscellaneous Test Selector

7.   Data Transfer Bus

Three complete sets of the first three items shown are included in the BITE subsystem to provide voting redundancy. It is assumed-to conserve power, that only one of each is normally active. Periodically (typically once per frame) the inactive two are activated to perform a voting test. The other BITE hardware elements are periodically tested under BITE processor control.

The functions of the subassemblers listed above are described below as follows.

Central Processor CPU

The CPU is the heart of the BITE System. With the help of its subassemblies and its program, it executes a comprehensive sequence of testing at a periodic rate which allows it to directly or indirectly assess the operation of all field replaceable units. The interconnect lines required to achieve this consist of an address bus (8 lines), a data bus (8 lines) and control lines. The address bus serves to steer information to or from the desired radar test point via the subassemblies. The data bus is the channel that drives the data to or from the selected point.

Program Memory

The CPU requires a memory in order to function. The memory usually contains both program and data. Because of the unattended nature of the system it is necessary to divide the program and data sections so that read only memories (ROM) may be used to contain the program so that noise or power transients will not effect it.

Data Memory

This section of the memory is the working section. Test data is stored for analysis and a file of each FRU status is maintained in it. The contents of this file is periodically sent to the logistics unit.

TR Selector Logic

The TR selector logic consists of an 8 bit register and a decoder which allows the eight bit code to activate one out of 256 selection lines. These lines are fanned out to each of the 256 TR modules and serve to make the selected one receptive to the selection command.

TR Test Selector

With the selection of a TR module, the computer places on the data bus, a 3 bit code which is sent to the selected module. This code is interpreted by the TR module as a specific test command of which it recognizes four, the transmitter test and three receiver channel tests. The transmitter test uses the data bus to return transmitter status to the CPU. Each of the three data bus lines contains the status of one frequency component of the transmitter pulse.

Miscellaneous Test Selector

The balance of the test commands are accomplished by the selector labeled miscellaneous selector. This unit, capable of controlling up to 32 selection lines allows the enabling of the injection signals such as the pilot pulse at the antenna and the receiver injection pulses at the receiver inputs. In addition it requests status information from the signal processor and the IFF unit.

The actual generation of the pilot and receiver test pulse is accomplished by the radar controller. The BITE processor merely enables or inhibits the test.

Relay Data To The Logistics Center

The transmission of BITE data to the logistics center relies on the use of the same communication link employed for radar information. Radar information is periodically sent by the signal processor via the modem and phone line. This message is assembled at a selected place in the signal processor memory into a serial data train. A portion of this data train includes BITE status data which the signal processor

2-137

obtains from the appropriate BITE memory area. A specific word in the BITE data serves as a flag to indicate that the latest data is being retrieved. After retrieving the data, the flag is reset and remains so until new BITE data is assembled by the BITE processor.

2.4.4 BITE SOFTWARE

To devise the appropriate BITE software algorithms for testing a radar with the complexity of the A type, time is an important dimension. It is not sufficient to determine that a power amplifier is functional. It must be determined that it is activated for a specified period and deactivated for another specified period. Since there are 256 power amplifier elements, a timing profile for each amplifier showing every azimuth position must be periodically taken. Rather than store such large amounts of test data at once, partial processing at each stage permits a vast reduction in required data storage. Only data which is suggestive of a potential fault is retained.

Fortunately, the highly regular nature of most of the radar system allows relatively simple go/no go tests to be used to accurately isolate a malfunctioning FRU.

Three basic techniques summarize the approach to be used to diagnose the entire radar. They are:

1. Signal injection at key points
2. Signal sensing at key points
3. Computer logical deduction

These tests have been functionally described earlier.

The software performing the diagnostic task consists of basic tests and associated fault isolation. These are:

1. The power amplifier, azimuth lens system
2. Receiver test
3. Signal processor test
4. IFF test
5. Communication link test

These tests are performed in sequence. The sequence is established by the master control program or executive. The executive program is in control of processor operation at all times except when it orders one of the tests to be performed. Two other functions are controlled by the executive, they are the local diagnostic message program and the diagnostic message to the logistics unit. The executive establishes priority of functions and initiates all the tests.

A typical sequence is as follows:

1. Executive calls for Xmtr/azimuth test

   a. Test is performed
   b. If OK, executive is notified
   c. If not, difficulty is reported

2. Executive calls next test if process one is OK. If not, executive incorporates fault data into local and remote diagnostic messages.

3. Next test performed as ordered

   a. If OK, executive is notified
   b. If not, difficulty is reported

4. Tests 3 and 4 are conducted in similar manner with appropriate updates of the diagnostic messages.

5. The local diagnostic message is available by keyboard command for display on a local CRT. This local indicator is used by the repair technician to ascertain that repairs he has made did in fact restore proper operation.

6. At the end of a test sequence the latest diagnostic message is deposited in the common element memory for incorporation into its radar message to the logistics unit.

A block diagram showing the flow of software control between the executive program and the individual test and utility program is contained in Figure 2.4.4-1.
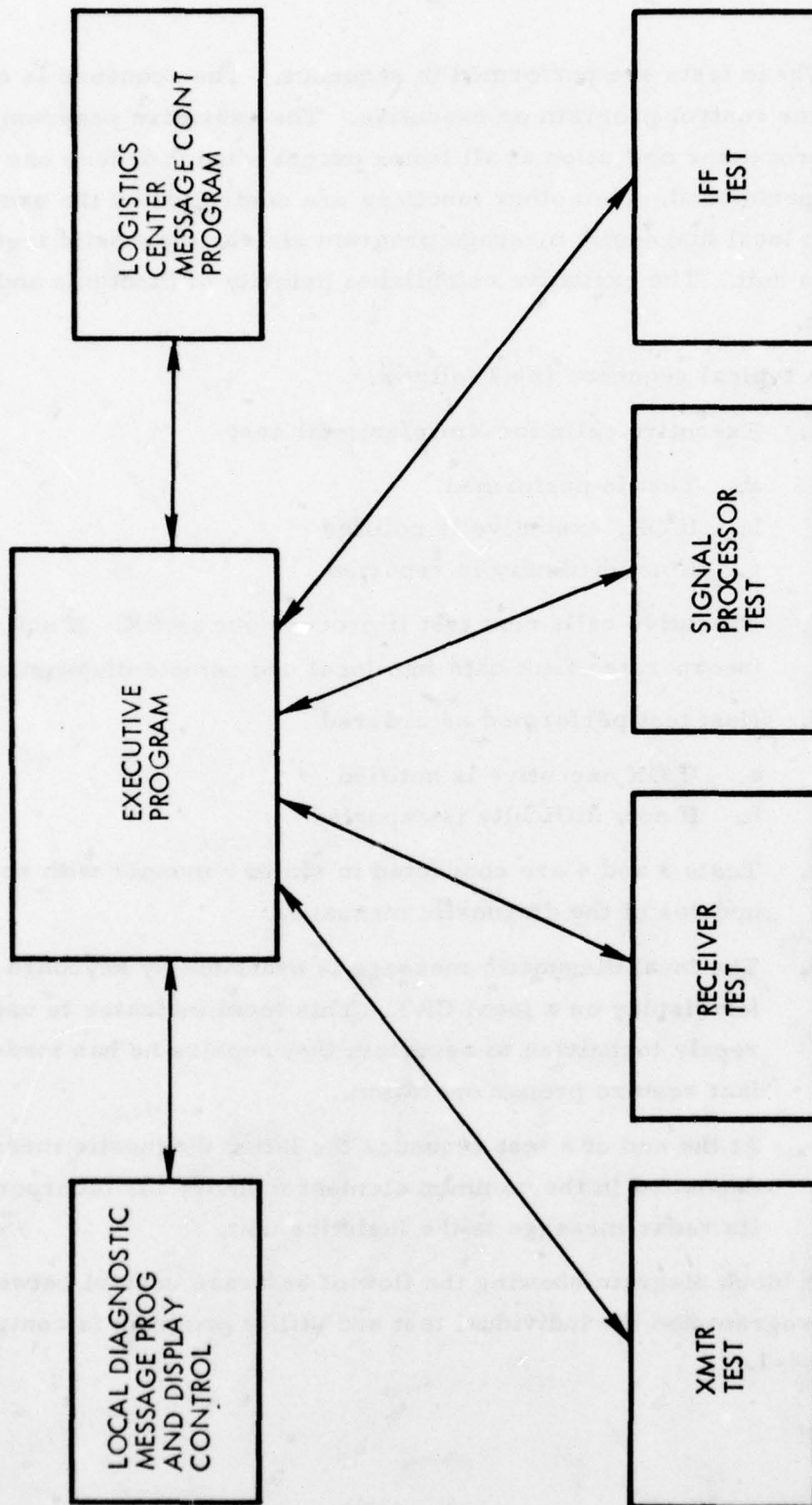
Figure 2.4.4-1   Simplified Software Control Flow Remote Site

2.4.5 LOGISTICS NODE BITE

The logistics site is the gathering point for all BITE information from 12 remote sites. Since the logistic site is a manned site it does not have the environmental or power constraints of the remote site as a result more latitude exists for incorporating increased capability in its equipment.

The CPU is unidentified because the option for its selection should be kept open until a more datailed sizing can be performed. If time is not important at the logistics node as it is not at the remote sites, it is quite possible that the same microprocessor unit will suffice (AMD 9080). The main difference between the two types of sites then becomes the memory complement. This consists of 16K of semiconductor random access memory and a one million byte magnetic disc for non volatile storage.

A display and keyboard is provided which allows maintenance personnel to interrogate the status of any remote site with a message query. The processor obtains the required data from disc storage and displays it on the CRT, performing any required manipulation of the data in the process. The printer provides hard copy of the same information and detailed repair instructions, if desired.

The software in the logistics center serves an entirely different function from that of the remote unit. Tasks to be accomplished include:

1. Data gathering (from modem) & storage
2. Data manipulation
3. Recognition of symbolic representation of FRU's and capability to ascertain effect of given FRU failure on system performance.
4. Alarms when operation drops below minimum acceptable threshold.
5. Capability to command remote switching of available spares of failed FRU's.
6. Capability to receive specialized raw processor data.
7. Processing of data from any site and displaying site performance graphically against a minimum acceptable threshold. Allows anticipation of performance degradation.

2-141

8. Inventories spaces both at repair center and at remote sites, alarming when spaces drop below minimum level.

9. Possibility of performing developmental software functions improving system performance both at logistics center and remote sites.

The logistics node like the remote site requires order in the execution of its functions. As such it also contains an executive program which organizes the performance of tasks and their sequence of occurrence. It responds to external questions posed at the console and calls out the necessary programs to answer the requests.

A simplified block diagram of the logistics node software is shown in Figure 2.4.4-2. The major functional software tasks are indicated.
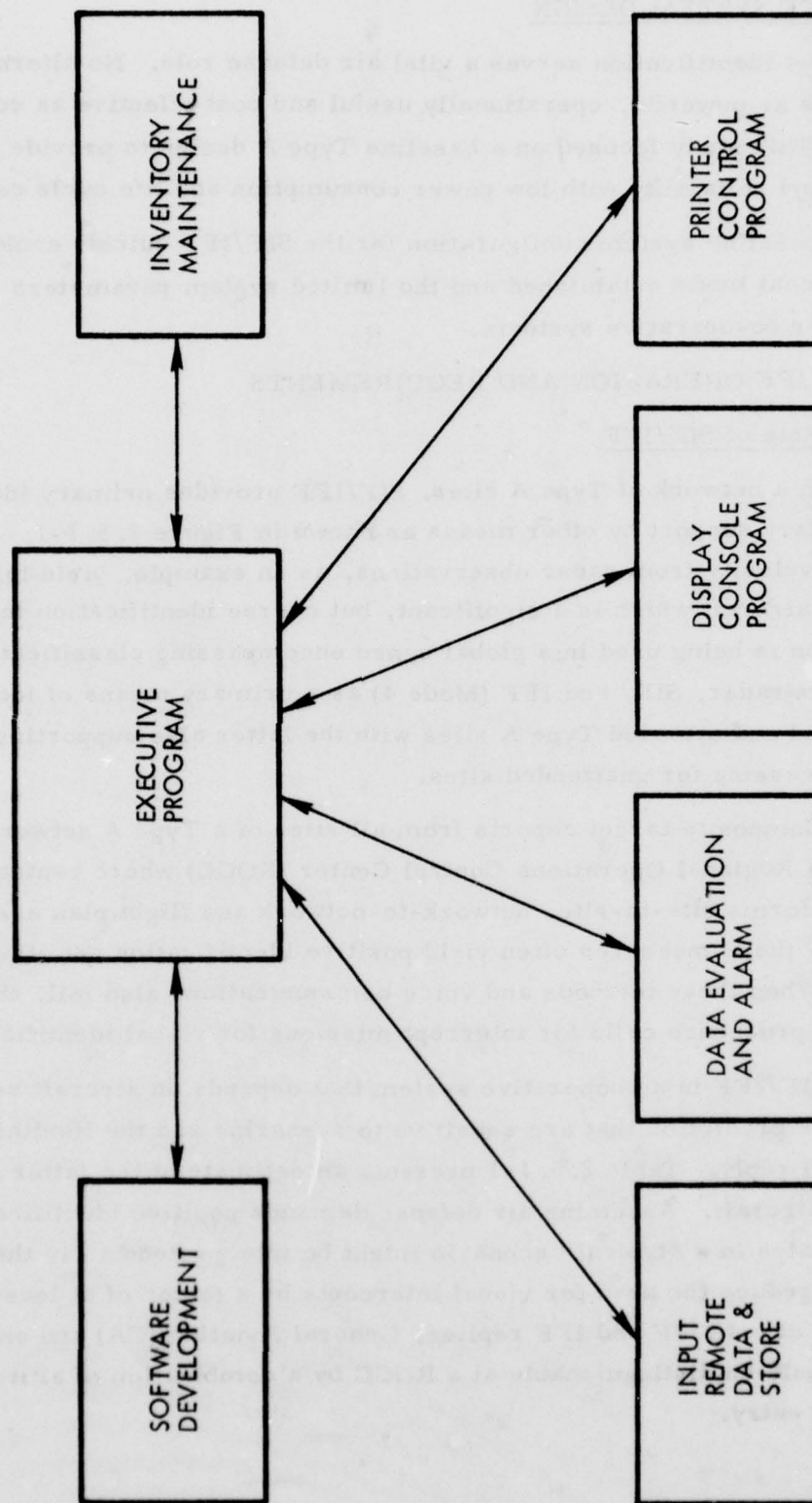
Figure 2.4.4-2   Simplified Software Control Flow Logistics Unit

2.5 SIF/IFF SYSTEM DESIGN

Target identification serves a vital air defense role. No alternative approach is as powerful, operationally useful and cost effective as conventional SIF/IFF. This study focused on a baseline Type A design to provide high performance and reliability with low power consumption and life cycle costs (LCC).

The baseline system configuration for the SIF/IFF quickly evolved from the operational mode established and the limited system parameters options available for co-operative systems.

2.5.1 SIF/IFF OPERATION AND REQUIREMENTS

a) Role of SIF/IFF

In a network of Type A sites, SIF/IFF provides primary identification with secondary support by other means as shown in Figure 2.5.1-1. Estimates of aircraft velocity from radar observations, as an example, yield information on class of aircraft which is a significant, but coarse identification input. Here identification is being used in a global sense encompassing classification. The figure shows radar, SIF, and IFF (Mode 4) as a primary means of identification at unattended and attended Type A sites with the latter also supporting remote Mode 4 processing for unattended sites.

Composite target reports from all sites of a Type A network are relayed to a Regional Operations Control Center (ROCC) where central processing performs site-to-site, network-to-network and flight plan associations. Collectively these measures often yield positive identification not otherwise possible. When these methods and voice communications also fail, then standard air defense procedure calls for intercept missions for visual identification.

SIF/IFF is a cooperative system that depends on aircraft replies and performance prediction that are sensitive to scenarios and the likelihoods that aircraft will reply. Table 2.5.1-1 presents an estimate of the latter for various classes of aircraft. Assuming air defense demands positive identification , those estimates in a "typical" scenario might be interpreted to say that the SIF/IFF should reduce the need for visual intercepts by a factor of at least 10. In the absence of both SIF and IFF replies, General Aviation (GA) and enemy hostile aircraft should be distinguishable at a ROCC by a combination of altitude, velocity, and point of entry.

2-144

RADAR   SIF   MODE 4

UNATTENDED SITE

- TGT DET & TRKG YIELDS FLGT PROFILE & CLASS OF A/C
- SIF/ATCRBS YIELDS ID & ALT
- SUPPORTS SECURE MODE 4

V77-38

RADAR   SIF   MODE 4

ATTENDED SITE

- TGT DET & TRKG YIELDS FLGT PROFILE & CLASS OF A/C
- SIF/ATCRBS YIELDS ID & ALT
- FULL MODE 4 & MODE 4 PROC FOR UNATTENDED SITES

SITE   FLGT   G/A/G VOICE
DATA   PLANS

MANNED ROCC

- MULTIPLE SITE TR CORR & ASSOC
- FLIGHT PLAN (CIVIL & MIL) AND ROUTE ASSOC
- VOICE COMM FOR ATC AND ADC
- INTERCEPT CONTROL

INTERCEPTOR(S)

- FLIGHT INTERCEPT FOR VISUAL IDENT

Figure 2.5.1-1. Means of Target Identification in Type A Network

2-145

Table 2.5.1-1

SIF/IFF Targets

Target Class	Expected SIF Replies	Expected Mode 4 Replies
International Civil Overflights	100% - 3/A and C	None
Local General Aviation	50% - None	None
	40% - 3/A	
	10% - 3/A and C	
Allied and Neutral MIL Overflights	90% - 3/A and C	None
Strategic High ALT MIL	70% - 3/A and C	70%
	20% - 2	
Low ALT MIL	-	-
Enemy Hostile	None	None
Enemy Non-Hostile	50% - 3/A and C	None

b) SIF/IFF Operation

Combined requirements for Type A sites pose a significant design challenge. This has been dealt with at the conceptual level by introducing a very low duty on-demand primary SIF/IFF operating mode. High duty and continuous modes are also available but are expected to be only occasionally used.

In the on-demand mode, the SIF/IFF system remains dormant until local radar processing requests interrogation and processing at designated radar cells. The SIF/IFF system then cycles through SIF modes 1 and 2, SIF/ATCRBS mode 3/A, ATCRBS mode C, and secure Mark XII mode 4. A composite SIF/IFF

target report outputs all replies decoded within the designated radar cell ($\pm 0.5^{\circ}$ x 0.25 nmi). This on-demand mode will be activated only when radar processing declares a target (correlation on 3 of 4 scans) which fails to associate with an existing radar track. This situation will always arise when new targets are first detected and will also occur when reacquiring dropped tracks and reidentifying crossing tracks. Present estimates of worst-case average daily SIF/IFF duty-cycles per site are based on mean times of 30 minutes or 50 cycles per day; each cycle requires about 1 second.

Figure 2.5.1-2, a simplified flow diagram, shows how radar processing attempts to correlate each newly declared radar target with an existing track and, upon failure, initiates a SIF/IFF cycle. Composite radar and SIF/IFF target reports are ultimately forwarded to a ROCC.

The cooperative nature of IFF permits azimuthal resolution well in excess of antenna beamwidth. The baseline design achieves better than 3° resolution with a 13 foot circular array having a 7° beamwidth.

The improvement in resolution is achieved by exploiting the Side Lobe Suppression (SLS) function of present generation transponders as explained in Figure 2.5.1-3. The top sketch shows IFF sum-difference antenna patterns and the transmission of IFF pulses P1 and P3 over the sum channel and P2 over the difference channel with all pulse amplitudes equal. Transponder processing inhibits replies except when P1 levels are 0 to 9 dB above P2 and, in the worst-case, this yields an effective azimuthal resolution equal to the crossover beam-width. In the middle sketch the sum transmission has been reduced to 1/10 the difference level and the crossover beamwidth is narrowed by a factor of 3. For the baseline antenna, this beam sharpening technique achieves a true resolution better than 3° even though the actual sum beamwidth is 7°. An exploded view of the crossover region in the bottom sketch shows interrogation beamwidths for transponder threshold extremes.

Beam sharpening trades off peak transmitter power for resolution and favorably affects antenna size, complexity, reliability, cost, and power consumption.
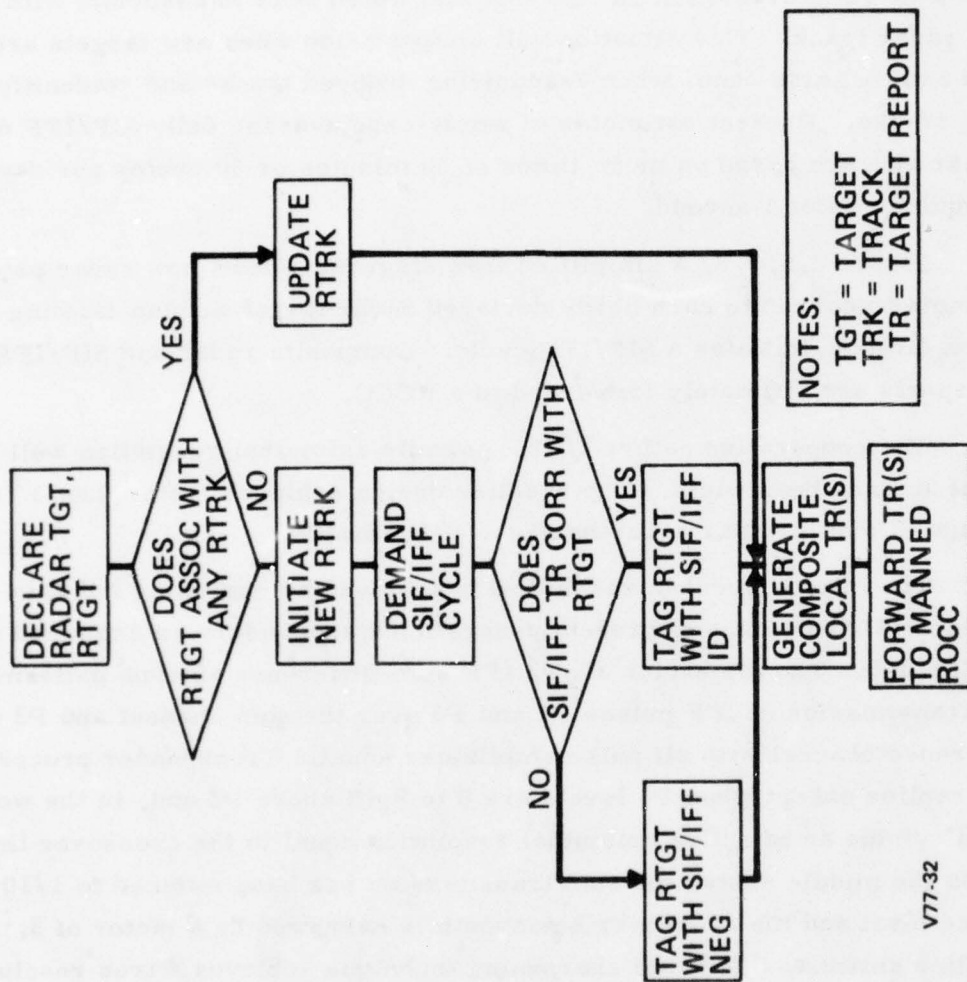
Figure 2.5.1-2. SIF/IFF Operation in Type A Sites

The flowchart contains the following elements:

DECLARE RADAR TGT, RTGT →

DOES RTGT ASSOC WITH ANY RTRK

YES → UPDATE RTRK

NO → INITIATE NEW RTRK → DEMAND SIF/IFF CYCLE →

DOES SIF/IFF TR CORR WITH RTGT

NO → TAG RTGT WITH SIF/IFF NEG

YES → TAG RTGT WITH SIF/IFF ID

GENERATE COMPOSITE LOCAL TR(S) →

FORWARD TR(S) TO MANNED ROCC

NOTES:
TGT = TARGET
TRK = TRACK
TR = TARGET REPORT

V77-32

2-148

Figure 2.5.1-3 Beam Sharpening and
Azimuth Resolution

c) SIF/IFF Requirements

Statement of Work (SOW) goals for the SIF/IFF system are less definitive than for the radar and appropriate measures of quality in performance are not so widely recognized. Definitive requirements have been assumed for operating range and volumetric coverage; implied requirements add range and azimuth resolution and accuracy comparable to the radar; and typical additional derived requirements include ISLS quality, uplink and downlink power budget margins, SIF and IFF processing parameters, SIF operating modes, and others. Table 2.5.1-2 lists major parameters of performance dealt with under this study for Type A.

2.5.2 SYSTEM DESCRIPTION

a) Functional Design

Type A networks have been configured so that every site has autonomous SIF/IFF except for separate Mode 4 encoding and target evaluation equipments (Termed Remote IFF), 28 of which are recommended to support 80 sites. Four would be installed at each of 7 manned sites and switched as available to service requests from approximately 12 dependent sites. Estimates based on expected demand and service durations show that this arrangement has no significant queing problem.

Referring to Figure 2.5.2-1, the SIF portion of Type A operates as follows:

- A SIF/IFF operating cycle begins at the instant a command is received from radar processing to interrogate a particular radar cell ($\pm 0.5^{\circ}$ x ± 0.25 nmi) designated by centermarked range (DMDR) and azimuth (DMDAZ). The equipment is then energized and the ESCAN antenna is steered to DMDAZ. (Between cycles all hardware except interface logic remains dormant.)

- Every SIF/IFF cycle sequentially examines designated radar cells on Modes 1, 2, 3/A, C and 4 and outputs a composite target report.

2-150

Table 2.5.1-2

Summary of Requirements Parameters for Type A

SOW and Implied			Derived Additional	
Parameter	Range of Values		Parameter	Range of Values
Range	1 to 60 nmi		SIF Modes	1, 2, 3
Range Resolution	0.5 nmi		ATCRBS Modes	A, C
Range Accuracy	0.25 nmi		IFF Mark XII Mode	4
Azimuthal Cover	360 degrees		Link Margins*	6 dB
Az Resolution	3 degrees		ISLS Punchthrough Margin	3 dB
Az Accuracy	0.5 degrees		Target Capacity	20 per 3°
Sidelobes*	-20 to -30 dB		Fruit Environment	20,000 per second
Elevation Cover	-10 to +50 degrees			
			Special Processing	SPI, MIL emergency, Hijack, Phantom Detect
Frame Time	4 seconds			
			Interrogation Rate	400 per second max
Prob of FA	1×10^{-6}		Special Capabilities*	ECM Warning ECCM
Prob of Detect	0.95			

*Clarified in later report discussions.
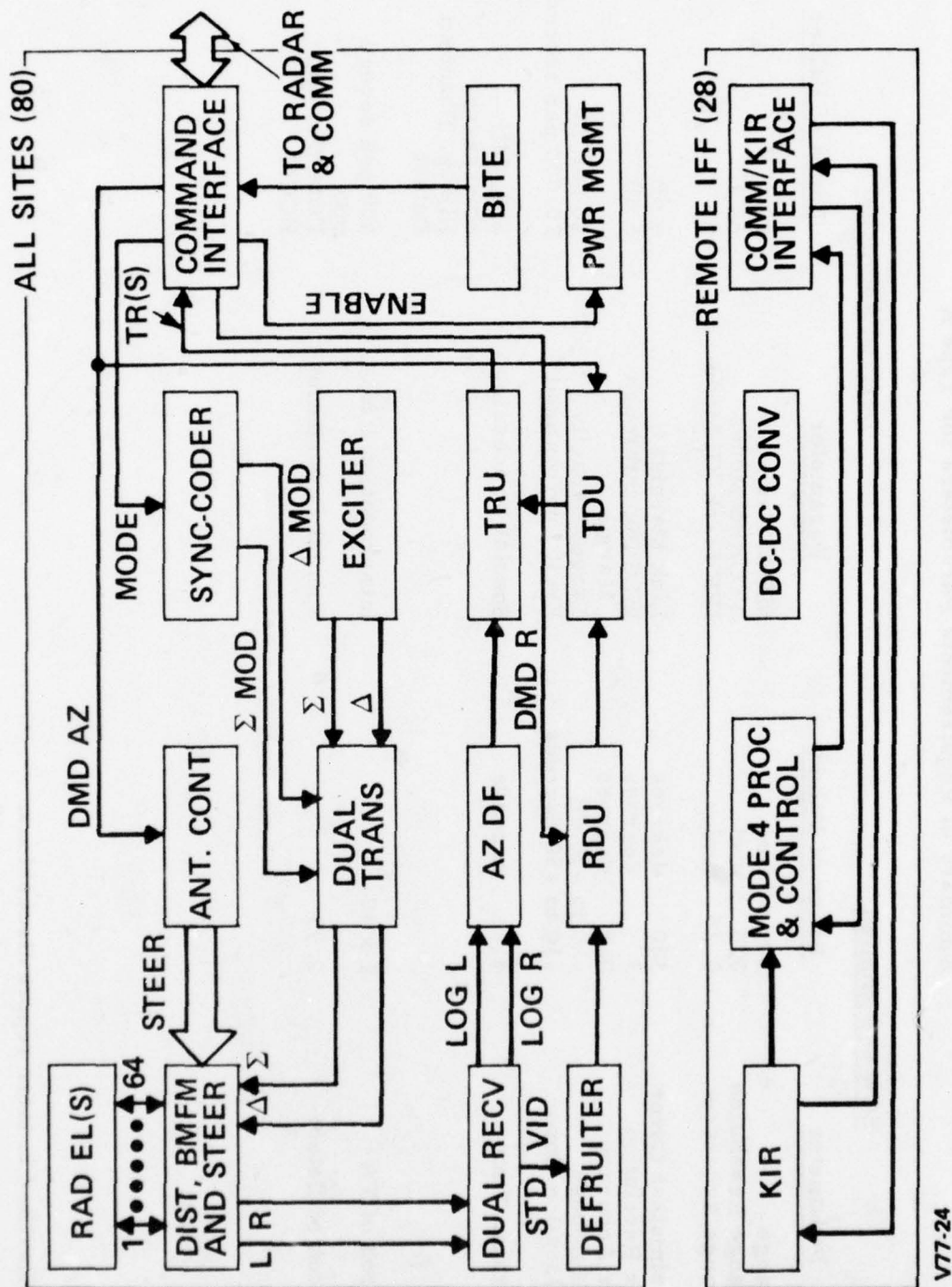
Figure 2.5.2-1. Type A Functional Block Diagram

V77-24

- Each sub-cycle (i.e., single SIF/IFF mode), except Mode 4, is carried out conventionally with P1 and P3 transmitted over a sum beam radiation pattern, and P2 over a difference pattern for ISLS.

- As shown in the figure, the antenna also generates left and right squint beams for amplitude monopulse DF on received transponder replies. Note that in contrast to conventional SIF and ATCRBS systems, the Type A design does not use rotating beams and sliding window detection for azimuthal DF.

- Defruiting, replay detection, target detection, and target reporting functions are carried out in a modern implementation of AN/TPX-42A Techniques.

Mode 4 operation is more complicated and is explained below with reference to Figure 2.5.2-2:

- Functional elements supporting Mode 4 are the SIF/IFF system at all sites (Figure 2.5.2-1), remote IFF equipment (including KIR) at manned sites, and an Interconnecting chain of communication relay links. Figure 2.5.2-2 includes an overview showing Mode 4 interrogations and replies at a local site with two-way data flow to a remote attended site.

- At the beginning of a Mode 4 sub-cycle the local SIF/IFF generates and relays a RQST for a valid Mode 4 code-of-the-day. Receipt of RQST at the remote attended site generates a KIR trigger.

- The KIR responds to the trigger with a realtime pulsetrain which is decoded and then relayed to the requestor as a static digital word.

- At the unattended site a realtime replica of the KIR pulsetrain is recreated and radiated as a Mode 4 interrogation. Measurements on decoded valid replies yield true azimuth and apparent range, the latter in error by an unknown transponder delay (1 of 16) inserted in accordance with information cryptographically buried in the KIR interrogation code. AZ and R data are then relayed back to the attended site.

REMOTE IFF

A. OVERVIEW

MODE 4
INT
RPLY

ATTENDED SITE

UNATTENDED SITES

COMM LINKS

CODE REQUEST
CODE
AZ & REPLY TIME

B. UNATTENDED

RANGE MEAS

IFF CONT

COMM MODEM

AZ PROC

MODE 4 DECODE

CODE STORE

ANT.

R/T

CODER

R

R & AZ

RQST

CODE

AZ

VID

C. ATTENDED

KIR

TGT EVAL

COMM KIR INTER

REAL-TIME PROC

COMM MODEM

TRIG
CODE
REPLY
CORR REPLY

CORR REPLY & AZ

REPLY

R

R & AZ

CODE

RQST
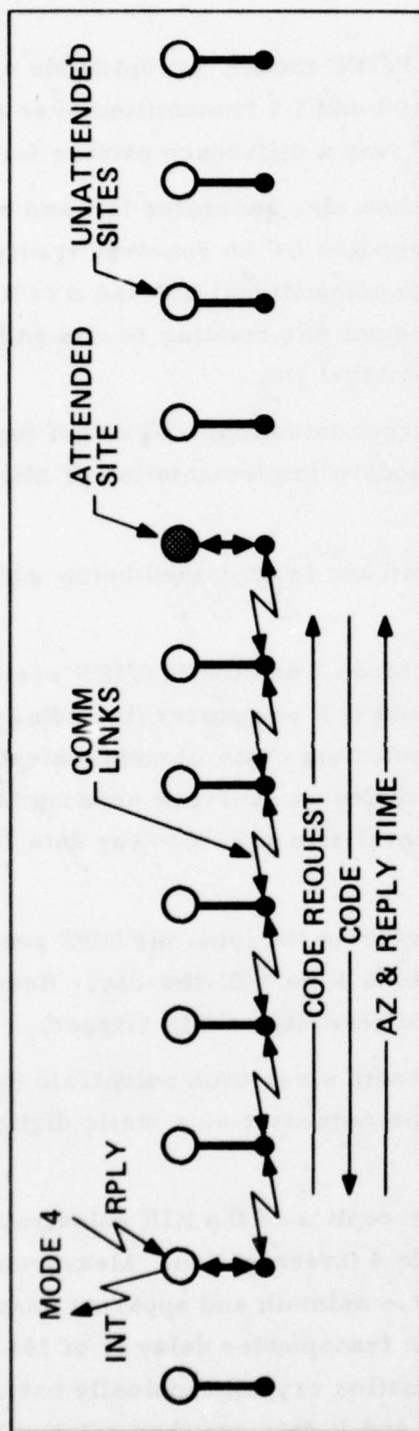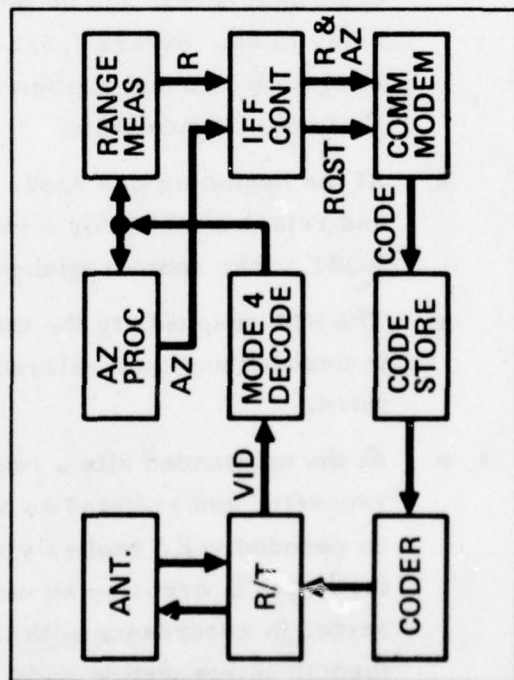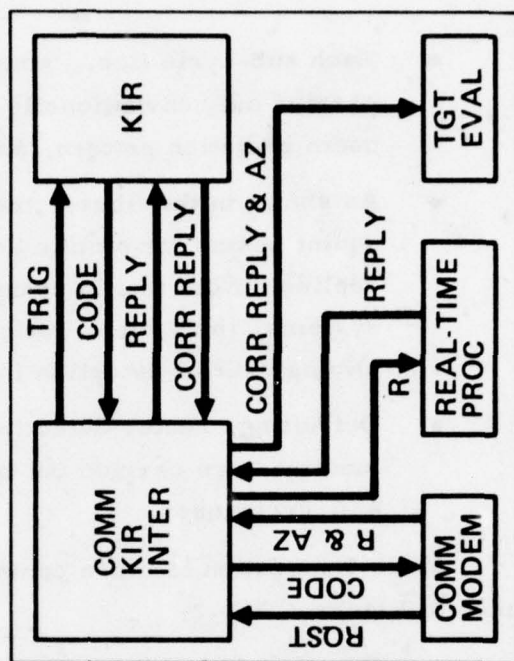
Figure 2.5.2-2. Type A Remote IFF (Mode 4)

- It is essential that the KIR run continuously between the original TRIG and the associated REPLY with no intervening TRIG's, because each new TRIG erases the delay correction corresponding to that buried in the original code. In response to a REPLY input pulse, the KIR outputs a delay-decorrelated range pulse.

- When AZ and R are received at the attended site, a realtime REPLY is generated and the observed time difference between that KIR input and its CORR REPLY output is subtracted from apparent R to yield true R.

- A Mode 4 target evaluator at the attended site accepts 12 to 20 sets of AZ and true R inputs in a full Type A Mode 4 sub-cycle, and generates "friend" and "no observed friend" outputs. With this method of Mode 4 operation, performance is in principle insensitive to communication delays and data rates.

b) Timing

Figure 2.5.2-3 shows how time is allocated in a worst-case SIF/IFF system cycle in the on-demand operating mode. Power transients in this worst-case not unexpectedly consume the larger part (1 second) of a total cycle (1.2 seconds). This is even more so in typical cases.

Allowing 25 milliseconds for each SIF and ATCRBS cycle assumes 10 interrogation sub-cycles of the sort illustrated in Figure 2.5.2-4. Allocating 116 milliseconds per Mode 4 cycle assumes, as shown in Figure 2.5.2-5, the maximum number (20) of challenges with maximum expected separation (400 nmi) between an unattended site and an attended site with supporting KIR and processing.

Although the total time may seem long, it should be stressed that 1.2 seconds is a small fraction (1/1500) of the mean interval (30 minutes) expected between operating cycles.

c) Power Budget

Uplink and downlink power budgets at 1030 and 1090 MHz, respectively, are presented for Type A in Table 2.5.2-1. Transponder minimum triggering

2-155
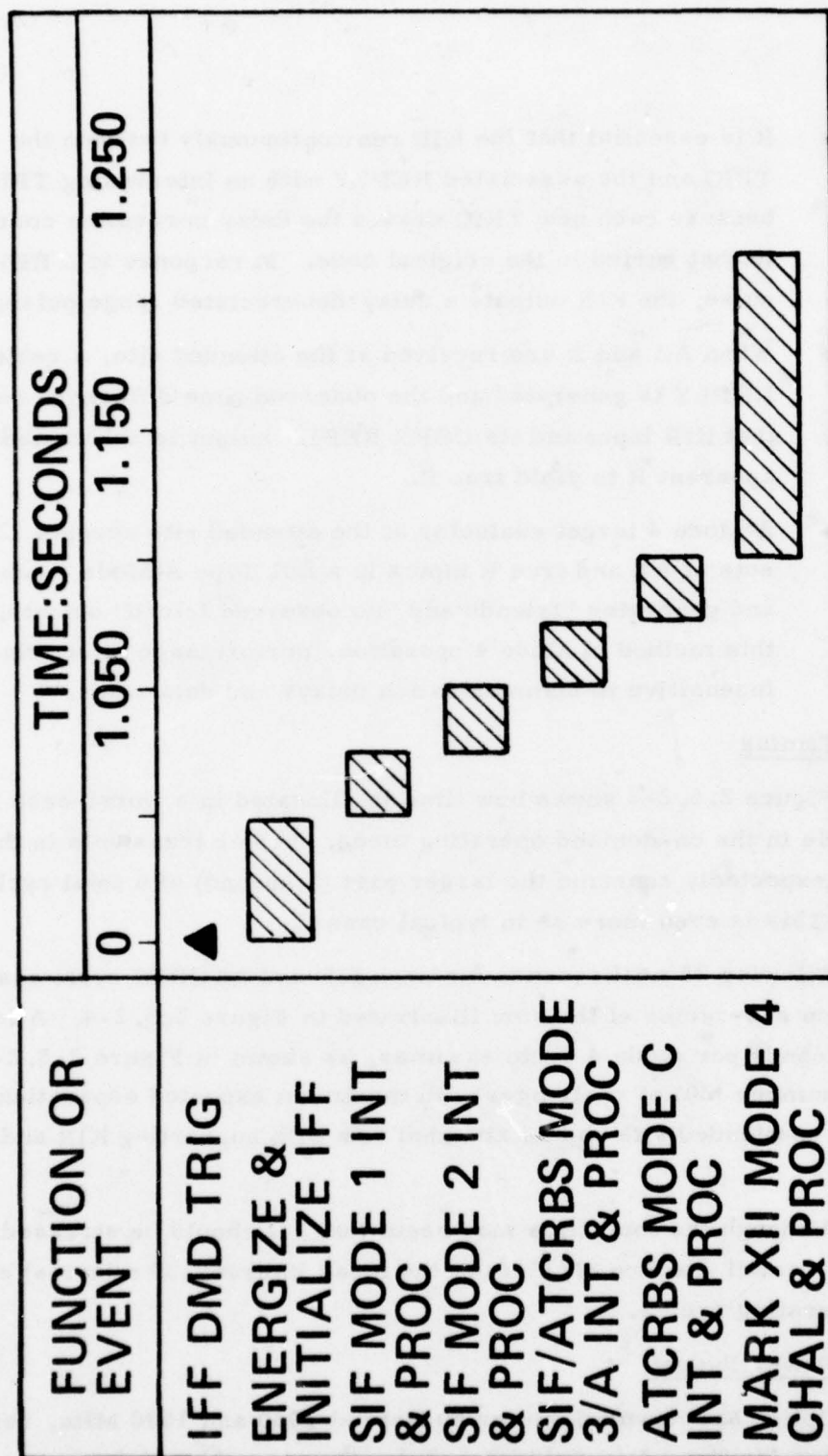
Figure 2.5.2-3. SIF/IFF System Cycles: Type A (Worst Case)
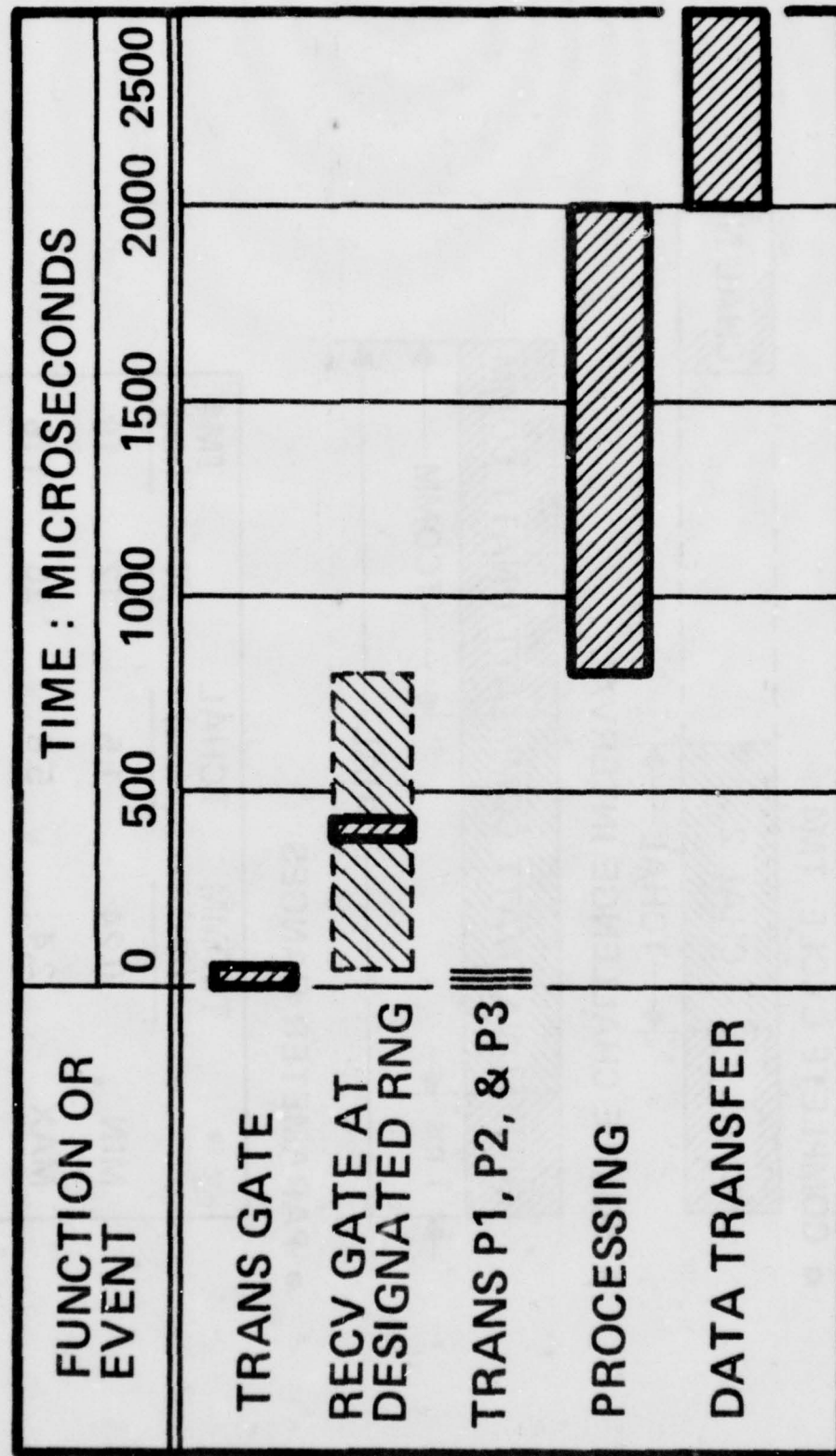
Figure 2.5.2-4. SIF/ATCRBS INT Interval: Type A

2-157

- **COMPLETE CYCLE; TM4**

  CHAL 1 | CHAL 2 — — — CHAL N

  TCHAL

- **SINGLE CHALLENGE INTERVAL**

  INT | UNATT/ATT COMM | ATT/UNATT COMM
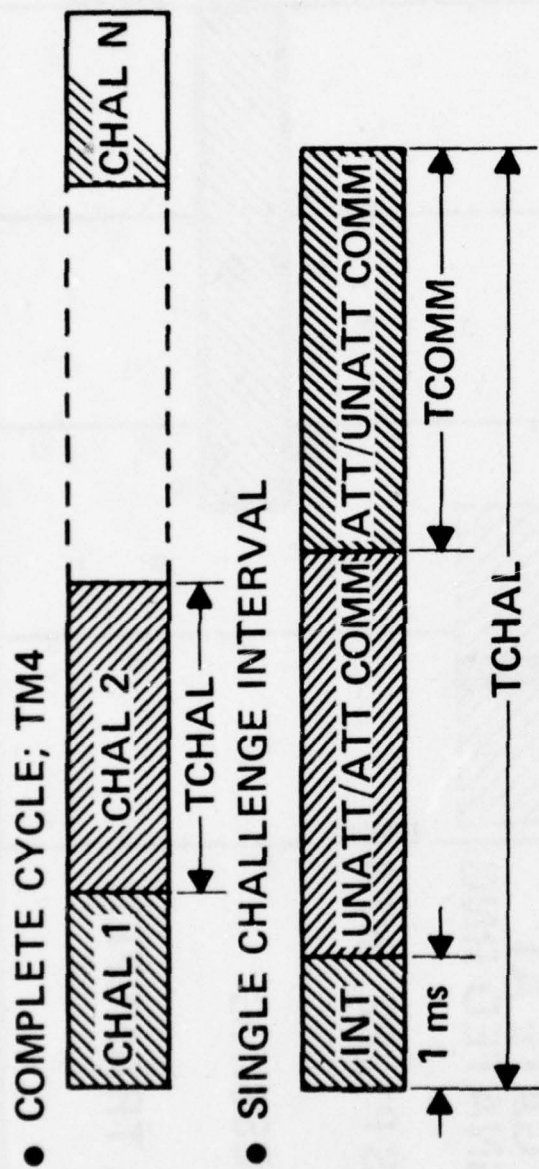
  1 ms — TCOMM — TCHAL

- **PARAMETER RANGES**

	TCOMM (ms)	TCHAL (ms)	N	TM4 (ms)
MIN	0.24	1.5	12	18
MAX	2.4	5.8	20	116
AVE	1.3	3.6	16	58

Figure 2.5.2-5. Mode 4 Cycle: Type A

Table 2.5.2-1

Link Power Budgets: Type A

Uplink

Trans Pwr	+57 dBm
Gnd Ant. Gain (Sum)	+16 dB
Beamsharpening Loss	-6 dB
EIRP	+67 dBm
Free-Space Loss (60 nmi)	-134 dB
A/C Ant. Gain	+2 dB
Recv Signal Level	-65 dBm
Recv Mtl	-70 dBm
Uplink Margin	+5 dBm

Downlink

Trans Pwr	+55 dBm
A/C Ant. Gain	+2 dB
EIRP	+57 dBm
Free-Space Loss	-134 dB
Gnd Ant. Gain (L & R)	+15 dB
Recv Signal Level	-62 dBm
Recv Noise Level	-94 dBm
Snr Reqd for DF	+23 dB
Downlink Margin	7 dB

load (MTL) in the uplink and transponder peak power in the downlink are the 95th percentile values for a mix of military and air carrier transponders based on recent data collected by Lincoln Labs in an extensive experimental program. Average transponders will yield higher link margins. In the downlink the indicated margin understates the true picture because system operation does not require the degree of DF accuracy (0.1°) implicit in the indicated SNR requirement. For Type A, the downlink is overpowered.

Although operating margins are essential to cover operations off boresight, aircraft antenna scalloping and shadowing, lobing losses, and poorer than expected transponder performance, the magnitudes need not be anywhere near the 20 dB margins customary in communications to accommodate fading.

d) Parameters and Performance

Table 2.5.2-2 summarizes major system performance parameters. ISLS punchthrough margin is the difference between P2 and P1 levels received outside the desired interrogation lobe and is clarified below.

Table 2.5.2-2

Type A SIF/IFF System Summary Sheet

System Operating Modes	On-Demand, STD Continuous, Spec Purpose
SIF/IFF Modes	1, 2, 3/A, C, and 4
Azimuth Coverage	360°
Elevation Coverage	-10° to $+50^{\circ}$
Range Coverage	0.5 to 60 nmi
Range Resolution	400 Feet
Range Accuracy	400 Feet
Azimuth Resolution	4°, Average
Azimuth Accuracy	0.3°
Target Capacity	32 in 4° AZ Wedge
Fruite Environment	30,000 per second
ISLS Punch Through Margin	3 dB, min
Uplink Power Budget Margin	+5 dB, Worst-Case

Table 2.5.2-2 (Continued)

Type A SIF/IFF System Summary Sheet

Downlink Power Budget Margin   +7 dB, Worst-Case
SIF Processing Capability   Full AN/TPX-42A
IFF Target Evaluator Capability   Full AWACS

Antenna Performance

The performance parameters, summarized in Table 2.5.2-3, meet or exceed all requirements and go well beyond conventional SIF/IFF designs. Parameter values listed in the table are estimates based on a combination of experimentally determined and calculated results. Azimuthal radiation patterns have been calculated and are shown in Figures 2.5.2-6, 2.5.2-7 and 2.5.2-8.

For cardinal beams (those in directions exactly between antenna radiators), 4-bit phase shifters give precisely the m $\pi/8$ radian incremental phase progression required at the input to the Butler matrix. This leads to faithful reproductions of a specified excitation at the radiators and the excellent uplink radiation patterns shown in Figure 2.5.2-6. For intermediate beams, (intercardinal), the required phase progression of n $\pi/64$ can be only approximated with 4 bit digital phase shifters and this leads to small excitation errors which tend to strengthen the relative level of sidelobes. These "quantization-induced" sidelobes are readily apparent in Figure 2.5.2-7 which shows the directional beam steered to the intercardinal position in which these quantization effects are worst. The left and right squinted receive beams (cardinal) are shown in Figure 2.5.2-8. The relatively strong sidelobes exhibited to the right of the left beam and to the left of the right beam are a consequence of the simple manner in which these beams are derived. These lobes could be suppressed by use of a more complex feed network, but the complication is unwarranted since these lobes occur outside of the narrow interrogation window.

Comparison of the computed patterns with measured patterns show excellent agreement in the main beam region. Over the range of elevation angles between ±30 degrees, the measured beamwidths varied from just under seven degrees to about 7.5°. The causes for the differences between measured and computed patterns is known and their effects can be reduced.

Table 2.5.2-3

Type A SIF/IFF Antenna Performance Parameters

A. Operating Frequencies   1030 MHz (transmit)
1090 MHz (receive)

B. Polarization   Vertical

C. Beam Types   Directional beam and
specially shaped SLS
beam (both steerable)
for transmission, left
and right squinted
directional beams for
reception)

D. Impedance/VSWR   50/1.3 to 1 maximum
in IFF band

E. Power Capacity   500W at 1% duty factor

F. Gain/Beamwidth (Directional Beam)

    o Beamwidth (3 dB) 7° nominal at 15° elev.

    o Interrogation Window 2° - 5° (depending on
transponder) with 6 dB
greater signal trans-
mitted by SLS pulse

    o Directivity   20.8 dBi

    o Losses (Network and Cables)   4.6 dB

    o Gain   16.2 dBi (Nominally 16 dBi)

G. Secondary Lobes and SLS Perf.

    o Worst Case Secondary Lobe   20 dB

    o Average Secondary Lobe Level   26 dB

    o SLS Punchthrough Margin   3 dB minimum

H. Beam Pointing Accuracy   2/3 degree throughout
elevation coverage

I. Elevation Beamwidth   40 degree 3 dB beamwidth
with beam tilted up 10
degrees

J. Steering Speed/Steering
Granularity   20 microseconds/512
steps per revolution

NOTES:
• FREQUENCY IS 1030 MHz
• GAIN REL TO ELEMENT GAIN
• ELEVATION 15°
• BEAMSHARPENING 6 dB
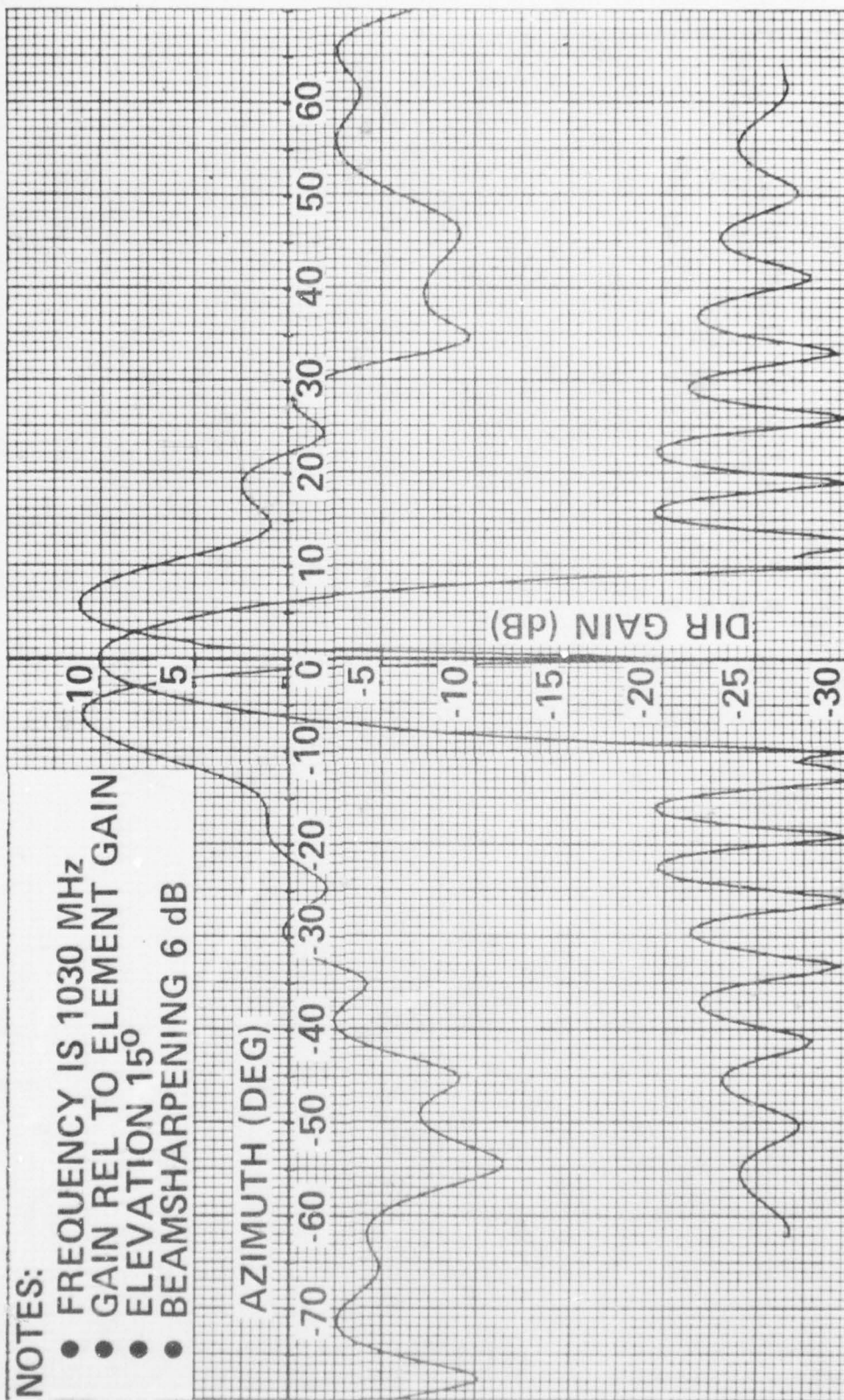
Figure 2.5.2-6. Computed Uplink Beams
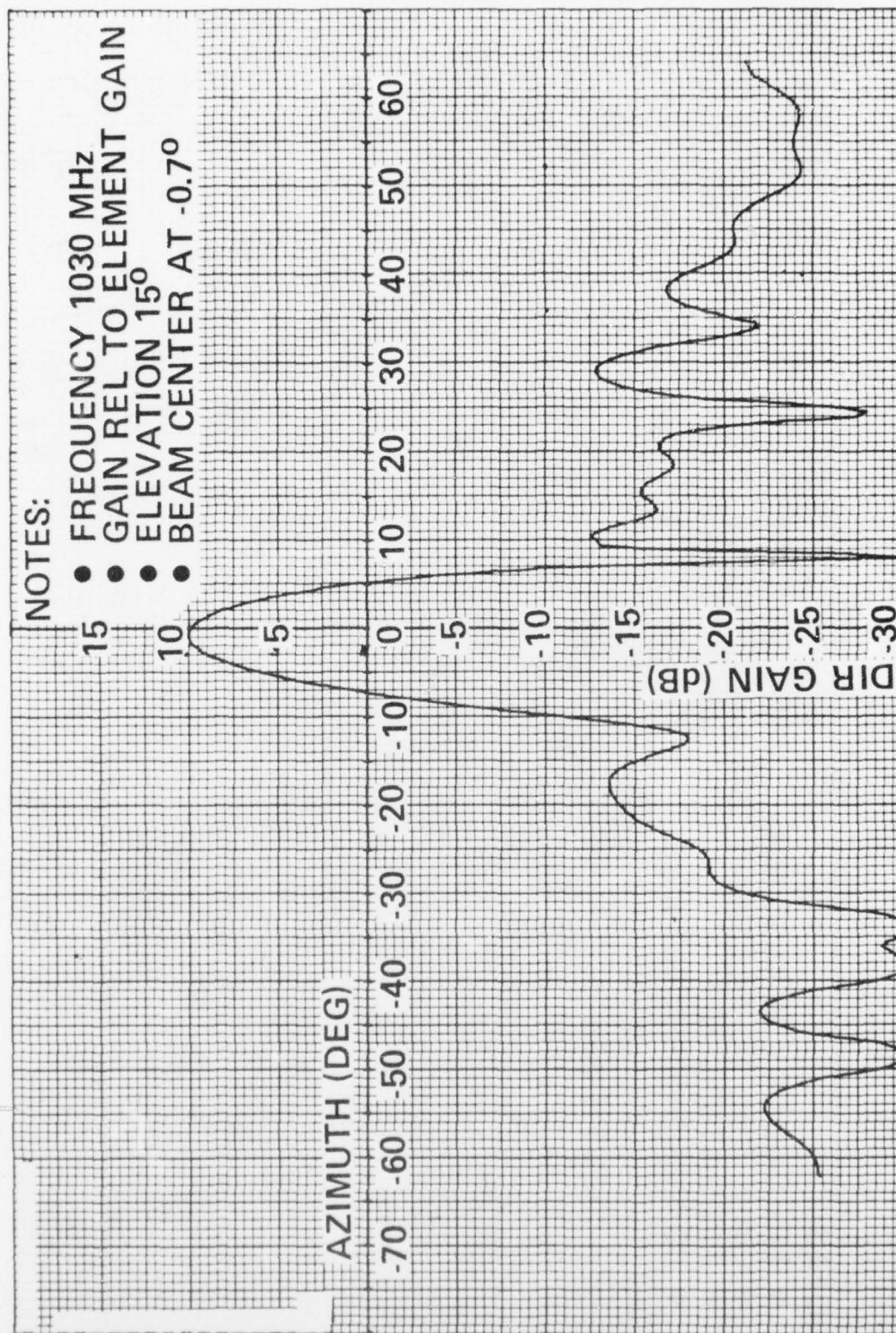
Figure 2.5.2-7. Intercardinal Directional (Uplink) Beam
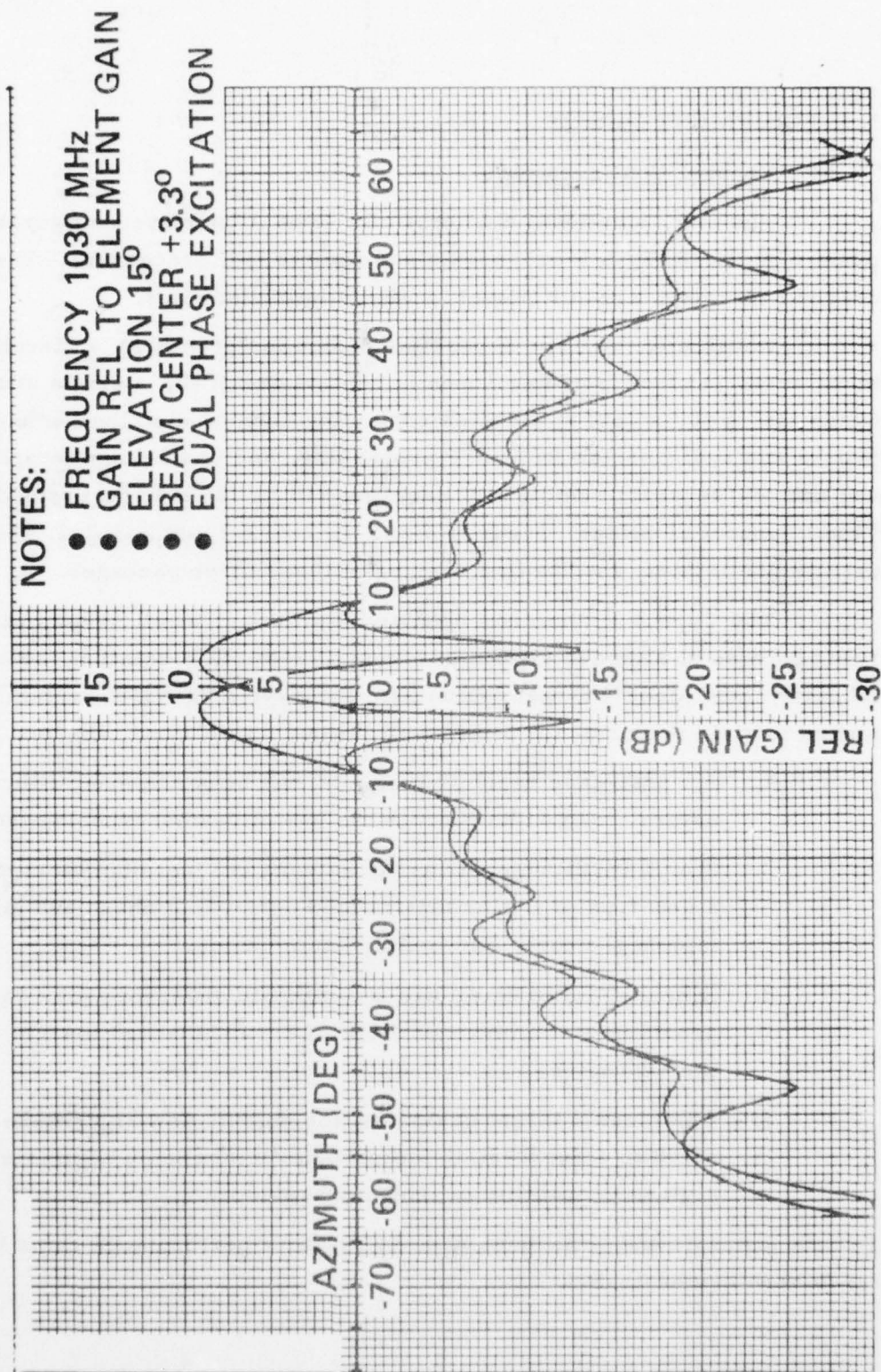
Figure 2.5.2-8. Left and Right Receive Beams

2.5.3 EQUIPMENT DESIGN

a) General Configuration

The main functional elements of a Type A baseline configuration are antenna system, R/T, SIF processing and remote IFF processing. The last is packaged separately with a KIR and located at attended sites.

Physically the Type A baseline design includes: (a) a circular antenna array (13 feet diameter, open in central area); (b) a single additional package (35" x 30" x 25") at all sites containing antenna distribution and steering networks and switches, an R/T, SIF processing, and control and interface hardware; and (c) separate remote IFF packages (18" x 12" x 12") at attended sites (28 total support 80 sites). Figures 2.5.3-1, 2.5.3-2 and 2.5.3-3, respectively, illustrate preliminary mechanical designs of these three packages.

The Type A system has been configured so that all cryptographic gear (KIR) is located at attended sites. In terms of azimuth resolution, beam control, ISLS purity, and Mode 4 target evaluation, the Type A SIF/IFF system has been designed to yield performance levels well beyond conventional designs.

1. A worst-case resolution of 3.5° has been achieved with a 7° natural beamwidth through the use of beamsharpening techniques.

2. The SIF/IFF circular array antenna (13 feet diameter) employs a new type of Butler matrix feed permitting phase and amplitude tapering, nearly eliminating beam coning.

3. Special ISLS patterns are a composite difference plus cardiod, providing a minimum of 3 dB ISLS punchthrough margin even in the aft region.

4. The mode 4 target evaluator implements new algorithms providing a 100 to 1 decrease in the probability of enemy admissibility for a given probability of friend acceptance.

All of the concepts and techniques underlying these performance gains have already been demonstrated.

152" - 64 ELEMENTS

7"
APPROX

0.65 λ

ELEMENT IN
CORNER
REFLECTOR
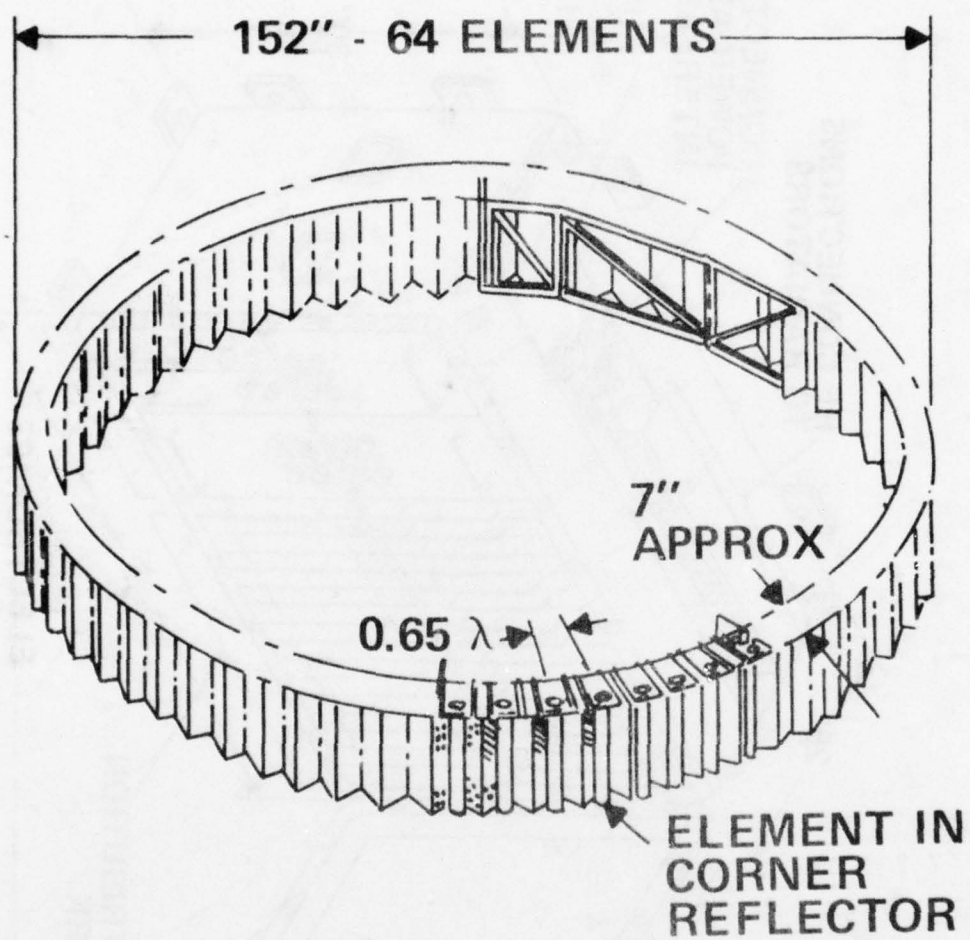
Figure 2.5.3-1. Type A SIF/IFF Circular Array

2-167

RF CONNECTIONS
TO RADIATORS

CONNECTIONS FOR
POWER AND
INTERFACE SIGNALS

PUSH FOR LED
ACTIVATION
(BITE)

30"

25"

35"

ELECTRONICS

RF DISTRIBUTION
NETWORK

Figure 2.5.3-2. Type A SIF/IFF Package: All Sites
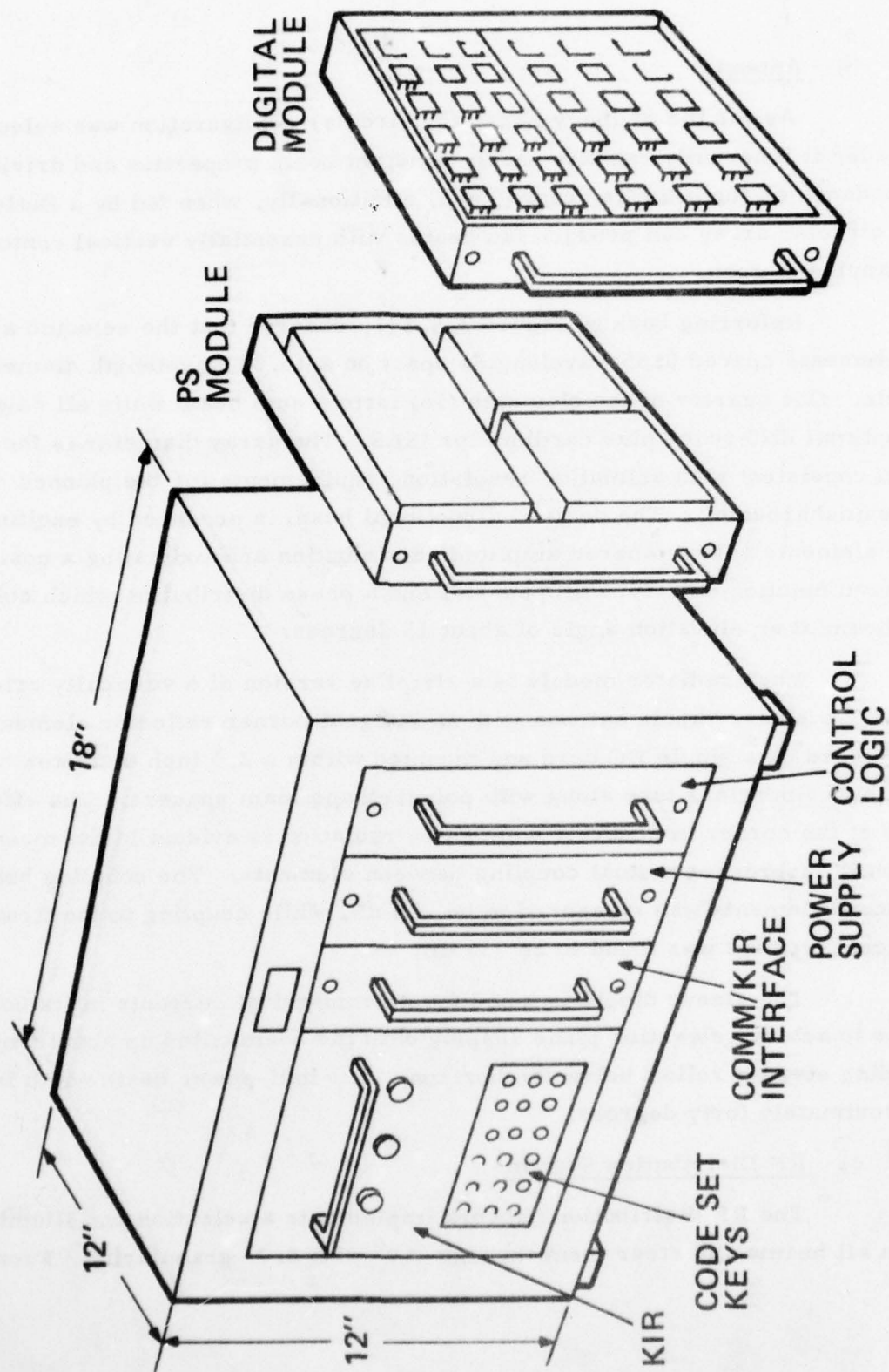
Figure 2.5.3-3. Type A Remote IFF Package

b)   Antenna

As for the primary radar the circular configuration was selected because it inherently exhibits nearly constant beam properties and driving-point impedance as the beam is scanned and, additionally, when fed by a Butler matrix the circular array can produce fan beams with essentially vertical contours for all angles of scan.

Referring back to Figure 2.5.3-1, observe that the selected array has 64 elements spaced 0.65 wavelengths apart on a 13.31 wavelength diameter circle. One quarter of the elements (16) form a sum beam while all 64 generate an optimal difference plus cardioid for ISLS. The array diameter is the minimum consistent with azimuthal resolution requirements for the planned degree of beamsharpening. The desired directional beam is produced by exciting sixteen elements with a tapered amplitude distribution approximating a cosine-squared function on a 10.5 dB pedestal and a phase distribution which collimates the beam at an elevation angle of about 15 degrees.

Each radiator module is a stripline version of a vertically oriented full-wave sleeve-dipole antenna with an integral corner reflector element; both are etched on a single PC card and mounted within a 2.5 inch diameter by 15 inch high fiberglass tube along with polyurethane foam spacers. The effectiveness of the corner in reducing wide angle radiation is evident in the manner in which it suppresses mutual coupling between elements. The coupling between adjacent elements was measured to be -26 dB, while coupling to the first non-adjacent element was found to be -36 dB.

The sleeve dipole is tuned for asymmetrical currents in its component arms to achieve elevation plane shaping with the beam tilted up about ten degrees, yielding steeper rolloff below the horizon. The half-power beam width is approximately forty degrees.

c)   RF Distribution System

The RF distribution network implements a selection and illumination to form all beams and steer them through 360° with 0.7° granularity. From earlier

discussions recall that the beams of interest are sum for uplink interrogation, difference plus cardioid for uplink ISLS, and left and right for downlink amplitude monopulse reception.

In the simplified block diagram of Figure 2.5.3-4, 16 sectoring switches (SP4T) are grouped so that the four outputs from each are connected to elements spaced by 90 degrees and are thus able to excite any one of the 64 sets of 16 contiguous array elements spanning a continuous 90 degree sector (shown in figure exciting elements 1 through 16).

With all phase shifters set to zero, the RF distribution network provides excitations at the switch inputs which form a sum pattern directed along the central radius of this group of elements. To achieve this result: (a) both amplitude and phase distributions must exhibit even symmetry; (b) amplitude must be tapered to achieve the desired side lobe level; and (c) phase must be controlled to collimate the beam. In concert, the Butler-matrix, collimating line lengths, and input power divider satisfy all of these requirements.

It is a property of the 16 x 16 Butler-matrix that when a linear phase ramp with incremental phase shift between adjacent terminals equal to $\pi/8$, is introduced at the Butler-matrix input terminals, then the original set of outputs is reproduced exactly except that each output now appears at the next higher numbered terminal and the output originally at the 16th output terminal appears at the first terminal with a 180 degree phase change. This enables the Butler-matrix and a set of phase shifters to act as a commutation switching matrix, in effect able to rotate a distribution about its output. Thus, as shown in Figure 2.5.3-4, if the output of sector switch 1 is relocated from array element 1 to element 17 and if, as is indeed the case, the path lengths through the sectoring switches differ by 180 degrees for outputs to elements in adjacent quadrants of the array, then the original sum pattern will now appear radiating in the direction midway between elements 9 and 10.

The 64 cardinal beam positions are the centers of 64 coarse steering intervals. To obtain the required 512 beam positions requires eight fine steering positions within each coarse steering interval. Eight equally-spaced fine steering positions are achieved approximately with incremental phase differences which are multiples of $\pi/64$.

2-171

SUM PATTERN BEAM DIRECTION
(ALL PHASE SHIFTERS SET TO ZERO)

SEGMENT OF THE
64-ELEMENT
CIRCULAR ARRAY

64
EQUAL-LENGTH
CABLES

16 SP4T
SECTORING
SWITCHES

16 x 16
BUTLER MATRIX

16 4-BIT
PHASE SHIFTERS

COLLIMATING
LINE LENGTHS

16:1 POWER DIVIDER
(TAPERED DISTRIBUTION)

SIGNAL INPUT
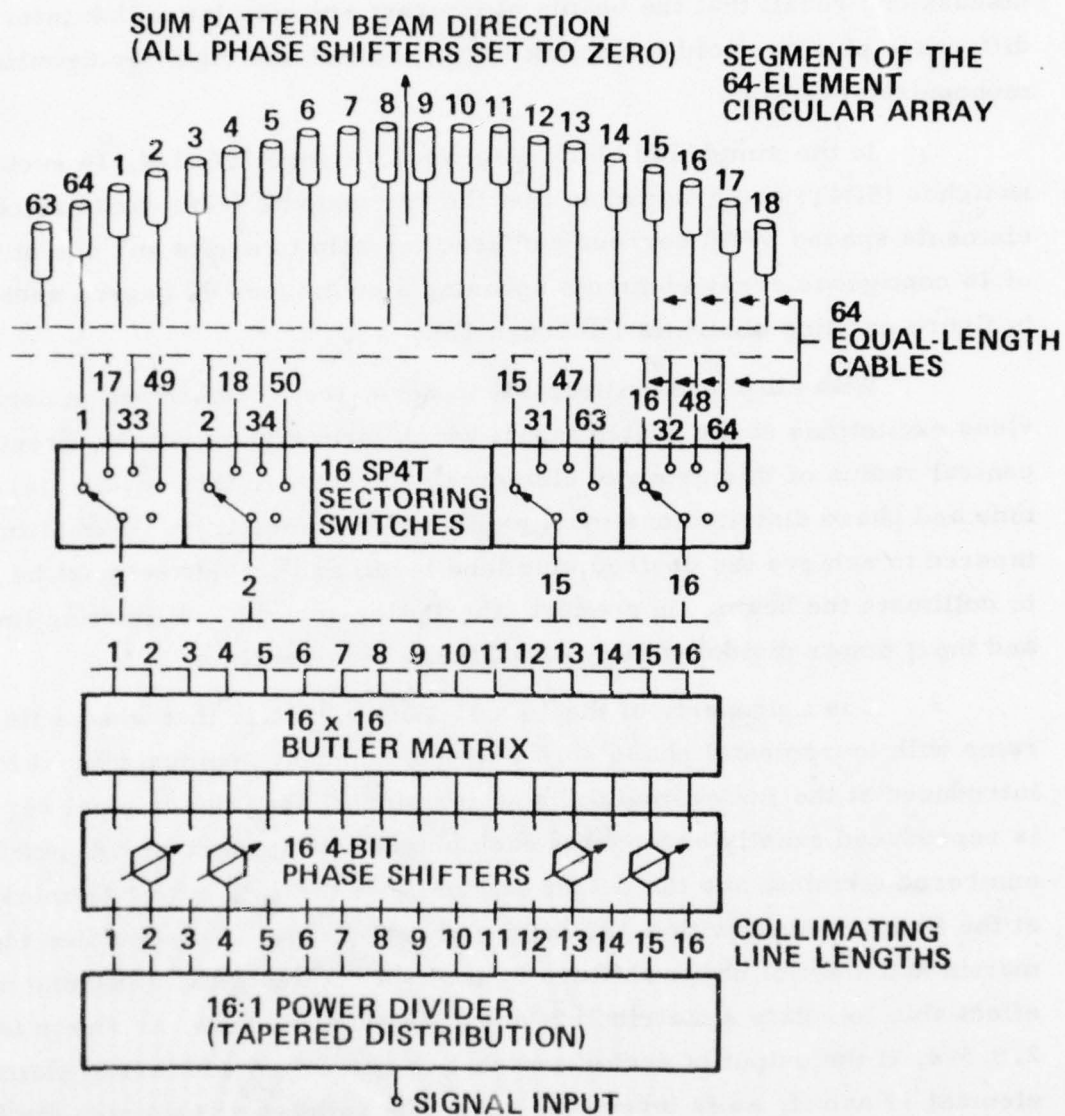
Figure 2.5.3-4.   Sector-Switched Butler Matrix RF Distribution Network

d) ISLS Pattern Generation

An ideal ISLS pattern is one which does not inhibit valid replies in the main beam sector of the directional (sum) pattern and inhibits all other replies. When a difference pattern is used to perform the ISLS function, the problem often encountered is that the difference pattern does not provide adequate backlobe coverage. With a separate omni-antenna to perform the ISLS function, there is usually adequate backlobe coverage but valid replies may sometimes be inhibited as a result of mismatched elevation plane patterns and/or multipath effects.

The AIL design combines the best features of both the difference and omni solutions to the ISLS problem. As shown by Figure 2.5.3-5, the sixteen elements in the active or forward quadrant generate a difference pattern which by itself, would satisfactorily perform the ISLS function in the forward quadrant. The remaining 48 elements, comprising the "backfill" sector, are excited with equal amplitudes and phases to generate a cardioid pattern which provides adequate backlobe coverage throughout the 270 degree backfill region. The two patterns are then combined to form the composite ISLS pattern shown in the sketch. Thus, all sixty-four elements of the array effectively contribute to the ISLS pattern.

The sum pattern and the difference pattern component of the ISLS pattern share a common aperture. This permits minimal displacements between the two radiation phase centers for all radiation angles throughout the forward sector. As a result, the elevation plane patterns associated with the ISLS and sum beams will be closely similar, and the ISLS pattern will provide satisfactory sidelobe coverage outside the sum pattern main beam for all elevation angles. Further, since the ISLS patterns null coincides with the sum pattern main-beam direction, small differences in elevation plane patterns will not inhibit any desired target replies. Thus, the ISLS pattern provides a clean reply sector.

e) Receiver/Transmitter (R/T)

The R/T is a single FRU comprised of a dual transmitter, dual receiver, and a video processor.
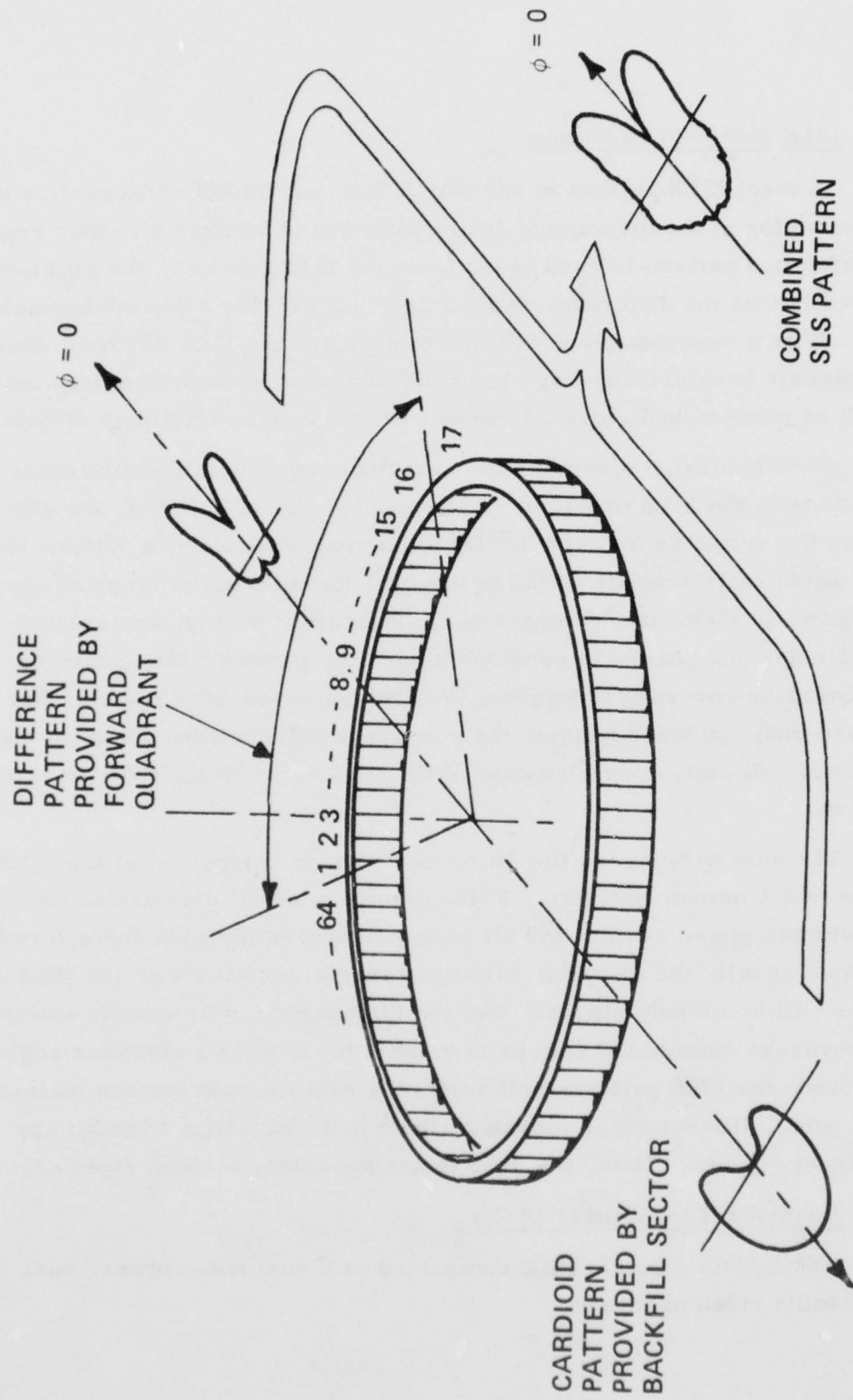
Figure 2.5.3-5. Generation of Optimum ISLS Pattern

The transmitter consists of two identical solid state transmitters with ISLS switches and an automatic fast switchover relay. The switching operation also flags a transmitter failure at the SIF/IFF BITE reporting unit. Redundancy was necessary to meet reliability requirements.

Each transmitter is an RF pulse amplifier operating Class C and fabricated in stripline. Collector voltages are kept low (40V) for increased reliability. Also, Class C mode of operation draws negligible power during key up period. An RF exciter in this LRU uses a crystal oscillator at 103 MHz feeding 5X and 2X multiplier stages to provide +15 dBm at 1030 MHz. This output feeds the transmitters and dual receiver mixers.

A dual receiver provides left and right channels to support amplitude monopulse DF; monopulse processing is implemented in a separate Video Processor.

The receivers implement conventional high reliability designs and operate at low voltage with low power consumption. Each receiver channel consists of a preselector for 1090 MHz, a mixer-preamp and a 60 MHz log IF strip. The log strip uses Plessy IC elements and provides a dynamic range greater than 60 dB. Since monopulse angle information is determined by the relative outputs of the receiver, the receiver must track within 1 dB over the dynamic range to meet azimuthal accuracy requirements.

Video processing function consists of pulse width preservation (PWP) and video GTC. This is done on both right and left channels. Summed (R&L) channel digitized video then is sent to the digital processor for determining the target range, SIF code, M4 replies.

Video processing functions are listed below:

- Monopulse Azimuth detection
- Modulation of transmitter
- BITE signal generation and fault detection

2-175

- Switchover control
- R/T I/O interface
- Pulse Width Preservation (PWP) and Video GTC

f) SIF/IFF Processing

This subsystem consists of an RDU/DEFRUITER and a TDU/TRU/ CODER. Both are all digital plug-ins made up of lower level plug-in PC cards. The RDU/DEFRUITER contains the following functions:

- Defruiter
- Reply detector
- Azimuth processor and test
- Transfer electronics

The TDU/TRU/CODER, built around a microprocessor, contains the following functions:

- MPU - Microprocessor unit
- Memory
- DMA - Direct memory access hardware
- CODER/SIF

Each of these FRU's is designed to accept an additional unit for Mode 4 when deployed in Type B sites.

SIF processing incorporates all of the field-proven AN/TPX-42A techniques (floating range bins, finger-gating, phantom elimination, full MIL emergency, etc.) in a new mechanization using a microprocessor. IFF processing (mode 4) embodies new target evaluation algorithms developed for AWACS.

g) Power Consumption

The SIF/IFF prime power is distributed by a power management FRU.

This FRU is basically a power supply with IDLE and ON modes. During idle, it supplies voltage to keep alive circuits, and when ON, full operating power is gradually turned on. Power is reduced immediately after each SIF/IFF operating cycle.
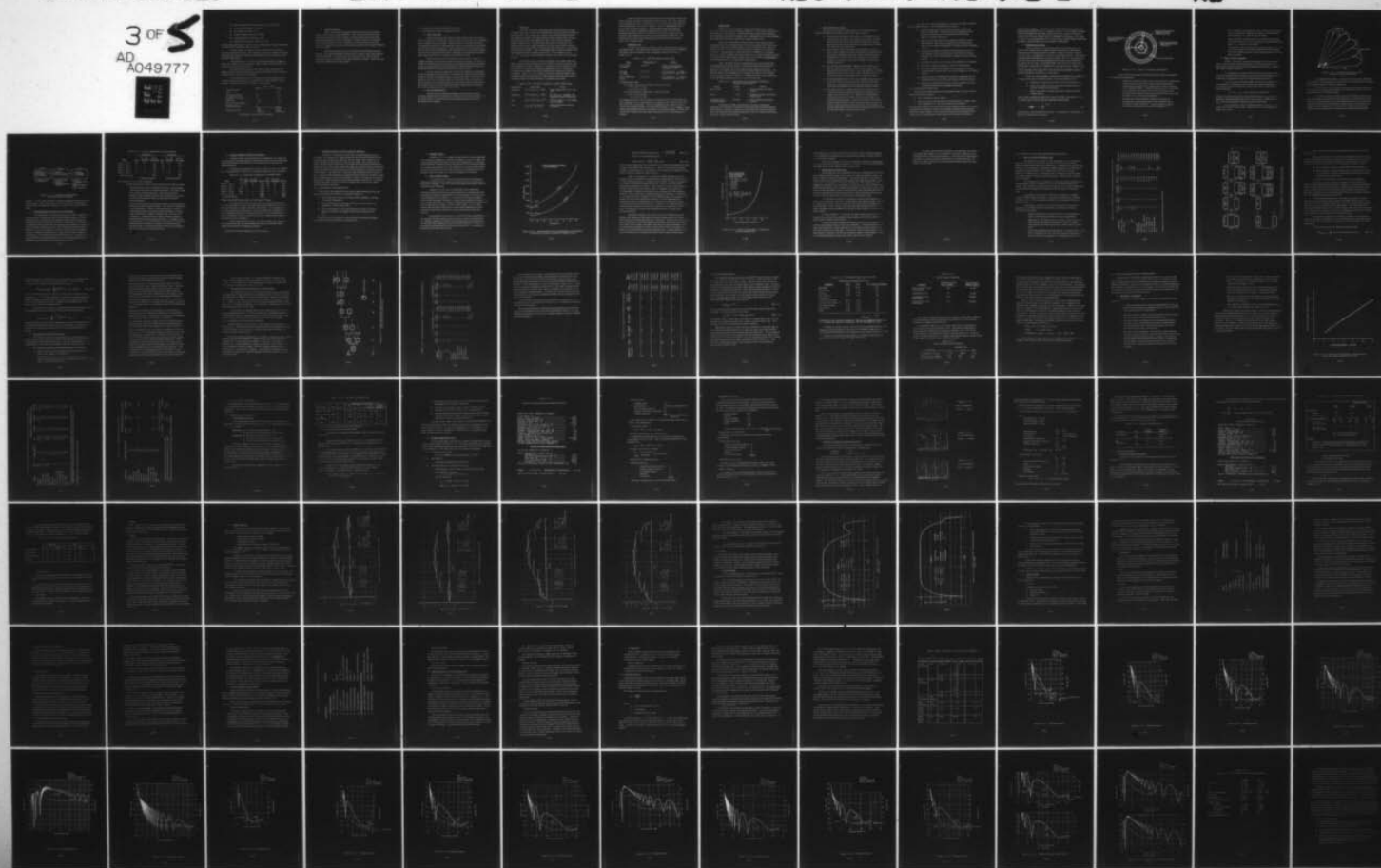
The unit is divided into 5 elements which are listed below.

- Keep-alive/BITE power converter

- Low voltage converter, 5V

- Medium voltage converter, ±15VDC

- Transmitter power converter, +40V

- PIN diode driver power converter, +2.3V

The keep alive/BITE power converter is on continuously to energize keep-alive circuits and the catastrophic failure alarms.

The low voltage and medium voltage elements are switched on by the keep-alive/BITE circuits. DC to DC power converters (chopper type, high efficiency) feed selected circuits so that a failure in one circuit does not take down the whole system.

Transmitter power converter is specifically designed to supply 40 volts and 33 amperes at 1 percent duty. This as well as all other power converters are short circuit protected.

The PIN diode driver power converter provides 4A peak at low voltage (2.3V) to ensure minimal voltage drop across diode driver transistors. This also ensures low power consumption.

This element operates at 65% efficiency and this translates to the estimates below for peak power consumption for the entire SIF/IFF Type A system. Average power is less by a factor of about 1000.

| | Power: Watts | |
	IDLE	ON
ANT Controller	0	.55
R/T	0	14.1
Command Interface	0.1	.68
SIF/IFF Processing	0	1.7
BITE HQ	.01	.01
Power & Power Manage	.1	--
Pin Diode Driver Power Converter	0	9.2
	.21	26.24
Conversion Loss	.07	9.17
	.27 watts	35.41 watts

Average power consumption is negligible.

h)   BITE Management

BITE is distributed throughout the SIF/IFF system with sampling, control, and processing within this FRU. Each ancillary BITE element pre-processes information prior to sending it to BITE central where processing determines appropriate actions, typically a corrective command to the failed FRU, a failure report, or both. Decisions are all pre-programmed within the unit. In addition to the above, the unit also contains a status report formatter and its own BITE.

Pre-processed BITE data are collected in the BITE data collection register. All expected symptoms of failures are stored in code in the symptom look-up table ROM. If symptoms call for corrective action, the corrective command is routed to the failed FRU and immediately retested. In any case, the results are reported in the status report.

2.6 RELIABILITY/MAINTAINABILITY ANALYSIS

2.6.1 RELIABILITY DESIGN CONSIDERATIONS

a) Basic Philosophy

Present day operational radars typically exhibit mean-time-between-failures in the orders of hundreds of hours. Many of these radars were primarily lineal evolutions of a prior design. This permitted a reasonably low risk procurement specification to be developed and radars procured with low acquisition cost and short delivery schedules. In these instances the low acquisition cost award criteria would stimulate the radar manufacturer to minimize the hardware content of his design while addressing a reliability requirement that permitted many single point failure mechanisms in the hardware design.

Radars designed for 90% probability of operational survival for 3 months and longer are not lineal evolutions of any prior design. The equivalent MTBF's of 20,000 hours and up will not permit single point failure mechanisms except in sub elements that are very difficult to make redundant and when that subelement has very few part with extremely low failure rates.

The key feature of radars with >20,000 hour MTBF's is parallelism both at the hardware and system level. Ideally this parallelism in the hardware should be inherent to meeting the basic system performance. In this case redundancy is "for free" and not needed for its own sake. The successful cost effective design of an unattended radar will exploit parallelism in ways that will permit specific amounts of graceful degradation at both hardware and system level without adding redundancy for its own sake.

b) Basic Building Blocks

The advances in reliability potential of current long life radar/electronic equipments can be examined in detail at the part, the assembly and the system level to see how they contribute to high life expectancy in the Unattended Radar designs.

2-179

Part Level

Part data, in general, shows that the present generation of "high reliability" parts have failure rates substantially lower than earlier generations of these parts. This is borne out by failure rate prediction sources such as MIL-HDBK-217B (Sept. 1974) which lists much lower failure rates for many parts and devices than MIL-HDBK-217A (Dec. 1965) or RADC Notebook Volume II (Sept. 1967). Not only did the data base for 217B grow over a longer period of time, but the inclusion of very early data (1950's) on tubed equipment and first-generation semiconductors was eliminated as inconsistent with contemporary parts. Thus, a high quality silicon diode in a ground, fixed environment would have a failure rate of .49 x 10^{-6} according to 217A, .22 x 10^{-6} according to RADC Notebook Volume II, and .023 x 10^{-6} according to 217B.

For devices such as RF power transistors, the failure rates were either lacking in earlier handbook sources (217A) or limited to low noise, low power applications (RADC, Volume II). Handbook data now available in 217B covers power, duty factor and frequency applications for RF transistors. Even the effect on failure rate of device metalization (aluminum or gold) is considered. Table 2.6.1-1 is a listing of RF power transistor failure rates, comparing several current sources of data and shows that the figure used in Unattended Radar reliability estimates is compatible with others.

Table 2.6.1-1. RF Power Transistor (L-Band) Failure Rates

Metalization	Failure Rate	Source
Aluminum	10^{-6} f/hr for T$_j$ 100°C	RADC Report TR-76-177, June 1976
Aluminum	10^{-6} f/hr for T$_j$ 100°C	W. Poole & L. Walshak, 1974 Reliability Physics Symposium
Gold	0.25 x 10^{-6}/0.44 x 10^{-6}	217B incl Notice 1 - for 914509, 510, 511 types
Gold	0.3 x 10^{-6} (at 0°C) to 0.6 x 10^{-6} (at 50°C)	Unattended Radar Reliability Predictions

Another indication of the improvement in part reliability comes from NASA experience on space experiments during the years 1965-1972. Data was collected during this interval on more than 190 individual experiment payloads in the Orbiting Solar Observatory, Pioneer, Explorer, Interplanetary Monitoring Probe and other programs. When the data on operating time and failures are reduced it shows that equipment on the order of 50,000 part complexity has attained MTBF's in excess of 2,700 hours without resort to the large scale redundancies possible for ground-operated equipment. This result would probably not have been possible with the parts and screening practices of a decade earlier.

Assembly Level

One of the key hardware elements of the Unattended Radar is the T/R solid state module. The failure rate estimated for this assembly is compatible with failure rates estimated for other comparable modules as shown in Table 2.6.1-2.

Table 2.6.1-2. Solid State Module Failure Rates

Type	Failure Rate (λ)	Source
TPS-59 SSM (L-Band)	36×10^{-6}	o RADC tests reported in Aviation Week issues of December 6, 1976
TSR SSM (L-Band)	21×10^{-6}	o 217B prediction - J. Sullivan memo 74:55, 21 May 1974
PAVE PAWS SSM (UHF)	8.7×10^{-6}	o 217B prediction - J. Sullivan memo 76:38, 13 Dec. 1976

Unattended Radar SSM

- L-Band (3 receivers, 40 w peak, 6 microsec pulse)

  $\lambda = 22.6 \times 10^{-6}$ at 50°C

  11.3×10^{-6} at 0°C

- UHF (2 receivers, 200 w peak, 6 microsec pulse)

  $\lambda = 18.4 \times 10^{-6}$ at 50°C

  9.2×10^{-6} at 0°C

The unattended radar S.S.M. estimates are double the actual 217 B predictions. This contingency factor was assumed in recognition of the impact this item has on system cost-of-ownership. The above unattended radar predictions apply only for the conditions stated. As can be seen in Table 2.3.2-2 a number of other module configurations have been considered with dramatic impact on system cost. The S.S.M. module is the only system element where 217 B predictions were doubled.

2-181

System Level

There is no way to properly compare distributed function systems, such as the Unattended Radar, with non-redundant, serial systems in which every part failure is a system failure. Distributed function systems with additional spares protection are highly redundant, have a substantial tolerance for individual part failures and exhibit very low effective system failure rates.

If the graceful degradation characteristics of the baseline Type A Unattended Radar are disregarded then at an average ambient of 0°C and every part failure considered a system failure, the non-redundant radar would have a failure rate of $3.677.4 \times 10^{-6}$ failures per hour, equivalent to an MTBF of 272 hours. With appropriate consideration for its redundancies, its failure tolerance, and the conditions of its maintenance for a 3 month unattended interval, the baseline radar behaves like a system which has an MTBF of 20,500 hours, a 75 fold improvement over an equivalent serial system.

Thus, distributed function systems should be compared with other distributed function systems if one is to properly evaluate the feasibility of attaining the potentially high MTBF's that long life designs can deliver. Table 2.6.1-3 compares several recently developed distributed systems. The effective MTBF of an Unattended Radar design is the highest of those listed because its possess a greater degree of redundant protection and is exposed to the low thermal operating stresses of an artic environment.

Table 2.6.1-3. Distributed Function Systems-Comparison of Effective System MTBF's

System	MTBF	Source
PAVE PAWS	4,208	o 217B prediction for mature system
SPG-34	1,964	o Ordnance Logistic Information System Data
Unattended Radar (3 months system)	20,500	o 217B prediction for mature system

On the basis of these comparisons at all levels of equipment complexity, the reliability projections for the Unattended/Minimally Attended Radar should be regarded as feasible and consistent with systems sharing the same kind of functionally parallel architecture, degree of redundant protection, and choice of high-reliability parts.

2-182

c) Basic Reliability Features

In terms of reliability the unique feature of the unattended radar concept is the highly fault tolerant nature of the entire system:

- The highly parallel nature of the system archietecture permit random hardware failures to be apportioned in range, azimuth and elevation such that the total randomized detection volume lost in a given time never exceeds that resulting from an equivalent 2 dB loss in transmit power.

- The radiating stack is entirely passive resulting in very low failure rates. Modern RF power transistors are obtainable with much better median life-times than earlier equivalent devices. TRSSM failure rates are such that redundancy for reliability purposes is not required for a radar capable of 12 months unattended operation.

- The azimuth steering network employs R-2R circular lens as the basic phasing mechanism. These lens are totally passive with extremely low failure rates. The active switches are highly parallel such that in most case a failure will affect but a few of the total available beam positions (1536 L-band, 256 UHF).

- The highly modular nature of the non-redundant subsystems such as receiver and exciter makes off-line sparing economically attractive. The extensive BITE and remote diagnostic facility make manual switching of off-line spares a practical reality.

- The signal processor common element (CE) architecture has considerable degree of natural parallelism coupled with the very simple sparing of off-line CE's. Sparing is accomplished by activating the address of a failed CE in an inactive spare connected to the bus structure. In any event failure of CE results in loss of only a fraction of the range coverage due to the assignment of range gate blocks between all CE's. With a simple progressive addressing change the block of range gates can be moved to a different position in range of each scan.

The above factors greatly simplify the achievement of high reliability for the unattended radar. Other helpful influences include:

- A totally benign operating environment where vibration and shock are eliminated. This issue is very important given the amount of cabling involved in controlling and distributing signals to a 44-foot ring array.

- System operation at a 0°C mean temperature thanks to arctic environments. This feature permits a two fold reduction in failure rates compared to typical 50°C required of more ubiquitous systems.

- A program development schedule which assigns to full year of soak testing to weed out latent defects in the hardware design. Extensive use of part and assembly acceptance screens and burn-in tests.

- Reduction of system requirements to the essentials for operation.

- Selection of minimal equipment to meet the requirements.

- *Use of all components in a highly derated fashion with respect to temperature, voltage, duty cycle, power handling or mechanical stress.*

- Selection of those technologies, materials, components and configurations that have demonstrated highly reliable performance.

- Provision of quality controls in purchasing, manufacturing and installation with extensive sampling and testing.

2.6.2 RELIABILITY MODELING

The cost and ultimate viability of the unattended radar concept is heavily influenced by two key factors:

- What constitutes a system failure.

- How long can this system failure be tolerated before a repair action is accomplished i.e., how much downtime is acceptable.

The first issue relates to the inherent mean-time-between-failure of the system and defines the redundancy needed to meet MTBF requirements assuming instantaneous repair actions. The second issue defines the acceptability of permitting remote reconfiguration repair actions from manned sites based on

remote failure diagnosis. This latter issue must be addressed from the viewpoint that the DEWLINE will be a contiguous network with overlapping coverage and that self-diagnosis/self repair actions for all non-redundant subsystems could become the major design risk in the equipment development. This study is based on the assumption that non-real time remote manual control of switching in off-line redundant subsystems is acceptable and desirable.

a) Definition of A Failure

Failure criteria for conventional radars are typically based on a single beams radiated from an effective point source and the maximum permissible degradation in performance would be related to the loss of effective detection range corresponding to a specific loss in radiated power. Diminished range detection capability is not sufficient by itself, however, to satisfactorily describe maximum permissible degradation of the Type A Unattended Radar. For radars like the Type A Unattended Radar which use 360° circular arrays and fill space completely with multiple beam coverage for each complete scan, it should be more practical to define loss of detection capability as loss of volumetric coverage and the specified 2 dB of detection loss should be allocated among all potential contributors to volume loss.

There are three possible contributors to reductions in the volumetric coverage in the Type A Unattended Radar as shown in Figure 2.6.2-1.

a. Reduction in maximum range due to loss of transmitted power.

b. Holes in the solid coverage due to loss of radiated beams for specific azimuths and elevations.

c. Holes in the solid coverage due to loss of range bins within radiated beams.

Each of these contributes measurable volume loss which may then be converted to effective power loss through the following transformation.

3/4

$$\frac{\Delta \text{VOL}}{\text{VOL}} = 1 - \frac{P_2}{P_1}$$ (b-1)

where P_2/P_1 is the fractional loss in power. For example, a 2 dB power loss equals a 29 percent loss in volume.
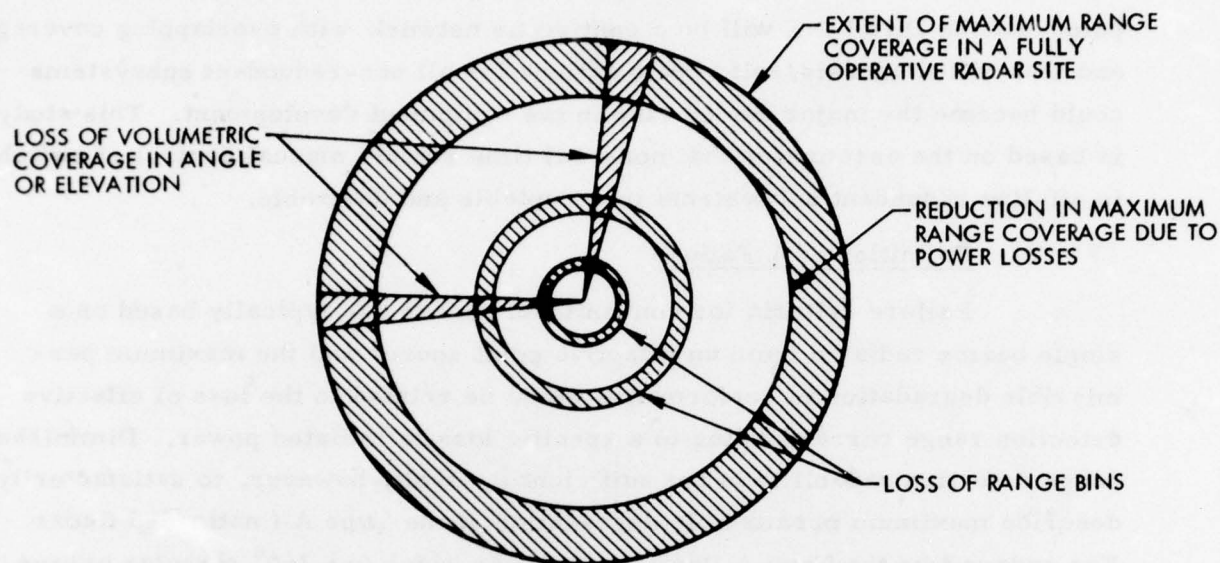
Figure 2.6.2-1. Types of Performance Degradation

In the reliability analysis that follows from these types of degradation, we made these assumptions:

- Reduction in maximum radar range coverage and the corresponding volume shrinkage is due only to losses in transmitted power resulting from failures of T/R modules and/or antenna elements of the Unattended Radar. Possible changes in receiver sensitivity as a contributor were ignored here because the failure rates affecting transmitted power loss are much higher than failure rates affecting receiver sensitivity degradation.

- Volume losses which are power-related may be directly combined with volume losses that are hole-related to obtain the system's total volume loss. Volume losses may then be converted to equivalent power losses using equation b-1.

2-186

-   When volumetric coverage loss is due to holes in given azimuth
    and elevation beams, the holes are randomly distributed over
    the full volume, i.e., they are not correlated.

-   When volumetric coverage loss is due to holes in given range
    bins within a beam, the holes are randomly distributed along the
    beam, i.e., they are not correlated.

-   The possible overlap in holes due to separate causes (e.g., loss
    in maximum range due to drop in transmitted power overlaps
    loss of the outermost range bin due to signal processor failures)
    may be ignored.

b) Setting Failure Threshold

Clearly, volumetric coverage losses which do not raise the total
volume loss beyond the required threshold do not bring the system into a
failure state in spite of some obvious degradation from the full up, complete
solid space coverage condition.

To be practical, any combination of volume losses which do not
exceed this threshold level constitutes acceptable system degradation and the
losses may be apportioned to internal system elements arbitrarily.

In order to relate internal hardware failures to the indicated volume
loss threshold, coverage space for the radar must first be defined in terms of
the maximum number of elemental "volume cells" which a fully operative
radar represents:

$$N_V = N_R \cdot N_{AZ} \cdot N_{EL}, \text{ where } N_R \text{ is the full-up} \qquad \text{Eq. c-1}$$

quantity of range bins delivered by the Signal Processor, N_{AZ} is the full-up
quantity of azimuth positions delivered by antenna and T/R SSM elements, and
N_{EL} is the full-up quantity of elevation beams in the system.

For the baseline, Type A Unattended Radar we have $N_V = (150) \times
(256) \times (6) = 230,400$ volume cells. Figure 2.6.2-2 is a representation of a
single volume cell.

Upper set

Lower set

One range bin in length
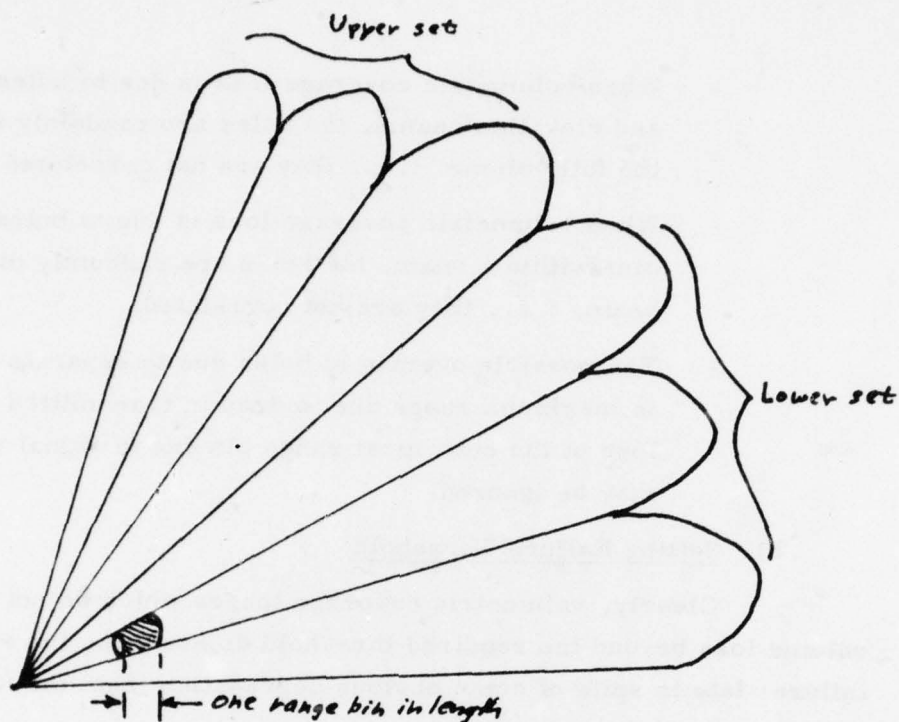
Figure 2.6.2-2.   A Single Volume Cell in a Set of
6 Beams at a Particular Azimuth

It is apparent that a close-in volume cell occupies less volume than
a far-out cell, but for simplicity of analysis all volume cells will be considered
to be equally important in detection capability.

At this point hardware failures can be categorized which produce sys-
tem failures according to the reliability block diagram of Figure 2.6.2-3 for
the baseline Type A Unattended Radar.

A reliability diagram of this type normally states that equipment in
each of the blocks is required to be fully operative for system success, but in
the case of radar designs, such as the Unattended Radar, where much of the
operational functions are distributed and shared among many elements at a
single site, the interpretation of the diagram is modified so that for site
system success at least some minimum amount of operative equipment in

2-188

BLOCK 1	BLOCK 2	BLOCK 3
EQUIPMENT AFFECTING REDUCTION IN MAXIMUM SPACE COVERAGE	EQUIPMENT AFFECTING "HOLES" IN SPACE COVERAGE	ALL OTHER SITE HARDWARE AND SOFTWARE

BLOCK 1
• ANTENNA ELEMENTS
• T/R MODULES

BLOCK 2
• AZIMUTH STEERING
• RECEIVERS
• BEAM SWITCHES
• SIG. PROC. COMMON ELEMENTS

BLOCK 3
• EXCITER
• DATA PROC. COMMON ELEMENTS
• BITE
• POWER DISTRIBUTION
• IFF
• SERIAL EQUIPMENT

Figure 2.6.2-3. Baseline Unattended Radar -
Simplified Reliability Diagram

Blocks 1, 2, and 3 of the diagram is required consistent with the 2 db power
loss threshold. When volume loss of coverage occurs, it is assignable to
integral numbers of parallel "channels" in Blocks 1 and 2 of the Unattended
Radar.

c) Relating Hardware Failures to Loss Threshold

For the purpose of computing volume loss in Block 1 equipment, it is
necessary only to consider the fraction of the antenna element/T/R module
group which is in a failed state and multiply the power loss represented by
this fraction by the 3/4 factor to convert it to volume loss. For the purpose
of computing volume loss in Block 2 equipment, it is necessary to compute the
number of volume cells that are lost due to failures and take the resulting
fraction of N_V as the volume loss. If Block 2 volume loss is considered
excessive, redundant protection will be required to eliminate volume loss
contributions. The example represented by Table 2.6.2-1 shows a hypothetical
Unattended Radar configuration before and after redundant protection and
should make clear the failure level computations involved.

Table 2.6.2-1. Losses in Hypothetical Unattended Radar

Item*	Unprotected			Protected		
	Qty.	No. Fail. Allowed	Assoc. Vol. Loss	Qty.	No. Fail. Allowed	Assoc. Vol. Loss
Block 1 - EL A	256	25	.073	256	28	.082
Block 2 - EL B	96	5	.052	96	7	.073
Block 2 - EL C	3	1	.333	4	1	0
Block 2 - EL D	6	1	.167	7	2	.167
Block 3 - EL E	1	0	0	1	0	0
Total Vol. Loss			.625			.322
			(outside threshold)			(within threshold)

*See Figure 2.6.2-3 for Block categories

Among the points to be made from the example of the table are these:

- The unprotected system configuration would be in a failed state with the indicated numbers of allowed failures. The system must have critical elements protected. When that protection is provided, other elements may have their failure tolerance level raised and the protected system is still within the system failure threshold.

- Some elements groups have natural redundancy if a high degree of functionally parallel hardware exists. This would be represented by element group A in Block 1 and element group B in Block 2. Other element groups do not have natural redundancy and spare units would have to be added to eliminate their contribution to volume loss. Element group C in Block 2 would be typical of equipment which requires spares protection. By adding a spare to the original 3, we can eliminate the contribution to volume loss represented by the failure of a single unit of Element group C and still satisfy a reliability requirement based on the permitted failure of a single unit of element group C.

d)   Relating Hardware Failures to Reliability

In addition to the need to satisfy the loss threshold, the criteria for establishing the acceptable quantities of hardware failures must simultaneously satisfy the reliability requirement of 0.90 probability of survival for the unattended period.

Returning to the hypothetical system of Table 2.6.2-1, the reliability for a 6-month period or 4320 hours of continuous operation can be calculated.

Table 2.6.2-2.   Reliability of Hypothetical Unattended Radar

Item	Unit *	Sys. Qty.	No. Fail. Allowed	P(6 mo)	Sys. Qty.	No. Fail. Allowed	P(6 mo)
Block 1 - EL A	11.9 **	256	25	.9994	256	28	.9999
Block 2 - EL B	.13	96	5	.9999	96	7	.9999
Block 2 - EL C	20.0	3	1	.9805	4	1	.9645
Block 2 - EL D	30.8	6	1	.8344	6	2	.9594
Block 3 - EL E	5.0	1	0	.9786	1	0	.9786
System Reliability				.8000			.9054

*These are assumed failure rates in failures per 10^6 hours.

The unprotected system not only exceeds the loss threshold (Table 2.6.2-1), but fails to meet the reliability requirement (Table 2.6.2-2), whereas the protected system complies with both requirements. It is entirely possible that some unprotected configuration would not meet the loss threshold, but would have computed probabilities of survival in excess of 0.90. Unless both the loss and the reliability criteria for that level of loss are simultaneously satisfied, the system is not in compliance.

In the Unattended Radar study, only those systems were considered by Raytheon which fully met the simultaneous loss and reliability criteria with the least hardware complements possible.

** Includes the antenna radiating stack and connectors.

2-191

e)   Additional Modes of Partially Degraded Operation

Methods to randomize the "hole" type coverage degradation can be conceived. For example, if a signal processor common element should fail and all spares have already been exhausted, then the range "hole" created by this failure could be moved around on a scan-by-scan basis. This would cover all angles, but the average revisit time is increased and the system is generally degraded over the entire volume rather than suffering complete outage in one section. Another possibility is the randomization of beam outages due to azimuth steering switch failures. The objective is to prevent large contiguous blocks of beams to fail. As the even/odd switching arrangement provides complete redundancy, beam failure randomization would prevent outages in beams at the expense of a general degradation. These and other concepts require further examination. The general objective should be to prevent any actual complete holes, and have the radar gracefully degrade uniformly.

2.6.3   RELIABILITY COST SENSITIVITY

Three of the most significant factors which exhibit sensitivity to the cost versus reliability trade-offs for any Unattended Radar are:

- Cost of hardware required to satisfy system reliability, a function of required redundancy;

- Cost of validating the reliability attained by a given system configuration, a major testing cost;

- Cost of maintenance crews and maintenance doctrine, carrying impact on operation and support for the entire system service life.

All of these are incorporated in the Life Cycle Cost models developed for the study, but some discussion is pertinent here.

a) Hardware Impact

In Table 2.6.2-1, it is shown that the addition of spare equipment to the hardware complement is generally necessary in order to comply with required probabilities that failure-induced loss thresholds not be exceeded. As the hardware complement grows, the acquisition and replacement spares cost of the hardware grows too. The growth occurs not only to the duplicate hardware involved but also to the fault sensing and switching hardware and software which must sense and report the equipment failure status.

b) Test Validation Impact

It is expensive to run tests which demonstrate with reasonable statistical validity the level of attained reliability because such tests take a long time to complete. The more reliable the system, the longer it takes to demonstrate that reliability.

Figure 2.6.3-1 is a plot of test duration versus statistical confidence in the test result for a system which has a constant failure rate and satisfies a reliability requirement of 0.90 probability of survival for an unattended period of 3 months (i.e., 2160 hours of continuous operation). To prove that the system reliability is that good with moderate confidence, say, 50%, it would take about 1-1/2 years of continuous operation of a single system without experiencing a single, scorable system failure. Or, you could achieve the same level of proof with a single system operating for about 4 continuous years with no more than a single system failure within that interval.

If probabilities of survival of 0.90 for even longer unattended periods are required, the test validation time and costs increase correspondingly. For example, Equation (b-2) shows that the least test time in system hours for demonstrating compliance for any unattended radar with 0.90 survival probability is proportional to the required system MTBF, or inversely proportional to the system failure rate:

2-193
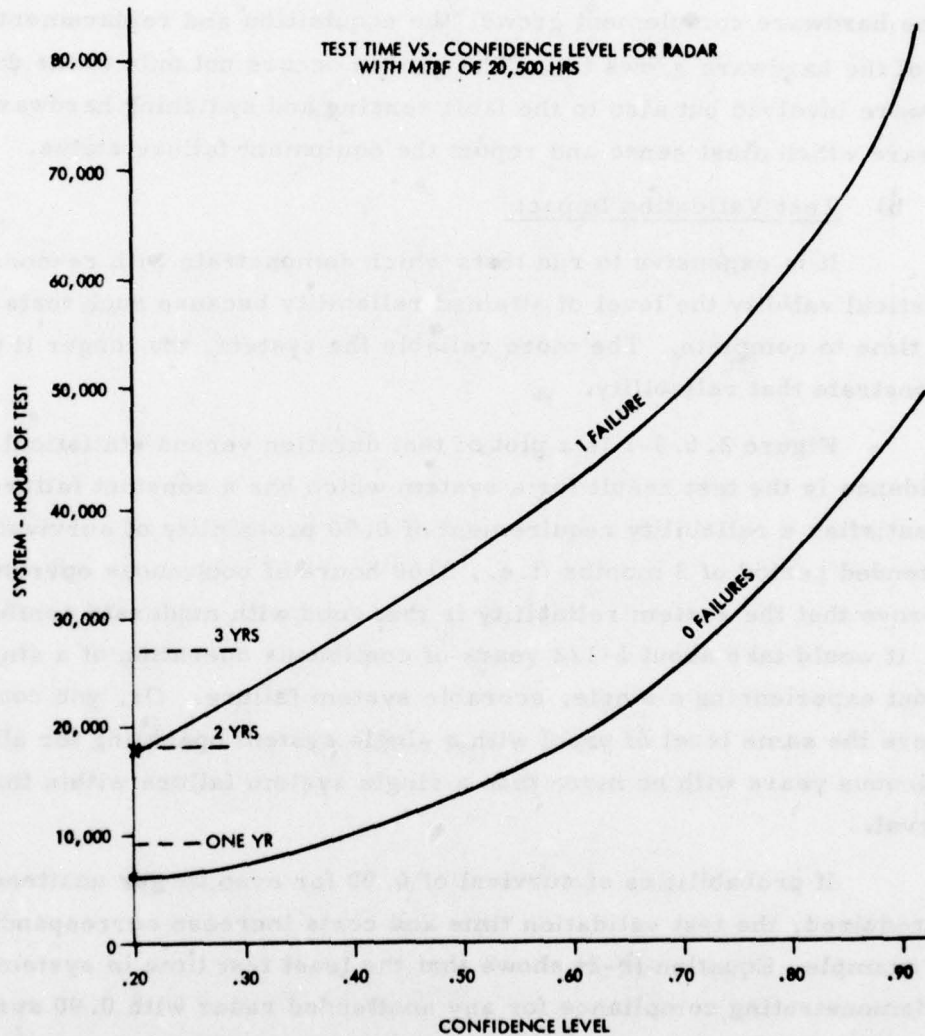
Figure 2.6.3-1. Required Test Time to Demonstrate 0.90 Probability
of Survival for 3 Months at Indicated Confidence Level

2-194

Required System Failure Rate, $\lambda = -\left[\dfrac{\ln 0.90}{t}\right]$, (Eq. b-1)

where t is the unattended period.

Least test time $= \dfrac{\theta \cdot \chi^2}{2} = \dfrac{\chi^2}{2\lambda}$, where (Eq. b-2)

χ^2 is the value of chi-square for zero failures at the desired confidence level and θ is the system MTBF, the reciprocal of λ. Since χ^2 increases as confidence increases, the test time has to be greater if more quantitative confidence in the result is desired as shown in Figure 2.6.3-1.

Suppose for example, it is planned to conduct the least amount of testing at arctic sites which would demonstrate 0.90 probability of survival for a 3-month unattended period at a confidence level of 90%. We could use equation b-1 to find λ, the effective system failure rate of 48.7×10^{-6} f/hr, which satisfies the probability of survival. Then equation b-2 would be solved for the amount of system test time using the value of λ together with a value of χ^2 corresponding to 2 degrees of freedom (for zero failures) and 90% confidence. Using $\chi^2 = 4.60$, the amount of required testing is 47,228 hours. If 18 months of continuous test time is available for the validation phase of the program, this amount of testing would require four systems to run simultaneously and continuously without a single failure for 11,800 hours or about 16.4 months - very close to the allotted validation time. Figure 2.6.3-1 could have been used to determine the required test time as an alternative to equations b-1 and b-2, since it is plotted for a system which satisfies the value of λ used in the preceding example.

Substantial savings in the duration and cost of validation tests are possible if the testing can take place at elevated temperatures at the contractor's plant instead of at the operational arctic environment. Figure 2.6.3-2 illustrates this for hypothetical electronic equipment containing a mix of parts as indicated. If the mix is close enough to the parts comprising the Unattended Radar, then a test conducted at an ambient of 95°C would accelerate failure mechanisms by a factor of 10 and diminish the required validation time. A single system tested at this temperature and running continuously without a failure would require

REDUCTION OF TEST TIME AT
ELEVATED TEMPERATURES FOR
ASSUMED MIX OF PARTS:

2 DIG IC (50 g), $T_i = T_A + 25°C$
1 LIN IC (48 tr), $T_i = T_A + 25°C$
1 NPN TRANS
1 DIODE, g.p.
2 PIN DIODE
2 RES, RLR
1 CAP, CKR

$\lambda 0° = .219 \times 10^{-6}$
$\lambda 50° = .482 \times 10^{-6}$
$\lambda 100° = 2.944 \times 10^{-6}$
} MIL-HDBK -217B
G_F env., S = .2

TIME ACCELERATION FACTOR

AMBIENT TEMPERATURE OF TEST/OPERATION °C
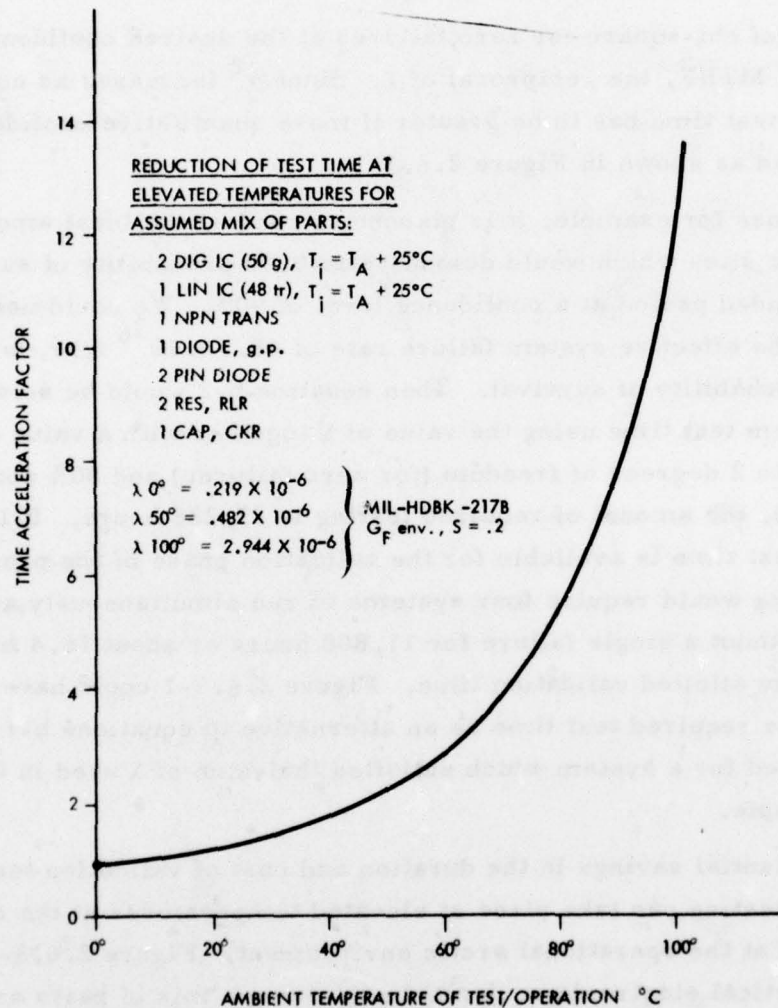
Figure 2.6.3-2. Effect of Temperature on Duration of
System Reliability Test

$1/10 \times 47,228 = 4,723$ hours or about 6-1/2 months to reach the same confidence level of 90% for 0.90 probability of survival that four systems required in more than 16 months of testing.

The curve of Figure 2.6.3-2 is a composite of Arrhenius relationships for the part mix shown and was extrapolated from failure rate versus temperature information given in MIL-HDBK-217B for those parts.

c) Maintenance Doctrine Impact

Maintaining the Type A unattended radar on a scheduled basis is not the only maintenance doctrine that could be used. It would be possible to service unattended sites on a demand basis instead. This would mean that a site would be visited when the level of performance degradation exceeded some amount, regardless of what was expected by a calendarized schedule. If the degradation level triggered a maintenance call, the system would rarely ever reach a system failure state since the demand could be based on anticipation of failure prior to actual failure and system availability would be extraordinarily high compared with scheduled visits for a maintenance doctrine which goes by a fixed schedule and on occasion results in visits to sites which have entered the system failure state.

An "anticipation-of-failure" maintenance concept would generally require more maintenance visits than a simple repair-when-failed concept. However, the radar net availability would be higher and the visits could be scheduled with more flexibility. Thus, repairs on systems exhibiting degradation close to the failure threshold could be scheduled for periods of clear weather or in anticipation of bad weather.

For this concept to be attractive, the radar would need to have a 'fine grained' rate of failure which permitted high confidence in the time available for repair before complete system failure.

A purely periodic scheduled maintenance would involve the highest risk of radar outage unless frequent visits were scheduled. A ninety percent survival factor between periodic visits would clearly not be adequate since ten percent of the radars would be in a failed state. The correct value with this concept is probably closer to 99 percent and the exact definition depends on the definition of what is a reasonable equipment outage time before repairs can be effected.

2-197

The most efficient trade-off between crew utilization and system availability would appear to be a combination of periodic maintenance and anticipated failure on-demand maintenance. The entire field of maintenance and logistics concepts including consideration of transportation and crew safety is a subject requiring careful and detailed analysis beyond the scope of this reported study.

2-198

2.6.4 PRIMARY RADAR BASELINE SYSTEM RELIABILITY

a) Baseline System Reliability Model

The baseline for the Type A Unattended Radar is an L band system which has 256 antenna elements and associated T/R solid state modules. Without considering the spare units required for redundant protection, the basic functions of the system up to the antenna/TRSSM elements are provided by an azimuth steering subsystem which contains three R-2R lenses, three receivers, a single exciter, a signal processor containing a requisite number of "common element" channels, an IFF subsystem, system power, BITE and interconnections.

The baseline system complement is also augmented by sufficient subsystem spares to satisfy a reliability of 0.90 for an unattended period of 3 months. The reliability is defined as the probability of surviving the unattended interval without exceeding internal failure levels that exceed a 2 db power loss.

For a Type A system which satisfies this reliability, redundant protection must be added to the basic, unprotected complement as indicated in Table 2.6.4-1. The corresponding reliability block diagram is shown in Figure 2.6.4-1.

The required reliability of the baseline system and alternate configurations of the Type A radar is achieved by a combination of factors, including, among others:

- Intrinsic parallelism for many functions, thus permitting some degree of internal failure without excessive degradation.

- Added spare, redundant elements to protect critical components from introducing excessive degradation at failure. Spares, when present, are used in a dormant, standby mode to conserve power.

- Use of high reliability parts and materials, typically, MIL-M-38510 class B integrated circuits, JANTXV transistors and diodes and ER type resistors and capacitors at reliability level R or better.

Table 2.6.4-1. Baseline Type A Unattended Radar (P_s (3 mos) = 0.90)

Subsystem	On-Line Qty.	Stdby. Spares	Allowable Failures	Element λ^*	Allowable Pwr. Loss	P (3 mos.)
ANT EL/TRSSM	256	0	12	11.90	.0469	0.98527
AZ STEER A	3	0	0	0.80	0	0.99482
B	24	0	0	0.21	0	0.98917
C	96	0	1	0.13	.0139	0.99964
DEF	192	0	3	1.46	.0208	0.99662
H	768	0	6	0.21	.0104	0.99999
BEAM SW	3	1		11.30	0	0.99744
RECEIVER	3	1		25.70	0	0.98758
EXCITER	1	1		19.20	0	0.99916
SIG. PROC. SERIAL	1	1		54.80	0	0.99352
D. P. COMM. EL.	2	1		21.50	0	0.99594
S. P. COMM. EL.	6	1	2	30.80	.2223	0.99331
PWR. DISTR.	1	0	0	5.00	0	0.98925
BITE/INTERCONN.	1	0	0	1.00	0	0.99784
IFF	1	0	0	6.00	0	0.98712
					.3143	0.91054

*Failure rates in units of failures per 10^6 hours.
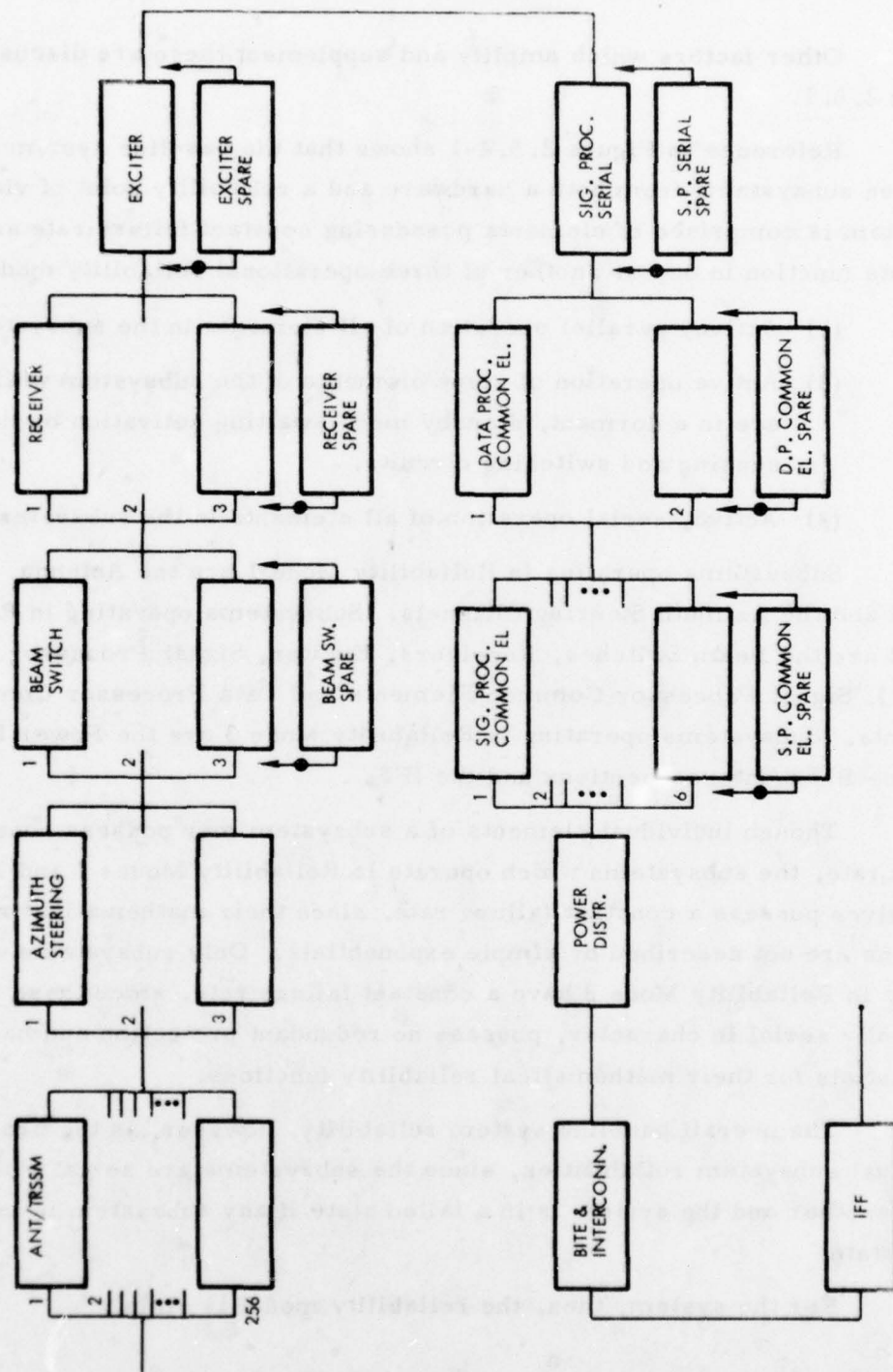
Figure 2.6.4-1. Reliability Diagram, Type A Baseline System
(With Redundant Protection For 3 Month Unattended Period)

Other factors which amplify and supplement these are discussed in Section 2.6.1.

Reference to Figure 2.5.4-1 shows that the baseline system consists of eleven subsystems from both a hardware and a reliability point of view. Each subsystem is comprised of elements possessing constant failure rate and the elements function in one or another of three operational reliability modes:

(1) Active, parallel operation of all elements in the subsystem,

(2) Active operation of some elements of the subsystem while others are in a dormant, standby mode awaiting activation by the fault sensing and switching circuits.

(3) Active, serial operation of all elements in the subsystem.

Subsystems operating in Reliability Mode 1 are the Antenna, the TRSSM and the Azimuth Steering Channels. Subsystems operating in Reliability Mode 2 are the Beam Switches, Receivers, Exciter, Signal Processor (serial portion), Signal Processor Common Elements and Data Processor Common Elements. Subsystems operating in Reliability Mode 3 are the Power Distribution, the BITE/Interconnections and the IFF.

Though individual elements of a subsystem may possess constant failure rate, the subsystems which operate in Reliability Modes 1 and 2 do not themselves possess a constant failure rate, since their mathematical reliability functions are not described by simple exponentials. Only subsystems which operate in Reliability Mode 3 have a constant failure rate, since these subsystems are totally serial in character, possess no redundant protection and have simple exponentials for their mathematical reliability functions.

The overall baseline system reliability, however, is the product of individual subsystem reliabilities, since the subsystems are serial with respect to one another and the system is in a failed state if any subsystem is in a fully-failed state.

For the system, then, the reliability model is simply

$$R(t)_{system} = \prod_{i=1}^{n} R_i(t), \text{ where the } R_i(t) \text{ are the} \qquad (Eq. a-1)$$

2-202

individual subsystems reliabilities for the n subsystems. An individual sub-system reliability may not be so simply expressed. For example, the reliability of the combined Antenna/TRSSM subsystems is

$$R(t)_{Ant/TRSSM} = \sum_{i=0}^{k} \binom{m}{i} r_a^{m-i} (1 - r_a)^i, \text{ where } k \qquad \text{(Eq. a-2)}$$

out of m = 256 elements may be permitted to fail without causing excessive degradation, $r_a = e^{-\lambda_a t}$ is the reliability of an element combined Antenna and TRSSM) possessing constant failure rate λ_a and t is the unattended period of interest. This illustrates the type of reliability function appropriate to sub-systems which operate in Reliability Mode 1.

Subsystems which operate in Reliability Mode 2 may be illustrated by the reliability function for the Receiver subsystem which has the form

$$R(t)_{Receiver} = \sum_{i=0}^{k} \frac{e^{-\lambda_r t} (\lambda_r t)^i}{i!}, \text{ where } k \qquad \text{(Eq. a-3)}$$

standby elements protect the basic complement of m receiver elements and may be permitted to fail without causing excessive degradation, λ_r is the constant failure rate of a single receiver element and t is the unattended period of interest.

b) Baseline System Reliability Estimate

The reliability estimate corresponding to a 3-month unattended period for the baseline Type A radar was computed from Equation a-1 after subsystem reliabilities were calculated with functions of the form of Equation a-2 or a-3, as appropriate. These have been tabulated in the last column of Table 2.6.4-1.

The following conditions and assumptions apply to the estimate:

- Failure rates for high reliability parts were taken from MIL-HDBK-217B, Tables 3-1 through 3-10.

- Modifying factors that were used corresponded to the ground, fixed environment; quality levels were appropriate to MIL-M-38510, class B, JAN TXV and ER level R.

2-203

- Connectors, printed circuit boards, and interconnecting cables were used in conjunction with parts lists derived from existing designs of similar complexity and function.

- Past failure history or statistically valid test data on certain critical items was used to modify 217B failure rates. Examples are pin diode failure rates based on billions of part hours in operation of the MSR phased array radars at Meck Island and North Dakota and RF power transistors at L band based on tests at Microwave Semiconductor Corp. and Raytheon TSR System.

- Mean arctic temperature excursions from -60°F to $+50^{\circ}$F were considered in applying an "average" operating ambient of 0°C and in reducing failure rates to correspond to such a cold temperature ambient.

- When spares redundancy was employed, the least amount of hardware required to satisfy the reliability for the degradation threshold was sought. This was done to minimize the acquisition cost and logistic cost of the system so "optimized".

- In modeling the system an antenna element is combined with its associated T/R solid state module so that the antenna function and the TRSSM function are combined into a single subsystem.

- The tree dependency of an Azimuth Steering Channel is shown in Figure 2.6.4-2. The reliability analysis treats each level in the tree independent of other levels. No failures are permitted at the "A" or "B" switch level and only from the "C" level onward is there any tolerance for failure-induced degradation. When degradation at any permitted level exists, it is treated as the maximum possible and all such degradations are added to obtain total degradation within the Azimuth Steering subsystem. This probably makes the reliability estimate conservative for this subsystem, since many switches could fail at a given level without causing the maximum possible power loss used in the analysis.

The reliability estimate for 3-month Unattended baseline Type A radar with consideration for these assumptions is 0.91 as indicated in Table 2.6.4-1. The required degree of redundant spare protection is shown in the third column of the table and in Figure 2.6.4-1.

b) Baseline Reliability Estimates for 6 and 12 Months

The reliability estimate provided was a baseline system configuration which satisfies 0.90 probability of not exceeding 2 db power loss for a 3-month unattended period. When the requirement is extended to satisfy 0.90 reliability for 6 months or 12 months, more spares must be added to the system configuration. Table 2.6.4-3, attached, for 6 and 12-month unattended periods of operation may be compared with Table 2.6.4-1 where the configuration for a 3-month unattended period has been described.

In summary, the baseline system may be optimized for 3, 6, or 12-month unattended operation. When this is done, the coresponding reliabilities for the specific optimum configurations are 0.910 for the three-month system, 0.897 for the six-month system and 0.896 for the twelve month system.

2.6.5 RELIABILITY OF ALTERNATE DESIGNS

Reliability analyses of the baseline, Type A Radar, have been given in Section 2.6.4. The baseline system is characterized as an L Band configuration with three lenses, three receivers, 256 antenna/TR solid state modules and 6 beams, among other attributes.

Many other alternative designs were considered, differing from the baseline system by having other quantities of lenses, beams, receivers, solid state modules, etc. 72 alternatives were listed, for example, in Table 2.2.2-2 of Section 2.2.4. These alternative configurations are believed to contain most of the potentially realizable systems within the bounding guidelines laid down in Section 2.1. Performance, reliability, cost and other significant variables were traded off against each other and against the baseline system for optimum Life Cycle Costs.

Figure 2.6.4-2. Reliability Diagram, Single Azimuth Steering Channel
(One of Three in Baseline System)

Table 2.6.4-3. Baseline Type A Radar - 6-Month and 12-Month Unattended Operation

Subsystem	On-Line Qty.	6-Month System				12-Month System			
		Stby. Spares	Allow. Fail.	Allow. Pwr. Loss	R(t)	Stby. Spares	Allow. Fail.	Allow. Pwr. Loss	R(t)
ANT EL/TRSSM	256	0	25	.0977	0.99943	0	40	.1563	0.99883
AZ STEER A	3	0	0	0	0.98968	0	0	0	0.97947
B	24	0	1	.0556	0.99977	0	1	.0556	0.99911
C	92	0	1	.0139	0.99861	0	1	.0139	0.99464
DEF	192	0	6	.0417	0.99975	0	10	.0695	0.99996
H	768	0	6	.0104	0.99999	0	6	.0104	0.99940
BEAM SW	3	1	1	0	0.99026	2	2	0	0.99663
RECEIVER	3	2	2	0	0.99519	3	3	0	0.99515
EXCITER	1	1	1	0	0.99674	1	1	0	0.98767
SIG. PROC. SERIAL	1	2	2	0	0.99814	2	2	0	0.98754
D. P. COMM. EL.	2	1	1	0	0.98474	2	2	0	0.99351
S. P. COMM. EL.	6	3	3	0	0.99098	5	5	0	0.99401
PWR. DSTR.	1	0	0	0	0.97863	1	1	0	0.99909
BITE/INTERCONN.	1	0	0	0	0.99568	0	0	0	0.99139
IFF	1	0	0	0	0.97441	0	0	0	0.97441
				.2192	0.89692			.3057	0.89590
				(1.07 db)				(1.58 db)	

The reliabilities of a number of the alternatives were examined in detail where it was felt that their designs possessed significant features that were interesting or attractive from a performance point of view or where it was believed that high reliabilities could be achieved with smaller complements of hardware. Some representative results are tabulated in Table 2.6.5-1. In all cases, the system complement of hardware was "optimized" to establish the smallest quantities of spares that would be consistent with reliability of 0.90 for the indicated unattended period. As before, the criterion for reliability is the probability of surviving the unattended interval without exceeding the 2 dB power loss threshold.

To facilitate the rapid and accurate calculation and optimization of the large number of cases represented by Table 2.6.5-1, a computer program was developed for this purpose.

The detailed failure rate, reliability and sparing data down to the field replaceable unit (FRU) level for the cases summarized in Table 2.6.5-1 are presented in Appendix B in the form of computer printouts from this reliability estimation program.

Table 2.6.5-1 Reliability of Alternate Type A Designs

Matrix No.*	Freq.	No. TRSSM	No. Lenses	No. Rcvrs.	No. S.P. Comm. El.	R(t)	Design Time
1 (Baseline)	L	256	3	3	6	0.91054	3 months
						0.89692	6 months
						0.89590	12 months
36	L	64	3	1	2	0.9173	3 months
						0.8963	6 months
						0.9082	12 months
39	L	64	3	2	16	0.9207	3 months
						0.9001	6 months
						0.9025	12 months
49	UHF	32	2	2	4	0.9200	3 months
						0.9005	6 months
						0.8804	12 months
62	UHF	32	1	1	2	0.8995	3 months
						0.9051	6 months
						0.8975	12 months

*per Table of Section 2.2.4

2.6.6 SIF/IFF RELIABILITY

The reliability analysis performed on the SIF/IFF used the same component failure rate data as for the primary radar. However, unlike the primary radar a very low duty cycle of operation is used. This duty cycle of two one-second transmission per hour has a dramatic impact on the reliability model. Normally, the IFF is in a dormant state until the radar senses a target and activates the IFF to perform its identification function. Thus, the operational profile for the IFF involves the effects of extremely low electrical stresses during dormancy along with the periodic turn-ons and turn-offs related to target detection or status tests. The appropriate model for the IFF supplements those given in the referenced memo below and is expressed as

$$R(t)_{IFF} \approx e^{-\lambda_s t},$$ (Eq. c-1)

where λ_s is the in-service failure rate of the IFF under dormancy and cyclic conditions. For the in-service rate we have

$$\lambda_s = [d + (1 - d) c + NKC] \lambda_E, \text{ where}$$ (Eq. c-2)

d is the duty cycle, C is the ratio of dormant to energized failure rate, N is the average cyclic rate and K is the ratio of cyclic to dormant failure rate. λ_E is the failure rate in the continuously energized condition.

Appropriate values of C and K have been published for many part types in documents such as RADC Report TR-73-248, "Dormancy and Power ON-OFF Cycling Effects on Electronic Equipment and Part Reliability". By averaging the values of C and K for the mix of parts in the IFF subsystem and by using reasonable estimates of cyclic rate and duty cycle we can generate Table 2.6.6-1 giving the effective failure rates for major assemblies of the IFF and for λ_s. The effects of cycling and dormancy reduce the active failure rate in the arctic environment by a factor of 30.

Table 2.6.6-1. IFF Failure Rates (Type A System)

Failure Rate Estimates x 10^{-6} f/hr.

Assembly	50°C	0°C	0°C, Cycled & Dormant
ANT Assy.	76.90	38.45	1.28
ANT Control	3.82	1.91	.06
Receiver	11.39	5.70	.19
Video Process.	4.97	2.49	.08
Transmitter			*
Processor RDU/DEF	15.47	7.74	.26
Processor TDU/Coder A	22.16	11.08	.37
Command Interface	5.01	2.51	.08
Power Mgmt.	3.38	1.69	.06
BITE	11.23	5.62	.19

$\lambda_{s\,3\,mos.}$ = 2.57

*Transmitter used in a dual arrangement, yielding time dependent failure rate.
For 3 months use .003; for 6 months use .007; for 12 months use .014.

The effect of the above failure rates is to provide a single thread SIF/IFF design with excess reliability to meet the 0.974 availability apportionment (80,000 hours MTBF) allotted to the equipment as part of the overall type A radar.

Table 2.6.6-2 shows the various levels of reliability achieved by the single thread system for each of the applicable factors.

Table 2.6.6-2

SIF/IFF System Reliability

Conditions	Effective Failure Rate: FPMH	Equiv Effective MTBF: Hours
Single Thread at 100% Duty and 50°C	154	6,500
Translation to 0°C	77	13,000
Translation to Low Duty (0.001)	2.6	390,000
Adjustment for 2 dB Degradation	1.5	670,000

Even without the last adjustment, these estimates yield 0.995, 0.989 and 0.978 probabilities of fail-free operation for periods of 3, 6 and 12 months, compared to an apportionment of 0.974.

At unattended Type A sites, IFF system operation is on demand and cycled on the average twice per hour at 0°C. The system configuration is illustrated in the reliability block diagram of Figure 2.6.6-1. For the 0° cycled condition, the probability of success was determined for 3, 6, and 12 months and listed in Table 2.6.6-3 together with effective failure rate and MTBF. In each case, the allocated value of .9734 is exceeded.

Table 2.6.6-3

Type A SIF/IFF System Reliability

Parameter	Period: Mos		
	3	6	12
Probability of Success	.9945	.98888	.9777
Effective F.R. (FPMH)	2.57	2.57	2.58
Effective MTBF (K Hrs)	389	388	388

2-212

The margin with which the system apparently meets reliability requirements provides the degree of confidence sought to offset the risk of error in interpreting the effects of dormancy and cycling discussed previously. The values presented in Table 2.6.6-3 were based on a 30 to 1 correction factor. It is interesting to note that the requirements can still be met in the worst case (12 months) if the correction factor is as low as 25 to 1. Further, the results tabulated thus far must be considered conservative in that the entire phased-array antenna subsystem has been treated as a serial item while in fact some antenna element failures can be allowed without undue degradation.

Although, IFF System performance at Type A sites is dependent upon operation of the remotely located SIF/IFF equipment, this equipment is not included in the reliability calculations for several reasons. Failure of the equipment, for example, does not necessitate a maintenance action at an unattended site since the equipment is located at a manned installation remote from the site it serves. Further it is assumed that 28 remote IFF's service 80 sites which translates to 4 per attended site and, based on duty-cycles, a negligible queing problem, even with the estimated reliability parameters for remote equipments and two failed units. Estimates of reliability parameters for remote IFF equipments for cycled operation at $0^{\circ}C$ are:

failure rate = 0.16 failures/10^6 hours

MTBF = 6.2 million hours

Probability success 3, 6, 12 mos. = .9996, .9993, .9986

These values are conservative since it is likely that the demand for mode 4 equipment will result in a duty cycle even less than that assumed.

2-213

2.6.7 BASELINE MAINTENANCE REQUIREMENTS

Failure rates for the Baseline subsystems and FRU's are given in Table 2.6.4-1 and 2.6.4-3. They may be used to make worst case estimates of the expected replacement/checkout workload that accumulates during the period of unattended operation. This worst case analysis assumes a scheduled maintenance concept with a time interval of 3, 6 or 12 months. The size of the workload and the constraint of a 3-hour maximum limit on the duration of a maintenance visit determine the required size of the work force.

a) Maintenance Groundrules

Groundrules assumed to apply for this study to the maintenance doctrine are:

- A single maintenance crew visits each unattended site at or near the end of each designated unattended period. In this concept 10% of the radars will be in a failed state.

- The crew travels in a single vehicle (helicopter) and may include the pilot as part of the working maintenance force.

- The crew/vehicle combination carries transportable heaters, illumination gear, test equipment and spares (certain spares that are physically large, such as antenna stack FRU's may be emplaced at each site, if necessary).

- Sites are visited sequentially. For maximum crew utilization the full set of 80 sites may be visited in turn at the average rate of 2 sites/working day taking 40 days to complete a full schedule where a single crew services the entire system, or taking less than 40 days if crews are limited to some fraction of the full set and return to a logistic mode takes place at the end of each work day.

2-214

- Repairs to FRU's are made at logistic nodes, depots or factory according to need for special test equipment, parts or skill levels. In any event, no repairs are made at sites; only FRU replacement takes place at sites.

- The fault detection system furnishes sufficient information to allow reasonable diagnosis at nodes so that crews have high probability of taking correct spares on maintenance trips.

- Each site is presumed to be fully restored to peak operational capability at the end of each visit BITE readout at the site will be used for verification.

- Crew efficiency estimated to be 75%, requiring elapsed time of 1.3 x replacement workload (see Table 2.6.7-2).

Table 2.6.7-1 gives the expected number of FRU's in a failed state at the end of the designated unattended period. Table 2.6.7-2 is an estimate of FRU replacement times and Figure 2.6.7-1 shows the required crew size compatible with the unattended period and 3 hour elapsed time per visit constraint. Table 2.6.7-2 neglects the replacement of any FRU with less than 50 percent probability of failing in the time specified. The numbers of maintenance personnel required were costed into the appropriate element of the LCC model. The FRU failure data was also used to determine spares required for system operation.
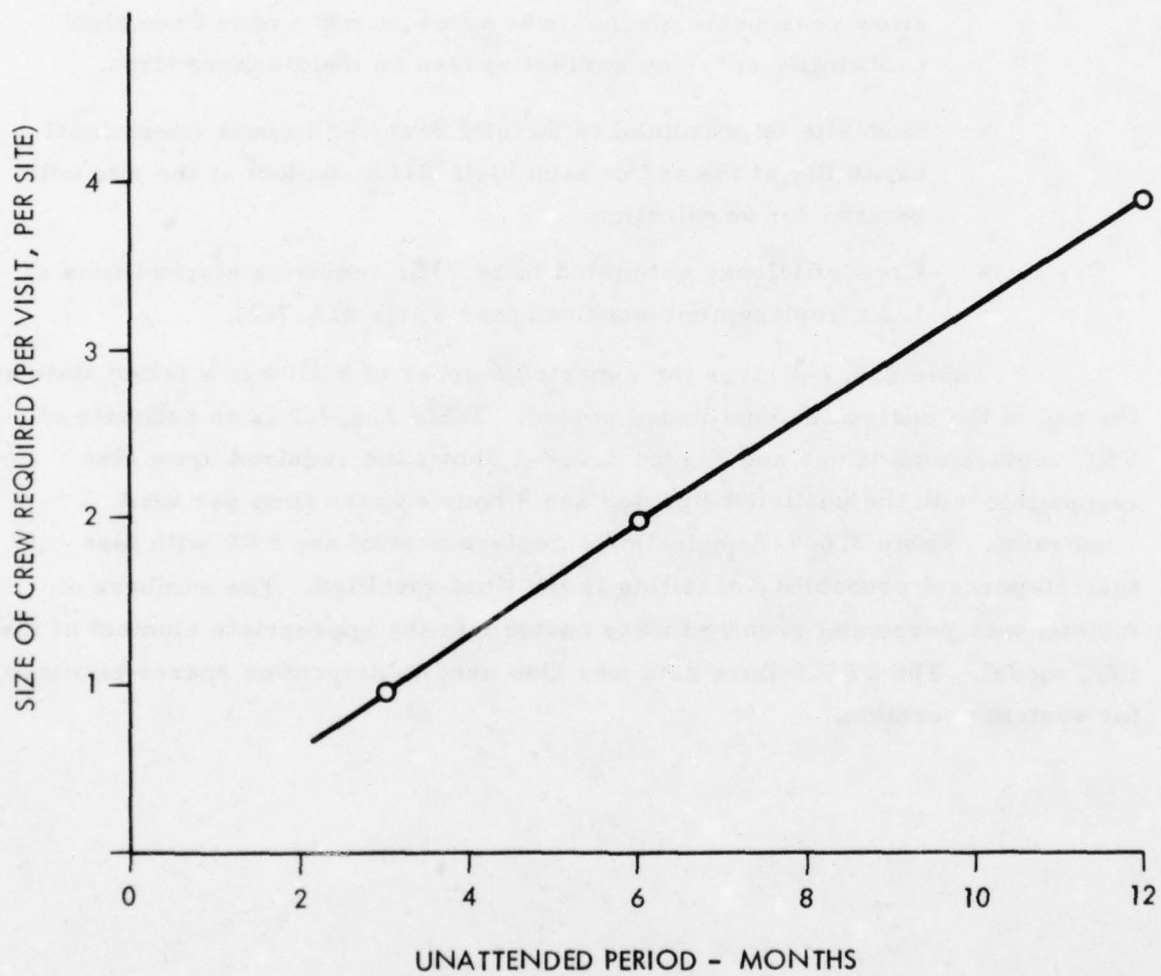
Figure 2.6.7-1. Maintenance Requirements - Baseline Radar,
(3 Hour Max. Elapsed Time Per Site Visit)

Table 2.6.7-1. Expected Replacement Levels - Type A, Baseline Radar

FRU	$n^{(1)}$	λ, Fail. Rate$^{(2)}$	$n\lambda$	Expected No. of Replacements, E (f)		
				3 mos.	6 mos.	12 mos.
Antenna	256	0.6	153.6	0.34	0.67	1.35
TRSSM	256	11.3	2892.8	6.34	12.67	25.34
AZ Steer AB	3	2.5	7.5	.02	.04	.08
AZ Steer CD	24	2.2	52.8	.11	.23	.46
AZ Steer EFH	192	2.1	403.2	.87	1.74	3.48
Beam Sw.	3	11.3	33.9	.07	.15	.29
Receiver	3	25.7	77.1	.17	.33	.67
Exciter	1	19.2	19.2	.04	.08	.17
Sig. Proc. Serial	1	54.8	54.8	.12	.24	.47
D. P. Comm. El.	2	21.5	43.0	.09	.19	.37
S. P. Comm. El.	6	30.8	184.8	.40	.80	1.60
Pwr. Distr.	1	5.0	5.0	.01	.02	.04
IFF	1	6.0	6.0	.01	.02	.04

[1]Unenergized standby spares assumed to have negligible contribution to logistic needs beyond initial installation. They are therefore not considered part of the on-line complement.

[2]All failure rates in units of failures per 10^6 hours.

Table 2.6.7-2. Maintenance Workload Per Visit

FRU Level	φ, Est Repl. Time-hrs.	Workload, Man hours* = φ · E (f)		
		3 mos.	6 mos.	12 mos.
Antenna	.33	.11	.22	.44
TRSSM	.25	1.58	3.17	6.34
AZ Steer AB	.33			
AZ Steer CD	.33			
AZ Steer EFH	.33	.29	.57	1.15
Beam Sw.	.25			
Receiver	.33			
Exciter	.33			
Sig. Proc. Serial	.50			
D. P. Comm. El.	.25			
S. P. Comm. El.	.25	.10	.20	.40
Pwr. Distr.	.33			
IFF	.33			
Σ =		2.09 hrs.	4.16 hrs.	8.33 hrs.
- Replacement time with assumed efficiency of 75%:		2.77	5.55	11.11
- Crew size (maintenance personnel) for 3-hour visit:		1.	2.0	4.0

*Workload man hours omitted from table where their contribution is negligible.

2-218

2.7 Type A Performance Evaluation

The performance of the Type A Baseline and alternate configuration has been analyzed for sensitivity (maximum range), clutter rejection, and ECCM capabilities. The results are presented in the following sub-sections and in Appendix C.

2.7.1 Maximum Range Performance

a) Track Initiation Criteria

Two track initiation criteria have been analyzed. Each of them requires that a target be detected on 3 out of 4 scans. The distinction between the criteria is as follows:

Criterion A
- One false track initiation per hour
- Same detection thresholds on all four scans

Criterion B
- One false track initiation per hour
- Average of ten (10) false alarms on scan #1
- Lower detection threshold on scans #2, 3 and 4

Criterion A applies to the more conventional scan types such as single frame or fence as defined in Section 2.1.1. All scans have equal probability of detection and thresholds are held constant. Criterion B result from the split-frame scan where subsequent target revisits are dependent on the first scan detection. Thresholds must be maintained higher on the first scan to keep initial false alarms to a reasonable level (10 per scan), but they can subsequently be lowered on succeeding scans and still meet the once per hour false track initiation rate.

The analysis is presented in Appendix C-1; the results are summarized in Table 2.7.1-1.

Table 2.7.1-1. Scan Detection Requirements

| Scan Type | Freq | N* | Parameters for Scan #1** | | | Track Initiation Criteria |
			P_d	P_{fa}	S/N (Batch)	
Single or Fence	L	2	0.902	3×10^{-4}	12.7 dB	A
Single or Fence	UHF	5	0.902	5×10^{-4}	7.3	A
Split [Baseline]	L	2	0.828	3×10^{-6}	13.1	B
Split	UHF	5	0.828	5×10^{-6}	7.7	B

* N = Number of 8-pulse batches in 3 dB beamwidth.

** For 6 microsecond transmitted pulsewidth.

The penalty for working with the adaptive split-frame type of scan is about 0.4 dB.

Included in the values of Table 2.7.1-1 is a 0.5 dB allowance for a typical correlation ("range-walk)" loss. A preliminary analysis is given in Appendix B-1.

The scan parameters shown in Table 2.7.1-1 are for a 6 microsecond pulsewidth (Baseline). The use of a 1.5 microsecond pulsewidth would result in somewhat different requirements. For example for the single frame, L-band system with a 1.5 microsecond pulse, the threshold must be raised to a P_{fa} of 6.7×10^{-4} for a corresponding S/N per batch of 12.4 dB ($P_d = 0.902$). Thus the net effect on S/N is only about 0.2 dB.

Table 2.7.1-1 also makes the assumption that all N batches on a scan are detectible, i.e., they do not fall into any blind zones, either around zero doppler or the blind speeds. Considering that:

- The Type A radar is a "tripwire" type system, i.e., detection on all cells is not necessary,

2-220

- The maximum range requirement of 60 NM is beyond the mask (maximum clutter range) for most sites,

- The clutter map implementation permits the system to take advantage of interclutter visibility even in clutter areas,

- Only the lowest elevation beam is affected (where the horizontal coverage is thickest), it appears that this factor can be safety neglected for maximum range calculations.

The effect of the "clutter notch" loss is also analyzed in Appendix C-1 and shown to be about 0.4 dB. An additional loss due to the simultaneous presence of clutter and noise is analyzed in Appendix C.2.4. This latter loss in approximately 0.6 dB for L-Band and 0.1 dB at UHF for an assumed doppler filter improvement limit of 50 dB.

b) <u>Baseline Range Performance</u>

The predicted radar range has been computed on Blake Chart Program and the result is shown in Table 2.7.1-2. This range calculation is for the peak of the lowest elevation beam averaged over azimuth. The peak of the lowest beam occurs at about $3°$. The individual entries are calculated as follows:

- Transmitter power (P_T):

  63 active TRSSM's x 40 watts peak/mod. = 2520 w.

- Pulsewidth (τ)

  6 μseconds transmitted into each beam

- Transmit and receive antenna gain (G_T, G_R)

  Total aperture: 44 ft. diameter ring array and 7 ft. high

  Active aperture (broadside)

  $A = 44 \times 0.707 \times 7 = 217$ sq. ft.

  Aperture gain (G_a)

  $$G_a = 4\pi \frac{A}{\lambda^2} = 4763 \rightarrow 36.78 \text{ dB}$$

  where $\lambda = .758$ ft. (f = 1.3 GHz)

Table 2.7.1-2

Baseline Configuration Maximum Range Calculation


```
RADAR AND TARGET PARAMETERS (INPUTS) --

PULSE POWER, KW ................................          2.6
PULSE LENGTH, MICROSEC .........................       6.0000
TRANSMIT ANTENNA GAIN, DB ......................         35.5
RECEIVE ANTENNA GAIN, DB  ......................         33.8
FREQUENCY, MHZ .................................       1300.0
RECEIVER NOISE FACTOR (FIGURE), DB .............          1.4
BANDWIDTH CORRECTION FACTOR, DB ................          0.
ANTENNA OHMIC LOSS, DB .........................          0.
TRANSMIT TRANSMISSION LINE LOSS, DB ............          1.5
RECEIVE  TRANSMISSION LINE LOSS, DB ............          1.5
SCANNING-ANTENNA PATTERN LOSS, DB ..............          1.3
MISCELLANEOUS LOSS, DB .........................          2.0
SIGNAL-TO-NOISE RATIO, DB ......................          7.5
TARGET CROSS SECTION, SQUARE METERS ............      16.0000
TARGET ELEVATION ANGLE, DEGREES ................         3.00
AVERAGE SOLAR AND GALACTIC NOISE ASSUMED
PATTERN-PROPAGATION FACTORS ASSUMED = 1.


*******************************************

CALCULATED QUANTITIES (OUTPUTS) --

NOISE TEMPERATURES, DEGREES KELVIN --
           ANTENNA (TA) ........................         79.3
           RECEIVING TRANSMISSION LINE (TR) .....        119.6
           RECEIVER (TE) .......................         110.3
           TE X LINE-LOSS FACTOR = TEI .........         155.8
           SYSTEM (TA + TR + TEI) ..............         354.8
TWO-WAY ATTENUATION THROUGH ENTIRE TROPOSPHERE, DB       1.3



RANGE =    81.9 N, MI.,  TROPOSPHERIC ATTENUATION =    1.11 DB

FOR SPECIFIED SIGNAL-TO-NOISE RATIO =    7.50 DB
```

The losses are:

Elevation taper	0.34
Azimuth taper	0.22 (uniform illumination)*
Feed network similarity	0.2
Radiator similarity & mismatch	0.3
TRSSM similarity	0.2

$$\overline{1.26}$$ *Due to TRSSM Class C Operation

Other losses due to cabling are included under transmitter loss or receiver noise temperature.

The net gain is then

$$G_T = 36.76 - 1.26 = 35.5 \text{ dB}$$

- Receiver antenna gain (G_R) (Reference b)

An additional azimuth taper loss of 1.85 dB is incurred due to natural taper of the R-2R lens. Also, the TRSSM similarity loss does not apply thus:

$$G_R = 35.5 - 1.85 + .2 = 33.85$$

- Target cross-section, frequency

$$\sigma_{50} = 16 \text{ sq. meters}$$

$$f_{MC} = 1300 \text{ MHz}$$

} as specified

- System noise temperature (T_{N1})

Receiver loss (L_R):

Antenna feed network (ohmic)	.8
Cables-TRSSM to antenna	.1
1:2 elevation switch	.2
Duplexer	.2
T/R limiter	.2

$$\overline{1.5} \text{ dB}$$

The other calculations are shown on the Blake Chart.

• Visibility Factor (V_o)

Let V_o is defined as the single pulse signal-to-noise ratio (S/N) required to produce the desired output. From the preceding section on Track Initiation Criteria, the Baseline requirement for S/N per pulse is 12.6 dB. The difference between the S/N per pulse and the S/N per batch (the effective processor gain) can be calculated:

Integration gain	+9.0
A/D loss	- .3
Range straddling	-1.0
Doppler weighting	-1.3
CFAR	- .8
	+5.6

Required S/N per pulse = 13.1 -5.6 = 7.5 dB [Baseline split-frame case]

• Bandwidth Correction Factor

This loss is assumed to be included in the signal processing losses (above).

• Transmitter Loss (L_T)

Antenna feed network (ohmic)	.8
Cables-TRSSM to antenna	.1
1:2 elevation switch	.2
Duplexer	.2
1:3 elevation switch	.2
	1.5 dB

• Antenna Scan Loss (L_p)

Two way scan loss in azimuth only is about 1.3 dB. (For UHF, this loss is considerably reduced due to greater overlapping of beams.

• Misc Loss (L_R)

A contingency loss of 2.0 dB is assumed. This value allows the system to degrade by 2 dB and still meet the coverage requirements as shown in Table 2.7.1-2.

2-224

The computed Baseline maximum range for these parameters as shown in Table 2.7.1-2 is 81.9 NM. This value represents the maximum range at the lower elevation beam peak as averaged over all azimuth angles. The average azimuth value is realized by including an allowance for average antenna scan loss (Lp).

The two-way elevation coverage diagram for this situation is shown in Figure 2.7.1-1. The antenna patterns calculated in the antenna study task (Section 2.3.1) were combined with the range analysis given above to derive the coverage shown. The desired coverage region bounded by 60 NM range, 100 KFT. altitude and 45° elevation is also indicated. It can be seen that deep nulls exist due to the low beam cross-over values associated with orthogonal beams. The nulls can be reduced by using elevation beams with closer spacing. The rapid fall-off in performance at high elevation angles is also evident. This is due to large defocussing losses caused by the use of only three azimuth steering lenses. A larger number of lenses would improve this. These alternatives are discussed in the following section.

c) Alternate Configuration Range Performance

The alternate configurations considered in this study (Section 2.2.2), impact the calculation of maximum range in the following areas:

Frequency: L, UHF
Scan type: Single or Fence, Split

Non-orthogonal beams with shallower crossover nulls can be used to fill in the nulls evident in the Baseline coverage of Figure 2.7-1-1. Cross-overs of 3.5 dB can be achieved. A mismatch loss of approximately 1.0 dB occurs for this case due to the closer than orthogonal beam spacing. The net loss in signal relative to the Baseline is thus 1.0 dB for an equivalent maximum range at the lower beam peak (averaged over azimuth) of 77.3 NM.

The 2-way elevation coverage corresponding to this reduced aperture case is shown in Figure 2.7.1-2. The coverage shown also assumes six azimuth steering lenses (one per elevation beam). The improvement in coverage is evident. Also shown in Figure 2.7.1-2 is the equivalent coverage against a 1 square-meter target. Advantage is taken of the effect of wider azimuth overlap at higher elevation angles (more pulses on target) as shown. The coverage shown is

2-225
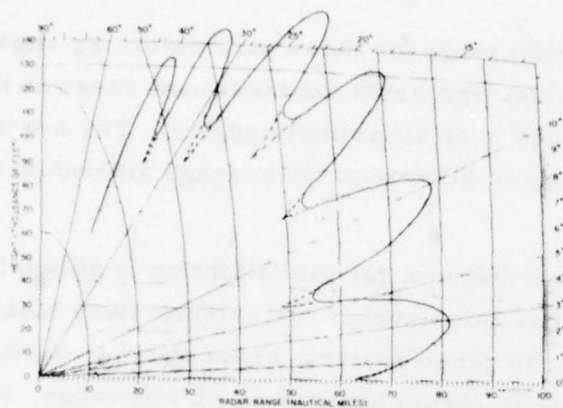
Figure 2.7.1-1

Two-way Elevation

L-Band - 3 Lenses
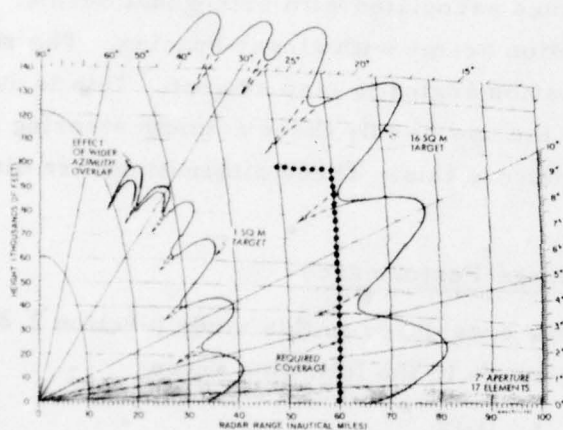
Figure 2.7.1-2

Two-way Elevation

L-Band - 6 Lenses
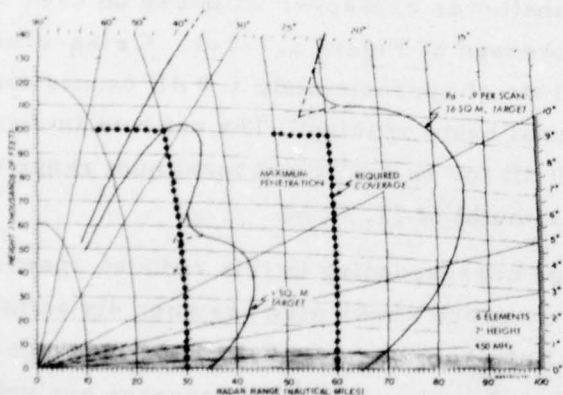
Figure 2.7.1-3

Two-way Elevation

UHF - 2 Lenses

consistent with the requirements for a 1 square-meter target with the exception of the region from about 85-100 KFT.

The UHF coverage diagram for a two lens configuration is shown in Figure 2.7.1-3. Coverage is good against both 16 and 1 square-meter tragets.

The important differences in parameters for UHF are indicated below:

Gain

Wavelength (λ): 2.46 feet

Aperture height: 7 feet

Aperture Gain: 27.6 dB

	T	R
Elevation taper	0.34	0.34
Azimuth taper	0.22	0.22 (uniform)
Lens taper		1.85 (5 dB taper)
Feed network similarity	0.1	0.1
Radiator similarity/mismatch	0.3	0.3
TRSSM similarity	0.2	
	1.16	2.81

Therefore: G_T = 26.4 dB ; G_R = 24.8 dB

Transmission Line Losses

	L_T	L_R
Antenna feed network (ohmic)	.4	.4
Cable	.2	Neg
1:2 elevation switch*	.2	.2
Duplexer	.2	.2
T/R limiter		.2
	1.0	1.0 dB

Required S/N per pulse

S/N = 7.7 - 5.6 = 2.1 dB [UHF, Split frame]

*Not present in UHF systems with two active receivers.

2-227

The range values calculated in Tables 2.7.1-2 and 2.7.1-4 are for the split-frame case. The ranges for the single frame or fence cases are greater by the signal-to-noise requirement variation (0.4 dB) as shown in Table 2.7.1-1. The maximum ranges at the lower elevation beam peak (averaged over azimuth) are summarized in Table 2.7.1-3. The range calculations are shown in Blake Chart format in Table 2.7.1-4 for a UHF, single scan, 7 ft. aperture height configuration.

All range calculations shown are for a 6 microsecond transmitted pulse. As indicated earlier, a 1.5 microsecond pulse results in a small additional loss; however, the effect on range is only about 1 percent.

Table 2.7.1-3. Maximum Range Summary

Scan Type	Freq	Beam Elevation	Maximum Range
Single/Fence	L	3°	83.8 NM
	UHF	9°	87.8
Split [Baseline]	L	3°	81.9
	UHF	9°	85.8

2.7.2 Clutter Performance

a) Clutter Rejection Requirements

The clutter environment given in the statement of work is shown in Table 2.7.2-1.

The subclutter visibility (SCV) of a radar system is a measure of its ability to detect moving-target signals superimposed on clutter signals. However, SCV is a power ratio between a clutter source and a moving target. Strictly speaking any ratio is without dimensions. It is this 'looseness' in the definition of SCV that has contributed to many interpretations how its qualities in a radar system can be measured.

2-228

Perhaps the most realistic definition of SCV is to relate it to the system Improvement Factor (I) by the following relationship:

$$SCV = 10 \log \frac{C_i}{S_i} = I - X$$

where $\frac{C_i}{S_i}$ = maximum input clutter-to-signal power ratio

Table 2.7.1-4
UHF Maximum Range Calculation

RADAR AND TARGET PARAMETERS (INPUTS) --

```
PULSE POWER, KW ..................................       4.7
PULSE LENGTH, MICROSEC ...........................    6.0000
TRANSMIT ANTENNA GAIN, DB ........................      26.4
RECEIVE ANTENNA GAIN, DB  ........................      24.8
FREQUENCY, MHZ ...................................     450.0
RECEIVER NOISE FACTOR (FIGURE), DB ...............       1.4
BANDWIDTH CORRECTION FACTOR, DB ..................       0.
ANTENNA OHMIC LOSS, DB ...........................       0.
TRANSMIT TRANSMISSION LINE LOSS, DB ..............       1.0
RECEIVE   TRANSMISSION LINE LOSS, DB .............       1.0
SCANNING-ANTENNA PATTERN LOSS, DB ................        .8
MISCELLANEOUS LOSS, DB ...........................       2.0
SIGNAL-TO-NOISE RATIO, DB ........................       2.1
TARGET CROSS SECTION, SQUARE METERS ..............   16.0000
TARGET ELEVATION ANGLE, DEGREES ..................      9.00
AVERAGE SOLAR AND GALACTIC NOISE ASSUMED
PATTERN-PROPAGATION FACTORS ASSUMED = 1.
```

****

CALCULATED QUANTITIES (OUTPUTS) --

```
NOISE TEMPERATURES, DEGREES KELVIN --
        ANTENNA (TA) ...........................    147.9
        RECEIVING TRANSMISSION LINE (TR) .......     75.1
        RECEIVER (TE) ..........................    110.3
        TE X LINE-LOSS FACTOR = TEI ............    138.9
        SYSTEM (TA + TR + TEI) .................    361.9
TWO-WAY ATTENUATION THROUGH ENTIRE TROPOSPHERE, DB      .3
```

RANGE =   85.8 N. MI., TROPOSPHERIC ATTENUATION =   .29 DB

FOR SPECIFIED SIGNAL-TO-NOISE RATIO =   2.10 DB

Table 2. 7. 2-1.   Clutter and Environment Data (Guide)

	UHF		L-Band		S-Band	
			Reflectivity (dB)			

	UHF		L-Band		S-Band	
Land Clutter						
Median	-39		-34		-32	
84th Percentile	-29		-24		-22	
Sea Clutter (Sea State 4)	(H)	(V)	(H)	(V)	(H)	(V)
One degree depression angle	-72	-53	-55	-48	-42	-41
three degree depression angle	-62	-5?	-50	-43	-42	-39

(H) is horizontal polarization

(V) is vertical polarization

Weather:

Rain up to 15 millimeters/hour from 0 to 30K feet for a storm cell size up to 5 miles in horizontal extent. Wind shear 0 to 80 knots from 0 to 50K feet with any arbitrary shear distribution over this altitude range.

I = clutter improvement factor (dB)

χ = detectability factor (dB)

The ratio C/S may be interpreted as the requirement imposed by the target size and the clutter; the detectability factor χ is a requirement imposed by the performance desired in terms of detection probability and false-alarm probability; and the improvement factor I is what the signal processor must deliver to meet these requirements.

$$I = SCV + \chi$$

The value that the clutter should be suppressed below the signal to prevent excessive additional loss in the presence of clutter plus noise is analyzed in Appendix C. 2. 4.

The SCV and improvement requirements are summarized in Table 2.7.2-2 for the various types of clutter versus the different system alternatives. It can be seen that the dominant clutter rejection (improvement) requirement is against ground clutter. UHF has an advantage of about 6 dB less improvement required. The analysis is given in Appendix C-2. Some comments follow.

Table 2.7.2-2. Clutter Rejection Requirements

	SCV (dB)		I (dB)	
	L	UHF	L	UHF
Land Clutter	33.4	32.4	49.8	43.4
Sea Clutter	6.9	6.0	23.3	17.0
Weather Clutter	9.3	-0.6	25.7	10.4
Aurora	-47	-22	-31	-11

Terrain Clutter

The terrain clutter characteristics given in the Statement-of-Work indicate a log normal distribution. The analysis is discussed in Appendix C-2.

A 30 NM range has been selected as a typical worst case range for maximum clutter return as this is the maximum range required against the 1 square meter target. This also approximately corresponds to the horizon between a radar at 200 feet height and a target flying at 100 feet.

Sea Clutter

The Baseline Type A radar use vertical polarization. The worst case should occur at about 30 NM range. A 1 degree depression angle value has been assumed.

Weather

With a rainfall rate of 15 mm per hour and the storm reaching up to
30 kft, the maximum rain cross-section will occur at maximum range.
The rain spectrum will be about 150 hertz wide at L-Band corresponding
to a 40 knot velocity width.

Aurora

Aurora occurs at altitudes of 80 to 150 Km. The reflection coefficient
is highly sensitive to the angle between the radar beam and the magnetic
field lines at the aurora location. The maximum reflections occur with
near normal incidence and reports indicate sensitivity to the aspect angle
of about 10 dB per degree. High dopplers have been measured up to
1200 meters per second (4000 m/sec on rare occasions). Aurora can be
detected over a wide azimuth span from the direction of the magnetic pole,
but the intensity falls off away from the pole direction. The aurora is
limited in elevation extent, with a height of 15 km reported and a typical
depth of 200 km in range.

Volume reflection coefficients of -100 dB (M^2/M^3) at L-band and
-80 dB at UHF are indicated as maximum intensities.

The typical aurora should appear at $3°$ elevation and at an altitude
of 110 km with a $1°$ elevation extent. The maximum cross-section will
be about 16 dBsm. Since the aurora at long range, about 500 NM, will
be competing with a target at 60 NM, the effective aurora cross-section
at this range at L-band is only ~20 dBsm. Also, with the aurora at long
range, only one pulse will be received before the batch frequency is
changed. This single pulse also occurs at the end of the batch and is
further reduced by the batch weighting. These factors are conservatively
estimated at about 15 dB. This is believed to be a worst case value and
indicates that aurora should not be a problem for L-band operation.

Aurora backscatter is increased at UHF due to the larger back-scatter
coefficient and the larger beamwidth. The net effect is 25 dB greater than
for L-band. Calculations show that super clutter visibility can be main-
tained on both the 1 sq. meter target at 30 nmi and the 16 sq. meter target
at 60 nmi.

b) Clutter Filtering

Given the clutter rejection requirements of Table 2.7.2-1, the next step is to design a filter network which can achieve these requirements in the best manner. Several different techniques can be utilized:

o Moving Target Indicator (MTI)
o Fast Fourier Transform (FFT)
o MTI followed by FFT
o Generalized Finite Impulse Response (FIR) Filter

The doppler response achievable by MTI, FFT or a combination of the two is analyzed in Appendix C-3. The results are summarized in Figures 2.7.2-1 through 2.7.2-4.

Figure 2.7.2-1 shows the response for an 8 point FFT only at L-band Hanning weighting is used. The maximum values of C/S for terrain and weather are used. A 40 knot wind is assumed. The other parameters are listed in the Figure. The spectrum shown is skewed due to the unidirectional wind velocity. Filter number 2 gives fair clutter rejection while filters 1 and 7 are poor. Filters 3 through 6 give excellent clutter rejection. Filter 0 is, of course, bad.

A similar clutter spectrum is shown in Figure 2.7.2-2 for UHF. The assymetrical effect of the wind-driven rain is much less evident as the relative spectral (doppler) spread is much narrower.

The response of an 8 point FFT preceded by a single delay line (2 pulse) canceller MTI is shown in Figure 2.7.2-3 and 2.7.2-4 for L-band and UHF respectively. Filters 1 and 7 are greatly improved at L-band. They are even more improved at UHF.

The use of a generalized Finite Impulse Response (FIR) or transversal filter has been reported in the literature (References 2.7-1 and 2.7-2). This type of filter forms a group of individual doppler filters with sidelobes optimally configured to reject a given interference spectrum model. Thus, each filter has a different sidelobe structure given its position.

2-233
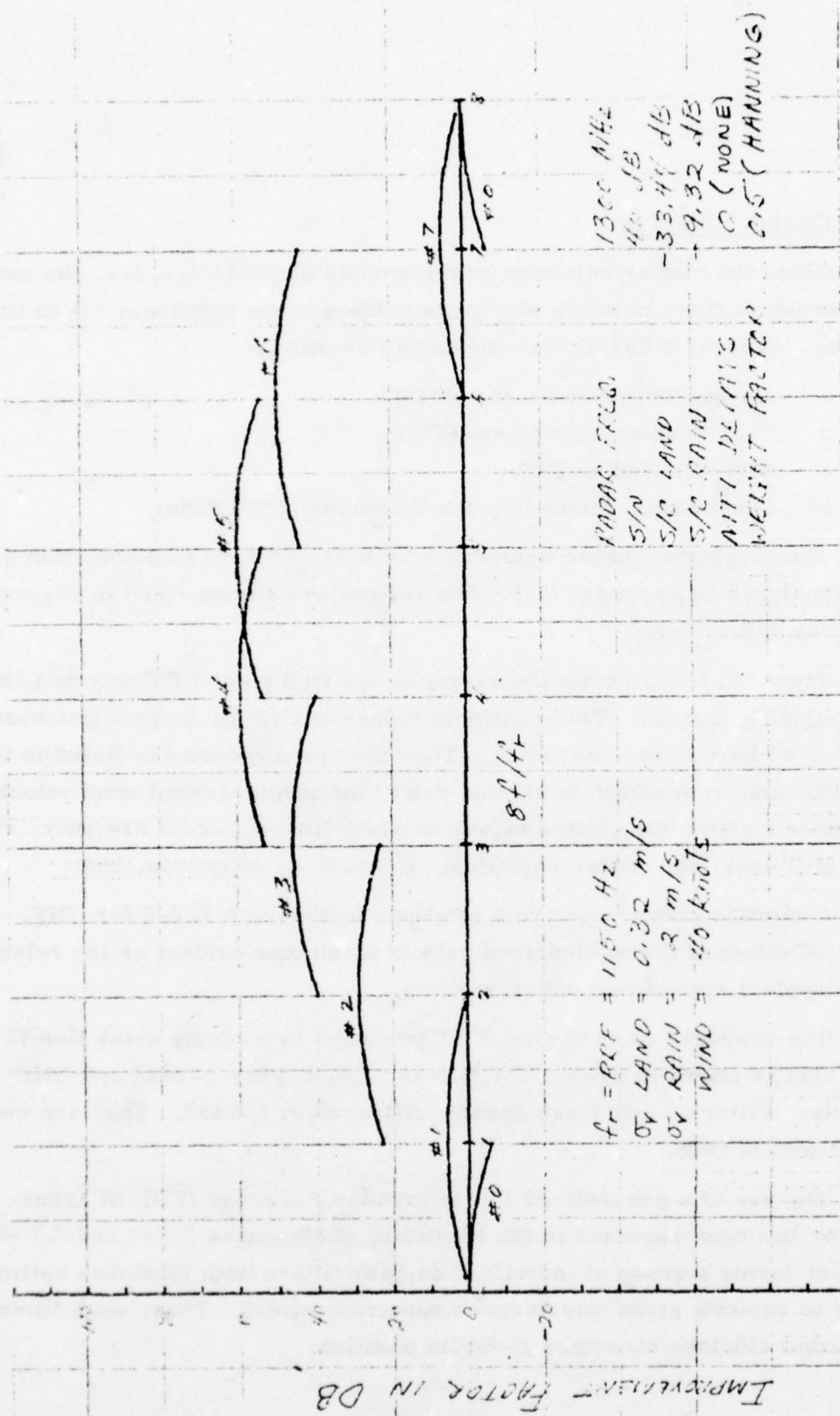
Figure 2.7.2-1. Clutter Improvement, FFT, L-Band

RADAR FREQ. = 1300 MHz
S/N = 40 dB
S/C LAND = -33.44 dB
S/C RAIN = -9.32 dB
ANT'I DELAYS = 0 (NONE)
WEIGHT FACTOR = 0.5 (HANNING)

$f_r = RCF = 1150 Hz$
$\sigma_V LAND = 0.32 m/s$
$\sigma_V RAIN = 2 m/s$
$WIND = 40 knots$

IMPROVEMENT FACTOR IN DB

2-234
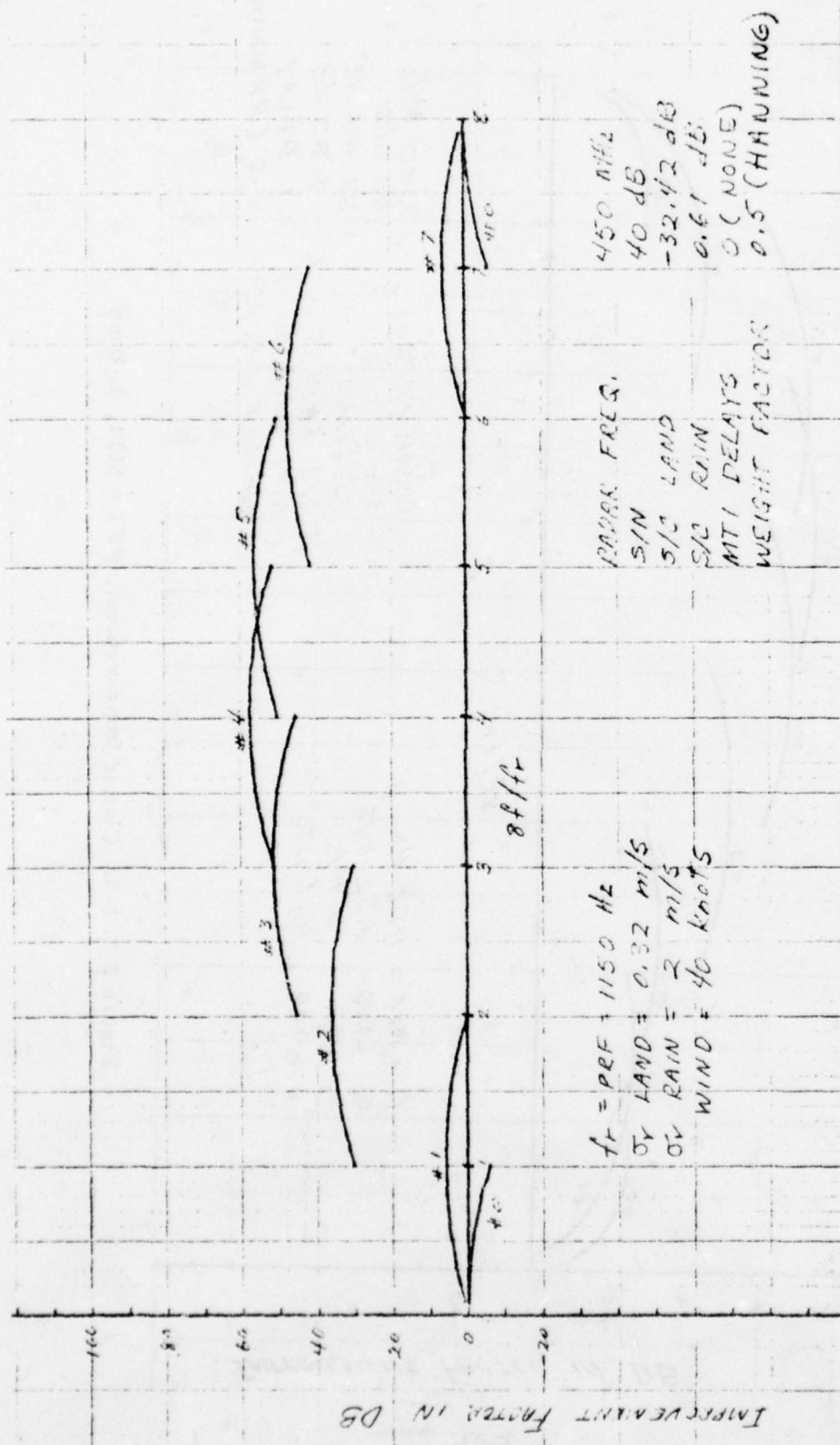
Figure 2.7.2-2. Clutter Improvment, FFT, UHF
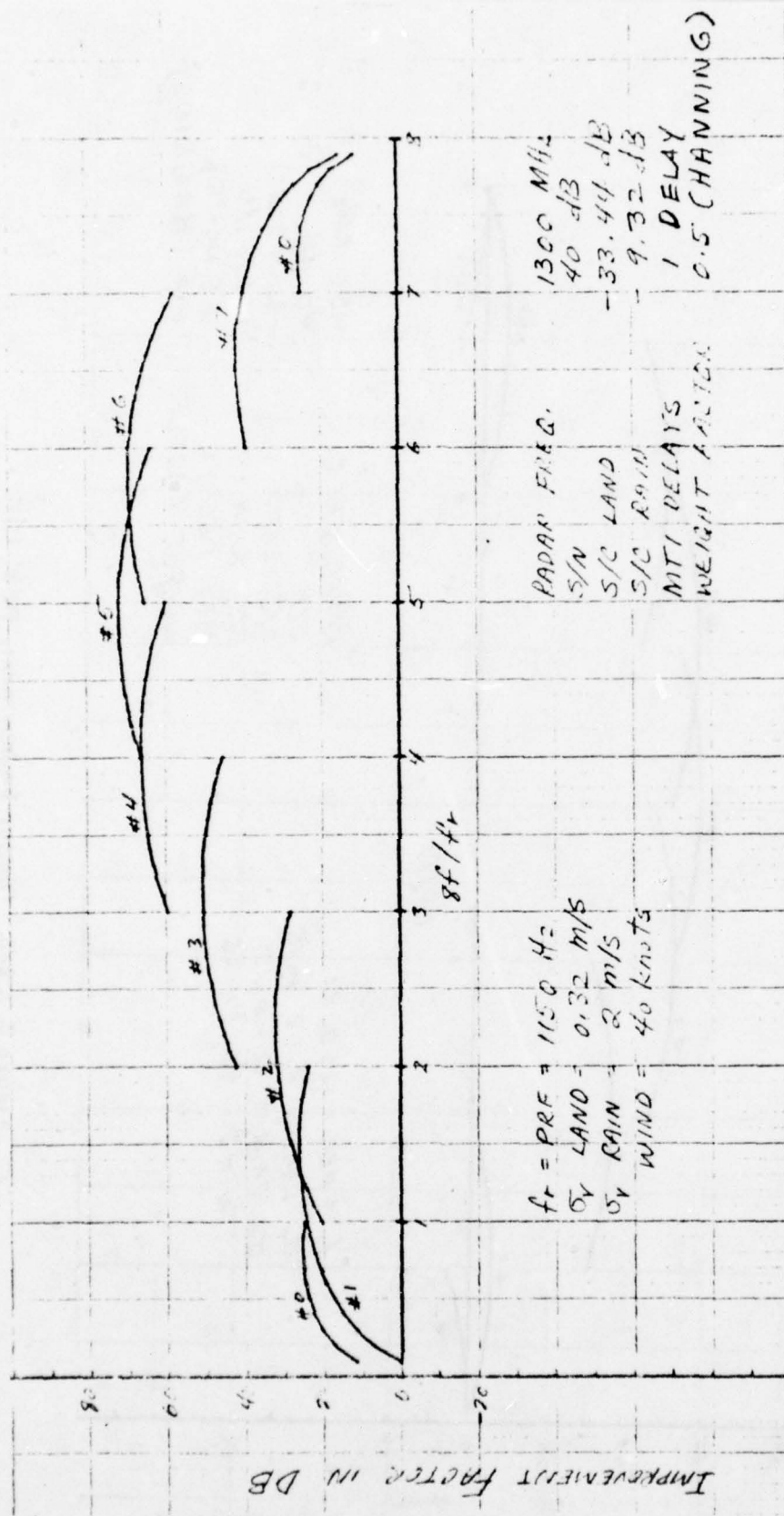
Figure 2.7.2-3. Clutter Improvement, FFT + MTI, L-Band
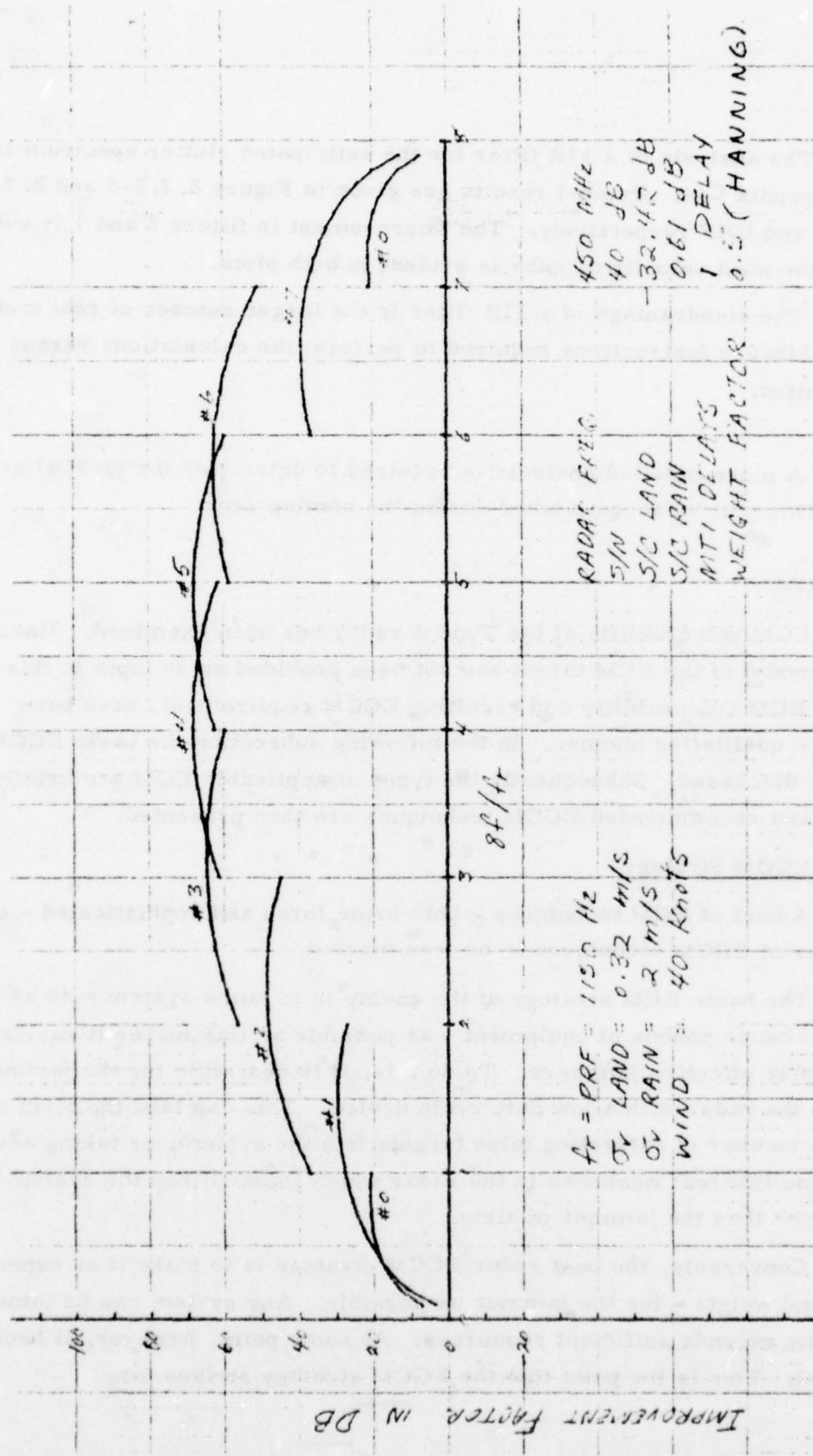
Figure 2.7.2-4. Clutter Improvement, FFT,+MT1, UHF

RADAR FREQ.   450 MHz
S/N   40 dB
S/C LAND   -32.47 dB
S/C RAIN   0.190 dB
MTI DELAYS   1 DELAY
WEIGHT FACTOR   0.5 (HANNING)

f_r = PRF = 115.0 Hz
σ_v LAND = 0.32 m/s
σ_v RAIN = 2 m/s
WIND = 40 knots

IMPROVEMENT FACTOR IN DB

The analysis of a FIR filter for the anticipated clutter spectrum is given in Appendix C-4. Typical results are given in Figure 2.7.2-5 and 2.7.2-6 for L-Band and UHF respectively. The improvement in filters 2 and 7 is evident. A notch at the wind velocity doppler is evident in both plots.

The disadvantage of a FIR filter is the larger number of real multiplies and hence software instructions required to perform the calculations versus the MTI/FFT filter.

A more detailed analysis is required to determine the most effective solution. This will be accomplished during the coming year.

2.7.3 ECCM

The ECM vulnerability of the Type A radar has been examined. Since a definitive model of the ECM threat has not been provided as an input to this study, the ECM vulnerability and resulting ECCM requirements have been handled in a qualitative manner. In the following subsection the basic ECCM strategy is discussed. Subsequently the types of applicable ECM are briefly discussed and recommended ECCM techniques are then presented.

a) ECCM Strategy

A host of ECM techniques - both brute force and sophisticated - exist. The number of ECCM techniques is no less myriad.

The basic ECM strategy of the enemy is to jam a system with as few watts - and hence pounds of equipment - as possible as this makes it easier for him to display effective jammers. To do this, it is desirable for the jammer to degrade the radar with a low duty cycle device. This can take the form of injecting a number of saturating false targets into the system, or taking advantage of some inherent weakness in the radar which immobilizes the system for a time longer than the jammer on time.

Conversely, the best radar ECCM strategy is to make it as expensive - in power and weight - for the jammer as possible. Any system can be jammed if the enemy expends sufficient resources. At some point, however, it becomes impractical. This is the point that the ECCM strategy strives for.

Improvement Factor in dB

80   60   40   20   0

0   1   2   3   4   5   6   7   8

$8f/f_r$

f_r = PRF = 1150 Hz
σ_v Land = 0.32 m/s
σ_v Rain = 2 m/s
Wind = 40 knots

CASE 2

Radar Freq	1300 MHz
S/N	40 dB
S/C Land	-33.44 dB
S/C Rain	- 9.32 dB
# of Samples	8
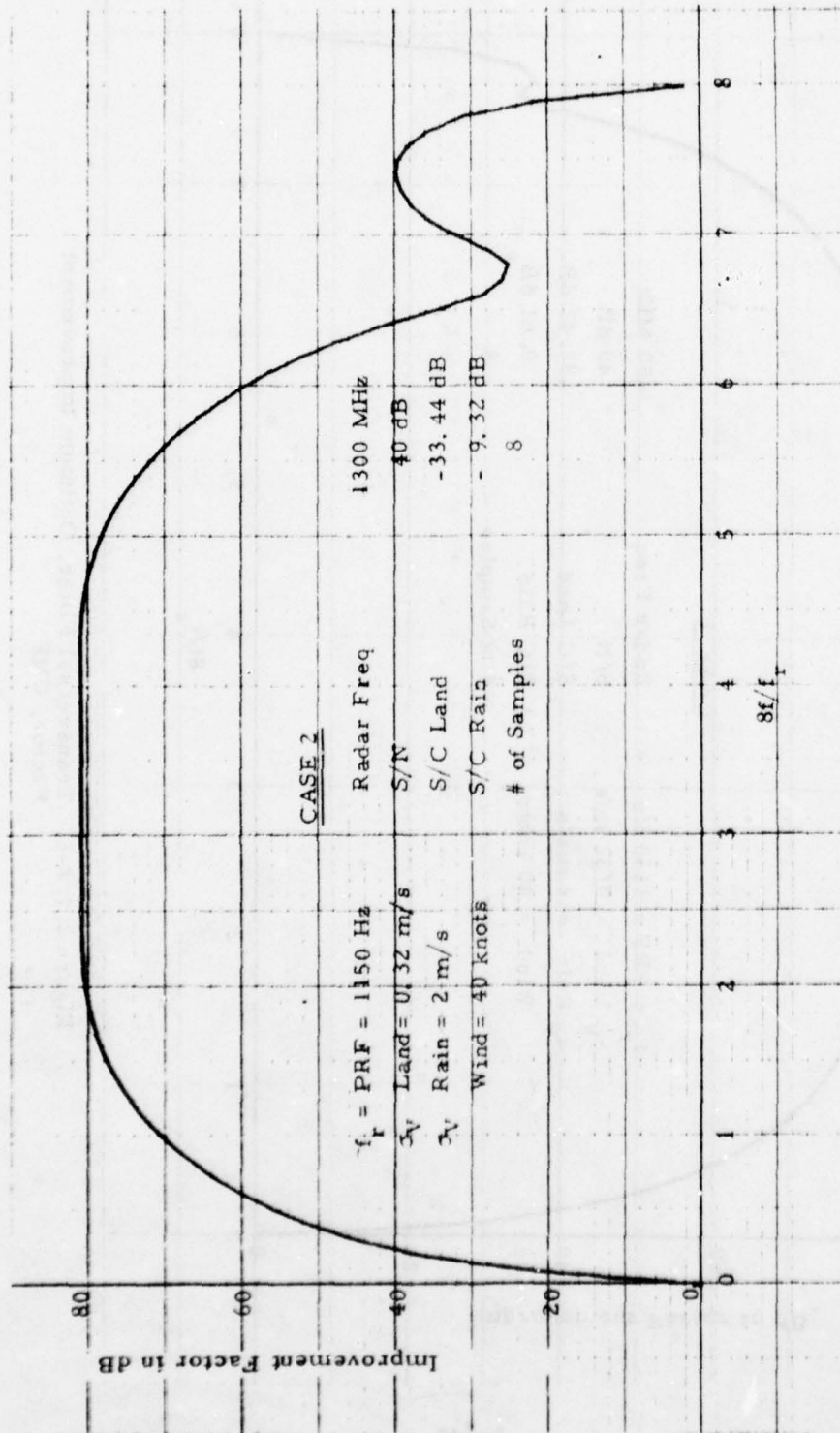
Figure 2.7.2-5. Transversal Filter, Optimum Improvement Factor, L-Band

2-239

CASE I

f_r = PRF = 1150 Hz

σ_V Land = 0/32 m/s

σ_V Rain = 2 ms/s

Wind = 40 knots

Radar Freq	450 MHz
S/N	40 dB
S/C Land	32.42 dB
S/C Rain	0.61 dB
# of Samples	8

Improvement Factor in dB

80

60

40

20

0

0 1 2 3 4 5 6 7 8

$8f/f_r$
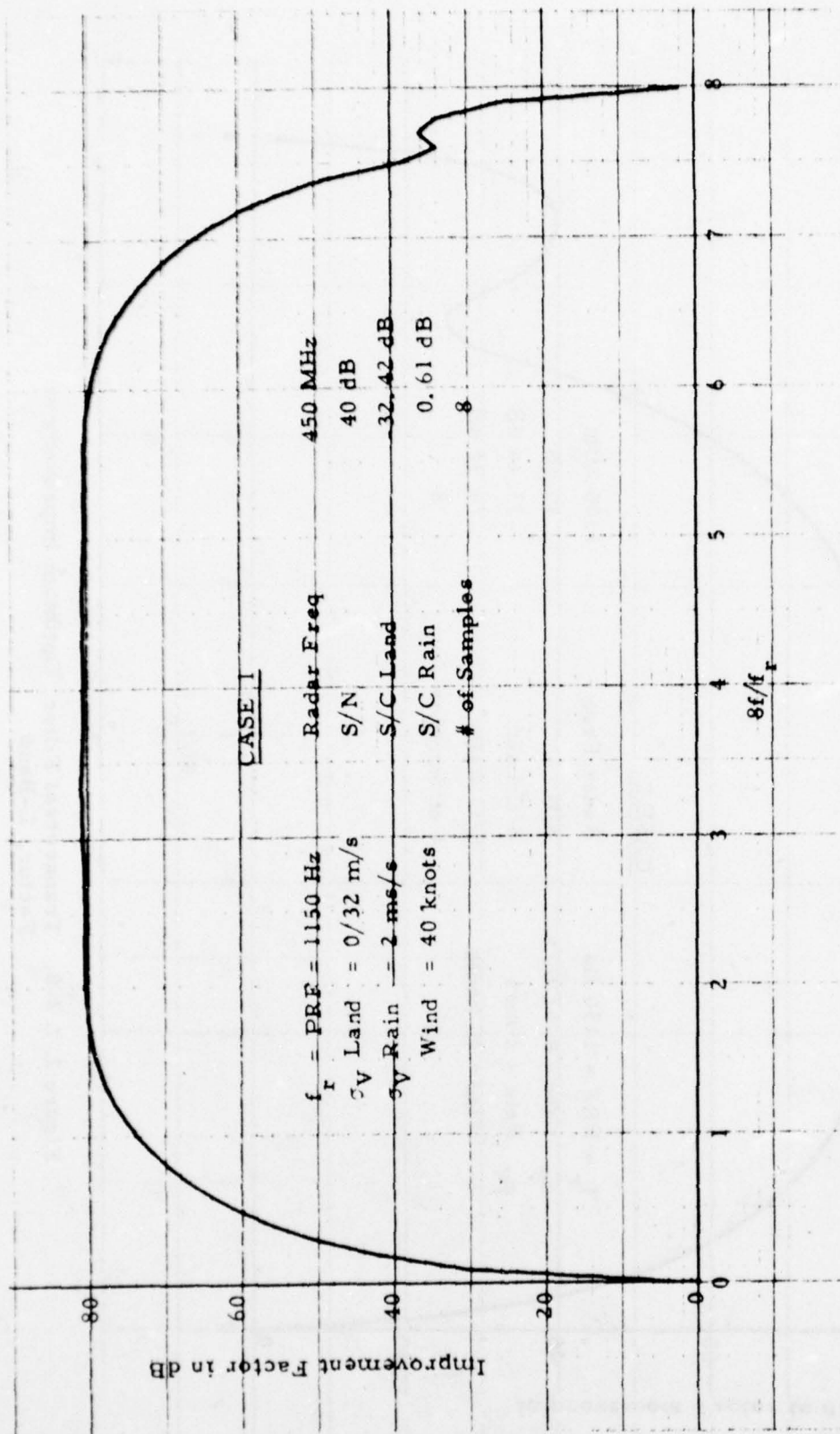
Figure 2.7.2-6. Transversal Filter, Optimum Improvement
Factor, UHF

To accomplish this goal for the Type A radar, a three level ECCM strategy is recommended:

1. Design the system to be relatively invulnerable to low-duty cycle ECM and thus force the jammer to a brute force random noise power duel.

2. Maximize the amount of average power random noise necessary to degrade system performance.

3. Provide means of detecting the presence of ECM and of locating the jammers.

The first strategy prevents the jammer from gaining an easy advantage of peak power versus average power by the use of deception jammers or impulse type jammers. The ECM/ECCM duel then becomes a contest of relative powers.

The second strategy attempts to force the jammer to use more random noise than be optimally has to. This is accomplished through frequency uncertainty, low receive antenna sidelobes, and coherent integration.

Finally, to combat a jammer which can bring an overwhelming amount of power to bear, means of detecting and locating the ECM source are provided.

b) Types of ECM

Jammers can be classified according to their tactical use or their type of modulation.

Tactics

Tactical uses can be broken up into:

1. Self-screening
2. Mainlobe screening
3. Stand-off

The first is not a primary threat as the jammer only screens himself (or someone close). The Type A is a "tripwire" system whose primary function is early warning of intruders actually penetrating the net of radars. Means shall

be provided to detect and locate (in azimuth) such jammers. Their intent - whether to actually penetrate or to act as an irritant - can then be assessed at the operational center and the appropriate action can be taken.

Mainlobe screening is a little more useful to the jammer as a corridor for a penetration is opened. However, with reasonably narrow radar beamwidths, and the overlapping coverage provided by adjacent (and opposite) beams, and adjacent sites, the amount of protection given to hostile intruders is minimal.

Stand-off jamming should be the primary ECM tactic against Type A radars. The purpose is to inject energy through the radar's sidelobes to cover all azimuth (and elevation) beams. The stand-off jammer may be just an irritant sent to test and spoof the radar net - but it may also mask actual penetrators. This is then the primary ECM tactic to counter.

Modulation

The various types of applicable ECM modulations are summarize in Table 2.7.3-1 and discussed below. The primary effect of the ECM modulation on the radar is also noted in the table. Many jamming modulations are designed strictly for self-screening and these are not discussed for the reasons expressed above.

• CW

This is a primitive form of jamming whose purpose is to interfere with weak signals and thus reduce sensitivity. As the exact radar frequency must be known, and as it is easily defeated by various techniques, this type of ECM modulation is not generally employed.

• Noise

This is the simplest type of ECM modulation (other than CW) to generate. It is created either by a low power noise source followed by direct amplification of noise (DINA) or at high power by frequency modulating a rapidly swept CW signal.

If the radar frequency uncertainty is relatively small, then the noise power can be concentrated as a spot jammer. Spot noise jamming,

Table 2.7.3-1. Types of Jammers

TYPE		PRIMARY EFFECT
• CW		LOSS OF SENSITIVITY
• NOISE		
	• SPOT	
	• SWEPT	
	• WIDEBAND	
• RCVR CAPTURE		LOSS OF SENSITIVITY
	• IF	
• TRACK BREAKER		RCVR SATURATION, LOSS OF SENSITIVITY
• PULSE		DEGRADATION IN R, $\dot{R}$, AZ, EL
	• RANDOM	FALSE ALARMS
	• REPEATER	FALSE ALARMS $(R > R_J)$
• SOPHISTICATED DECEPTION		FALSE ALARMS
(COHERENT WAVEFORM ANALYSIS & GENERATION)		

2-243

against a frequency changing radar, requires some means of locating frequency occupany. This usually takes the form of a set-on or look - through technique.

On a set-on system, the frequency occupancy is measured in the absence of ECM. Jamming is then generated. The danger to the jammer occurs if the radar changes frequency sufficiently to clear the ECM. The jammer can then pause again, set-on and recommence jamming. If the radar changes frequency rapidly, the jammer can be seriously degraded.

Look-through tends to circumvent this problem at the cost of complexity. Jamming is periodically interrupted for a short period to receive and analyze the radar spectrum. The transmission interruption can be sufficient to examine a complete radar interpulse period or a very rapid on-off transmission such as "click" or "flicker" jamming where one very short sample is taken every pulsewidth.

The disadvantage of spot jamming, by whatever method, is the additional complexity as a receiver, duplexer and processor are required. The effective ECCM against this ECM is to force the jammer into a broad-band mode by the use of frequency changes.

As the radar frequency uncertainty grows, the jammer may try to sweep the noise spot. The purpose of swept jamming is to temporarily cause the receiver to go into saturation or "ring". If the jammer can sweep back before the receiver unblocks, then continuous jamming is achieved over a wide band at a fraction of the normal power required.

Swept ECM can be made ineffective if sufficient dynamic range and IF limiting are provided in the receiver, so that the receiver only puts out its impulse response (≈ 1 pulsewidth) without blocking when hit by an impulse. The sweeping must then become faster until the entire radar uncertainty spectrum is filled. The jammer is then a wide band noise jammer; this can also (and usually is) achieved by DINA jammers using wide band RF power amplifiers.

2-244

• Receiver Capture - IF Jamming

There are several variations of this type of ECM. All involve prior knowledge of the victim receiver IF and all operate by creating a beat IF between two separate frequencies. Either two separate frequencies separated by the IF can be transmitted by the jammer or only a single frequency above the radar's by the IF. In the latter case, the radar itself provides the other frequency. This technique is defeated if the first IF is higher than the receiver bandpass.

• Track-Breaker

Many types of track breakers are possible. The primary goal is to capture one element of the radar resolution cell (range, azimuth, elevation, range rate) which is tracking the jammer and cause it to go off target. So the Type A radar is a track-while-scan system which periodically reexamines all resolution cells, this type of jamming is not very applicable. The extent in degradation possible is loss of azimuth accuracy by some types of angle modulation techniques.

• Pulse Jamming (Unsynchronized)

This type of ECM has the same purpose as swept jamming, i.e., cause the receiver to become inoperative due to saturation. This is another attempt for the jammer to obtain a duty cycle advantage.

With the coherent signal processing of the FFT, the unsynchronized pulses will not achieve any coherent gain. In addition they will appear in one particular range gate and doppler filter and thus will block only a relatively small number of resolution cells. Frequency changes will be effective unless the jammer employs a sophisticated set-on receiver.

• Pulse Repeaters and Deception ECM

The purpose of these forms of ECM is to saturate the signal and data processor with excessive false alarms. There are an extremely large number of different techniques used; however, for the Type A

application, where PRR synchronization is required, the basic
technique is that of a repeater. This type of jammer amplifies and
retransmits the received pulse. It may also retransmit a replica of
the pulse at fixed delay intervals to provide a string of false targets
spread out in range.

This type of jammer cannot create targets ahead of itself unless
it delays pulses to the next interpulse period. (It then in effect anticipates
the next pulse.) PRR agility is effective aginst this type of jammer,
particularly if it lies beyond the instrumented range.

The Type A PRR is shifted after each group of 8 pulses; the frequency
is also shifted, but must remain stable in PRR for the complete 8 pulses.

If the jammer is beyond the instrumented range, then its simulated
returns will be rejected in the target verification test where two successive
pulse group returns at different PRR's are required to be directed in coin-
cidence. However, if the target is within the instrumented range, only
one out of 8 pulses will be lost and the jamming can effectively appear
as false targets.

To avoid being attenuated in the dc clutter notch, the jammer can
offset the received signal by a suitable doppler. This doppler can also
be made to vary to cover different doppler filters. Other, more sophis-
ticated modulation which can simulate a moving target, can be added
with a suitable processor. The radar pulse can also be anticipated if
the radar waveform and frequencies are highly regular.

There are several possible countermeasures against this type of
ECM. One is to turn the CFAR thresholds down until an acceptable
number of false alarms occur. This is done automatically under pro-
cessor control.

An even more effective ECCM is to switch the exciter into a Coherent
Oscillator (COHO) mode. In this mode, a random phase variation is in-
serted into the transmitted pulse every pulse period. As the same reference

is used to generate the local oscillator, the pulse shift is effectively re-moved for those pulses returning during the same interpulse period. As the jammer cannot anticipate the phase shift to be added next pulse. Thus the jammer can successfully insert false targets only behind itself; anticipated pulses before its range, are dispersed in the FFT due to their random phases. The target jammer can then not only be located in azimuth but also in range as its return is the first.

This ECCM cannot be left in operation on a continuous basis as some degradation does occur. Multiple time around clutter cancellation deteriorates in a COHO mode. Thus a switch must be provided to move the system temporarily into this mode to clear the false alarms and to locate the jammer. The exact location of such a control - whether on the console or at the pallet has not yet been determined; however, its inclusion is a relatively simple matter.

c) Inherent Baseline System ECCM

Many of the ECCM features discussed above have been incorporated into the Baseline Configuration as normal measures against natural interference (noise, ground clutter and weather). The specific capabilities and the ECM techniques that they counter are summarized in Table 2.7.3-2.

Most of these ECCM capabilities are self evident from the foregoing discussion. Those that might require further discussion are given below.

Range Average CFAR

The Type A signal processor utilizes a range average constant false alarm rate (CFAR) technique to combat weather returns. Eight range gates from each side are added and a threshold above the average is computed. The target must be above this threshold for detection. Continuous noise or CW will raise the levels in all gates and thus will not create any additional false alarms. A loss of sensitivity naturally occurs, but this is the expected outcome in a radar/ECM power duel.

Table 2.7.3-2. Baseline System Inherent ECCM Capability

CAPABILITY	AGAINST
TYPES A BASELINE	
● 2ND IF > RF BAND	IF
● WIDE DYNAMIC RANGE	SWEPT
● IF LIMITING	CW, SWEPT
● FREQUENCY AGILITY	CW, SPOT, RANDOM PULSE
● SPECTRAL FILTER	NOISE, RANDOM PULSE
● RANGE AVERAGE CFAR	NOISE, CW
● INTERFERENCE EDITOR	PULSE
● TRACK SMOOTHING	ANGLE TRACK DEGRADATION
RECOMMENDED FOR ECCM CONFIGURATION	
● LOW RECEIVE SIDELOBES	ALL TYPES FROM SIDELOBES
● SIDELOBE BLANKING	PULSE, DECEPTION IN SIDELOBES
● STROBE REPORTING	NOISE, CW, PULSE

Interference Editor

The signal processor has the capability of determining if the signal in a given range gate exceeds the linear limits of the system, i.e., goes into saturation. Range gates indicating saturation are suppressed. This effectively prevents high level pulse signals from causing false alarms.

Track Smoothing

Continued track will average out angle errors caused by angle track breaker type jammers.

d) Additional ECCM for ECCM Configuration

Several other techniques, not included in the Baseline configuration are desirable for an ECCM configuration. These additional techniques are also shown in Table 2.7.3.2. The penalities for these addition is increased cost and power consumption. These penalities are quantitifed in Section

Low Receive Sidelobes

As the sidelobe jammer is probably the primary ECM threat, it is highly desirable to suppress sidelobes on receive. The effect of antenna taper on sidelobes is discussed in Section 2.3.1, Figure 2.3.1-4. The method of achieving such tapers is by adding a group of digital attenuator with appropriate logic and control as described in Section 2.2.3. Approximately 10 dB of taper is sufficient to keep all sidelobes below 30 dB (with the possible exception of sidelobes about 3-4 dB higher at $\pm 90^{\circ}$). As five dB is furnished by the natural R-2R lens taper, only five dB further is required by the attenuators.

The effectiveness of taper on sidelobe control is partially degraded if antenna elements are allowed to fail. The sidelobes will tend to rise as TRSSM's or some of the final azimuth switch, e.g., quadrant switches, fail. For eight failed elements, peak sidelobes will rise about 2 to 5 dB at random azimuths. The RMS sidelobes are still well down.

For a UHF antenna, the peak gain is about 24 dB. Thus, the average sidelobes are probably no better than 27-29 dB. The net effect of taper then would be to suppress near in sidelobes.

One additional advantage of suppressing near-in sidelobes is that target ambiguities due to detection of large targets on sidelobes are avoided.

Sidelobe Blanking

An effective countermeasure against low duty cycle sidelobe jammers is a sidelobe blanking feature. Sidelobe blanking effectively compares the signal from an omnidirectional antenna and the normal directional antenna. If the return from the omni is higher, than the signal is being received from the sidelobes and is suppressed.

The omni-signal for the Type A radar is derived from the IFF cardiod-difference pattern which covers all angles uniformly with the exception of the mainlobe (when it is not required). For an L-band configuration, the antenna would be designed somewhat broader-banded. For UHF, the IFF antenna cardioid generating elements will be double tuned to cover both the UHF and IFF bands. This level of integration between the radar and IFF systems would only be used for an ECCM requirement.

An additional receiver is required for the omni signal. As it is desirable to make the blanking decision after the FFT integration, some additional processing capacity and logic will be required.

Strobe Reporting

The CFAR thresholds generated during an ECM event are the best indicator of jamming. Sidelobe jamming will tend to raise CFAR levels at all azimuths, but will be much higher in the mainlobe. Thus ECM detection can be accomplished by comparing average clutter levels to preset thresholds. Jammer location in angle (azimuth and crudely in elevation) can be determined by finding the CFAR processing interval with the highest average CFAR level. An ECM strobe report can then be forwarded to the operational site. Depending on the anticipated threat it may be necessary to insert attenuation in the receive path if saturation of the sidelobes is experienced.

Triangulation

Further jammer localization can then be accomplished at the operational site by comparing strobe reports from adjacent sites (triangulation). This ECCM technique, however, is beyond the control of the radar system design.

Other Techniques

Techniques such as pseudo-random COHO, sidelobe cancellers and adaptive beam forming are not recommended for Type A due to their complexity and power consumption.

2.7.4 Multipath Analysis

The multipath problem is due to contamination of the direct signal return from a source by the indirect return which arrives by a reflected path. Multipath can be either specular or diffuse or both. Specular multipath is caused by scattering from an essentially smooth surface while diffuse scattering occurs when the surface is rough.

The diffuse component is generally negligible when

$$\sigma_n < \frac{0.065\lambda}{\sin\Psi}$$

where:

σ_n = rms surface height variation

λ = wavelength

Ψ = specular reflection angle

For both L-Band (λ = 0.76 feet) and UHF (λ = 2.5 feet), both inequalities are satisfied for most terrains of reasonable flatness. Most of the current DEWLINE sites are situated such that they overlook relatively flat terrain or water. Several sites located on Baffin Island appear to overlook more rugged terrain.

2-251

The worst specular scattering conditions will occur when the radar over-looks the sea or long fields of ice. Either of these conditions can occur for many DEWLINE sites depending on the season of the year. Both sea water and ice conditions were assumed in the analysis to assess the full range of the multi-path problem.

An existing multipath program at Raytheon was employed to evaluate the effects of multipath at L-Band and UHF. This program utilizes the specular multipath equations (Appendix D) for a curved earth. Surface roughness is taken into consideration. This multipath computer program was developed under the Wide Area Active Surveillance (WAAS) study for the Naval Electronic Systems Command (Contract No. N00039-75-C-0435).

The parametric variations examined are summarized in Table 2.7.4-1. The target and radar heights were varied parametrically as shown in the table. The corresponding figure for these parameters is also indicated. Figures 2.7.4-1 through 2.7.4-14 compare L-Band and UHF multipath over ice for various target/radar height combinations. The same comparison is made over sea water in Figures 2.7.4-15 and 16 for two selected cases. The effectiveness of frequency agility in filling in the multipath nulls is demonstrated in Figures 2.7.4-17 and 18.

The multipath curves shown are accurate out to 2-3 NM of the horizon where the simplistic multipath model used is deficient as it neglects the transition region between interference and diffraction near the horizon. A discussion of the model employed is given in Appendix D.

In all figures, the expected L-Band signal-to-noise ratio (S/N) is shown as a function of target range for constant target altitude. The system parameters employed are those for the L-Band Baseline and an essentially similar UHF split-frame configuration. These parameters are summarized in Table 2.7.4-2.

All of the multipath figures show the system sensitivity (single pulse S/N) to achieve 0.9 probability of detection per scan for both a 16 M^2 target to 60 NM and a 1 M^2 target to 30 NM. Two S/N scales are shown for the two target sizes. The sensitivity values are 7.5 dB for L-Band and 2.1 dB for UHF. The derivation of these values is discussed in Section 2.7.1. The effects of Sensitivity Time Control (STC) are also shown on the figures. The STC assumes an R^4 STC curve which disappears at about 25 NM. The plots shown end at the radar horizon or at 60 NM, whichever is smaller.

The results against a 16 M^2 target at L-Band overlooking ice(Figures 2.7.4-1 to 6) are substantially similar to those shown for UHF (Figures 2.7.4-7 to 12). Minor excursions do drop below the sensitivity/STC lines at both frequencies, but the large majority of the returns exceed the thresholds. The effect or greater radar height (Figures 2.7.4-6 and 12) is to produce faster variations in signal strength as the target moves in.

In general, the range intervals of increased signal-to-noise ratio are longer at UHF. This should provide an edge in detecting fast targets.

Against a 1 M^2 target, some noticeable differences begin to occur. For low target altitudes, the 0.9 detection threshold is crossed earlier at L-Band. The difference in threshold crossing range is about 4-5 NM up to 500 feet target altitude. Above 500 feet, the differences do not appear substantial.

The ice surface conditions analyzed represent a worst case as the reflection coefficients are highest and the attenuation is the least of all surfaces. A different surface condition which would probably predominate at warmer times of the year is that of sea water. Two cases are shown in Figures 2.7.4-13 and 14. Comparison with the equivalent ice cases shows that the results are similar except that the null and peak excursion are not as extreme.

2-252a

Table 2.7.4-1.   Parametric Cases for Multipath Analysis

Frequency	Surface	Radar Height	Target Height	Figure For Result
L-Band (1300 MHz)	Ice	100 Ft.	100 Ft.	2.7.4-1
			200	2
			500	3
			1,000	4
			10,000	5
		500	500	6
UHF (450 MHz)	Ice	100	100	7
			200	8
			500	9
			1,000	10
			10,000	11
		500	500	12
L (1300 MHz)	Sea Water	100	500	13
UHF (450 MHz)	Sea Water	100	500	14
UHF (425 & 475)	Ice	100	1,000	15
UHF (425 & 475)	Ice	100	10,000	16

L Band
Ice Surface
100 Ft. Target Ht.
100 Ft. Radar Ht.
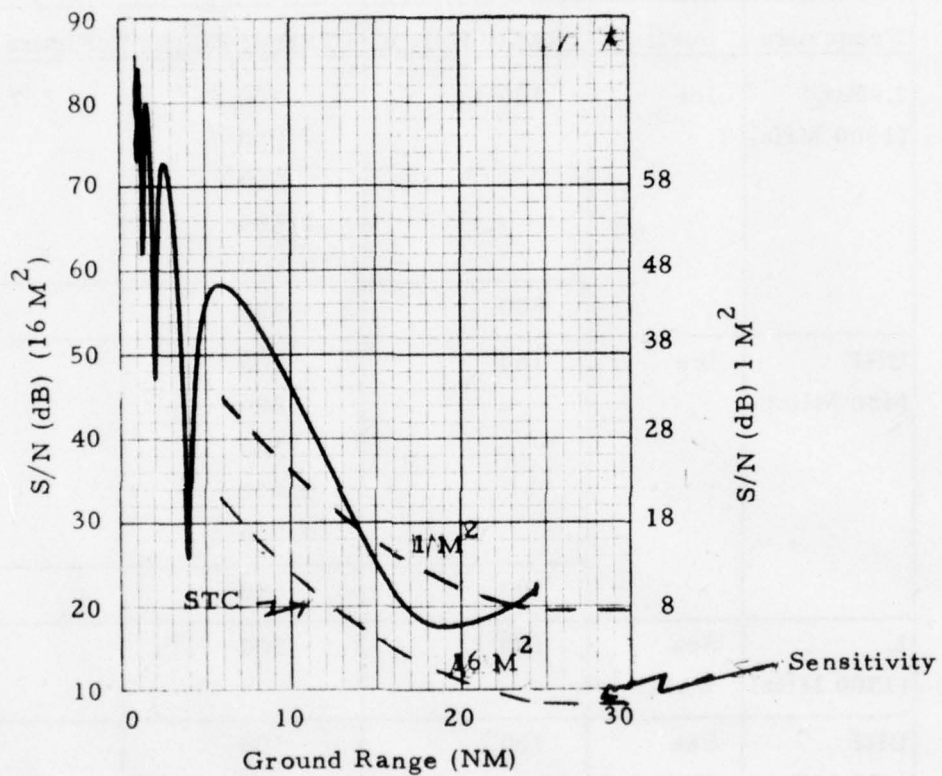
Figure 2.7.4-1. Multipath Results

2-254

L-Band
Ice Surface
200 Ft. Target Ht.
100 Ft. Target Ht.

Ground Range (NM)
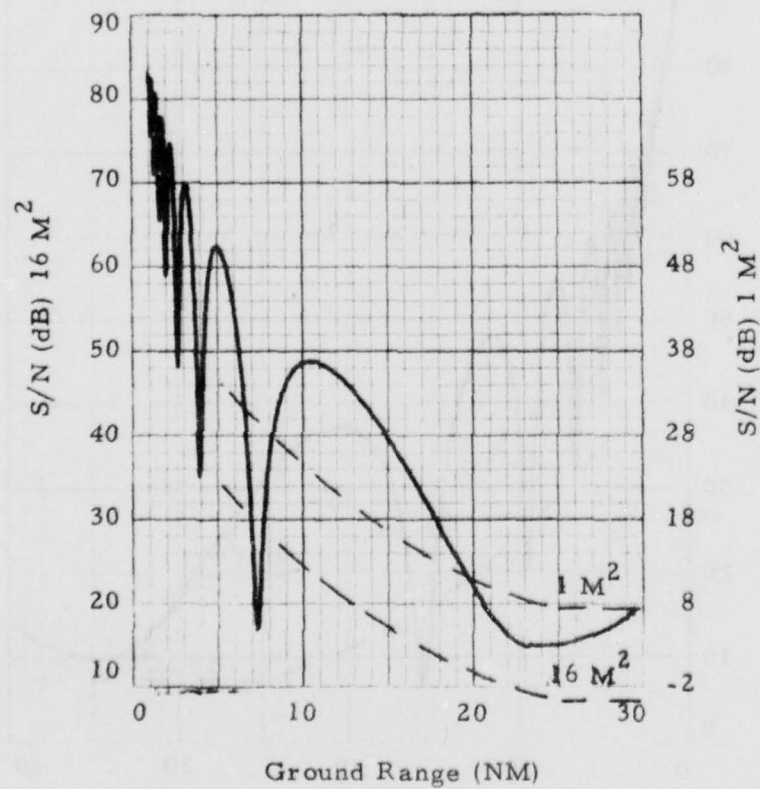
Figure 2. 7. 4-2.   Multipath Results
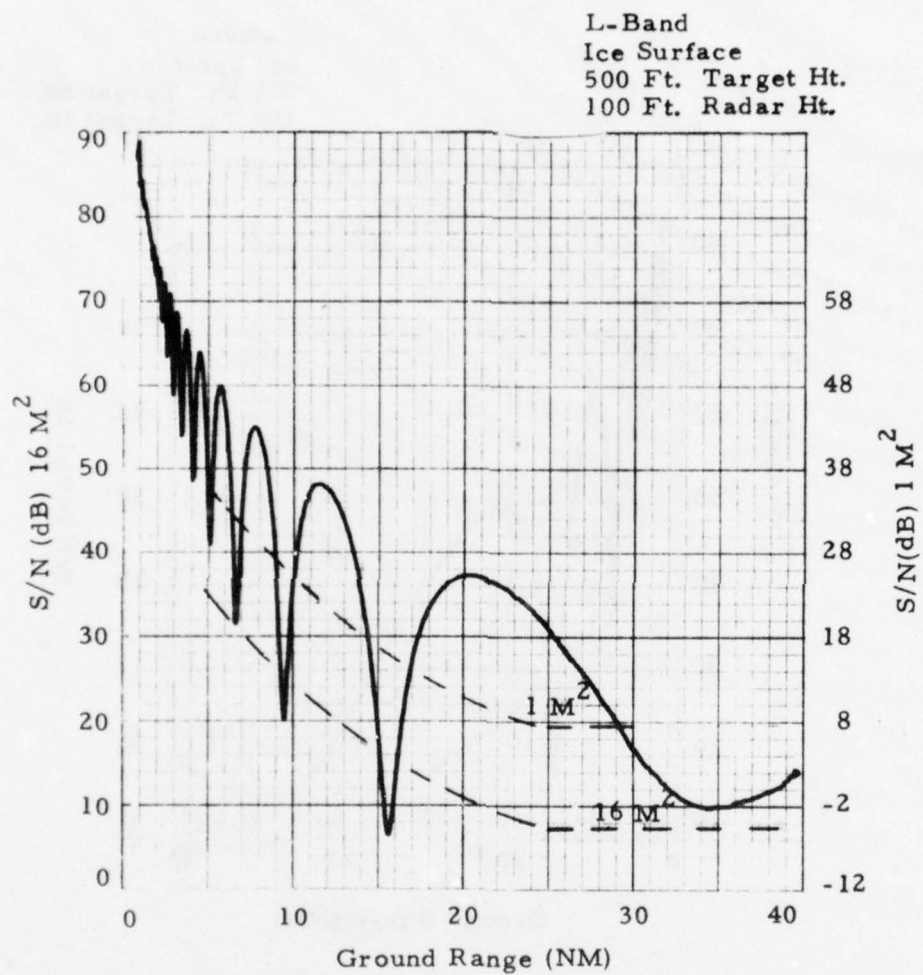
Figure 2. 7. 4-3.   Multipath Results

2-256
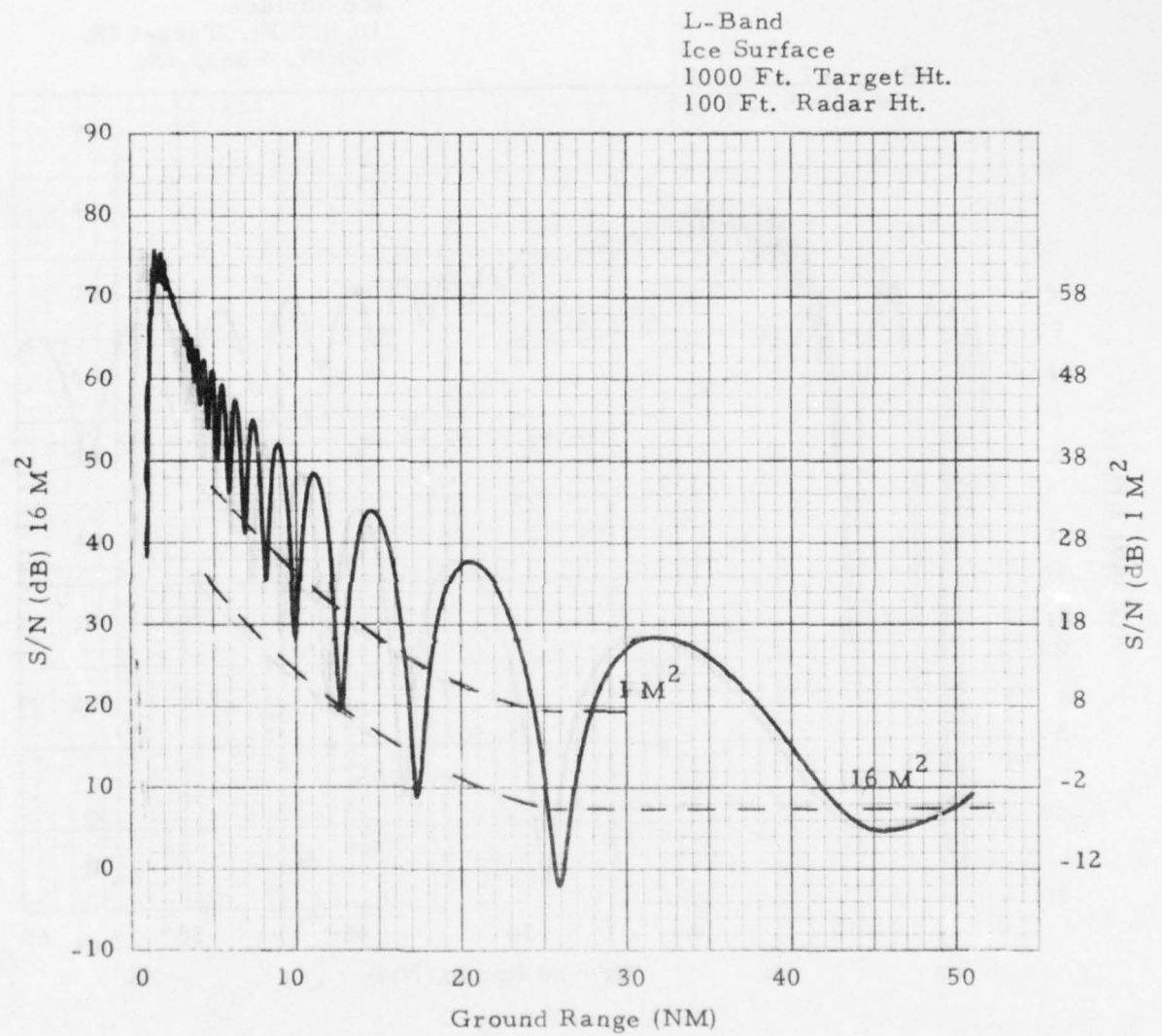
Figure 2.7.4-4. Multipath Results

2-257

L-Band
Ice Surface
10,000 Ft. Target Ht.
100 Ft. Radar Ht.
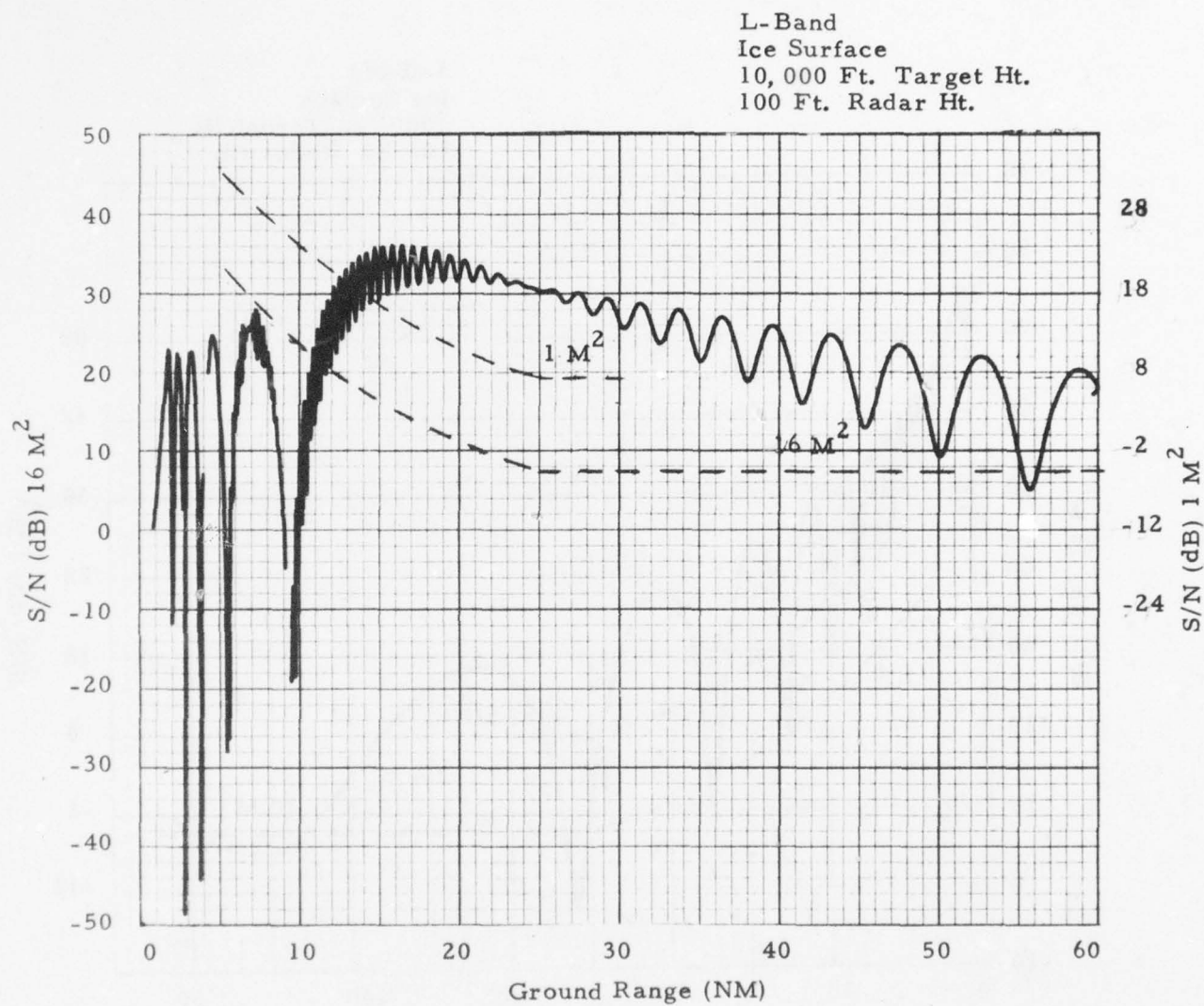
Figure 2.7.4-5. Multipath Results

L-Band
Ice Surface
500 Ft. Target Ht.
500 Ft. Radar Ht.
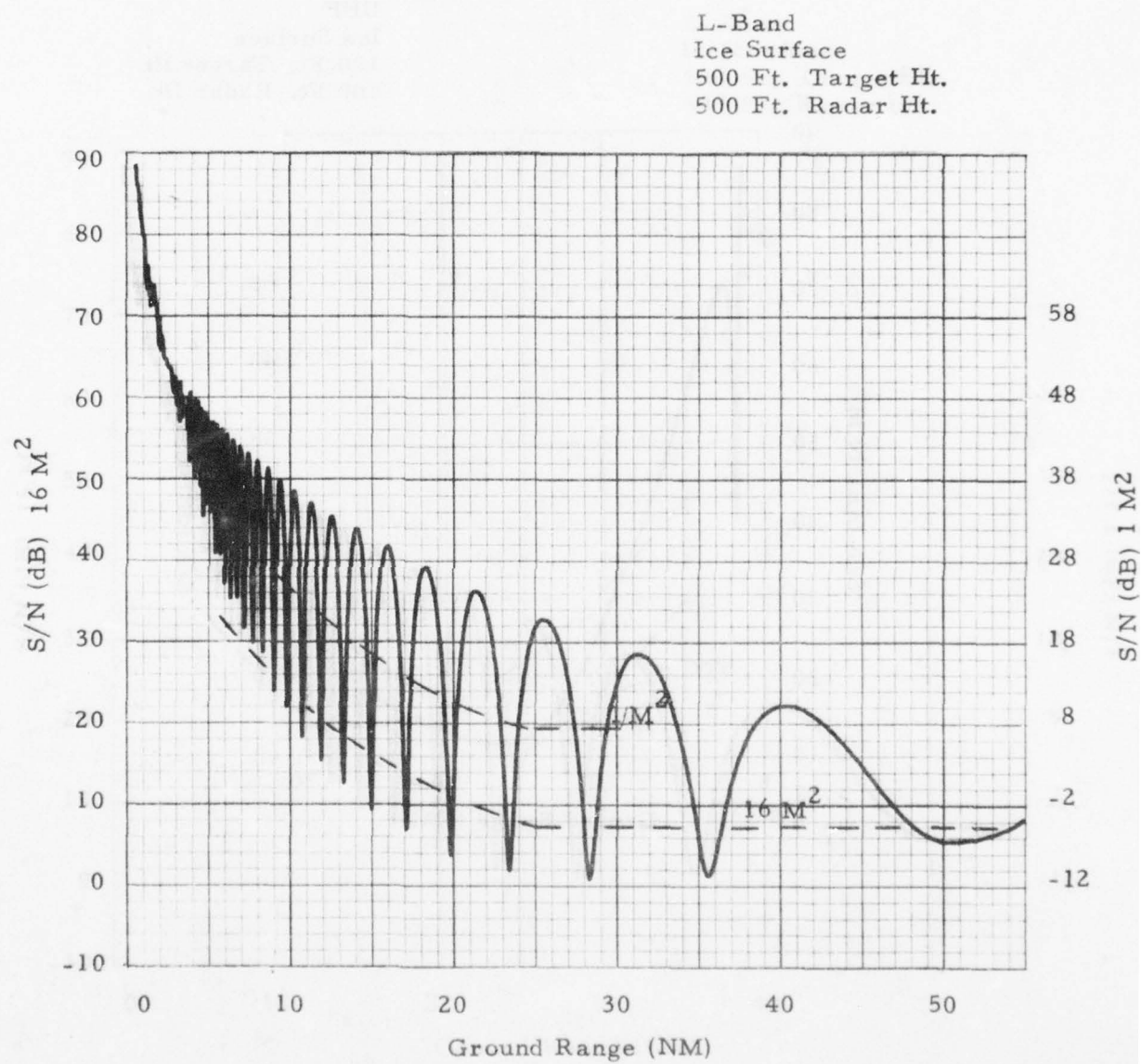
Figure 2.7.4-6.   Multipath Results

UHF
Ice Surface
100 Ft. Target Ht.
100 Ft. Radar Ht.
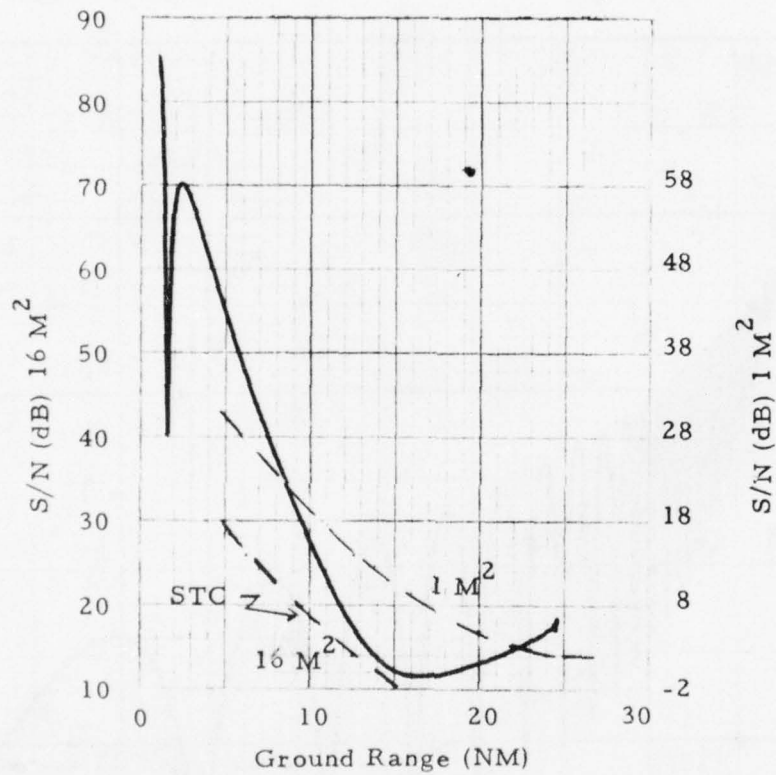
Figure 2.7.4-7.   Multipath Results
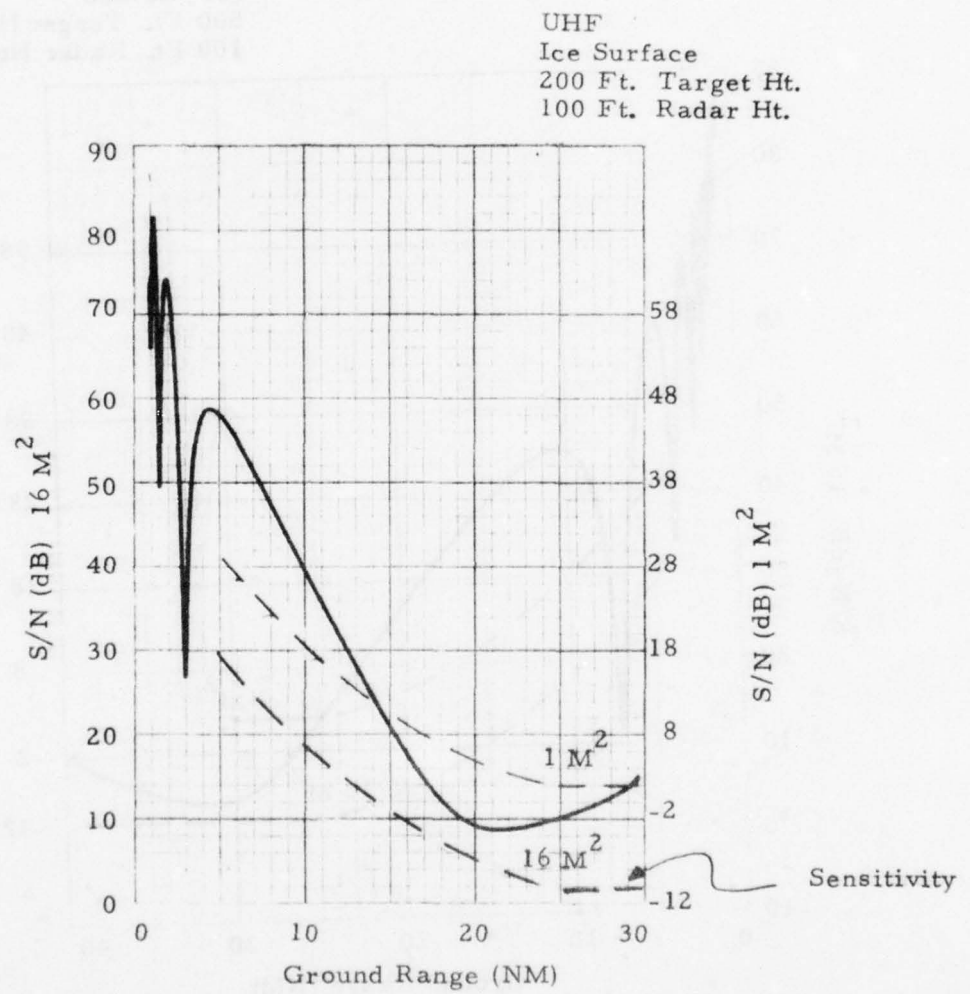
Figure 2.7.4-8.   Multipath Results

2-261

UHF
Ice Surface
500 Ft. Target Ht.
100 Ft. Radar Ht.
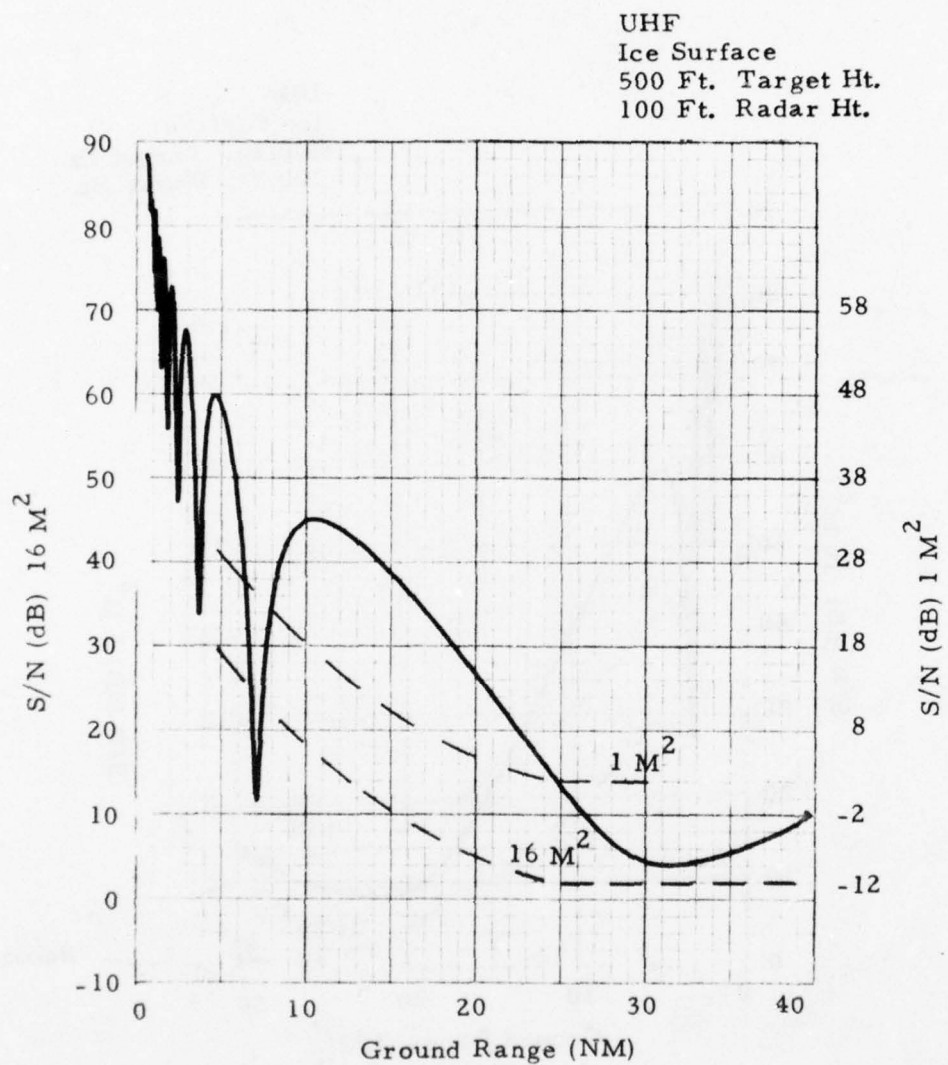
Figure 2.7.4-9. Multipath Results

2-262

UHF
Ice Surface
1000 Ft. Target Ht.
100 Ft. Radar Ht.
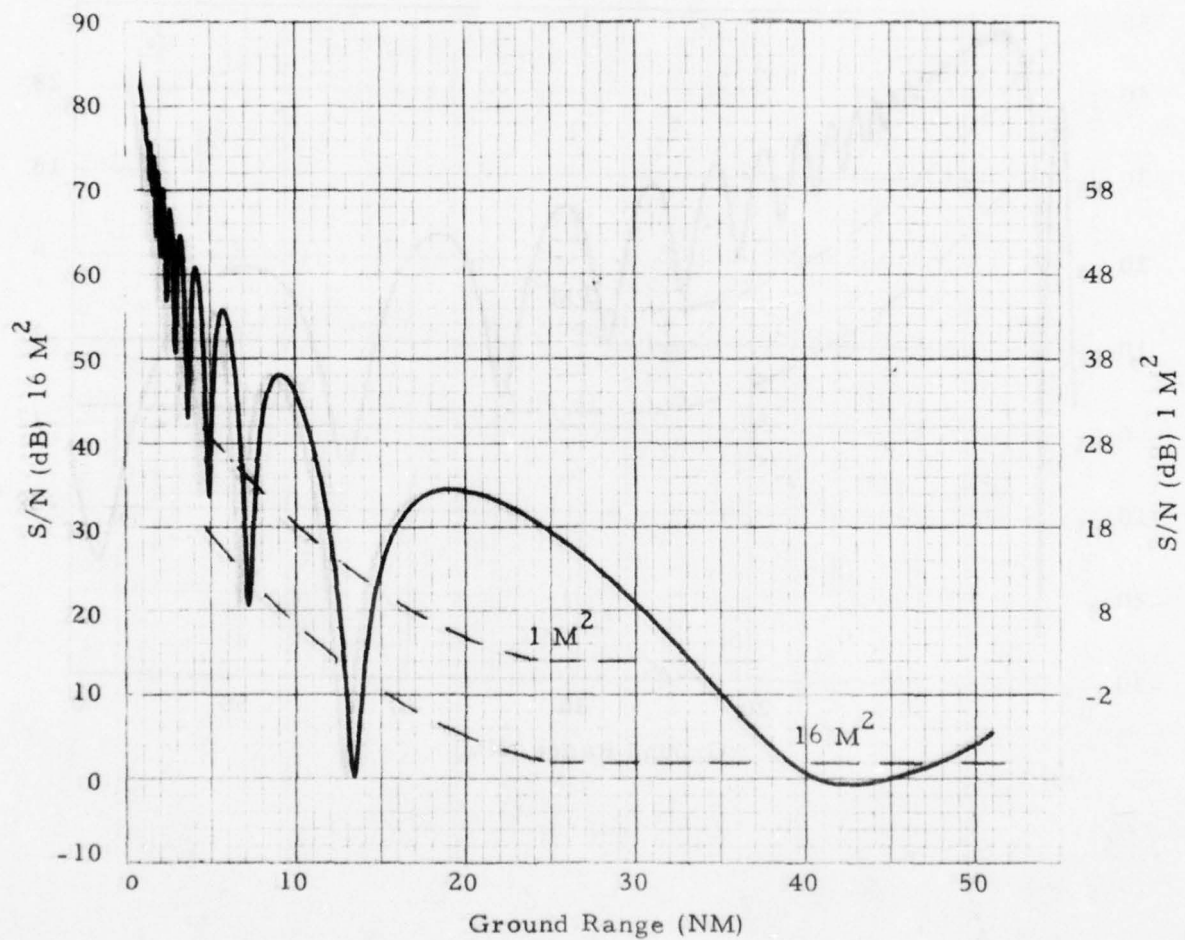
Figure 2.7.4-10.   Multipath Results

UHF
Ice Surface
10000 Ft. Target Ht.
100 Ft. Radar Ht.
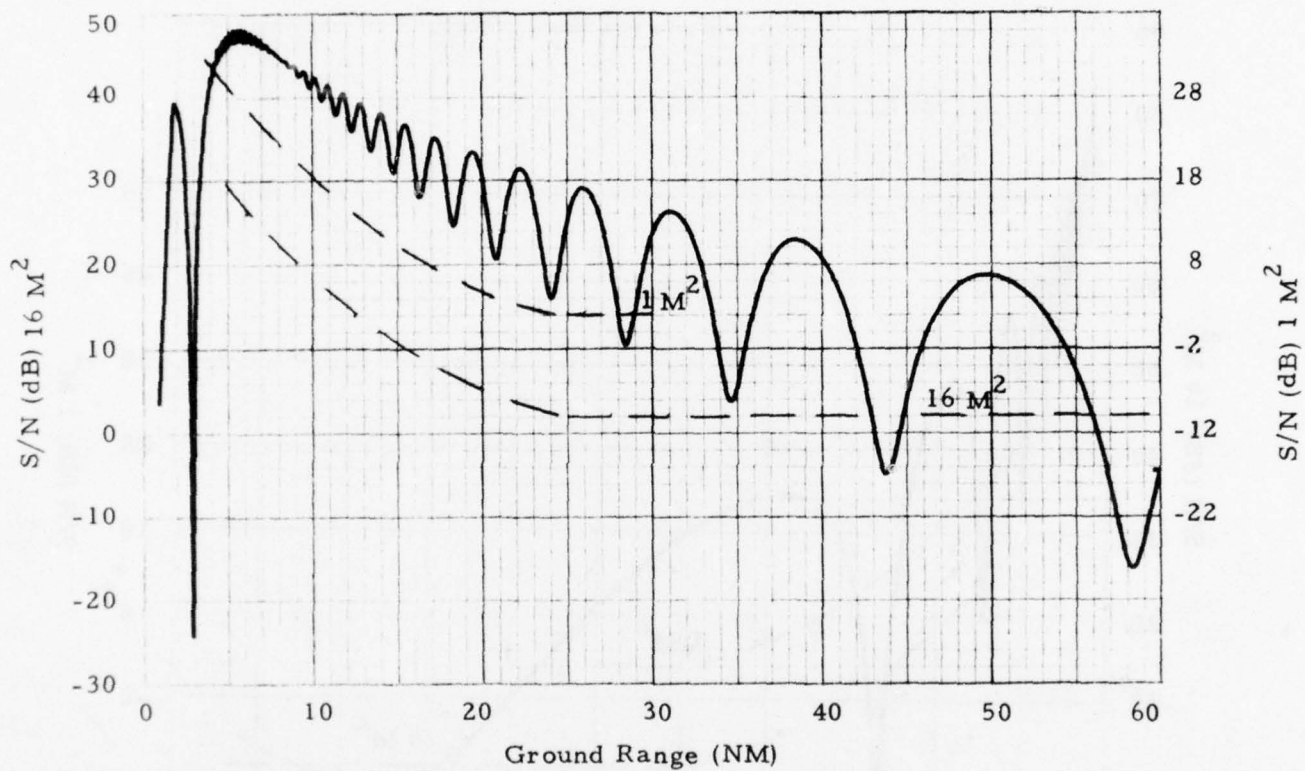
Figure 2.7.4-11.   Multipath Results

UHF
Ice Surface
500 Ft. Target Ht.
500 Ft. Radar Ht.
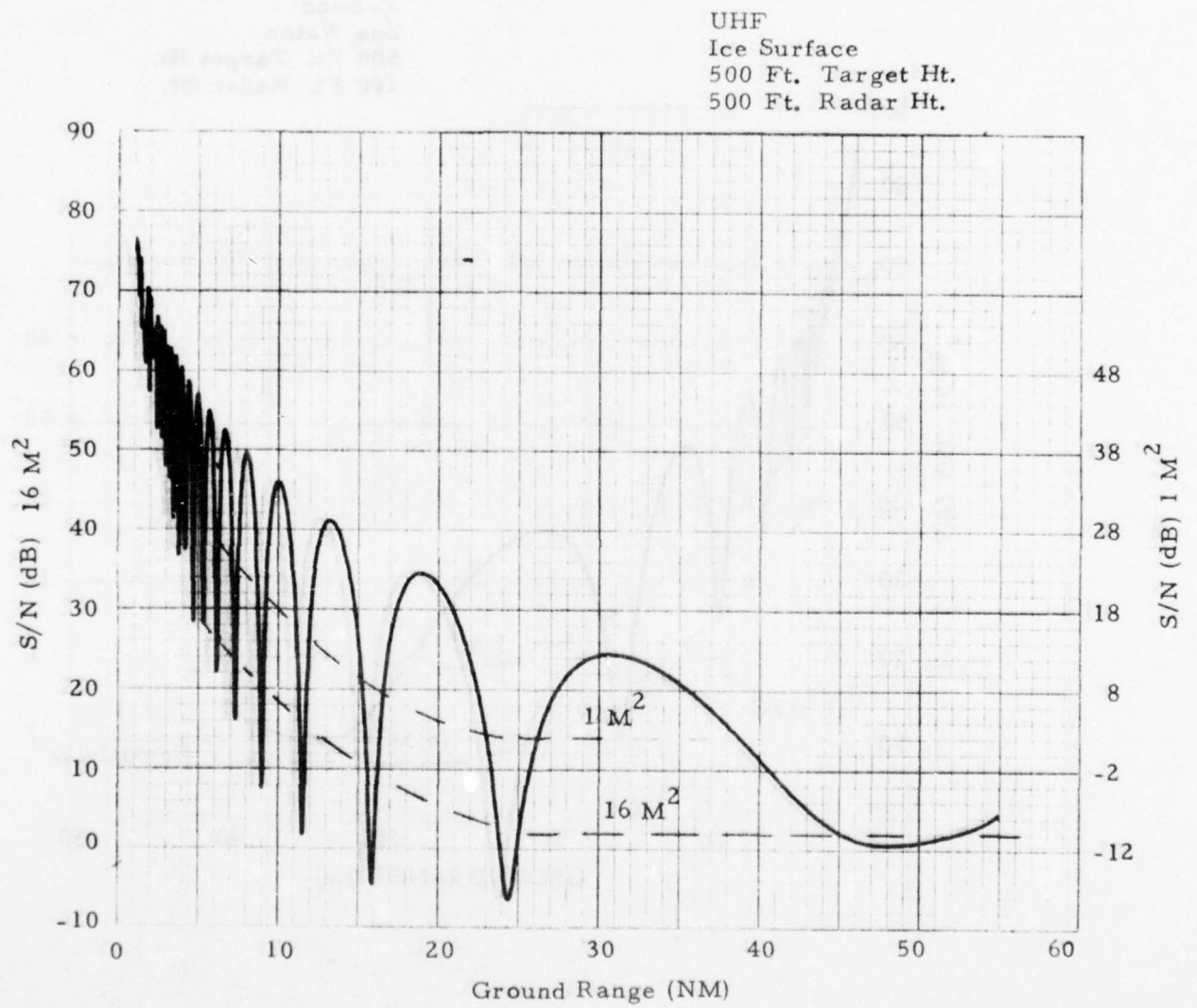
Figure 2. 7. 4-12. Multipath Results

2-265

L-Band
Sea Water
500 Ft. Target Ht.
100 Ft. Radar Ht.
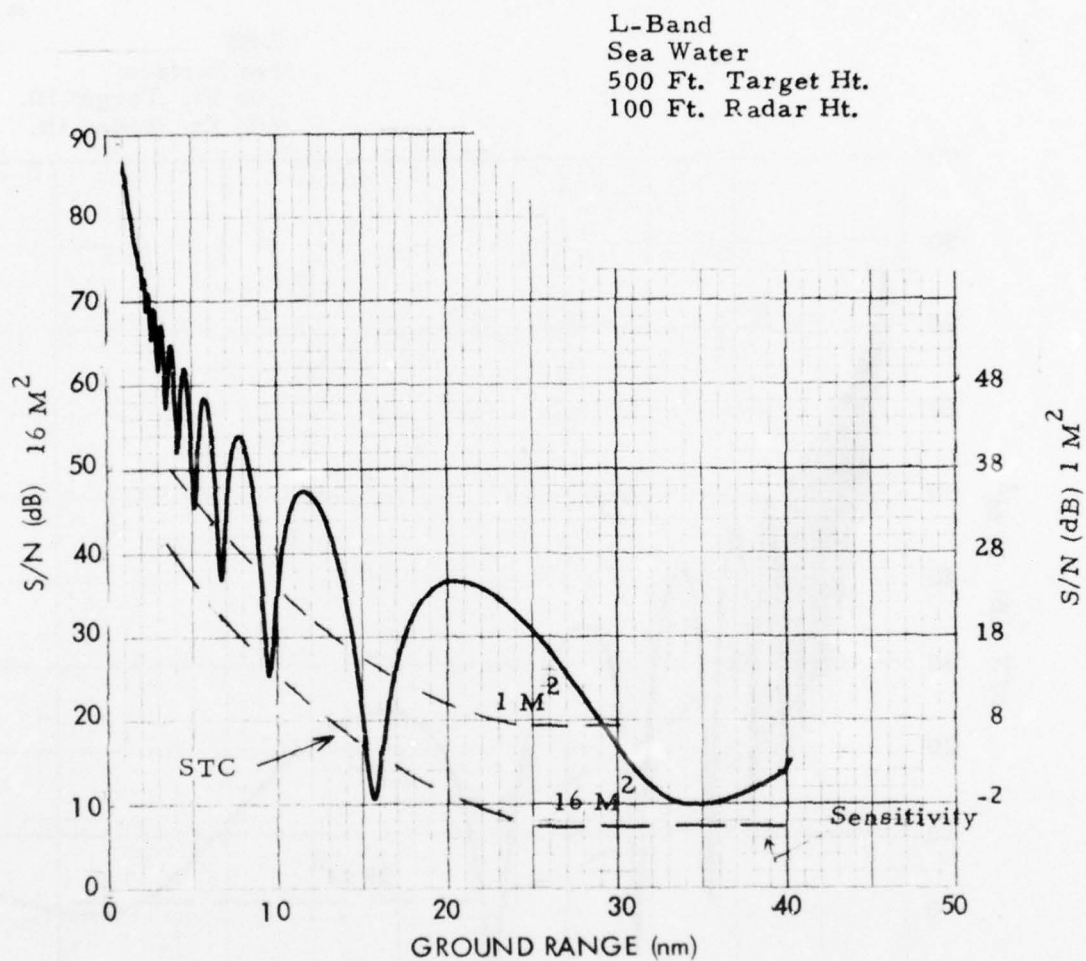
Figure 2.7.4-13.   Multipath Results

2-266

UHF
Sea Water
500 Ft. Target Ht.
100 Ft. Radar Ht.
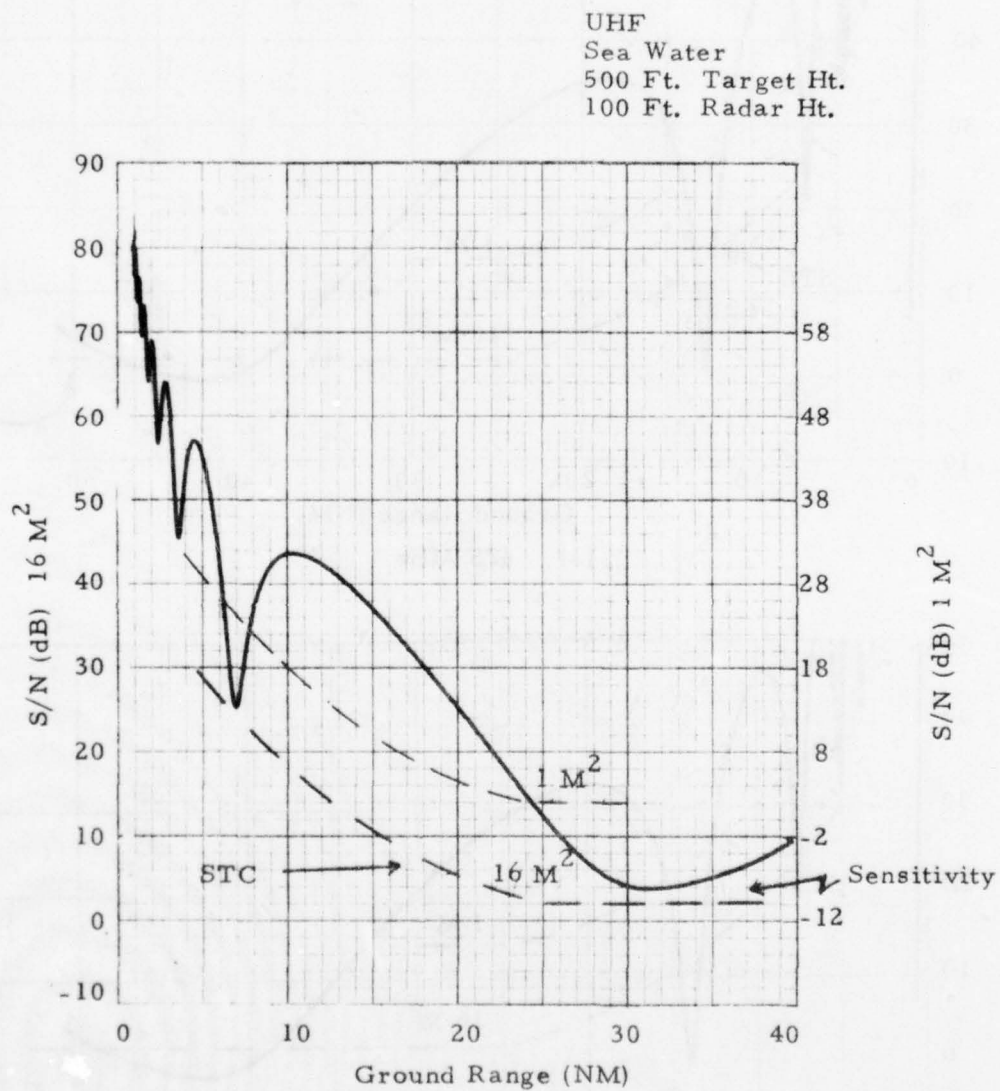
Figure 2.7.4-14.   Multipath Results

UHF
Ice Surface
1000 Ft. Target Ht.
100 Ft. Radar Ht.

(a) 425 MHz

(b) 475 MHz
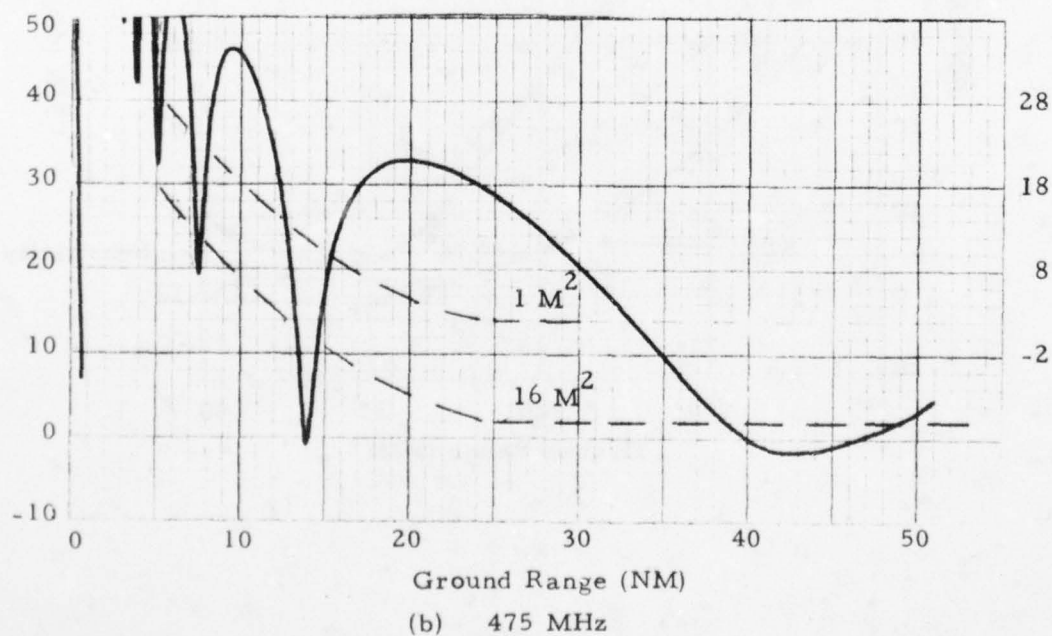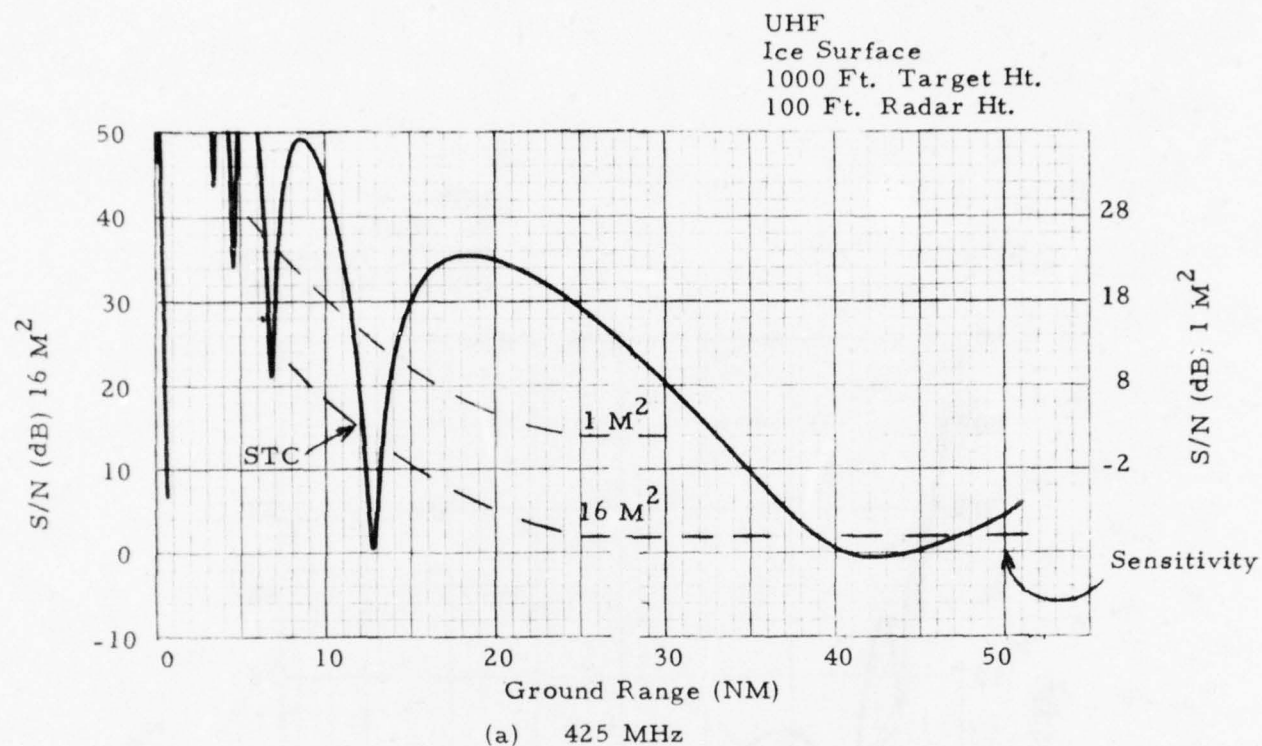
Figure 2.7.4-15. Multipath Frequency Agility Results

UHF
Ice Surface
10000 Ft. Target Ht.
100 Ft. Radar Ht.

(a) 425 MHz

(b) 475 MHz
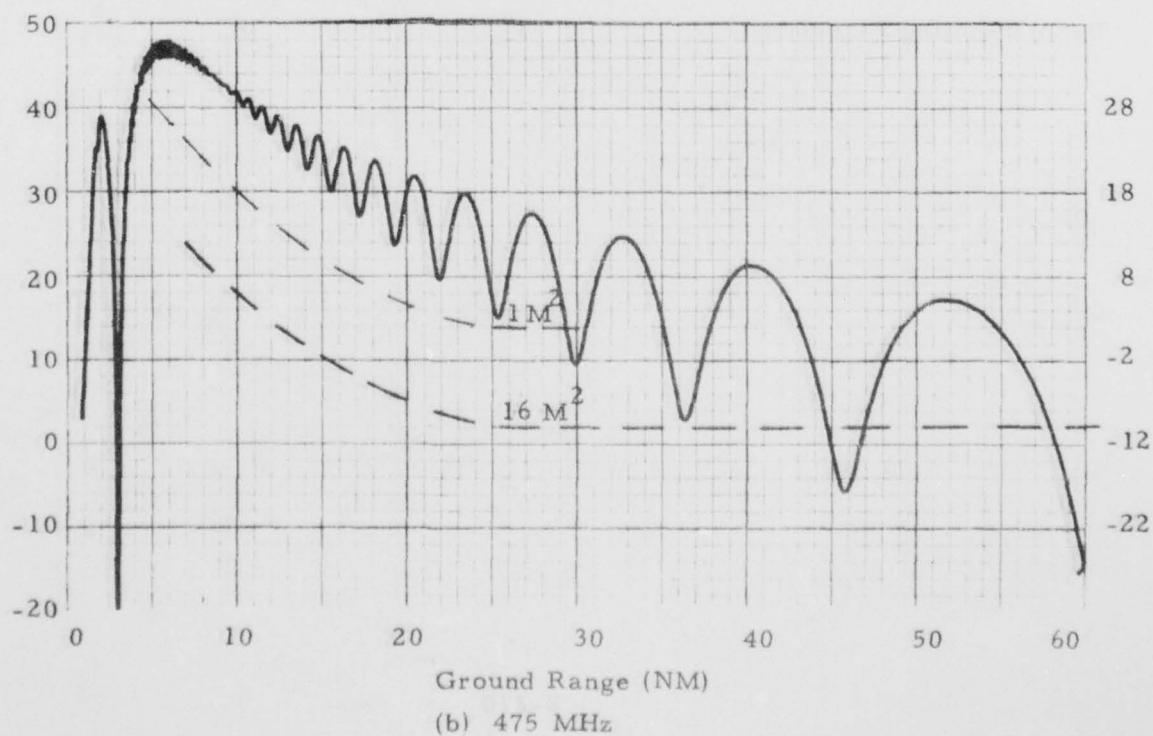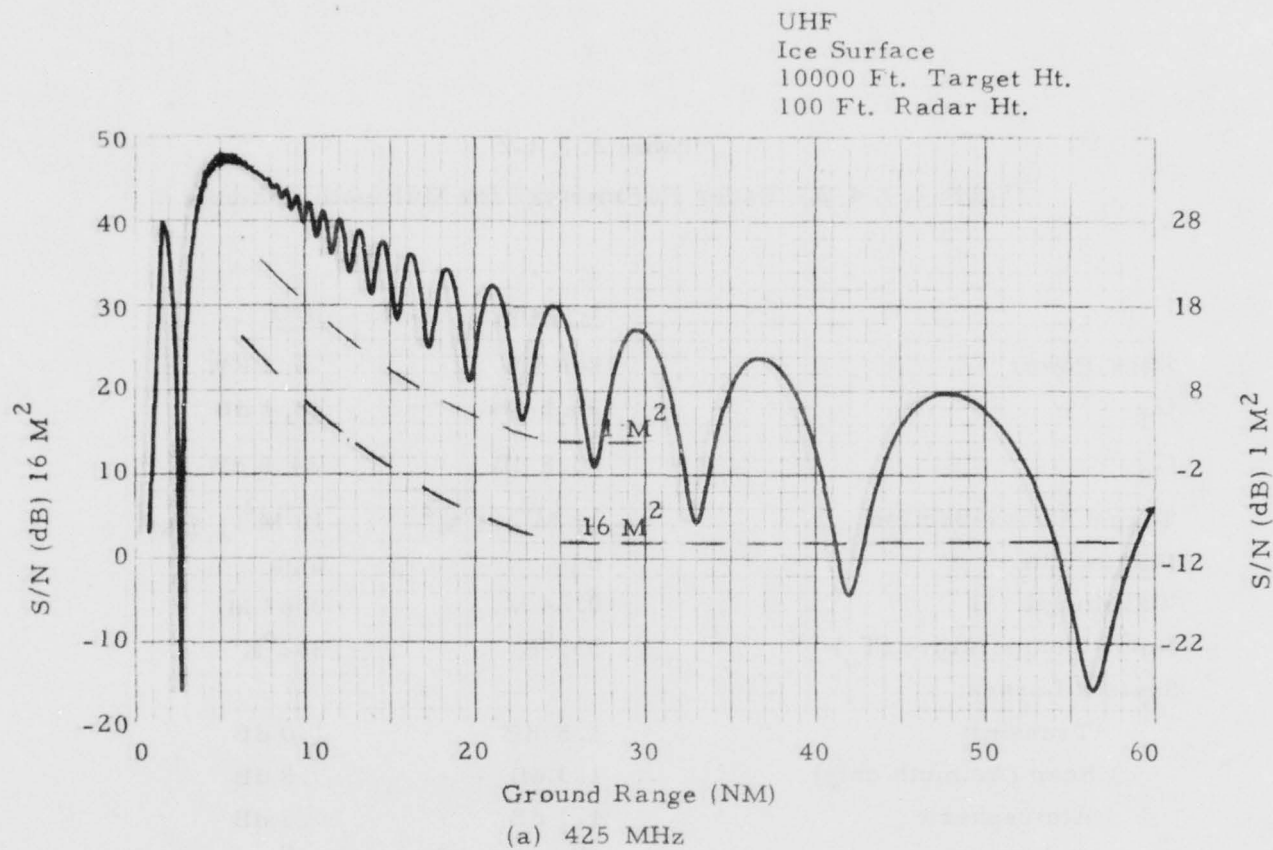
Figure 2. 7. 4-16. Multipath Frequency Agility Results

2-269

Table 2.7.4-2

Table 2.7.4-2. Radar Parameters for Multipath Analysis

	L-Band	UHF
Peak Power	2.6 KW	4.7 KW
G_T	35.5 dB	26.4 dB
G_R	33.8 dB	24.8 dB
Target Cross-Section	16 M^2, 1 M^2	16 M^2, 1 M^2
Pulsewidth	6 μs	6 μs
Wavelength (λ)	0.24 M.	0.67 M
Noise Temperature (T_e)	355°K	362°K
System Losses:		
Transmit	1.5 dB	1.0 dB
Scan (Azimuth only)	1.3 dB	.8 dB
Atmospheric	1.1 dB	.3 dB
Elev. Beamwidth	6°	18°
Beam Pointing Direction	3°	9°

The effect of multipath nulls can be minimized by the use of frequency agility. This effect is illustrated in Figures 2.7.4-15 and 16 for ice surface conditions at UHF with a frequency change of 50 MHz (425 and 475 MHz) substantially the same effect would occur at L-band for the same percentage bandwidth (150 MHz). In both Figures 2.7.4-15 and 16, the plots at the two frequencies are shown on the same figure for convenience in assessing the difference. The nulls, particularly at longer ranges, can be seen to be substantially filled.

Multipath comparisons at UHF and L-band with the radar parameters assumed indicate that in the case of a 16 sq meter target both UHF and L-band have adequate detection capability and if comparisons are made on an equal prime power basis UHF would be preferred. In the case of a 1 sq meter target UHF is preferred for a target above 500 ft and L-band for a target below 500 ft.

In general both UHF and L-band appear to satisfy a 'trip-wire' detection process in the presence of multipath. However, it will be the ultimate definition of the 'trip-wire' detection requirements that determine the choice of frequency. In this context it will be necessary to define not just detection but also tracking requirements, particularly as they relate to duration of the periods of continuous track and how many such periods are required. This latter question will also determine if 360 degree coverage is needed.

Thus, it is concluded that

- No significant difference is likely between UHF and L-band in the presence of multipath with the exception of a 1 sq meter target below 500 ft in which case L-band is preferred.

- For equal prime power consumption UHF would have the advantage under all conditions except below 500 ft for a 1 sq meter target.

- It will be necessary for mission planners to define the cumulative detection requirements, duration and number of periods of continuous track data particularly below 500 ft altitude before a frequency choice can be made.
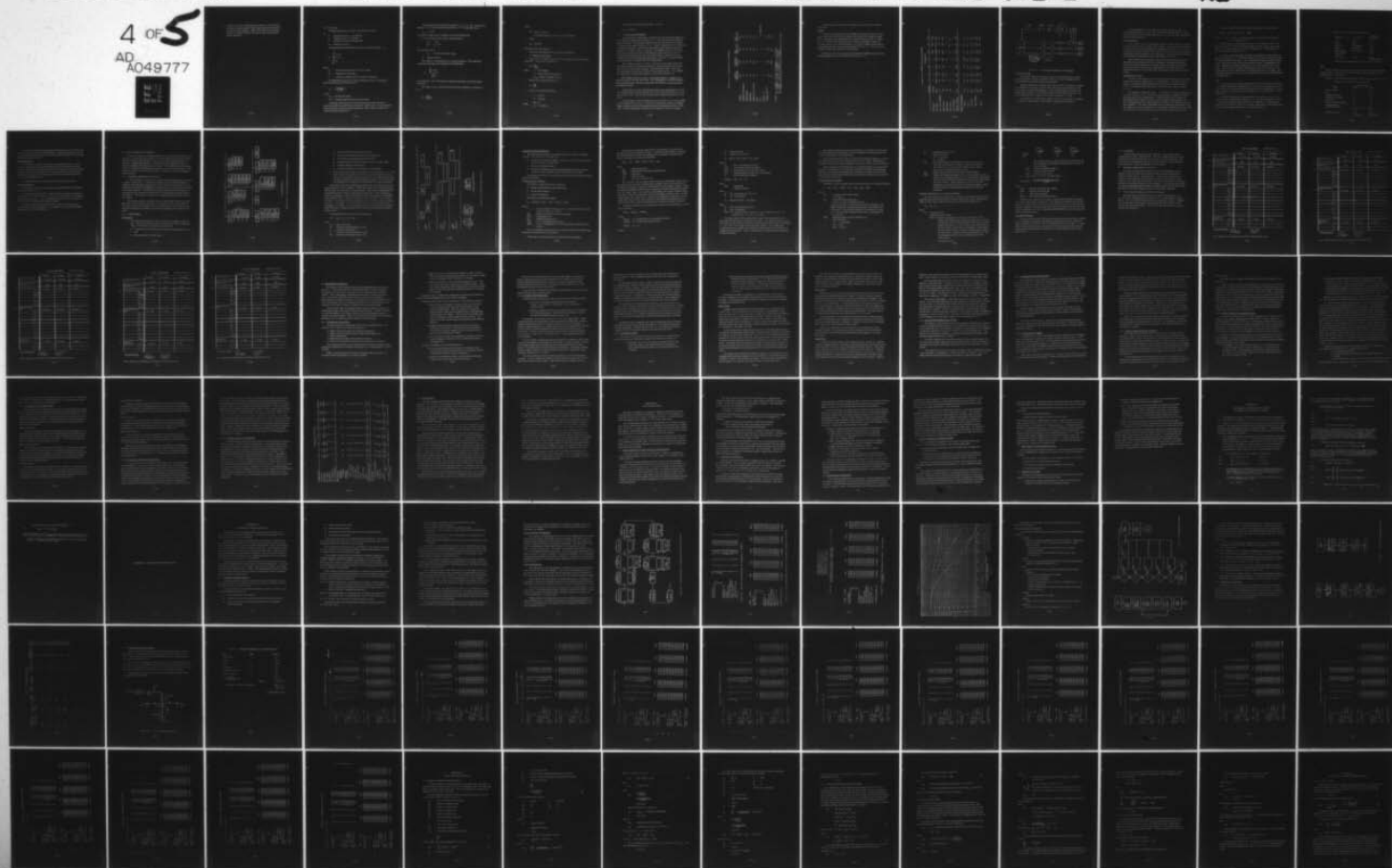
● A further and more comprehensive evaluation is recommended
to assess the performance of both frequencies for low altitude,
low cross-section targets. Model of the expected low altitude
intruder (minimum altitude cross-section and velocity) would
also be desirable.

2.7.5 Accuracy

The specified system accuracy in the Statement of Work is:

- Azimuth accuracy = 0.5 degrees
- Range accuracy = 0.25 NM
- Range rate accuracy (not specified)

(a)   Azimuth Accuracy

The target azimuth is estimated by a beam centroid technique, i.e.,

$$\hat{A} = \frac{\sum\limits_{i=1}^{n} A_i M_i}{\sum\limits_{i=1}^{n} M_i}$$

where

A_i =   antenna boresight azimuth for ith sample

M_i =   magnitude of ith sample

n =   number of samples (batches) between 3 dB points

The theoretical accuracy for uniform illumination over a rectangular aperture (Reference 2.4.3) is given by:

$$\sigma_A = \frac{0.62 \, \Delta A}{\sqrt{2n \, S/N}}$$

where

ΔA =   azimuth beamwidth

S/N =   average signal-to-noise ratio per batch

In general, other sources of error limit practical achievement of accuracy to about one-tenth to one-twentieth of a beamwidth. The specification does not call for accuracies approaching these values, thus the noise error will be the determining error.

2-273

The baseline system batch S/N is (Table 2.7.1-1) 13.1 dB. The number of batches, n, is 2 and the azimuth beamwidth is 1.4°. Using these values

$$\sigma_A = 0.15°$$

at maximum range which is adequate to meet the specification.

For an equivalent UHF system with parameters:

$$\Delta A = 3.5°$$
$$S/N = 7.7 \text{ dB}$$
$$n = 5$$

The azimuth error is

$$\sigma_A = 0.45° \text{ at maximum range.}$$

(b)   Range Accuracy

The range is also estimated by a centroid technique. The magnitudes in adjacent range gates are compared by the algorithm,

$$\hat{R} = \frac{\sum_{i=1}^{3} R_i M_i}{\sum_{i=1}^{3} M_i} -$$

where samples 1 and 3 correspond to adjacent range gates around the biggest magnitude.

The range accuracy associated with this type of technique is (Reference 2.4.3):

$$\sigma_A = \frac{\Delta R}{\sqrt{2 \ S/N}}$$

where

ΔR = range resolution

= 0.5 NM for baseline system (6 μsec pulsewidth).

Then,

σ_R = 0.08 NM

which meets the specification.

This value also applies to an equivalent UHF system.

(c) Range Rate Accuracy

Range rate is estimated by selecting the doppler filter with the biggest magnitude. The velocity resolution is,

$$\Delta V = \frac{\lambda}{2} \frac{fr}{N_{df}}$$

where λ = wavelength

fr = pulse repetition frequency

N_{df} = number of doppler filters.

The error in selecting one filter is,

$$\sigma_V = \frac{\Delta V}{\sqrt{12}}$$

Using, for the Baseline system,

λ = 0.23m

fr = 1150 Hz

N_{df} = 8

Then,

σ_V = 4.8 m/sec

For the equivalent UHF system with $\lambda = 0.67m$,

$$\sigma_V = 13.9 \text{ m/sec}$$

2.7.6 Prime Power Consumption

The estimates of prime power consumption for four selected system configurations are summarized in Table 2.7.6-1. Two L-band and two UHF systems are shown. The Baseline L-band system has been described at length elsewhere in this report (Section 2.2.3). L-band Configuration 13 is essentially a "maximum-hardware" system and represents a worst case for power consumption. It utilizes 6 lens, 6 receivers, 256 TRSSMs and a 1.5 µsec pulsewidth which increases the size of the signal processor (section 2.3.5). It probably also represents the best performing system in terms of coverage uniformity and inherent hardware parallelism. However, it is also the most costly and power consuming of all the configurations.

UHF configuration 49 is a 2 lens, 2 receiver system which means that the search volume is covered in elevation by "machine-gunning" on transmit between the two beams and listening simultaneously on both. Thus it has excellent frame-time and track initiation time characteristics. The TRSSMs are assumed to lie behind the quadrant switch (see Section 2.2.4).

UHF Configuration 62 is nearly a "minimum hardware" configuration in that it uses only 1 receiver and 1 lens. This configuration is the UHF analogue of the L-band baseline with the exception that the TRSSM's are located behind the Quadrant switch.

The variation in power consumption between the configurations is evident. The L-band baseline uses nearly 700 watts while L-band Configuration 13 uses better than 1.6 kW. The two UHF systems shown range from about 400 to 600 watts.

The two biggest power consumers shown in Table 2.7.6-1 are the TRSSM and the signal/data processor. The effect of reducing the number of TRSSMs (lower frequency and moving the modules behind the quadrant switch), and the effect of pulsewidth (range resolution) on the signal processor are evident.

2-276

Table 2.7.6-1. Typical Power Consumptions

	L-BAND BASELINE	L-BAND CONF 13[1]	UHF CONF 49[2]	UHF CONF 62[3]
TRSSM	248	455	258	122
AZIMUTH STEERING	63	126	38	19
RECEIVERS	75	150	44	22
EXCITER	40	40	28	28
SIGNAL/DATA PROC	195	825	155	135
BITE	15	15	15	15
IFF	1	1	1	1 (AVERAGE)
COMM. I/O	5	5	5	5
POWER DIST.[4]	25	25	25	25
	667	1642	569	372

NOTES: 1) 6 LENSES, 6 RCVRS, 256 TRSSM's, 1.5 μs PULSE
2) 2 LENSES, 2 RCVRS, 32 TRSSM's, 6 μs PULSE
3) 1 LENS, 1 RCVR, 32 TRSSM's, 6 μs PULSE
4) ASSUMES REGULATED DC INPUTS AT APPROPRIATE VOLTAGES

The derivation of these power estimates is discussed in the following paragraphs.

TRSSM

The power consumption for each TRSSM configuration (frequency output power, and number of receiver channels) was analyzed on a stage-by-stage basis. The power input diagram for the L-band baseline is shown in Figure 2.7.6-1. Three driver stages and two parallel final amplifier stages are required to produce 40 watts peak output. Low power CMOS is proposed for the switching and logic functions described in Section 2.3.2. Three low noise amplifiers (LNA) are required for the baseline.

The total power input required for the baseline TRSSM and several other TRSSM configurations are summarized in Table 2.7.6-2.

Table 2.7.6-2 TRSSM Power Requirements

	Baseline				Configuration			
		6	13	36	39	49	58	62
Frequency	L-Band	L	L	L	L	UHF	UHF	UHF
Scan Type	Split	Split	Single	Fence	Fence	Single	Split	Split
No. Active TRSSM's	67	67	70	65	66	34	33	33
Peak Power	40w	80	160	80	320	200	150	200
Pulsewidth	6µs	6	1.5	6	1.5	6	6	6
Duty Cycle	2%	6	1	2	1	1.4	0.7	0.7
Rcvr Channels	3	3	6	1	2	2	1	1
TRSSM Location	Ant	Ant	Ant	Q Sw	Q Sw	Q Sw	Ant	Q Sw
Power Consumption:								
Trans.	2.5w	5.0	5.0	5.0	10.0	7.0	2.6	3.5
Rcvr	0.4	0.4	0.7	0.1	0.3	0.3	0.1	0.1
Logic/Sw	0.8	0.8	0.8	0.6	0.6	0.3	0.6	0.1
Pwr/TRSSM	3.7w	6.2	6.3	5.7	10.9	7.6	3.3	3.7
Total	248w	415	455	370	719	258	109	122
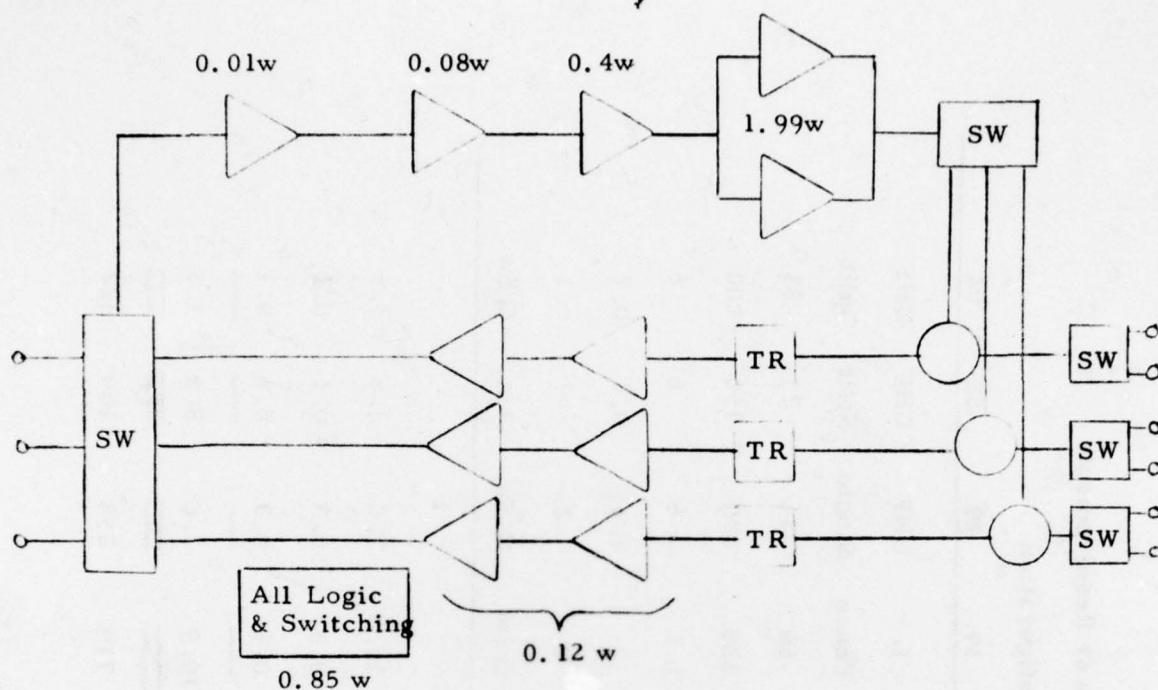
Figure 2.7.6-1 Baseline TRSSM Power Dissipation

Azimuth Steering

The switch design was selected to require a minimal amount of control power dissipation.   All logic is CMOS with very low power dissipation (less than 500 mW for all of the azimuth steering logic).

Because of the slow switching rates of the switches (10-30 μsec), a simple low dissipation switch driver can be used, and power is consumed only when the switch is activated (forward bias).   There are 205 diodes (per lens) in the forward bias condition.   At 100 mW per driver and 500 mW for the logic, the power dissipation for a single R-Lens switch assembly is 21 watts.

As the Baseline configuration contains 3 lens, the total power consumption is 63 watts.   Configuration 13 with 6 lenses consumes twice as much.

2-280

Fewer diode/driver switch pairs are required for UHF as there are fewer antenna elements to drive. Approximately 19 watts for logic and diode driver dissipation will be required per lens. For a two lens UHF configuration, 38 watts will be required.

Receiver/Exciter

The receiver and exciter designs are based on simplifications of existing Transportable Surveillance Radar (TSR) designs. Extrapolating (by comparison of relative parts counts) from TSR power dissipation data, the d. c. power consumption per receiver channel will be between 25 and 35 watts, and the exciter requirement will be between 40 to 50 watts range. The total power consumption for the baseline configuration will be a minimum of 115 watts.

This is felt to be a conservative effort as time has not permitted full evaluation of new promising receiver technology. Anticipated in the near future are receiver designs that utilize microwave monolithic integrated circuits and L-band A/D converters. Employment of such devices should substantially reduce the predicted power consumation values for the receiver/exciter.

Signal/Data Processor

The power requirements for the signal and data processors hinges on the design of an efficient, high speed, processing element. The design of such an element, called the Common Element (CE) is described in detail in Section 2.3.5. The speed-power trade-offs for such a device are shown in Figure 2.3.5-6.

The numbers of signal processing CEs required for various configurations is given in Figure 2.3.5.7. Two data processing CEs are adequate to handle the target load for all configurations. Using the early 1980's estimate for Integrated-injection logic (I^2L) and silicon on sapphire (SOS) memory, the power dissipation per CE is approximately 15 watts for a 100 nanosecond cycle time capability. The power requirement for the remaining, serial, portion of the signal processor is estimated as 75 watts based on predicted IC count. This serial portion includes the synchronizer and the input-output (I/O) circuits.

Thus, the signal data processor power dissipation can be predicted,

$$Power = (15) \quad (N_{CE} + 2) + 75 \quad watts$$

where N_{CE} = number of signal processor CEs, which can be obtained from Figure 2.3.5.7.

For the various configurations, N_{CE} is 6 for the baseline, 48 for configuration 13 (twice as many instrument beams and four times as many range gates), 4 for configuration 49 and 2 for configuration 61. This leads to the power level shown on Table 2.7.6-1.

It can be seen that the signal processor represents one of the major consumers of prime power. The present estimates are based on predictions using I^2L and SOS/CMOS technologies. It is evident that the signal processor design is one of the areas where a major improvement in power consumption is possible. Raytheon is presently studying a C.C.D. signal processor for use in space. This technology applied to the unattended radar holds promise of reducing the total power consumption of the signal processor to <10 watts. The technology application of C.C.D.'s to the unattended radar will be studied during the coming year.

Bite

The Bite processing speed requirements are modest and thus permit the use of CMOS digital logic building blocks. Such devices typically draw current on the order of microamperes and only during the switching transition. In their static position they present both input loading so that one CMOS gate can drive many others.

An AMD 9080 militarized processor has been selected. The power requirements are summarized in Table 2.7.6-3. The power dissipation is about 2.5 watts for a quiescent state and 10 watts for dynamic. It is proposed to use three active BITE processors in a voting configuration. The average power load is conservatively estimated as 15 watts for all three.

2-282

Table 2.7.6-3.   BITE Power Requirements

Function	Type	Power Dissipation
A LU	9080	1.5w
Buffer	8228	0.8
Decoder	MC14028AL	0.01
ROM	MC1452AL	0.02
Bus Register	MC14039AL	0.02
Hex Tristate Driver	-	0.05
Misc Logic	CMOS	0.01

$\sim \overline{2.4w}$ (Quiescent)

Dynamic power consumption $\cong$ 4 x Quiescent $\cong$ 10 watts.

IFF

The IFF subsystem is only activated upon receipt of a target designation from the radar.   When not used, the entire IFF is deactivated except for a small amount of control logic.

The power consumption breakdown for the IFF is shown in Table 2.7.6-4.

Table 2.7.6-4.   IFF Power Requirements

FRU	Power: Watts	
	IDLE	ON
ANT Controller	0	.55
R/T	0	14.1
Command Interface	0.1	.68
SIF/IFF Processing	0	1.7
BITE GQ	.01	.01
Power and Power Manage	.1	---
Pin Diode Driver Power Converter	0	9.2
	.21	26.24
Conversion Loss	.07	9.17
	.27 watts	35.41 watts

It is estimated that the average target designation rate to the IFF will be about two per hour (one true target and false). Interrogation takes only one to two seconds including warm-up. Thus, a conservative estimate of the average IFF power drain is one watt.

Communication I/O

The expected output data rate of the communication I/O device will be very low. Essentially, the communication link will be activated only when a target alarm, IFF interrogation or BITE status message is ready to be transmitted. This would probably occur at a maximum of once per scan but will probably be much slower. Advantage can be taken of this inherent low duty cycle by using CMOS devices.

It is estimated that five watts will be sufficient for this function.

Power Distribution

A small factor for power distribution (current diversion and routed) is included in Table 2.7.6-1.

It should be noted that power conversion efficiency (power supplies and regulation) have not been estimated. The general uncertainty as to the type of prime power source (a. c., d. c., regulation, etc.) was felt to be too great to permit accurate estimation of this power function.

The input power, for the purpose of this study, has been assumed to take the form of well regulated d. c. at the appropriate currents and voltages (primarily $\pm 5V$, $\pm 15V$ and 28V d. c.).

2.8 COST SENSITIVITY ANALYSIS

As shown in Figure 2.1-2 the approach to the cost sensitivity analysis was to examine in considerable detail all the cost related aspects of the baseline system. This was achieved at the hardware level by the generation of detailed bills-of-material, engineering design data, and 'similar too' information from which a rigorous manufacturing estimate was developed. Cost sensitivity at the program level was developed by establishing a program cost model and assumptions. This section describes the hardware and program cost elements and the resulting sensitivity analysis.

2.8.1 BASELINE HARDWARE COST DATA

A work breakdown structure at the system hardware elements was developed as shown in Figure 2.8-1. Against each element a bill-of-material (BOM) was developed using engineering design data for sub-elements where previous design relationships could not be established and 'similar too' data where previous designs were judged applicable. The BOM's and design data were provided to Raytheon manufacturing cost estimators who performed a rigorous cost estimate based on 1977 dollars. This estimate involved many vendor quotations to ensure maximum cost validity.

This baseline hardware cost data was then extrapolated to the other system alternative configurations by factoring the complexity of each involved element. The ground rules and assumptions used to generate the actual prototype and production lot estimates are detailed in the following definition of the program cost model.

2.8.2 COST MODEL

Assumptions

a. The model will consider only those costs directly related to radar design. Government costs will not be included except where specifically noted. The following costs also are not included:

- Transportation of hardware and materials to and from the Arctic sites.

- Site preparation for Arctic tests.
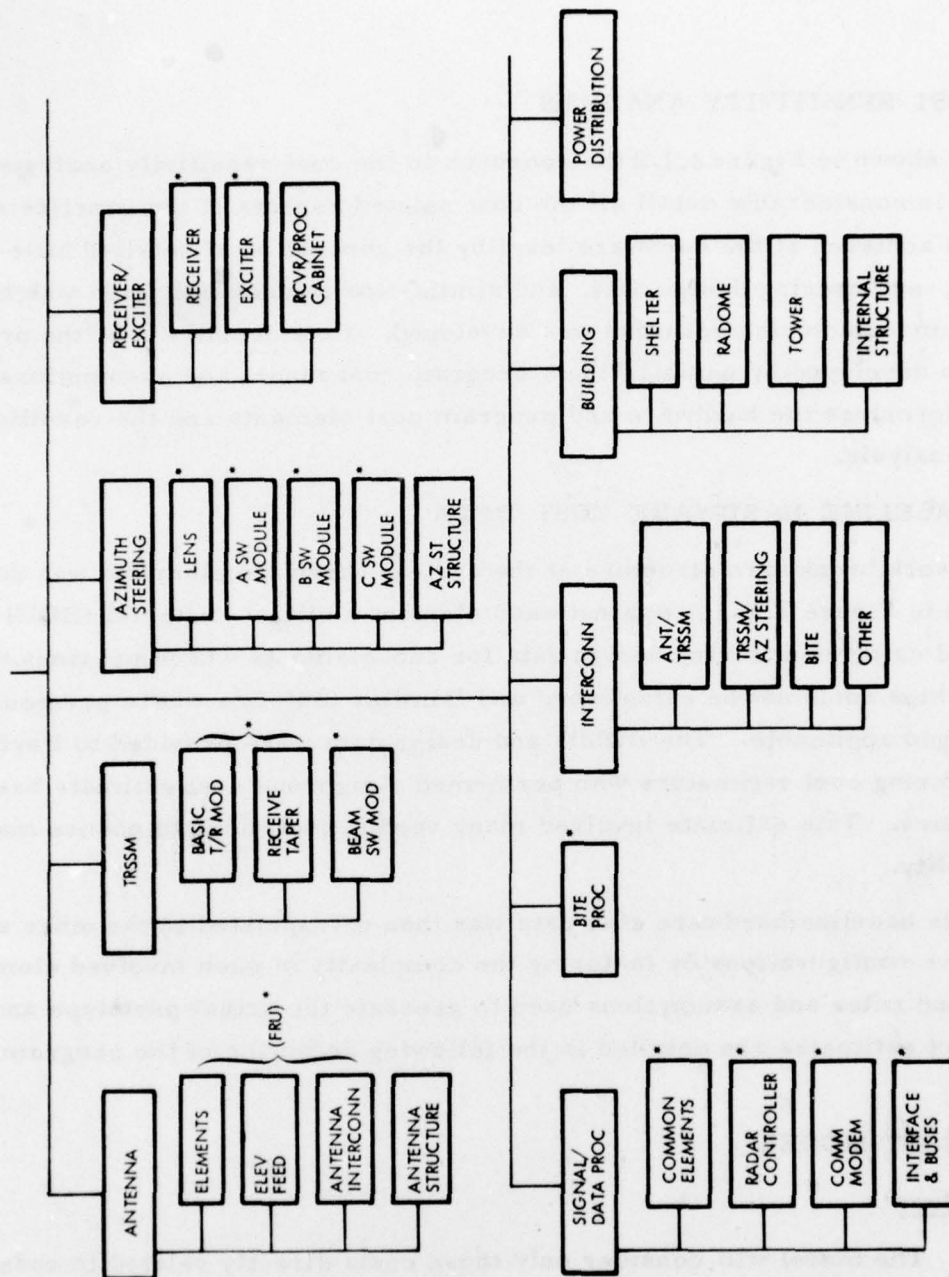
Figure 2.8-1. Type A Radar Hardware Cost Elements

* FRU = FIELD REPLACEABLE UNIT

- Site construction for operational system.

- Intersite transportation operation and maintenance.

- Life support and overhead personnel at sites.

- Transportation of failed modules to and from a repair depot.

- Logistics pipeline requirements.

- Contractual risk and turnkey prime responsibilities.

b. The program will consist of four phases as shown in Figure 2.8-2. The level of pricing commitment is also shown at each of the four phases. It can be assumed that it will be necessary for the Government to maintain price competition through the validation phase. This analysis does not consider the cost impact to the Government of price competition.

Also shown are the time relationships between the four phases for the three design times (3, 6, and 12 months). A fixed development and contractor factory test time has been assumed for all design times. The number of prototypes and the duration of Arctic testing varies with the design time. These parameters (number of prototypes, Arctic test time) have been chosen to give an essentially equal confidence level in system reliability for the three times. For example, the number of prototype Arctic testing hours for the 12 month system (4 prototype x 3 years = 12 prototype - years is four times that of the three month option (2 prototypes x 1.5 years = 3). The confidence achieved with this level of testing is about 50 percent. Confidence level versus test time tradeoffs are discussed in Section 2.6.3.

The total life cycle cost (LCC) can be expressed:

$$LCC = CF_c + V_c + I_c + OS_c$$

where

LCC	=	Life Cycle Costs
CF	=	Concept Formulation Phase Costs
V_c	=	Validation Phase Costs
I_c	=	Production (Investment) Phase Costs
OS_c	=	Operation and Support Phase Costs
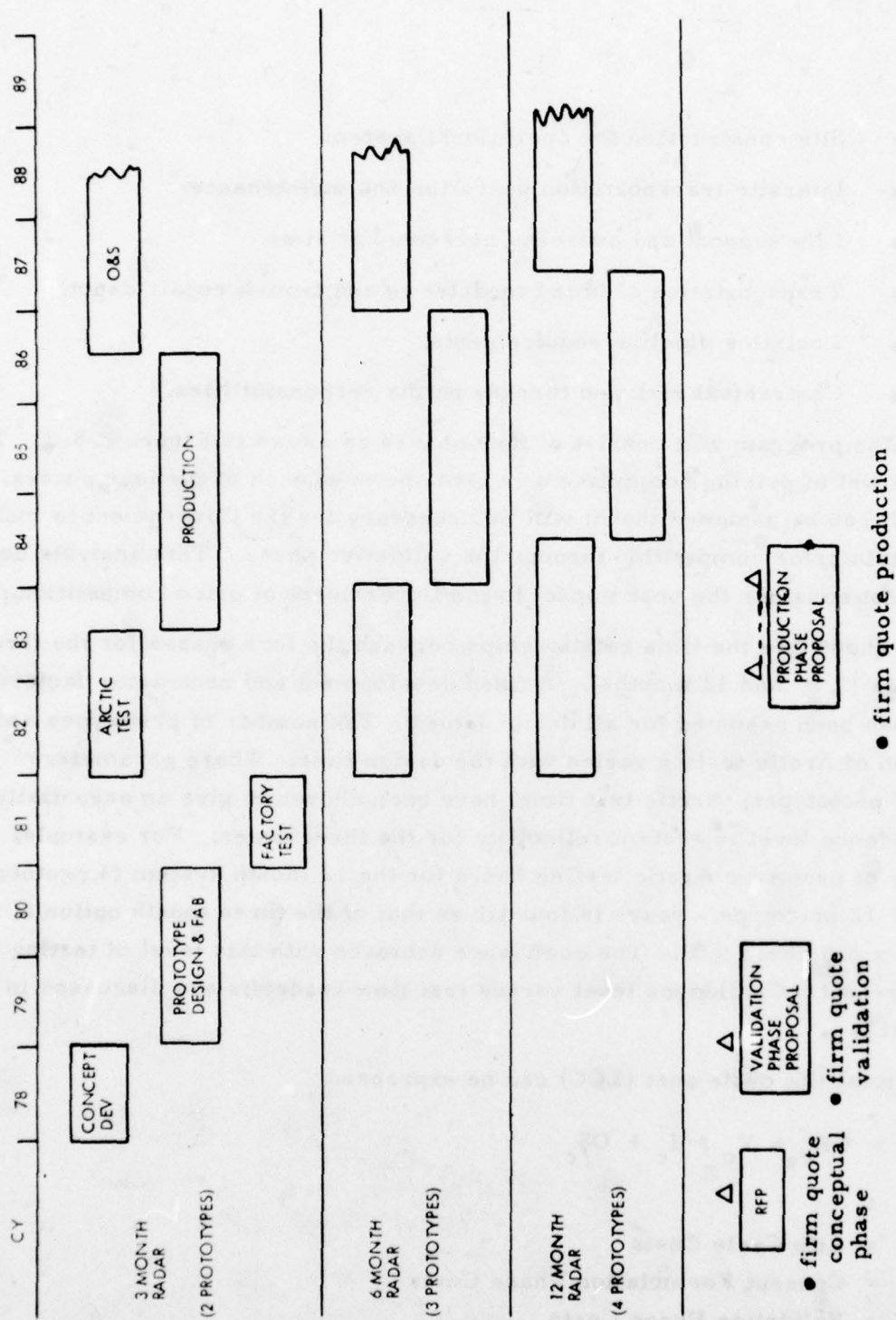
Figure 2.8-2. Type A Program Phasing

Concept Formulation Definition

This program phase will be 12 months duration for all three reliability variants. The elements to be costed are:

- Engineering design and analysis, selection of preferred configuration to meet minimum requirements.

- Pricing for validation phase.

- Establish reliability test plan including detailed agreement with Air Force as to test conditions, failure modes and ground rules.[*]

It has been assumed that in all instances the cost of the concept formulation phase will be $500K.

Validation Phase Definition

This phase is separated into three elements.

- Design and fabrication of prototype units.
- Factory test program.
- Arctic test program.

The following relationships apply:

$$V_c = (N)(TH_c) + DEV_c + SE_c + RMT_c + MOD_c$$

where

N	=	No. of prototpyes required (2 for 3 month radar; 3 for 6 month radar; 4 for one year radar)
TH_c	=	Hardware fabrication cost per prototype
DEV_c	=	Development cost
SE_c	=	Support equipment cost
RMT_c	=	R & M demonstration test cost
MOD_c	=	Cost of modifications to convert prototypes to pre-production models

TH_c was estimated rigorously from the bills-of-materials and design data provided to manufacturing cost estimators.

[*] This item is one of the major risk areas in the total program.

The design and fabrication phase (DEV_c) is assumed to be of two years duration for all three reliability variants. The intent of this activity is to design and build the required number of prototypes with a minimum of documentation (Form 3 drawings and engineering sketches).

$$DEV_c = E_c + MPS_c + DAT_c + SW_c + TE_c$$

where

E_c = Engineering costs

MPS_c = Management and program support costs

DAT_c = Data costs

SW_c = Software costs

TE_c = Test and evaluation cost

SE_c and DEV_c was estimated from the hardware fabrication cost per prototype (TH_c) using parametric relationships developed from seven previous radar development programs considered representative of relationships involved. These parametric relationships which involve proprietary Raytheon information establish SE_c, E_c, MPS_c, DAT_c, SW_c and TE_c as percentages of the total validation phase cost which in turn is a constant (K) x the total prototype hardware costs. In these relationships, SE_c, MPS_c, DAT_c, and SW_c are independent of the number of prototype built, TH_c and TE_c direct functions of the number of prototypes and E_c a weak function of the number of prototypes since subsystem testing is involved.

The total reliability and maintainability demonstration costs (RMT_c) is based on two elements.

$$RMT_c = RMTC_c + RMTA_c$$

where

$RMTC_c$ = R & M demo test cost at contractor factory

$RMTA_c$ = R & M demo test cost at Arctic

$$RMTC_c = P_c + S_c$$

where

P_c = Personnel cost

S_c = Support cost (10% TH_c)

$$P_c = (M)(5)(CPY)(NOY) + PO_c(NOY)$$

where

M = No. of personnel per shift (3)

CPY = Cost of person per year ($65K)

NOY = No. of years R & M test (1 year)

PO_c = Program office cost per year (4 personnel)

S_c = Cost of spares and repairs

$$RMTA_c = INS_c + P_c + S_c$$

where

INS_c = Installation

= $(M)(0.25\ CPY)(N)$

where

M = No. of personnel per site (15)

N = No. of prototypes

$$P_c = M(NOY)(CPY)(N) + PO_c(NOY)$$

where

M = No. of personnel per site (4)

N = No. of prototypes

NOY = No. of years Arctic Test (1.5 yr. for 3 month radar, 2 yr. for 6 month radar, 3 yr. for 1 yr. radar)

The factory test activity is intended to upgrade the configuration to pre-production and will last for 12 months in all cases. The assumed strategy is for one system to prove system electrical performance while the remaining prototypes (1, 2 or 3) are 'soak tested' to eliminate latent defects. Full configuration management will be initiated at the beginning of this activity and all engineering changes fully documented. Form 1 drawings will be available at the completion of this test activity.

The support equipments must be transportable and yet able to demonstrate all system performance parameters with the exception of antenna patterns which must be demonstrated on qualified range.

The Arctic test activity will be 1.5 years for 20,000 hour system, 2.0 years for 40,000 hour system and 3.0 years for 80,000 hour system. Equipment installation personnel and support equipment costs at the Arctic site are considered.

At the completion of the Arctic test, it is anticipated that no more than 50% confidence of achieving 20,000, 40,000 or 80,000 hours MTBF will be possible. The issue of who takes responsibility for committing to production at 50% confidence and the contractual penalties/incentives that are involved is not considered as a cost item at this time.

Production Phase Definition

Investments costs associated with the production phase are defined as follows:

$$I_c = PR_c + PF_c + MPS_c + IT_c + LN_c + SE_c + IRS_c$$

where

PR_c = Prototype refurbishment costs

= $(0.4 \ TH_c)(N)$

PF_c = Production fabrication costs

= $(80-N)$ x average manufacturing cost.

This cost element was developed by rigorous estimation from bills-of-material, engineering design data, and 'similar too' references. The production program was assumed to consist of a 1 year lead time followed by two years of manufacture at a constant rate.

MPS_c = Management and program support costs

= $(M)(CPY)(NOY)$

M = 15 personnel

CPY = $65K

NOY = 3 years

IT_c = Installation and test costs

= (M)(0. 25 CPY)(N)

   M = 15 personnel

   N = 80 sites

LN_c = Permanently manned site additional radar hardware costs.
This item includes BITE computer and display equipment
IFF Mode 4 K·I·R unit and radar control panel. Seven
permanently manned sites were assumed.

SE_c = Support equipment for the permanently manned sites.

IRS_c = Initial and replacement spares costs. These spares were com-
puted on the assumption that over a 20 year Operation and Support
period 5% of all module (FRU) failures would require replacement
with new modules. These replacement modules were also
assumed to be manufactured during the production phase. Addi-
tional modules for logistics pipeline requirements were not
estimated.

Operation and Support (O & S) Phase Definition

The costs associated with this phase considered only the direct maintenance
personnel per manned site required to bring a failed radar back to full operation
within a 3 hour visit, and the cost of repair for 95% of the failed FRU's.

$$\text{OS}_c = \text{P}_c + \text{R}_c$$

where

P_c = Personnel costs

= (NPLN)(NLP)(CPY)(NOY)

NPLN = Number of maintenance personnel required for 3 hour
repair visit.[*] Based on an analysis of mean-time-to-replace
and failure rate for each of the radar FRU's, the personnel
required to bring a 3, 6 and 12 month radar back to full per-
formance with a 3 hour visit was estimated. This estimate
did not consider safety, overhead or transportation aspects
but did assume a 75% factor for personnel efficiency. The
following table lists the direct maintenance personnel
requirements.

[*]See Section 2.6.7.

2-293

	90% P_s/ 3 months	90% P_s/ 6 months	90% P_s/ 12 months
L-Band	1.0	2.0	4.0
UHF	1.0	1.0	2.0

All estimates assume a priori knowledge of all failures and that performance verification is based on BITE readout at the visited site.

NLN = Number of logistics nodes (7)

CPY = Cost/person/year ($65K)

NOY = Number of years (20)

R_c = Cost of repair for 95% of the failed FRU's.

$$R_c \text{ per FRU} = \frac{8760(QPS)(NSYS)(NOY)(0.4\ UP)}{MTBF}$$

where

QPA = Quantity of that FRU per system

NSYS = Number of systems (80)

UP = Unit production price

MTBF = FRU mean-time-between-failure.

Because of the spread of FRU costs, an upper limit of $1000 was assigned to the FRU repair costs. In this case, it was apparent that FRU's with a production price in excess of $2500 could be assumed to have lower level modules which while not suitable for removal in the field would permit repairs far less than 40% of FRU production cost. FRU's with prices below $2500 were assumed repairable at 40% of production price.

Cost Model Summary

It can be seen that within the guide line that only those costs directly related to radar design be considered, the resulting assumptions severely restrict the inputs to the life-cycle-costs (L·C·C), particularly in the O & S Phase. In recognition of these omissions, it is considered more appropriate that the costs computed in the following section be assessed as a cost sensitivity analysis rather than a L·C·C.

2.8.3 Cost Data

The following charts represent the tabulated costs of selected radar configurations at both L-band and UHF. The radar configurations chosen are considered to bound the most attractive options at the two frequencies. The cost model and assumptions of section 2.8.3 was used in all cases, however it is necessary to clarify cost options for certain items:

- Building including shelter and radome.

The structure material as costed is based on the assumption that an integral radome matched to the antenna radiating elements is necessary to minimize radome losses. In this instance ~ 1 dB of loss is predicted for a separate space frame type of radome primarily due to the closely matched contours of the ring array to the radome. However as can be seen, an integral radome and additional structure is not inexpensive. Costs for this item could be reduced by approximately one half if a separate space frame radome (55 ft. diameter) is used with resulting increase in prime power demands.

- Tower Costs (Validation and Investment Phases)

The costs shown against this item are material estimates only. In the case of the Validation phase the estimate is for modifications to existing towers. The cost for the Investment phase assumes 80 new towers. However, it is obvious that a large number of the existing AN/FPS-19 towers can be used for the replacement radars. This cost saving in materials has not been considered at this time.

2-295

		3-Month	6-Month	12-Month
I.	Total LCC (20 yr.)	315.9M	341.8M	374.8M
II.	Concept Formulation Phase (CF_c)	500K	500K	500K
III.	Validation Phase (V_c)	40,404K	47,069K	54,067K
	IFF			
	(N)(TH)			
	DEV_c			
	SE_c			
	RMT_c			
	Tower			
IV.	Investment Phase Cost I_c	223,122K	230,975K	236,209K
	IFF			
	PR_c			
	PF_c			
	MPSC			
	IT_c			
	IRS_c			
	SE_c			
	LN_c			
	Tower			
V.	Operation & Support Cost (OS_c)	51,847K	63,299K	84,059K
	P_c			
	R_c			

CONFIGURATION: L-Band   6 μsec Pulse
                      Split-Frame   3 Receivers
                      256 TRSSM's   3 Lenses

Note: Detailed cost breakdown was submitted under separate cover.

		3-Month	6-Month	12-Month
I.	Total LCC (20 yr.)	231.2M	257.1M	281.3
II.	Concept Formulation Phase (CF_c)	500K	500K	500K
III.	Validation Phase (V_c)	32,633K	38,326K	43,479K
	IFF			
	(N)(TH)			
	DEV_c			
	SE_c			
	RMT_c			
	Tower			
IV.	Investment Phase Cost I_c	174,389K	182,962K	183,349K
	IFF			
	PR_c			
	PF_c			
	MPSC			
	IT_c			
	IRS_c			
	SE_c			
	LN_c			
	Tower			
V.	Operation & Support Cost (OS_c)	23,694K	35,324K	54,003K
	P_c			
	R_c			

CONFIGURATION: L-Band   6 µsec Pulse
                  Fence/Bowl   1 Receiver
                  64 TRSSM's   3 Lenses

Note: Detailed cost breakdown was submitted under separate cover.

		3-Month	6-Month	12-Month
I.	Total LCC (20 yr.)	264.2M	293.8M	331.5M
II.	Concept Formulation Phase (CF_c)	500K	500K	500K
III.	Validation Phase (V_c)	35,683K	41,884K	49,243K
	IFF			
	(N)(TH)			
	DEV_c			
	SE_c			
	RMT_c			
	Tower			
IV.	Investment Phase Cost I_c	190,394K	199,575K	209,248K
	IFF			
	PR_c			
	PF_c			
	MPSC			
	IT_c			
	IRS_c			
	SE_c			
	LN_c			
	Tower			
V.	Operation & Support Cost (OS_c)	37,606K	51,800K	72,480K
	P_c			
	R_c			

CONFIGURATION: L-Band   1.5 μsec Pulse
                  Fence/Bowl   2 Receivers
                  64 TRSSM's   3 Lenses

Note: Detailed cost breakdown was submitted under separate cover.

2-298

LIFE CYCLE COSTS   Configuration # 49

		3-Month	6-Month	12-Month
I.	Total LCC (20 yr.)	171.7M	194.6	225.6
II.	Concept Formulation Phase (CF_c)	500K	500K	500K
III.	Validation Phase (V_c)	22,817K	26,967K	31,320K
	IFF			
	(N)(TH)			
	DEV_c			
	SE_c			
	RMT_c			
	Tower			
IV.	Investment Phase Cost I_c	128,158K	135,821K	140,016K
	IFF			
	PR_c			
	PF_c			
	MPSC			
	IT_c			
	IRS_c			
	SE_c			
	LN_c			
	Tower			
V.	Operation & Support Cost (OS_c)	20,250K	31,270K	53,774K
	P_c			
	R_c			

CONFIGURATION: L-Band   6 μsec Pulse
                Single Frame   2 Receivers
                32 TRSSM's   2 Lenses

Note: Detailed cost breakdown was submitted under separate cover.

2-299

		3-Month	6-Month	12-Month
I.	Total LCC (20 yr.)	153.8M	171.9M	202.9M
II.	Concept Formulation Phase (CF_c)	500K	500K	500K
III.	Validation Phase (V_c)	20,993K	24,297K	29,066K
	IFF			
	(N)(TH)			
	DEV_c			
	SE_c			
	RMT_c			
	Tower			
IV.	Investment Phase Cost I_c	115,070K	119,307K	123,624
	IFF			
	PR_c			
	PF_c			
	MPSC			
	IT_c			
	IRS_c			
	SE_c			
	LN_c			
	Tower			
V.	Operation & Support Cost (OS_c)	17,230K	27,553K	47,666K
	P_c			
	R_c			

CONFIGURATION: UHF   6 μsec Pulse
                   Split Frame   1 Receiver
                   32 TRSSM's   1 Lens

Note: Detailed cost breakdown was submitted under separate cover.

2.9 DISCUSSION OF RESULTS

The study has been conducted within the bounding guidelines described in Section 2.1. This was necessary to reduce the number of system variables to be examined to those that met assumed 'top-level' operational and hardware criteria. Thus a preliminary assessment of several key variables was made early in the study to eliminate what was felt to be obvious non-contenders. These decisions included elimination of all frequencies with the exception of UHF and L-Band and the choice of a maximum aperture size to minimize power consumption while holding installation problems within reasonable bounds.

In this section, these bounding guidelines and key parameter options are reexamined in light of the results achieved during the study. In effect, the intent is to test the integrity of the study to discover if any interesting configuration variants have been excluded. While such an effort can by no means be completely exhaustive, it is a further test of the validity of the study model.

2.9.1 FREQUENCY SELECTION

The study effort has concentrated on UHF and L-Band frequencies. Frequencies above L-Band were eliminated because of:

- Higher clutter backscatter for equivalent beamwidth
- Higher fluctuation losses/reduced signal processing gain for reduced beamwidths
- Higher insertion losses from microwave devices
- Reduced power generation efficiency from microwave transistors

The resulting reduction in power/aperture efficiency and increased clutter suppression problems was considered undesirable for a minimum power unattended radar.

Higher frequencies have two primary advantages both of which are considered of reduced importance for a tripwire system:

- Higher 'roll-off' of elevation beam pattern for a given aperture. This will minimize multipath and maximize 3D low angle tracking accuracy providing a basic 2D detection is possible.

- Wider bandwidths for same percentage frequency spread. This will increase the power required by a successful jammer. However, higher frequencies allow higher gains from mobile antennas and for a fixed site target beam pointing problems for a jammer is minimized.

Frequencies above L-Band were considered to increase the 2D detection problem while contributing little by way of their advantages.

Frequencies below UHF are also unattractive for the following reasons:

- It is desirable to maintain a minimum of two elevation beams to allow a different sensitivity-time-control (STC) on the lower and upper beams. The lower beam STC retains the system dynamic range while the upper beam is concerned with weather clutter and "angels". The use of the same STC would cause a reduction in close-in high elevation coverage. Two beams at 150 MHz would require an undesirably large elevation aperture.

- Antenna noise temperatures due to cosmic noise increase dramatically below UHF. At 450 MHz, the sky temperature (for nearly all elevation angles) is about 150 degrees Kelvin, while it exceeds 1000°K at 150 MHz.

- The azimuth beamwidth for an aperture constraint of 50 feet is about 10 degrees at 150 MHz. This considerably increases tracking errors.

The basic advantages of lower frequencies are:

- For any given antenna area the number of elements in an array varies directly with the square of the frequency thereby minimizing complexity at power frequencies.

- Reduction in detrimental effects of ground clutter and back-scatter from weather and large flocks of birds.

2-302

However, given the proposed low cost honeycomb sandwich construction, printed radiating elements and elevation network, the antenna cost at UHF is minimal therefore reduced number of radiators will have a negligible impact. Increased beamwidth from the 50 ft. max aperture will illuminate more clutter and diminish any backscatter improvements.

It was therefore concluded that a frequency window between UHF and L-Band offered the best region to study in depth.

2.9.2 ANTENNA ARCHITECTURE

An electronically scanned ring array was chosen for the following reasons:

- Low power consumption dictated the need to eliminate friction, wind resistance and inertia of any mechanically rotated system.

- Moving mechanical systems have single point failure mechanisms due to bearing seizures. These failures are difficult to repair in Arctic environments during a 3 hour visit.

The multiface array is not economic for a 360° scan requirement. It generates essentially cone shaped beams when scanned off boresight and as such has difficulty achieving the goal of 0.5 degree azimuth accuracy on all targets. In addition, targets detected in overlapping sectors must be correlated which requires a more complex correction algorithm to reduce the off-axis angle errors for correlation. A planar array also requires phase shifters, which are inherently more complex to fault isolate. For these reasons, a four-faced planar array was eliminated.

If the azimuthal coverage required of the system was reduced to 180° or less a planar array antenna would require re-evaluation. However, given the problems of mounting antennas high off the ground and considering that the most likely threat is from high-speed aircraft at 100-500 ft. altitudes, a 360 degree scanning system is highly desirable to ensure adequate track time (>2 minutes) for high confidence identification as a hostile.

The Dome antenna provides an alternate approach to improve hemispheric coverage. It uses a single active planar array to illuminate a passive dome lens, which forms a pencil beam in space. This antenna however suffers from gain

2-303

degradation at low elevation angles and has difficult polarization problems in certain directions. The resulting development risk make this configuration undesirable.

The Hourglass antenna, using a concave cylindrical reflector (shaped like an hourglass) and a ring array feed, represents an excellent antenna geometry for the 360° azimuth coverage. However, due to the requirement of an exterior feed array, the horizontal dimension of the antenna tends to be large. For example, if a 44' diameter cylindrical reflector is used, the feed array diameter is approximately 60'. Furthermore, to achieve the desired elevation pattern shaping, the antenna also requires an oversized aperture. This configuration is not desirable given the tower mounting constraints and radome problems.

The cylindrical array offers the best solution to the tower/radome constraints, (44 ft. diameter with integral low loss radome) and possesses a number of other distinct advantages; the beam steerability, the pattern invariance, the effective usage of the radiating aperture and the ease of protection for weather. The pattern invariance is a property realizable with all circularly symmetric arrays, such that the azimuth beam is electronically steered without scanning loss.

Cylindrical arrays configured with vertical radiating stacks can be economically constructed using recently developed low cost honeycomb sandwich stripline technology. Given the advent of this low cost technology and the advantages for 360° coverage the ring array was the preferred choice.

2.9.3 SCAN STRUCTURE

This is the most fundamental of all system parameter variables and is derived from the basic decisions relating to the antenna parameters i.e.:

- Electronic step - scan in azimuth to eliminate friction wind resistance, inertia, and single point failure problems of rotary joints (bearing seizure) while maximizing beam time-on-target.

2-304

• Electronic beam forming in elevation to permit maximum aperture efficiency at all elevation angles. A 7 ft. high elevation aperture has been selected requiring 6 beams at L-Band and 2 beams at UHF to cover 0 to 45 degrees. More beams at L-Band would produce excessive processing requirements and more beams at UHF are unnecessary and undesirable unless height information is required.

On transmit the pulse is sequentially 'machine-gunned' into each beam. On receive all beams are processed simultaneously also maximizing beam time-on-target. The resulting systems configuration options from the above 'degrees' of freedom are identified below.

Single Frame

A single frame scan permits all elevation beams to be searched on each azimuth scan. If all elevation beams are simultaneously instrumented, then a good frame time (3.6 sec. for 16 pulses on target), and subsequent track initiation time (14.4 sec) can be achieved (See Table 2.2.2-2). However, this type of single frame scan leads to a higher duty cycle ($\sim 4\%$ L-Band, 1.4 % UHF) with consequent higher power consumption. It also requires more hardware in that a separate receiver and signal processor channel is needed per beam. This amounts to 6 channels at L-Band and 2 for UHF.

An alternative form of single frame scan occurs when only half the number of beams are simultaneously instrumented. The two groups of beams are searched in sequence, but still on the same scan. Half of the receiver and signal processor channels are saved (relative to the fully instrumented single frame scan); however, the frame and track initiation times are also doubled to 7.2 and 28.8 sec, respectively. This frame time can be reduced by using a smaller number of pulses in each beam position, however, the full advantages of either frequency agility or 8 pulse coherent integration must be given up. This is considered an undesirable option.

The single frame system has an intrinsic appeal as it represents the most straightforward and least complex of all scan structures. The radar scan is not required to 'adapt' to the motions of the target. This scan type, also possesses the advantage of covering the complete surveillance volume each scan.

It is difficult to satisfy all requirements (low frame time, low power consumption, low complexity) simultaneously at L-Band with a single frame scan where six elevation beams are required to fill the search volume for the 30 NM, 1 square meter cross-section target. These requirements can be met at UHF where only two elevation beams are needed to implement a single scan system with a 4 second frame rate.

Split Frame

The split frame scan was conceived to provide further options to the frame time/hardware complexity dilemma at L-Band. This scan type was chosen as the baseline system as it appeared to offer the simultaneous advantages of less hardware (3 receiver/processor channels), good track initiation rate (16.6 seconds), and less power consumption. In brief, a split-frame scan searches one half of the elevation volume on each scan and the remaining half on the succeeding scan. If a target is found on a particular beam on a scan, that group of elevation beams is revisited for the next 3 scans on the same azimuth beam. The frame time is 7.2 seconds but the average track initiation time is 16.2 seconds.

The disadvantages of a split-frame are the decreased surveillance update rate and the additional control complexity required in moving beams in response to previous target detections. In addition, a penalty of about 0.4 dB is extracted due to higher false alarm threshold requirements.

The use of a split-frame is more attractive at L-Band because of the 6 channels involved. Three receiver/processor channels can be saved while the two beam UHF system will only save one channel at the expense of twice the frame rate.

Fence/Bowl

A minimum energy system can be constructed if the concept of a "tripwire" system is applied literally. Fence/Bowl configuration permits all elevation beams to be searched each scan but only at predetermined range intervals. The advantage is reduction in receiver channels and signal processor memory. Additional data processing logic can be used to maintain update on target in track, however targets entering the coverage from above the predetermined 1 sq/meter target track initiation fence and tracked targets entering the cone-of-silence would be

difficult to pick-up until they penetrate the 1 sq/meter target track initiation fence again. This is likely to prevent two minutes of track time on a high speed target.

Even more than the split-frame, the use of a fence/bowl concept is more suited to L-Band than UHF. A minimum of about 110 NM of range gates must be searched per azimuth beam position for an L-Band fence/bowl as opposed to 360 NM for a fully instrumented single frame scan. This can be accomplished with one receiver channel at a frame time of 6.8 seconds or two receivers at a frame rate of 3.6 seconds. The difference at UHF is about 60 NM in range gates for a fence/bowl as opposed to 120 NM for a fully instrumented, two beam, configuration.

The primary disadvantage of the fence/bowl is the absence of full volume search. Apart from the frame time increase suffered if a single receiver concept is used the lack of a full range 'bowl' on the low beam will prevent the maintenance helicopter from being acquired on departure from the visited site until the 30 NMI fence is reached. This may be undesirable for safety reasons and may dictate that a 2 receiver fence/full range bowl is the minimum system configuration acceptable. In this case the U.H.F. fence/bowl would offer little significant hardware advantage over a full volume single scan configuration at U.H.F.

2.9.4 ELEVATION PLANE FOCAL STEPS

The number of elevation plane focal steps determines the number of parallel azimuth steering networks required. As it is desirable to minimize the number of such networks from cost and power consumption considerations, it was attempted to utilize one network for every pair of beams by focussing between them. This turned out to be feasible; however, a substantial focussing loss resulted at high elevation angles particularly at L-Band.

The choice between the reduced performance at high elevation angles with the decreased cost and a higher performance/higher cost system must depend on the degree of strictness with which the goals set forth in the SOW are to be interpreted.

This appears to be more of an issue at L-Band as the cost difference between 6 and 3 networks is considerable. At UHF, the choice is between a 1 or 2 focal plane network and the overall system cost impact is reduced accordingly.

2-307

2.9.5 TRANSMITTER PULSE LENGTH

This parameter is one of the most potentially significant differences between UHF and L-Band. At L-Band it is estimated that for a constant $10^{-5} P_{fa}$ the signal processor CFAR threshold must be 10 dB higher if only 3 as opposed to 15 samples of weather data are available. The question as to how many samples are available is a function of the size of the weather cell and the transmitter pulse length. If weather cells are approximately 1 nmi in depth a 6 microsecond pulse would require a 10 dB increase in CFAR threshold as opposed to a 1.5 microsecond pulse. At UHF backscatter from weather is diminished to a point where a 6 microsecond pulse is more than adequate to ensure minimum CFAR thresholds. The major impact of a 1.5 microsecond transmit pulse at L-Band is to increase the signal processor size, power requirements and failure rate.

Some portions of the DEWLINE are virtual deserts and intense storms rarely occur. Other regions, particularly in Alaska, however, do experience such storms and appropriate CFAR measures should be taken to prevent excessive false reporting.

The issue of pulse length for operation at L-Band requires much more detailed evaluation before any final conclusion can be drawn. The tests planned by Lincoln Laboratory on the AN/FPS 20 radar will contribute valuable empirical data in this regard.

2.9.6 LOCATION OF TRSSM

To minimize R.F. losses the TRSSM's should be mounted at each radiating stack of the antenna. However, for a 44 ft. diameter ring array there are 256 stacks at L-Band and 128 at UHF. This represents a major acquistion and repair cost because of the numbers involved. In order to minimize acquisition and repair costs the number of TRSSM's should be reduced to that required to form each instantaneous beam position. In this case 64 radiating stacks need energizing at L-Band and 32 at UHF.

This can be achieved by 'walking' 64 or 32 modules around the array controlled by the azimuth steering switches. In this case the modules are located behind

the quadrant switch (Q switch). The disadvantage to this technique is that increased power is required from each module because of switching and cable insertion losses. At L-Band this loss is about 3 dB and at UHF 1.5 dB. The increased loss at L-Band is largely due to the higher cable losses compared to UHF. The increased prime power required to overcome these losses is considered a desirable trade-off in life-cycle-cost.

The peak power required for the L-Band module located behind the Q switch is 320 watts for a 1.5 microsecond pulse and 80 watts for a 6 microsecond pulse while the 6 microsecond pulse at UHF requires 200 watts peak. The decision to place the TRSSM either at the antenna or behind the Q switch depends exclusively on the relative cost impact on the system. The effect on cost is not just the acquisition costs of the modules but also includes additional spares and maintenance costs if the module is more complex and thus less reliable. A higher failure rate module would also require a higher level of redundancy in other parts of the system to meet a specified survival time with a stated probability.

Table 2.3.2-2 compares several TRSSM configurations in terms of TRSSM production costs, failure rate and estimated impact on repair costs during the 20 year Operations and Support phase. Figures 2.3.2-3 through 2.3.2-8 shows simplified block diagrams for each configuration. The relative complexity of the modules is evident.

2.9.7 SIGNAL PROCESSING TECHNIQUES

The clutter model provided in the statement of work requires spectral filtering to preserve an acceptable level of false alarms. The general choice lies between MTI or MTD. The distinction is that the MTI has a single bandpass after clutter filtering while the MTD has banks of contiguous filters. The MTI is obviously the simplest mechanism with resultant savings in number of components, failure rate and cost. However, the MTI with non-coherent integration has ~2dB gain loss over 8 pulses compared to the coherently integrated MTD. This statement assumes that frequency agility is still applied every 8 pulses to reduce fluctuaion loss.

It is desirable that coherent integration be used to minimize the system prime power consumption for a given detection sensitivity providing the additional hardware complexity does not produce excessive power consumption, failure

rates and cost.

This latter criteria depends on pulsewidth, and number of channels to be processed.

L-Band systems have the most demanding processing load due to the 6 beam configuration. Further the lack of circular polarization from the antenna makes processing of the upper beams highly desirable to provide a degree of subweather visibility. As can be seen from Table 2.7.6-1 many of the L-Band configurations particularly with 1.5 microsecond pulses will more than swamp the prime power reduction due to a 2 dB sensitivity improvement making MTD processing questionable with presently available technology. However, the UHF configurations with 6 microsecond pulses and two channel (beam) processing permit the necessary reductions in MTD hardware complement that make coherent processing highly desirable. The only L-Band configuration to permit the same MTD hardware complement is the fence/bowl scan structure.

2.9.8 POWER APERTURE CONSIDERATIONS

As can be seen from Section 2.1 a 44 ft. diameter by 7 ft. ring array was selected as the antenna configuration for both UHF and L-Band. In terms of power/aperture the L-Band system has a 3 dB advantage, while UHF has a 2 fold increase in frequency diversity to reduce fluctuation losses and a 2 fold increase in the number of coherent processing intervals (CPI) to increase the signal processing gain. The net result was that similar average power per system is required on the assumption that the TRSSM's are located at the radiating stack.

However, at L-Band 256 radiating stacks were required while at UHF only 128 are needed. This immediately provided a cost advantage in favor of UHF. This advantage was further compounded when the benefits of locating the TRSSM's behind the Q switch were explored.

- The higher co-axial cable losses (3 dB two way) at L-Band provided a 1.5 dB advantage for UHF when the TRSSM's are located behind the quadrant switch. The magnitude of this difference is determined by the lengths of cable involved, therefore the larger ring array diameter the more advantage for UHF.

2-310

- Mounting the TRSSM's behind the quadrant switch required the module peak power to be increased to overcome the additional losses. The impact of this increase can be seen from Table 2.3.2-2 in which resulting the acquistion costs, failure rates and repair costs are tabulated showing an increasing advantage for UHF primarily because component state-of-the-art permits less complexity for higher peak powers than L-Band. This is particularly true if a 1.5 microsecond pulse is used at L-Band.

Based on the above considerations it would appear much of L-Band's problem rests with the number of stacks in the antenna and the diameter of the ring array.

An L-Band antenna with 128 radiating stacks would be approximately 22 ft. in diameter and have an azimuth beamwidth of 2.8 degrees. The aperture-gain product of this antenna would be reduced by 6 dB while the 2 fold increase in frequency diversity and CPI's would recover 4 dB making a total system gain reduction of 2 dB over the equivalent L-Band system with a 44 ft. diameter array. If we evoke the same logic to locate the modules behind a Q switch the number of switches involved is the same as for the 44 ft. diameter UHF array and the reduced cable run length will help compensate for the higher cable losses at L-Band. The overall R.F. power increase required at L-Band for a 22 ft. diameter array with the modules located at the Q switch compared to L-Band modules located in the same position in a 44 diameter array, is approximately 0.5 dB. As half the number of L-Band modules are used compared to the 44 ft. diameter array equivalent, this requires a module with 720 watts peak power for 1.5 microsecond pulses and 180 watts peak for 6 microsecond pulses. This higher L-Band peak power level requires a still more complex TRSSM module with attendant increases in cost, failure rate and power consumption compared to the UHF modules shown in Table 2.3.2-2.

Based on preliminary cost and performance analysis of a L-Band fence/bowl using a 22 ft. diameter by 7 ft. high ring array and:
- 6 microsecond pulsewidth
- 180 watt peak power modules (35 total) mounted behind the Q switch
- 2 receiving systems to permit a full range bowl (see Section 2.9.3)

the resulting L.C.C. compared to a UHF 2 beam single frame scan (configuration

49) are 15% higher using the cost model of Section 2.8.2 and power consumption is 3 dB more. For the same L-Band system with 1.5 microsecond pulse width the L.C.C. is 24% higher than configuration 49.

2.9.9 TECHNOLOGY CONSIDERATIONS

This study has been conducted with emphasis on minimizing the technology risks. This is considered consistent with the direction in the Statement-of-Work to limit hardware to that realizable in the 1980 time frame. However as can be seen from the proposed program milestones (Figure 2.8-2) the first production system will not appear until 1983. In the light of this timetable it is desirable to review the technology assumed in the study and comment on possible improvements in the near future.

Antenna Technology

The basic technology assumed for the antenna is shown in Figure 2.2.3-2. This technology is presently under development at Raytheon and will be directly applicable to the proposed radars. It is considered unlikely that a more cost-effective technology will evolve in the near future. Therefore this technology area is considered well within state-of-the-art.

Beam Steering Switches

These switches are well within state-of-the-art. However, they are also relatively expensive at present due to the broadband characteristics that component vendors have opted to produce. A cost-reduction program is required to match the performance requirements for the radar to a minimal cost solution. Raytheon has performed similar performance/cost matching in other radar systems with encouraging results.

Azimuth Steering

The baseline system uses a dielectric lens. Raytheon is confident that such a device is well within state-of-the-art. A more pertinent question in this area is whether the lens is the most cost-effective solution to the azimuth plane focussing requirement. It is intended to evaluate differential length cable networks as an alternative. Use of alternatives will be based solely on cost.

2-312

Transmit/Receive Modules

Raytheon is deeply involved in both UHF and L-Band module development and therefore well aware of the present and near term potential of this technology. The proposed modules are considered well within state-of-the-art. Future efforts in this area should be directed at cost-reduction rather than performance improvement.

Receiver/Exciter

This is one of two areas where technology improvements are desirable. The designs used in this study did not capitalize on the full range of analogue monolithic I.C.'s that are becoming available. It is intended to study increased applications of L.S.I. to the receiver/exciter in the coming year.

Signal/Data Processor

This is the other area where component technology improvements are desirable particularly from a power consumption viewpoint. The technology assumed for the signal/data processor is a programmable microprocessor using I^2L and SOS/CMOS technology.

While the programmable element is highly desirable as a fault tolerant building block, the power consumption using I^2L and SOS/CMOS is still undesirably high. Charge Coupled Devices (CCD) hold promise of dramatic reductions in complexity and power consumption. It is intended to evaluate CCD's further in the coming year.

2.9.10 FAILURE THRESHOLDS REVISITED

As can be seen from the reliability model (Section 2.6.2) the definition of what constitutes a system failure is perhaps the highest risk element in the ultimate realization of a radar designed to minimize system cost-of-ownership. This is because of the sensitive balance required between inherent hardware complement of the radar particularly for redundancy purposes and the frequency with which repair visits are required. More redundancy will permit extended periods of unattended operation but will also require higher acquisition and repair costs. The cost-effective realization of an operational system of unattended radars particularly in a network of radars with overlapping coverage will depend

2-313

to a large extent on the data availability required and the downtime permissable at any radar. This issue has to be ignored in the present study because of the reliability design requirements specified in the contract statement-of-work (SOW). Similarly, the S.O.W. permitted a 2 dB system degradation. This was modeled (Section 2.6.2) to permit a total coverage volume reduction equal to that resulting from a 2 dB drop in transmitter power. However, a conservative interpretation of the 2 dB degradation was used in the power budget estimations. In this case the R.F. power computed for each system configuration provides a 2 dB margin so that the degraded system still meets the equivalent volume of an 'all-up' system specifically tailored to the detection requirements of the SOW. If the 2 dB degradation had been taken starting from a system just satisfying the detection requirements a drop in module peak power would result. However, given the conceptual nature of the radar design and the occurrence with which dB's are lost in the translation to hardware, the conservative interpretation of 2 dB degradation was considered more realistic.

2.9.11 SYSTEM LEVEL COMPARISONS

The following table summarizes the salient cost and performance characteristics of selected L-Band and UHF configurations. It can be seen that if minimum power consumption with good performance at a reasonable cost is desired configuration 49 is very attractive. Configuration 49E has been included to establish the impact of designing in features specifically for ECCM. These features do not include those considered undesirably complex as identified in Section 2.7.3. The nearest minimum power and cost L-Band configuration is number 35 with a 2 receiver fence/full range bowl scan structure and 6 microsecond pulses. The primary advantage of L-Band is the ability to grow to 3D operation although not without additional processing complexity. This configuration assumes a 6 microsecond pulse is acceptable at L-Band - an assumption that is in question. As previously identified in Section 2.9.8 a reduced cost L-Band fence/ bowl is possible using a 22 ft. ring array but only at the expense of 3 dB more prime power. If growth to 3D is an important issue this configuration would be preferred.

2-314

Configuration Trade-Offs

Configuration	1	6	13	36	39	49	62	49 (A/J)
Frequency	L	L	L	L	L	UHF	UHF	UHF
Scan Type	Split	Split	Single	Fence	Fence	Single	Split	Single
No. TRSSM	256	64	256	64	32	32	32	32
Pulsewidth	6	6	6	1	1.5	6	6	6
No. Receivers	3	3	6	1	2	2	1	2
No. AZ Networks	3	3	6	3	3	2	2	2
Performance								
$16M^2$ TGT								
0-100 Kft	E	E	G	E	G	E	E	E
$1M^2$ TFT								
0-500 ft	G	G	G	G	G	G	F	F
500 ft - 80 Kft	F	F	G	F	F	G	G	F
80 - 100 Kft	P	F	F	P	P	G	G	G
Frame Time	F	F	E	E	E	E	F	G
Trk. Init. Time	E	E	E	E	E	E	E	E
CFAR	F	F	E	F	E	E	E	E
Growth to 3D	G	G	G	F	F	P	P	P
ECM	G	G	G	G	G	G	F	G
Power Consump. (W)	667	897	1642	679	1263	569	372	606
Cost ($ Sell)								
Concept Formulation	0.5	0.5	0.5	0.5	0.5	0.5	0.5	0.5
Validation	40	40	48	33	36	23	21	27
Investment	223	219	273	174	190	128	115	155
O & S	52	26	54	24	38	20	17	27
Total	316	286	386	231	264	172	154	210

P = Poor   F = Fair (below goals)   G = Good (meets goals)   E = Excellent (exceeds goals)
A/J = anti-jam

2.10 CONCLUSIONS

A family of unattended radars has been studied for application on the DEWLINE. These radars were designed for operation at both UHF and L-band. There is no one configuration that stands out as a recommended solution for the DEWLINE application. This is particularly true in the case of small targets (1 sq meter) at low altitudes (< 500 ft). Selection of the operating frequency for the DEWLINE will only be possible when a better definition of cumulative detection including duration and number of continuous track periods for specific targets are established. This latter issue will also determine the need for 360 degree azimuth coverage.

The UHF variants of the radar family are less expensive than the nearest L-band equivalent. For this reason UHF is very attractive. However UHF has relatively few ECCM features and virtually no growth potential to 3D operation.

A design goal of 500 watts prime power for the radar/operation was established at the study outset. This requirement became the driving influence in the system design. In retrospect this prime power constraint was a good influence in that the resulting radar configuration contained the features needed for very high reliability, such as parallelism, and minimum parts count. Very low power is considered fundamental to the ultimate realization of unattended radar systems: An unattended radar cannot function without an unattended power source. The lower the power demanded, the more viable the realization of a highly reliable power source. Minimum power dissipation in the radar is consistent with maximum reliability. The more internal heat generated by a component the higher the failure rate. The actual goal of 500 watts may be achievable at UHF but not L-band. It is considered more realistic to increase the available prime for any operational system to at least 1000 watts. If L-band configurations with 1.5 microsecond transmit pulses are ultimately required to satisfy mission requirements, 1500-2000 watts of prime power will be needed.

The IFF system for use with unattended radars is also shown to be readily attainable with proven techniques. Because of a proposed mode of on-demand IFF operation for Type A radars which requires IFF interrogations only for

new or dropped tracks and the predicted low aircraft populations at DEWLINE sites, a 30:1 improvement in equipment failure rates over continuous operation has been conservatively estimated, greatly simplifying IFF reliability and power consumption demands.

The nature of the IFF mission, the modularity and small physical size of the equipment, coupled with a proposed near-dormancy operational mode, make a highly reliable IFF system a much simpler proposition than the primary radar.

Technology is potentially available to build radars with MTBF's on order of magnitude greater than that exhibited by present radar systems. Whether radars with >20,000 hours MTBF are practical or even necessary depends on the commitments required of the manufacture for his emplaced equipment and a detailed understanding with the customer as to what constitutes a failure. A sensitive balance is required between inherent hardware complement of the radar particularly for redundancy purposes and the frequency with which repair visits are required. More redundancy will permit extended periods of unattended operation but will also require higher acquisition and repair costs. The cost-effective realization of an operational system of unattended radars particularly in a network of radars with overlapping coverage will depend to a large extent on the data availability required and the downtime permissable at any radar.

The greatest unknown, and therefore risk identified in the study is the acceptability of the reliability model assumptions. These assumptions in turn impact the redundancy requirements and hence the cost and viability of radars for extended periods of unattended operation.

SECTION 3.0
TYPE B RADAR STUDY

This radar is defined as a 'minimally' attended 3D/200 NMI radar with 'minimal' power consumption requirements. Periods for 90% probability of operational success are 2 weeks, 1 month and 3 months. As with the Type A radar operational success permits a '2 dB' system degradation.

The recommended solution for the Type B system is an L-Band, mechanically rotated, planar array which uses a shaped beam on transmit and a stacked beam on receive. A bootlace lens is used to achieve the elevation beam forming and shaping. The antenna aperture has been sized to fit within a 55 foot radome. The transmit power is provided by a group of solid state modules.

A number of Type B system candidates were examined in arriving at the above choice. These alternatives included different frequency bands, antenna scan techniques and antenna feeds. The rationale by which these alternate solutions were rejected and by which the preferred choice evolved are summarized in the following paragraphs.

3.1 IMPLICATIONS OF TYPE A RADAR CONFIGURATION

The question that must first be addressed is whether the generalized system design guidelines of the Type A radar (Figure 2.3) are equally applicable to Type B.

The Type A design guidelines basically evolved from the unattended operational requirement of the system and were driven by very low power consumption, and 3 hour repair visits. If 'minimally' attended is interpreted to mean an on-site complement of not more than 3 maintenance personnel, the justification for low power is questioned since life support will determine the power requirements and a 3 hour repair visit is no longer at issue. If the requirement of unattended operation is imposed on Type B the question becomes whether or not the Type A radar configuration is technically feasible for the Type B application.

This latter question can most easily be addressed by considering the additional system gain required on a 1 sq. meter target at 200 NMI as opposed to 30 NMI. In this case an additional 33 dB of gain is required. This additional gain can basically be achieved in two ways:

- Increase in transmitter power
- Increase in antenna aperture.

Increase in transmitter power can be achieved by either increase in pulse length and/or peak power. Increasing pulse length introduces two potential complexities:

1) Pulse compression to maintain 0.5 NMI range resolution
2) Short range gap filler pulse following the main pulse to meet a minimum range requirement (unstated).

If a minimum range requirement of 5 NMI is assumed (1 NMI is FAA requirement) then the time available for transmission is 62 microseconds. Transmission of pulses longer than 62 microseconds will require additional short range gap filler pulses to ensure a minimum range of 5 NMI.

If machine-gunning of the transmitter into a set of stacked elevation beams is attempted as in the case of the Type A, the question becomes how many beams are involved and can the peak power generated by the transmitter into each beam prevent the need for pulse compression and gap filler pulses. The number of beams required is a function of operating frequency, height accuracy and low angle tracking requirements.

3.2 FREQUENCY SELECTION

The only goal stated in the SOW is a height accuracy of $\pm$ 2000 ft at 100 NMI ($\pm$ 33 milliradians). If we assumed a practical limit of 15 times for reliable beam splitting, each stacked beam should not exceed 2.8 degrees. This requires 7 beams to cover from 0 to 20 degrees in elevation. The resulting physical aperture at S, L and UHF is 6 ft, 15 ft and 45 ft, respectively.

It should be noted that using the 1/2 beamwidth rule for simple low angle tracking the resulting height at 100 NMI below which 3D accuracy is suspect is about 22 kft (including the effects of earth curvature). This can be reduced to about 12 kft by use of sophisticated low angle tracking techniques. Any further

improvement in low angle tracking can only be achieved by a narrower elevation beamwidth on the low beam which while not necessarily increasing the total number of beams will increase the physical aperture requirements.

If we now consider the practical and cost-effective issues of the Type B system it is obvious that only S-Band holds promise of minimizing the physical size of the antenna while achieving acceptable height accuracy and low angle tracking accuracies. However, before system accuracies can be claimed a basic detection must be possible, before minimum power consumption can be claimed R. F. power generation must be efficient, and before unattended operation can be claimed high voltages should be eliminated.

S-Band is considered undesirable for the Type B system because of:
- Higher clutter backscatter makes detection more difficult
- Higher spectral spread from weather which for a 200 NMI radar operating with unambiguous P. R. F. can extend over the P. R. F. doppler interval
- More complex antenna in that circular polarization is required to combat high backscatter and spectral spread from weather
- Higher insertion losses from microwave devices
- Microwave transistors not yet practical for R. F. power generation at the levels required.
- Generation of R. F. with high voltage devices required making overall power efficiency and reliability more difficult to achieve.

The above reasons for eliminating S-Band are similar to those for the Type A system; however, unlike the Type A radar, the elevation accuracy and low angle tracking issues of the Type B radar make the required minimum elevation aperture at UHF (45 ft) too large for practical consideration. Therefore L-Band was selected as the preferred frequency choice for the Type B system.

3.3 SYSTEM SCAN TECHNIQUE

A set of seven stacked beams would permit a machine-gunned pulse width per beam of approximately 9 microseconds before a gap filler pulse became necessary. The peak power per beam position assuming a 44 ft x 15 ft high array at L-Band is 750 kw. This translates to 12 kw peak per radiating stack

assuming a 256 stack antenna. These are patently impractical requirements per stack given the state-of-the-art in solid-state microwave power devices. The only recourse is to increase the pulse length, and compression ratio and accept the need for the added complexity of a gap filler pulse.

The only viable ring array configuration would be to locate the transmitter behind the quadrant switch as for some of the Type A variants. The increased losses (~3 dB) from the azimuth steering network would again double the power of the transmitter while the R.F. power handling requirements for the azimuth steering switches make the technical realization of a ring array configuration impractical unless a power division in the elevation plane is made prior to the distribution in the azimuth plane. The resulting overall complexities make a Type A ring array configuration impractical for a 200 NMI radar. The preferred solution is a mechanically rotated planar array using shaped beam on transmit with the first R.F. power division in the elevation plane via a high power passive network and reception via multiple stacked beams.

3.4 POWER/APERTURE CONSIDERATIONS

The stacked beam configuration is necessary to maximize the hits per target over the full volume coverage. Two considerations apply:

- The more pulses available to form the clutter filter the deeper the rejection notch.

- The more pulses available the more transmit frequency changes are possible for a given clutter rejection notch and the lower the target fluctuation loss if post detection integration (PDI) is employed.

The first consideration relates only to system improvement factor while the latter is helpful in minimizing transmitter R.F. power generation requirements.

The objective of minimizing the R.F. power generation requirements for the Type B radar is very important if a solid-state transmitter is to be cost-effective. Unlike the Type A radar where the minimum number of solid-state transmitter modules was determined by the number of antenna active radiating stacks and not limitations in state-of-the-art component technology, the number of transmitter modules for the Type B radar is very dependent on component

technology limitations. This limitation will result in an increase in module count and hence failure rate. Both these latter issues will increase cost-of-ownership.

Apart from frequency diversity/PDI transmitter power reduction can be achieved by:

- Increasing the antenna aperture

- Minimizing RF transmission line insertion losses

Since the mechanically rotating antenna requires a separate radome, a reasonable maximum diameter for the radome is 55 ft. A 55 ft. diameter radome will accommodate a 27 ft. high by 32 ft. wide planar array. At L-Band this array produces an azimuth beamwidth of 1.4° and a full aperture elevation beamwidth of 1.7°. Assuming the total elevation coverage is 0 to 20° approximately 12 elevation beams are required for an elemental beamwidth of 1.7°. If the same vertical stack antenna configuration as for the Type A radar is used, the elevation network would require a 12 x 70 matrix - a clearly impractical requirement for a Butler or Blass/Lopez network. The only viable elevation network in this instance is the bootlace lens.

3.5 PREFERRED SYSTEM CONFIGURATION

The selected Type B system is therefore an L-Band stacked-elevation-beam-on-receive (SEBOR) and shaped beam on transmit with the following primary features:

- 27 ft. high by 32 wide planar array operating inside a 55 ft. radome.

- Maximum of 12 stacked elevation beams.

- Air dielectric 'bootlace' lens for elevation beam forming.

- Solid-state transmitter

3.6 UNRESOLVED ISSUES

Using the above building blocks a detailed cost/performance sensitivity analysis is required to resolve the following issues:

- Should the antenna be totally passive or should transmit/receive modules be mounted close to the radiating elements.

- Should a range ambiguous P.R.F. be used to increase the number of samples available for post detection integration.

- Is a 3 pulse integrate and dump type MTI with frequency agility/PDI more cost-effective than an 8 pulse MTD with 9 dB more coherent gain but 3/8 less samples for frequency agility/PDI. This issue is influenced by transmission bandwidth available assuming a minimum of 35 MHz is required to achieve backscatter frequency decorrelation, and the desirability of achieving subweather and chaff visibility.

- What is the minimum number of receive/signal processor channels that can be shared between the stacked pencil beams without undesirable compromises in 2D and 3D data rates or increase in transmitter power.

The system configuration combinations resulting from permutating all the degrees-of-freedom in each of the above issues results in an overall study task at least equal to that carried out for the Type A radar. In accordance with the S.O.W. directions the major effort under this study was concentrated on the Type A radar. It has not been possible within the time constraints of this study to conclude the type of rigorous trade-offs needed to produce the same overall cost/performance visibility as for the Type A radar. Raytheon intends to pursue the 3D radar configuration trade-offs in the coming year.

APPENDIX A

SECONDARY PATTERN CALCULATIONS
FOR CIRCULAR CYLINDRICAL ARRAYS

This appendix describes a formulation employed for calculating approximate secondary antenna patterns for a circular cylindrical array configuration.

Figure 2.3.1-1 shows the array element geometry with certain restrictions imposed. The elements are located (M per horizontal layer) on circular rings (of radius, R) at equi-angular spacings (setting the angle η = 360/M degrees) such that colinear vertical stacks (of N elements each) are formed (with an equal spacing, h, between the elements).

For convenience, the (m, n)-ordering of the array elements was taken such that the element, (m = 1, n = 1), falls in the xz-plane along the positive x-axis with the xyz-coordinate origin located at the center of the lowest circular ring. The index, n, counts off rings (or layers) proceeding in the positive y-axis direction. The index, m, then counts off elements proceeding away from the positive x-axis toward the positive z-axis.

The coordinates of the array elements can be written

(1a) $\qquad x_{mn} = R \cos\left[(m-1)\alpha\right] \qquad\qquad 1 \leq m \leq M$

(1b) $\qquad y_{mn} = (n-1)h \qquad\qquad\qquad 1 \leq n \leq N$

(1c) $\qquad z_{mn} = R \sin\left[(m-1)\alpha\right] \qquad\qquad 1 \leq m \leq M$

The secondary (power) pattern calculation is always made either in an azimuth plane cut (i.e., with the elevation angle, $\emptyset$, held constant and the azimuth angle, Θ, varying) or in an elevation plane cut (i.e., with Θ held constant and $\emptyset$ varying).

Excitation amplitudes (in voltage) at the array elements are taken to be of a separable product form

(2) $\qquad A_{mn} = (A_m)(A_n)$

where the horizontal ring amplitude distribution, A_m, is restricted such that only elements within a given angular sector (typically less than 90°) of the circular cylinder will be non-zero.

Excitation phases (in turns) at the array elements are taken to be of a separable additive form

(3)
$$\delta_{mn} = \delta_m + \delta_n + \epsilon_n$$

with

(4a)
$$\delta_m = (R/\lambda) \cos \phi_0 \cos [(m-1) \alpha - \theta_p]$$

and

(4b)
$$\delta_n = (h/\lambda) (n-1) [\sin \phi_0 + \sin \phi_p]$$

where the angle, ϕ_0, is an elevation angle selected to optimize certain azimuth plane focusing behavior; the angle, ϕ_p, is an elevation angle associated with a desired beam pointing direction; the angle, θ_p, is an azimuth plane angle associated with the beam pointing direction; and ϵ_n is a tabular input of relative phases determined by previous insight should a shaped beam elevation pattern be involved. Note that the vertical amplitude distribution, A_n, would also be so determined.

The radiation pattern of the array elements is taken as

(5)
$$E_m(\theta, \phi) = \left\{ \cos q \left[\theta - (m-1) \alpha \right] \right\}^P \left\{ \cos t\phi \right\}^s$$

where the constants, q and t, are typically near unity; the constants, p and s, as exponents taper the element voltage pattern; and some precaution is exercised to correct the angular factor, $[\theta - (m-1)\alpha]$, into the proper range for m-values passing from $m = M$ to $m = (M + 1 =)1$. E_m is made zero when either angular argument is greater than 90°.

The secondary power pattern is given by

(6)
$$P(\theta, \phi) = [R(\theta, \phi)]^2 + [I(\theta, \phi)]^2$$

where

(7a)
$$R(\theta, \phi) = \sum_{m=1}^{M} \sum_{n=1}^{N} E_m(\theta, \phi) A_{mn} \cos[2\pi \psi_{mn}(\theta, \phi)]$$

(7b)
$$I(\theta, \phi) = \sum_{m=1}^{M} \sum_{n=1}^{N} E_m(\theta, \phi) A_{mn} \sin[2\pi \psi_{mn}(\theta, \phi)]$$

and

$$\psi_{mn}(\theta, \phi) = [(x_{mn} \cos \theta \cos \phi + y_{mn} \sin \phi + z_{mn} \sin \theta \cos \phi)/\lambda] - \delta_{mn}$$

A-2

The power pattern is converted to dB down by

$$(9) \qquad P_{dB} = -10 \ \log_{10} \ (P/P_{max})$$

where ascertaining the value of P_{max} may require several trial-and-error calculations at spatial points surrounding the estimated beam pointing direction.

The above formulation was (FORTRAN) programmed for use with time-sharing access to the Raytheon Bedford computer.

APPENDIX B. RELIABILITY PREDICTION DATA

APPENDIX B

RELIABILITY PREDICTION DATA

The approach to the reliability modeling and the general results for the Type A radar are presented in Section 2. 6. The substantiating details are presented in summary form in this appendix.

A large number of system candidates had to be examined in detail during a short time period (see Section 2. 2. 2). It was also necessary to configure candidates to satisfy different, specific reliability requirements, namely: probabilities of system survival for 3 months, 6 months and one year. The reliability analysis was also required to provide inputs to the life cycle cost model, as the individual equipment reliabilities determined the redundancy required to meet the different survival times. The redundancy in turn affected acquisition costs and operations and support costs (see Section 2. 8, Cost Model).

A computer program was developed during the study to facilitate the rapid and accurate computation of a large number of variant configurations. This model is briefly described below. The computer output data for a number of candidate configurations is also presented. Finally, a selected detailed reliability estimate for one hardware element analyzed is shown to illustrate the depth of reliability analysis practiced in this program.

B-1. Reliability Computer Program

Complex reliability models are readily described and solutions to system reliability problems are quickly obtained using an interactive computer program developed at Raytheon in APL language.

Input data consists of any number of equipment groups in the system, each group being defined in terms of:

- total quantity used in the system

- number of active or dormant standby elements within each group

- number of elements within each group permitted to fail without failing the system

- element active failure rates

- standby dormancy factors

- computational method appropriate for exact reliability solution

- time intervals of interest

Variations of input data, as for alternate design candidates, may be easily exercised, enabling the computer to aid the user in optimizing the choice and type of equipment needed for least cost system solutions.

The versatility of the program lies in its ability to treat systems containing hardware groups in active and inactive standby conditions simultaneously as well as systems with non-zero standby failure rates.

The computer program which mechanizes the reliability model was developed independent of existing computer programs, such as RELCOMP[1], CARE[3], RMS[4], ARIES[5] and others which address a similar problem. The advantages of the Raytheon program are that its input data code is simpler than most, its output format is easily assimulated, it has a high degree of generality and it is both fast and economical.

Most complex systems are describable as a serial string of hardware groups. A group can be composed of serial equipment or it can be partially or highly redundant. The individual elements of the Type A radar were identified according to three types of reliability architecture:

Case (1): Parallel operation of n elements with m spares. Failure rates of spares are non-zero and may range from a fraction of active failure rate, as with dormant operation, to the full active failure rate, as with active, redundant n-tuples including voters.

Case (2): Parallel operation of n elements with m spares where spares have zero failure rate, as with completely inactive standby redundancy.

Case (3): Simple, serial operation of elements within the group.

The notation used to input data into the computer program has the form: N-S-M-F-D-C, where

N is the number of parallel, on-line elements within a group

S is the number of standby spares

M is the number allowed to fail before failing the group

F is the failure rate of an active, on-line element in units of failures per 10^6 hours

D is the dormancy factor for spares, expressed as a decimal fraction in the range $.005 < D < 1.0$

C is the computational algorithm used in the program to compute the group reliability.

In connection with parallel elements, the use of a single dormancy factor, D, within any one group limits the application to only two different failure rates within the group. This we find is not an important limitation since we have not had to impose more than two different failure rates in any practical, single parallel group of elements encountered thus far.

C, the computational algorithm, is designated by the numbers 1 through 5, calling up, respectively, reliability calculations based on transition rates from state-to-state, the binomial process, the Poisson process, an arbitrary process or one-shot relative frequency.

As an example, the entry code 150-0-10-5.8-1.0-2 describes a group consisting of 150 parallel elements with no provision for standby spares and up to 10 elements may fail before the group fails. Each element has an active failure rate of 5.8 failures per 10^6 hours, the dormancy factor is 1, since nothing is dormant within the group and the binomial reliability function will be used to compute the reliability value when the appropriate value of mission time is entered into the program.

As another example, the entry code 1-1-1-20.5-.5-1 describes an active on-line unit supported by a dormant standby spare. The failure rate of the active element of the group is 20.5 failures per 10^6 hours, the failure rate of the standby is half of that and equations derived from the state transition rate process will be called up to compute the group reliability.

The program proceeds with the entries for all groups within the system. If any group consists of redundant subordinate architecture, there is provision

B-4

through algorithm 4 to make the appropriate reliability calculation and enter it with all other computed group reliabilities so that the final system product of reliabilities is obtained.

System Computer Run Example

The program and the input data are given in APL language using any remote time-sharing terminal. Essentially, what the computer is directed to do is to compute group reliabilities at times of interest and then obtain the system reliabilities as products of the group string of reliabilities. This will be made more clear by modeling the configuration of Figure B-1 through the data entry codes as shown in Figure B-2. The output, formatted for time periods of 1/2, 1, 3, 6 and 12 months is shown in Figure B-3. Interactive editing instructions which alter the model are shown in Figure B-4 and the corresponding, new reliabilities are computed and printed out as shown in Figure B-5. Figure B-6 is a plot of the reliability functions for an original system configuration (mod 0) and two variants (mods 1 and 2).

Machine Instructions

The program user calls the program out of the library with the appropriate code and gives the command "ENTER". The machine interrogates the user for the name of each group in the model and the data entry code which describes it. In this way, the input data matrix is built row-by-row until the model is complete.

Along with the data entry codes, the specific time periods of interest must be inputted. The present program accepts up to five arbitrary times so that the reliability behavior over any portion of a life cycle may be computed and analyzed.

The matrix of data entries may be called up at the command "MODEL" (see Figure B-2). The reliability calculation methods are assigned at the time of data input and the computed group and system reliability outputs are printed at the command "REPORT" (see Figure B-3).

Editing changes to the data entry code may be undertaken at any time but must be followed by an instruction to perform a new set of computations for the new set of parameters and a new report results to complete the interaction between machine and user.
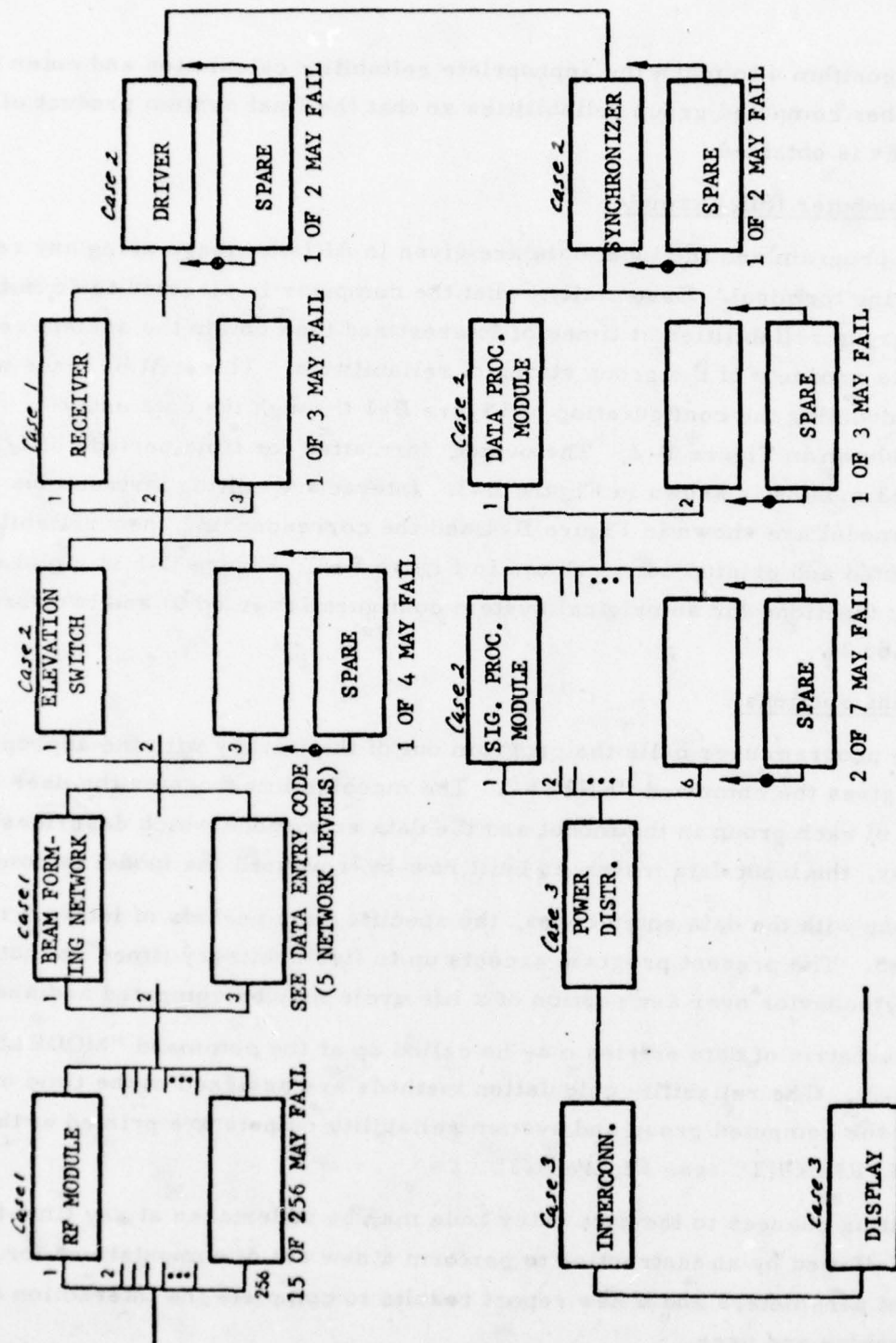
Figure B-1. Reliability Diagram, Candidate System Designated "Mod 0"

RF MODULES	256	0	15	11.90	1.000	2
BEAM FORM NET-A	3	0	0	1.25	1.000	1
-B	24	0	0	0.21	1.000	1
-C	96	0	1	0.13	1.000	1
-D	192	0	3	1.46	1.000	1
-E	768	0	6	0.21	1.000	2
ELEVATION SW	3	1	1	8.30	0.000	3
RECEIVER	3	0	1	25.70	1.000	1
DRIVER	1	1	1	19.20	0.000	3
SYNCHRONIZER	1	1	1	54.80	0.000	3
DATA PROC MODULES	2	1	1	21.50	0.000	3
SIG PROC MODULES	6	1	2	30.80	0.001	1
POWER DISTR	1	0	0	5.00	1.000	1
INTERCONNECTIONS	1	0	0	5.00	1.000	1
DISPLAY	1	0	0	6.00	1.000	1

Figure B-2. Data Entry Matrix Printed Out in Response to "MODEL"

ITEM↓ \ TIME→	360	720	2160	4320	8640
RF MODULES	0.99999	0.99999	0.99903	0.78349	0.01750
BEAM FORM NET-A	0.99865	0.99730	0.99193	0.98393	0.96811
-B	0.99818	0.99637	0.98917	0.97846	0.95738
-C	0.99999	0.99996	0.99964	0.99861	0.99464
-D	0.99999	0.99994	0.99662	0.96610	0.77809
-E	0.99999	0.99999	0.99999	0.99999	0.99940
ELEVATION SW	0.99996	0.99984	0.99860	0.99461	0.97992
RECEIVER	0.99974	0.99900	0.99156	0.96919	0.89684
DRIVER	0.99997	0.99990	0.99916	0.99674	0.98767
SYNCHRONIZER	0.99980	0.99924	0.99352	0.97603	0.91773
DATA PROC MODULES	0.99988	0.99953	0.99594	0.98474	0.94591
SIG PROC MODULES	0.99996	0.99970	0.99332	0.95938	0.80871
POWER DISTR	0.99820	0.99640	0.98925	0.97863	0.95771
INTERCONNECTIONS	0.99820	0.99640	0.98925	0.97863	0.95771
DISPLAY	0.99784	0.99568	0.98712	0.97441	0.94948
SYSTEM RELIABILITY	0.99044	0.97949	0.91740	0.60168	0.00665

Figure B-3. System Reliabilities of "MOD 0" Printed Out in Response to "REPORT"

```
IN[1;]+256 0 25 11.9 1 2
IN[3;]+24 0 1 .21 1 1
IN[5;]+192 0 6 1.46 1 1
IN[8;]+3 1 1 25.7 1 1
IN[10;]+1 2 2 54.8 0 3
IN[12;]+6 2 3 30.8 .001 1
```

Figure B-4. Set of Editing Instructions Changing Rows 1, 3, 5, 8, 10 and 12 of the Data Entry Matrix - Creating "MOD 1"

ITEM↓ \ TIME→	360	720	2160	4320	8640
RF MODULES	0.99999	0.99999	0.99999	0.99943	0.55190
BEAM FORM NET-A	0.99865	0.99730	0.99193	0.98393	0.96811
-B	0.99999	0.99999	0.99994	0.99977	0.99911
-C	0.99999	0.99996	0.99964	0.99861	0.99464
-D	0.99999	0.99999	0.99999	0.99975	0.98878
-E	0.99999	0.99999	0.99999	0.99999	0.99940
ELEVATION SW	0.99996	0.99984	0.99850	0.99461	0.97992
RECEIVER	0.99949	0.99803	0.98373	0.94266	0.82054
DRIVER	0.99997	0.99990	0.99916	0.99674	0.98767
SYNCHRONIZER	0.99999	0.99999	0.99974	0.99814	0.98754
DATA PROC MODULES	0.99988	0.99953	0.99594	0.98474	0.94591
SIG PROC MODULES	0.99999	0.99999	0.99934	0.99228	0.93127
POWER DISTR	0.99820	0.99640	0.98925	0.97863	0.95771
INTERCONNECTIONS	0.99820	0.99640	0.98925	0.97863	0.95771
DISPLAY	0.99784	0.99568	0.98712	0.97441	0.94948
SYSTEM RELIABILITY	0.99222	0.98316	0.93550	0.83491	0.31570

Figure B-5. New System Reliabilities for "MOD 1", After Changes to "MOD 0".
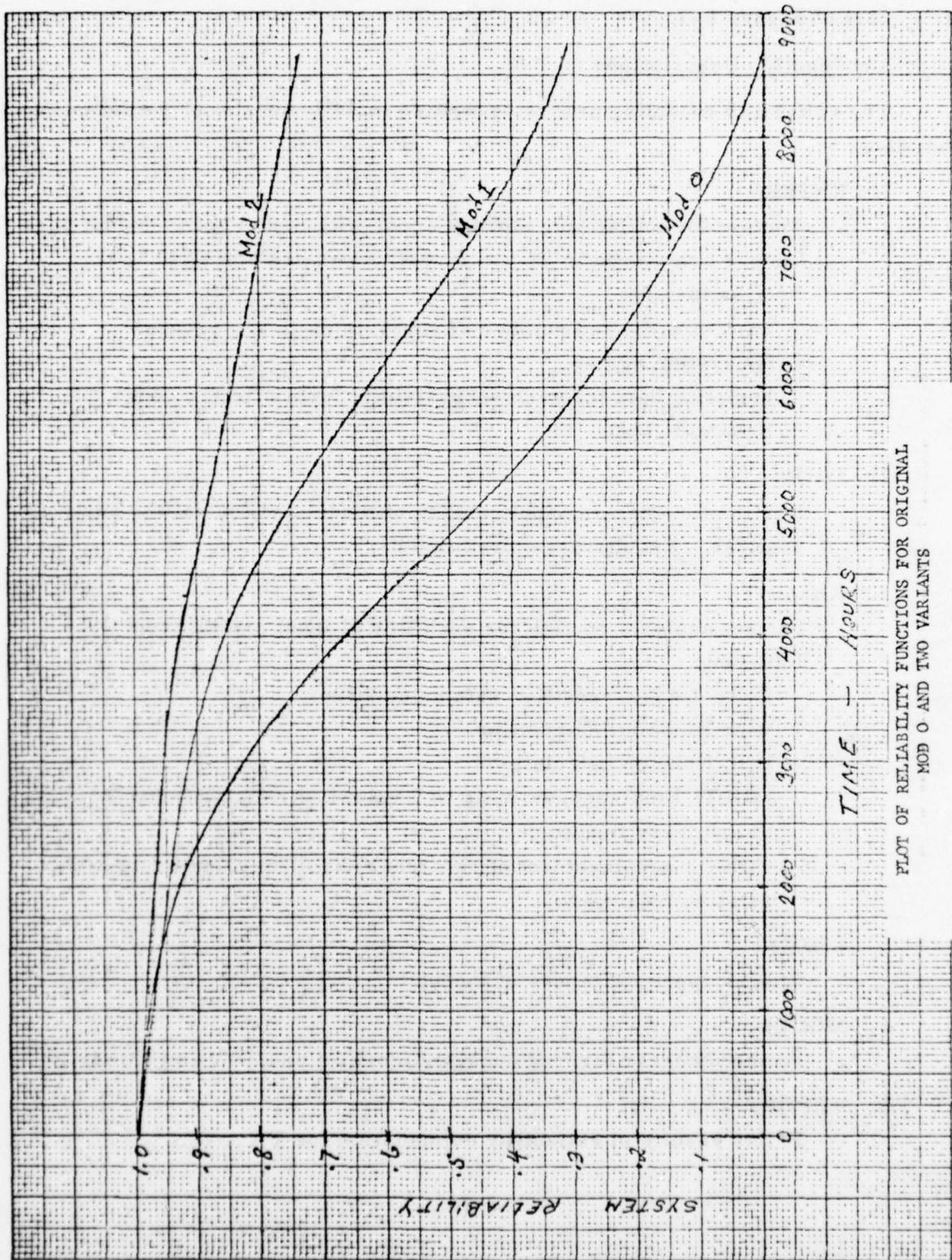
PLOT OF RELIABILITY FUNCTIONS FOR ORIGINAL
MOD O AND TWO VARIANTS

Figure B-6.

The significant instructions and their interrelationship are shown in the flow chart of Figure B-7.

Program Function Descriptions

The reliability modeling programs written in APL consist of the following functions:

1. ENTER

    - Routine for initializing storage areas with model data. Model parameters are stored in IN and model names are stored in LIST. Entries include:

        - System name and number of subsystems (i. e., groups)
        - Subsystem names
        - Modeling data for each subsystem in form of entry code N-S-M-F-D-C.

2. FROM

    - Routine for checking applicability of model and for calling analysis routines. Results are stored in TB.

3. RAL

    - Selects analysis routine for each line of input matrix from the following:

        - REL, DAT; Transition rate calculation
        - BIN; Binomial calculation
        - POI; Poisson calculation
        - MULT; Emplacement of up to 5 values of reliability for $T_1 \ldots T_5$ of arbitrary function.
        - CONST; Emplacement of constant reliability value for one-shot relative frequency.

4. CHECK

    - Checks appropriateness of model

5. MODEL

    - Prints model in form of subsystem names and data entry matrix

6. REPORT

    - Prints results of reliability computation for $T_1 \ldots T_5$.
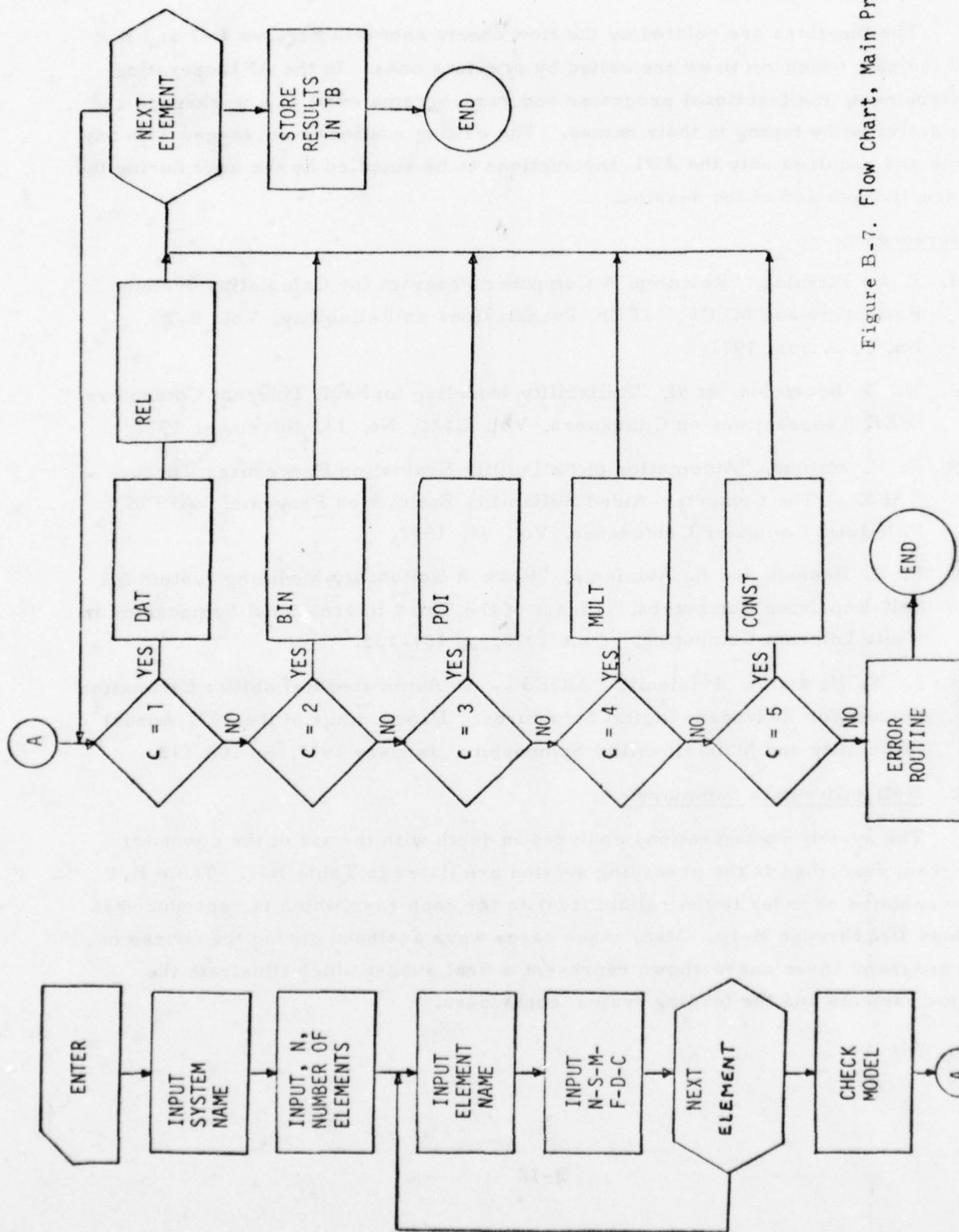
Figure B-7. Flow Chart, Main Program

The functions are related by the flow charts shown in Figures B-7 and B-8 and indicate which routines are called by previous ones. In the APL operating environment, the functional programs and subprograms exist in a workspace and are activated by typing in their names. The editing routine is not tagged with any name and requires only the APL instructions to be supplied by the user during the interactive portion of the session.

References:

B-1. J. L. Fleming, "Relcomp: A Computer Program for Calculating System Reliability and MTBF," IEEE Transactions on Reliability, Vol. R-20, No. 3, August 1971.

B-2. W. G. Bouricius, et al, "Reliability Modeling for Fault Tolerant Computers," IEEE Transactions on Computers, Vol. C-20, No. 11, November 1971.

B-3. F. P. Mathur, "Automation of Reliability Evaluation Procedures Through CARE -- The Computer-Aided Reliability Estimation Program," AFPIS Fall Joint Computer Conference, Vol. 41, 1972.

B-4. D. A. Rennels and A. Avizienis, "RMS: A Reliability Modeling System for Self-Repairing Computers," Digest of the Third International Symposium on Fault Tolerant Computing," June 1973, pp 131-135.

B-5. Y. W. Ng and A. Avizienis, "ARIES -- An Automated Reliability Estimation System for Redundant Digital Structures," Proceedings of the 1977 Annual Reliability and Maintainability Symposium, January 1977, pp 108-113.

B-2. Reliability Data Summary

The system configurations analyzed in depth with the aid of the computer program described in the preceding section are listed in Table B-1. Table B-1 also contains an index to the reliability data for each case which is reproduced in Tables B-2 through B-16. Many other cases were analyzed during the course of the program; those cases shown represent a final subset which illustrate the major variants and the leading system contenders.
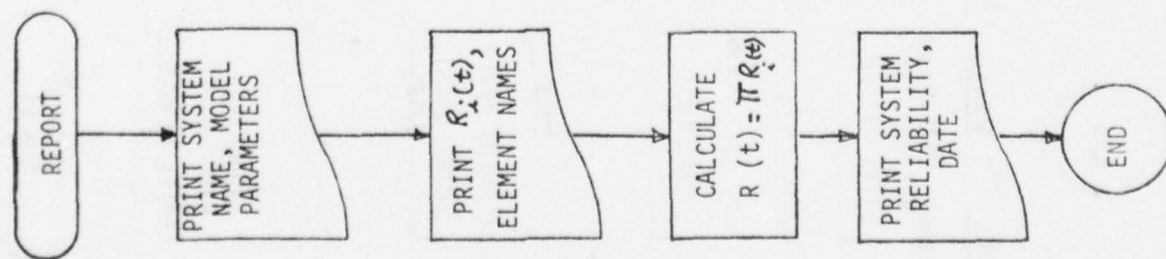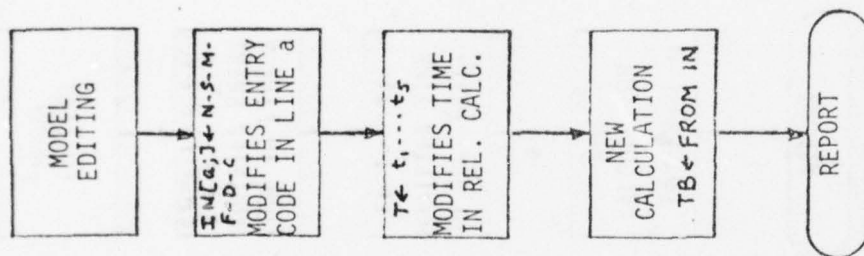
Figure B-8. Flow Chart, Supplementary Programs

Table B-1. Reliability Data Index

Matrix No.*	Freq.	No. TRSSM	No. Lenses	No. Rcvrs.	No. S.P. Common. El.	Design Time (Months)	Results Table
1 (Baseline)	L-Band	256	3	3	6	3	B-2
						6	B-3
						12	B-4
36	L	64	3	1	2	3	B-5
						6	B-6
						12	B-7
39	L	64	3	2	16	3	B-8
						6	B-9
						12	B-10
49	UHF	32	2	2	4	3	B-11
						6	B-12
						12	B-13
62	UHF	32	1	1	2	3	B-14
						6	B-15
						12	B-16

B-3. Reliability Calculation Example

A typical switch circuit from the azimuth steering subsystem is shown in Figure B-9. The reliability estimates by component parts is shown in Table B-17. Failure rates were taken from MIL-HDBK-217B with modifying factors as described in Section 2.7.4(b).

This level of reliability prediction is typical of the reliability analysis performed on this study. Reliability values for most of the baseline field replaceable units were generated from a parts list. In a few instances where a complete design was not available. The type and quantity of parts was estimated.

These baseline reliability values were then extrapolated to other system configurations as appropriate.
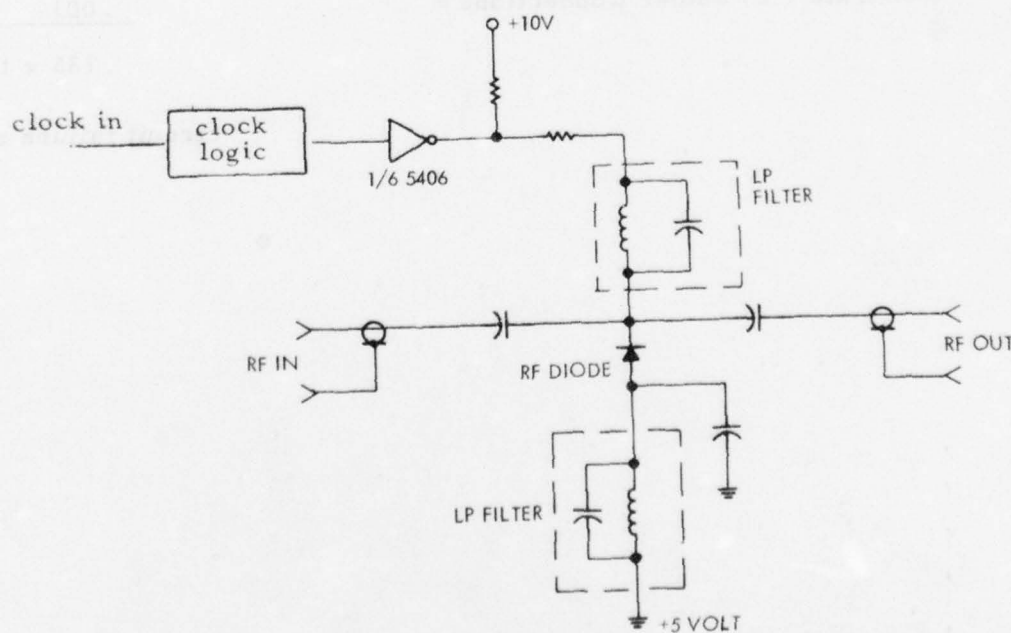
Figure B-9. "C" Level Switch Schematic

Table B-17. Reliability Estimate: "C" Level Switch at 0°C

Item	Qty.	Total F_R
Clock Logic	1	.029
Buffer	1	.0025
RES	2	.0007
PIN Diode	1	.075
Capacitors (Etched)	3	.001
Filters (Etched)	2	.001
RF Connector (Apportioned 1/4)	1	.025

$$\text{TOTAL:} \quad .134 \times 10^{-6}$$

+ Substrate + 25 Solder Connections =

$$.001$$

$$.135 \times 10^{-6} =$$

circuit failure rate.

Table B-2. Configuration 1, 3 Months

VARIANT: 3 MOS OFTM- LED, 3L, 3R, 256M, 6S, CASE 1A, MOD 5

BASELINE

ITEM						
ANT EL/TR SSM	256	0	12	11.90	1.000	2
AZ STEER A	3	0	0	0.80	1.000	1
B	24	0	0	0.21	1.000	1
C	96	0	1	0.13	1.000	1
DEF	192	0	3	1.46	1.000	1
H	768	0	6	0.21	1.000	2
BEAM SW	3	3	1	11.30	0.000	3
RCVR INCL S/H	3	1	1	25.70	0.000	3
EXCITER	1	1	1	19.20	0.000	3
SIG PROC SERIAL	1	1	1	54.80	0.000	3
D.F. COMM EL	2	1	1	21.50	0.000	3
S.F. COMM EL	6	1	2	30.80	0.005	1
PWR DISTR	1	0	0	5.00	1.000	1
BITE > INTERCONN	1	0	0	1.00	1.000	1
IFF	1	0	0	6.00	1.000	1

ITEM↓ \ TIME→	360	720	2160	4320	8640
ANT EL/TR SSM	0.99999	0.99999	0.98527	0.47977	0.00213
AZ STEER A	0.99913	0.99827	0.99482	0.98968	0.97947
B	0.99818	0.99637	0.98917	0.97846	0.95738
C	0.99999	0.99996	0.99964	0.99861	0.99464
DEF	0.99999	0.99994	0.99662	0.96610	0.77809
H	0.99999	0.99999	0.99999	0.99999	0.99940
BEAM SW	0.99992	0.99970	0.99744	0.99026	0.96462
RCVR INCL S/H	0.99962	0.99851	0.98758	0.95543	0.85587
EXCITER	0.99997	0.99990	0.99916	0.99674	0.98767
SIG PROC SERIAL	0.99980	0.99924	0.99352	0.97603	0.91773
D.F. COMM EL	0.99988	0.99953	0.99594	0.98474	0.94591
S.F. COMM EL	0.99996	0.99970	0.99331	0.95936	0.80862
PWR DISTR	0.99820	0.99640	0.98925	0.97863	0.95771
BITE > INTERCONN	0.99964	0.99928	0.99784	0.99568	0.99139
IFF	0.99784	0.99568	0.98712	0.97441	0.94948
SYSTEM RELIABILITY	0.99219	0.98265	0.91054	0.37007	0.00079

DATE: 12 9 1976

Table B-3. Configuration 1, 6 Months

VARIANT: 6 MOS OPTM- LED, 3L, 3R, 256M, 6S, 1A MOD 7

Case

Item					
ANT EL/TR SSM	256	0	25	11.90	1.000	2
AZ STEER A	3	0	0	0.80	1.000	1
B	24	0	1	0.21	1.000	1
C	96	0	1	0.13	1.000	1
DEF	192	0	6	1.46	1.000	2
H	768	0	6	0.21	1.000	2
BEAM SW	3	1	1	11.30	1.000	3
RCVR INCL S/H	3	2	2	25.70	0.000	3
EXCITER	1	1	1	19.20	0.000	3
SIG PROC SERIAL	1	2	2	54.80	0.000	3
D.F. COMM EL	2	1	1	21.50	0.000	3
S.P. COMM EL	6	3	3	30.80	0.000	3
PWR DISTR	1	0	0	5.00	1.000	1
BITE > INTERCONN	1	0	0	1.00	1.000	1
IFF	1	0	0	6.00	1.000	1

ITEM↓ \ TIME→	360	720	2160	4320	8640
ANT EL/TR SSM	0.99999	0.99999	0.99999	0.99943	0.55190
AZ STEER A	0.99913	0.99827	0.99482	0.98968	0.97947
B	0.99999	0.99999	0.99994	0.99977	0.99911
C	0.99999	0.99996	0.99964	0.99861	0.99464
DEF	0.99999	0.99999	0.99999	0.99975	0.98878
H	0.99999	0.99999	0.99999	0.99999	0.99940
BEAM SW	0.99992	0.99970	0.99744	0.99026	0.96462
RCVR INCL S/H	0.99999	0.99997	0.99932	0.99519	0.96984
EXCITER	0.99997	0.99990	0.99916	0.99674	0.98767
SIG PROC SERIAL	0.99999	0.99999	0.99974	0.99814	0.98754
D.F. COMM EL	0.99988	0.99953	0.99594	0.98474	0.94591
S.P. COMM EL	0.99999	0.99998	0.99922	0.99098	0.92164
PWR DISTR	0.99820	0.99640	0.98925	0.97863	0.95771
BITE > INTERCONN	0.99964	0.99928	0.99784	0.99568	0.99139
IFF	0.99784	0.99568	0.98712	0.97441	0.94948
SYSTEM RELIABILITY	0.99459	0.98874	0.96013	0.89692	0.38072

DATE: 12 7 1976

Table B-4. Configuration 1, 12 Months

Case

VARIANT: 12 MOS OPTM- LBD, 3L, 3R, 256M, 6S, IA MOD 7

ITEM						8640
ANT EL/TR SSM	256	40	11.90	1.000	2	0.99883
AZ STEER A	3	0	0.80	1.000	1	0.97947
B	24	1	0.21	1.000	1	0.99911
C	96	1	0.13	1.000	1	0.99464
DEF	192	10	1.46	1.000	2	0.99996
H	768	6	0.21	1.000	2	0.99940
BEAM SW	3	2	11.30	0.000	3	0.99663
RCVR INCL S/H	3	3	25.70	0.000	3	0.99515
EXCITER	1	1	19.20	0.000	3	0.98767
SIG PROC SERIAL	1	2	54.80	0.000	3	0.98754
D.F. COMM EL	2	2	21.50	0.000	3	0.99351
S.F. COMM EL	6	5	30.80	0.000	3	0.99401
PWR DISTR	1	1	5.00	0.000	3	0.99909
BITE > INTERCONN	1	0	1.00	1.000	1	0.99139
IFF	1	0	3.00	1.000	1	0.97441

ITEM↓ / TIME→	360	720	2160	4320	8640
ANT EL/TR SSM	0.99999	0.99999	0.99999	0.99999	0.99883
AZ STEER A	0.99913	0.99827	0.99482	0.98968	0.97947
B	0.99999	0.99999	0.99994	0.99977	0.99911
C	0.99999	0.99996	0.99964	0.99861	0.99464
DEF	0.99999	0.99999	0.99999	0.99999	0.99996
H	0.99999	0.99999	0.99999	0.99999	0.99940
BEAM SW	0.99999	0.99999	0.99993	0.99953	0.99663
RCVR INCL S/H	0.99999	0.99999	0.99997	0.99960	0.99515
EXCITER	0.99997	0.99990	0.99916	0.99674	0.98767
SIG PROC SERIAL	0.99999	0.99999	0.99974	0.99814	0.98754
D.F. COMM EL	0.99999	0.99999	0.99987	0.99906	0.99351
S.F. COMM EL	0.99999	0.99999	0.99999	0.99981	0.99401
PWR DISTR	0.99999	0.99999	0.99994	0.99977	0.99909
BITE > INTERCONN	0.99964	0.99928	0.99784	0.99568	0.99139
IFF	0.99892	0.99784	0.99354	0.98712	0.97441
SYSTEM RELIABILITY	0.99765	0.99523	0.98452	0.96407	0.89590

DATE: 12 7 1976

Table B-5. Configuration 36, 3 Months

VARIANT: 3 MOS OPTM CASE 36

ITEM						
ANT EL/TR SSM	64	0	0	9.50	1.000	2
AZ STEER A	3	0	0	0.80	1.000	1
B	24	0	0	0.21	1.000	1
C	96	0	1	0.13	1.000	1
DEF	192	0	3	1.46	1.000	1
H	768	0	6	0.21	1.000	2
BEAM SW	1	0	0	8.90	0.001	1
RCVR INCL S/H	1	1	1	25.70	0.000	3
EXCITER	1	1	1	19.20	0.000	3
SIG PROC SERIAL	1	1	1	54.80	0.000	3
D.P. COMM EL	2	1	1	21.50	0.000	3
S.F. COMM EL	2	1	1	30.80	0.000	3
PWR DISTR	1	0	0	5.00	1.000	1
BITE + INTERCONN	1	0	0	1.00	1.000	1
IFF	1	0	0	6.00	1.000	1

ITEM↓ \ TIME→	360	720	2160	4320	8640
ANT EL/TR SSM	0.99999	0.99999	0.99967	0.98576	0.76181
AZ STEER A	0.99913	0.99827	0.99482	0.98968	0.97947
B	0.99818	0.99637	0.98917	0.97846	0.95738
C	0.99999	0.99996	0.99964	0.99861	0.99464
DEF	0.99999	0.99994	0.99662	0.96610	0.77809
H	0.99999	0.99999	0.99999	0.99999	0.99940
BEAM SW	0.99680	0.99361	0.98095	0.96228	0.92598
RCVR INCL S/H	0.99995	0.99983	0.99851	0.99427	0.97871
EXCITER	0.99997	0.99990	0.99916	0.99674	0.98767
SIG PROC SERIAL	0.99980	0.99924	0.99352	0.97603	0.91773
D.P. COMM EL	0.99988	0.99953	0.99594	0.98474	0.94591
S.F. COMM EL	0.99975	0.99904	0.99189	0.97028	0.89987
PWR DISTR	0.99820	0.99640	0.98925	0.97863	0.95771
BITE + INTERCONN	0.99964	0.99928	0.99784	0.99568	0.99139
IFF	0.99784	0.99568	0.98712	0.97441	0.94948
SYSTEM RELIABILITY	0.98922	0.97731	0.91732	0.77767	0.34831

DATE: 3 25 1977

Table B-6. Configuration 36. 6 Months

VARIANT: 6 MOS OPTM CASE 36

ANT EL/TR SSM	64	0	6	9.50	1.000	2
AZ STEER A	3	0	0	0.80	1.000	1
B	24	0	0	0.21	1.000	1
C	96	0	1	0.13	1.000	1
DEF	192	0	3	1.46	1.000	1
H	768	0	6	0.21	1.000	2
BEAM SW	1	1	1	8.90	0.001	1
RCVR INCL S/H	1	2	2	25.70	0.000	3
EXCITER	1	1	1	19.20	0.000	3
SIG PROC SERIAL	1	2	2	54.80	0.000	3
D.P. COMM EL	2	2	2	21.50	0.000	3
S.P. COMM EL	2	2	2	30.80	0.000	3
PWR DISTR	1	1	1	5.00	0.000	3
BITE + INTERCONN	1	0	0	1.00	1.000	1
IFF	1	0	0	3.00	1.000	1

ITEM↓ \ TIME→	360	720	2160	4320	8640
ANT EL/TR SSM	0.99999	0.99999	0.99967	0.98576	0.76181
AZ STEER A	0.99913	0.99827	0.99482	0.98968	0.97947
B	0.99818	0.99637	0.98917	0.97846	0.95738
C	0.99999	0.99996	0.99964	0.99861	0.99464
DEF	0.99999	0.99994	0.99662	0.96610	0.77809
H	0.99999	0.99999	0.99999	0.99999	0.99940
BEAM SW	0.99999	0.99997	0.99981	0.99927	0.99718
RCVR INCL S/H	0.99999	0.99999	0.99997	0.99979	0.99845
EXCITER	0.99997	0.99990	0.99916	0.99674	0.98767
SIG PROC SERIAL	0.99999	0.99999	0.99974	0.99814	0.98754
D.P. COMM EL	0.99999	0.99999	0.99987	0.99906	0.99351
S.P. COMM EL	0.99999	0.99998	0.99964	0.99742	0.98305
PWR DISTR	0.99999	0.99999	0.99994	0.99977	0.99909
BITE + INTERCONN	0.99964	0.99928	0.99784	0.99568	0.99139
IFF	0.99892	0.99784	0.99354	0.98712	0.97441
SYSTEM RELIABILITY	0.99584	0.99155	0.96986	0.89634	0.50582

DATE: 3 25 1977

Table B-7. Configuration 36, 12 Months

VARIANT: 12 MOS OPTM CASE 36

ITEM					
ANT EL/TR SSM	64	0	12	9.50	1.000	2
AZ STEER A	3	0	0	0.80	1.000	1
B	24	0	2	0.21	1.000	1
C	96	0	2	0.13	1.000	1
DEF	192	0	10	1.46	1.000	2
H	768	0	6	0.21	1.000	2
BEAM SW	1	1	1	8.90	0.001	1
RCVR INCL S/H	1	2	2	25.70	0.000	3
EXCITER	1	1	1	19.20	0.000	3
SIG PROC SERIAL	1	2	2	54.80	0.000	3
D.F. COMM EL	2	2	2	21.50	0.000	3
S.F. COMM EL	2	3	3	30.80	0.000	3
PWR DISTR	1	1	1	5.00	0.000	3
BITE + INTERCONN	1	0	0	1.00	1.000	1
IFF	1	0	0	3.00	1.000	1

ITEM↓ \ TIME→	360	720	2160	4320	8640
ANT EL/TR SSM	0.99999	0.99999	0.99999	0.99999	0.99870
AZ STEER A	0.99913	0.99827	0.99482	0.98968	0.97947
B	0.99999	0.99999	0.99999	0.99999	0.99998
C	0.99999	0.99999	0.99999	0.99997	0.99981
DEF	0.99999	0.99999	0.99999	0.99999	0.99996
H	0.99999	0.99999	0.99999	0.99999	0.99940
BEAM SW	0.99997	0.99997	0.99981	0.99927	0.99718
RCVR INCL S/H	0.99999	0.99999	0.99997	0.99979	0.99845
EXCITER	0.99997	0.99990	0.99916	0.99674	0.98767
SIG PROC SERIAL	0.99999	0.99999	0.99974	0.99814	0.98754
D.F. COMM EL	0.99999	0.99999	0.99987	0.99906	0.99351
S.F. COMM EL	0.99999	0.99999	0.99998	0.99983	0.99780
PWR DISTR	0.99999	0.99999	0.99994	0.99977	0.99909
BITE + INTERCONN	0.99964	0.99928	0.99784	0.99568	0.99139
IFF	0.99892	0.99784	0.99354	0.98712	0.97441
SYSTEM RELIABILITY	0.99766	0.99526	0.98479	0.96554	0.90816

DATE: 3 25 1977

Table B-8. Configuration 39, 3 Months

VARIANT: 3 MOS OPTM CASE 39

ANT EL/TR SSM	64	0	6	12.62	1.000	2
AZ STEER A	3	0	0	0.80	1.000	1
B	24	0	0	0.21	1.000	1
C	96	0	1	0.13	1.000	1
DEF	192	0	3	1.46	1.000	1
H	768	0	6	0.21	1.000	2
BEAM SW	2	0	1	12.02	0.000	3
RCVR INCL S/H	2	1	1	25.70	0.000	3
EXCITER	1	1	1	19.20	0.000	3
SIG PROC SERIAL	1	1	1	54.80	0.000	3
D.F. COMM EL	2	1	1	21.50	0.000	3
S.F. COMM EL	16	0	3	30.80	0.001	1
PWR DISTR	1	0	0	5.00	1.000	1
BITE + INTERCONN	1	0	0	1.00	1.000	1
IFF	1	0	0	6.00	1.000	1

ITEM ↓ \ TIME →	360	720	2160	4320	8640
ANT EL/TR SSM	0.99999	0.99999	0.99834	0.94749	0.50387
AZ STEER A	0.99913	0.99827	0.99482	0.98968	0.97947
B	0.99818	0.99637	0.98947	0.97846	0.95738
C	0.99999	0.99996	0.99964	0.99861	0.99464
DEF	0.99999	0.99994	0.99662	0.96610	0.77809
H	0.99999	0.99999	0.99999	0.99999	0.99940
BEAM SW	0.99996	0.99985	0.99869	0.99496	0.98119
RCVR INCL S/H	0.99983	0.99933	0.99427	0.97871	0.92624
EXCITER	0.99997	0.99990	0.99916	0.99674	0.98767
SIG PROC SERIAL	0.99980	0.99924	0.99352	0.97603	0.91773
D.F. COMM EL	0.99988	0.99953	0.99594	0.98474	0.94591
S.F. COMM EL	0.99997	0.99965	0.98329	0.87103	0.46568
PWR DISTR	0.99820	0.99640	0.98925	0.97863	0.95771
BITE + INTERCONN	0.99964	0.99928	0.99784	0.99568	0.99139
IFF	0.99784	0.99568	0.98712	0.97441	0.94948
SYSTEM RELIABILITY	0.99245	0.98356	0.92066	0.68294	0.11955

DATE: 3 25 1977

Table B-9. Configuration 39, 6 Months

VARIANT: 6 MOS OPTM CASE 39

ITEM					
ANT EL/TR SSM	64	0	8	12.62	1.000	2
AZ STEER A	3	0	0	0.80	1.000	1
B	24	0	1	0.21	1.000	1
C	96	0	1	0.13	1.000	1
DEF	192	0	5	1.46	1.000	2
H	768	0	6	0.21	1.000	2
BEAM SW	2	1	1	12.02	0.000	3
RCVR INCL S/H	2	2	2	25.70	0.000	3
EXCITER	1	1	1	19.20	0.000	3
SIG PROC SERIAL	1	2	2	54.80	0.000	3
D.F. COMM EL	2	1	1	21.50	0.000	3
S.F. COMM EL	16	6	6	30.80	0.000	3
PWR DISTR	1	0	0	5.00	1.000	1
BITE + INTERCONN	1	0	0	1.00	1.000	1
IFF	1	0	0	6.00	1.000	1

ITEM↓ \ TIME→	360	720	2160	4320	8640
ANT EL/TR SSM	0.99999	0.99999	0.99994	0.99350	0.78773
AZ STEER A	0.99913	0.99827	0.99482	0.98968	0.97947
B	0.99999	0.99999	0.99994	0.99977	0.99911
C	0.99999	0.99996	0.99964	0.99861	0.99464
DEF	0.99999	0.99999	0.99996	0.99852	0.96490
H	0.99999	0.99999	0.99999	0.99999	0.99940
BEAM SW	0.99996	0.99985	0.99869	0.99496	0.98119
RCVR INCL S/H	0.99999	0.99999	0.99979	0.99845	0.98949
EXCITER	0.99997	0.99990	0.99916	0.99674	0.98767
SIG PROC SERIAL	0.99999	0.99999	0.99974	0.99814	0.98754
D.F. COMM EL	0.99988	0.99953	0.99594	0.98474	0.94591
S.F. COMM EL	0.99999	0.99999	0.99987	0.99370	0.86077
PWR DISTR	0.99820	0.99640	0.98925	0.97863	0.95771
BITE + INTERCONN	0.99964	0.99928	0.99784	0.99568	0.99139
IFF	0.99784	0.99568	0.98712	0.97441	0.94948
SYSTEM RELIABILITY	0.99463	0.98891	0.96233	0.90012	0.51397

Table B-10. Configuration 39, 12 Months

VARIANT: 12 MOS OPTM CASE 37

ANT EL/TR SSM	64	0	12	12.62	1.000	2
AZ STEER A	3	0	0	0.80	1.000	1
B	24	0	1	0.21	1.000	1
C	96	0	1	0.13	1.000	1
DEF	192	0	8	1.46	1.000	2
H	768	0	6	0.21	1.000	2
BEAM SW	2	2	2	12.02	0.000	3
RCVR INCL S/H	2	2	2	25.70	0.000	3
EXCITER	1	2	2	19.20	0.000	3
SIG PROC SERIAL	1	3	3	54.80	0.000	3
D.F. COMM EL	2	2	2	21.50	0.000	3
S.F. COMM EL	16	10	10	30.80	0.000	3
PWR DISTR	1	1	1	5.00	1.000	1
BITE + INTERCONN	1	1	0	1.00	1.000	1
IFF	1	0	0	3.00	1.000	1

ITEM↓ \ TIME→	360	720	2160	4320	8640
ANT EL/TR SSM	0.99999	0.99999	0.99999	0.99997	0.98717
AZ STEER A	0.99913	0.99827	0.99482	0.98968	0.97947
B	0.99999	0.99999	0.99994	0.99977	0.99911
C	0.99999	0.99996	0.99964	0.99861	0.99464
DEF	0.99999	0.99999	0.99999	0.99999	0.99920
H	0.99999	0.99999	0.99999	0.99999	0.99940
BEAM SW	0.99999	0.99999	0.99997	0.99982	0.99872
RCVR INCL S/H	0.99999	0.99999	0.99979	0.99845	0.98949
EXCITER	0.99999	0.99999	0.99998	0.99991	0.99932
SIG PROC SERIAL	0.99999	0.99999	0.99999	0.99989	0.99856
D.F. COMM EL	0.99999	0.99999	0.99987	0.99906	0.99351
S.F. COMM EL	1.00000	0.99999	0.99999	0.99998	0.99550
PWR DISTR	0.99999	0.99998	0.99988	0.99954	0.99821
BITE + INTERCONN	0.99964	0.99928	0.99784	0.99568	0.99139
IFF	0.99892	0.99784	0.99354	0.98712	0.97441
SYSTEM RELIABILITY	0.99768	0.99532	0.98538	0.96790	0.90249

Table B-11. Configuration 49, 3 Months

VARIANT: 3 MOS OPTM CASE 49

ANT EL/TR SSM	32	0	8.56	1.000	1
AZ STEER A	2	0	0.78	1.000	1
B	4	0	0.82	1.000	1
C	16	0	0.82	1.000	1
DEF	64	0	1.70	1.000	1
H	1	0	0.00	1.000	1
BEAM SW	2	1	7.96	0.000	3
RCVR INCL S/H	2	1	23.13	0.000	3
EXCITER	1	1	13.44	0.000	3
SIG PROC SERIAL	1	1	54.80	0.000	3
D.F. COMM EL	2	1	21.50	0.000	3
S.F. COMM EL	4	1	30.80	0.000	3
PWR DISTR	1	0	5.00	1.000	1
BITE + INTERCONN	1	0	1.00	1.000	1
IFF	1	0	6.00	1.000	1

ITEM \ TIME→	360	720	2160	4320	8640
ANT EL/TR SSM	0.99999	0.99999	0.99972	0.99440	0.92583
AZ STEER A	0.99943	0.99887	0.99663	0.99328	0.98661
B	0.99881	0.99764	0.99294	0.98593	0.97205
C	0.99998	0.99995	0.99963	0.99854	0.99439
DEF	0.99999	1.00000	0.99999	0.99988	0.99753
H	1.00000	1.00000	1.00000	1.00000	1.00000
BEAM SW	0.99998	0.99993	0.99942	0.99774	0.99136
RCVR INCL S/H	0.99986	0.99945	0.99532	0.98250	0.93853
EXCITER	0.99998	0.99995	0.99958	0.99837	0.99375
SIG PROC SERIAL	0.99980	0.99924	0.99352	0.97603	0.91773
D.F. COMM EL	0.99988	0.99953	0.99594	0.98474	0.94591
S.F. COMM EL	0.99904	0.99629	0.97028	0.89987	0.71206
PWR DISTR	0.99820	0.99640	0.98925	0.97863	0.95771
BITE + INTERCONN	0.99964	0.99928	0.99784	0.99568	0.99139
IFF	0.99784	0.99568	0.98712	0.97441	0.94948
SYSTEM RELIABILITY	0.99252	0.98239	0.91996	0.78144	0.45382

DATE: 3 25 1977

Table B-12. Configuration 49, 6 Months

VARIANT: 6 MOS OPTM CASE 49

ITEM						
ANT EL/TR SSM	32	0	4	8.56	1.000	1
AZ STEER A	2	0	0	0.78	1.000	1
B	4	0	0	0.82	1.000	1
C	16	0	1	0.82	1.000	1
DEF	64	0	4	1.70	1.000	1
H	1	0	0	0.00	1.000	1
BEAM SW	2	1	1	7.96	0.000	3
RCVR INCL S/H	2	2	2	23.13	0.000	3
EXCITER	1	1	1	13.44	0.000	3
SIG PROC SERIAL	1	2	2	54.80	0.000	3
D.P. COMM EL	2	2	2	21.50	0.000	3
S.P. COMM EL	4	2	2	30.80	0.000	3
PWR DISTR	1	0	0	5.00	1.000	1
BITE + INTERCONN	1	0	0	1.00	1.000	1
IFF	1	0	0	6.00	1.000	1

ITEM↓ \ TIME→	360	720	2160	4320	8640
ANT EL/TR SSM	0.99999	0.99999	0.99972	0.99440	0.92583
AZ STEER A	0.99943	0.99887	0.99663	0.99328	0.98661
B	0.99881	0.99764	0.99294	0.98593	0.97205
C	0.99998	0.99995	0.99963	0.99854	0.99439
DEF	0.99999	1.00000	0.99999	0.99988	0.99753
H	1.00000	1.00000	1.00000	1.00000	1.00000
BEAM SW	0.99998	0.99993	0.99942	0.99774	0.99136
RCVR INCL S/H	0.99999	0.99999	0.99984	0.99885	0.99209
EXCITER	0.99998	0.99995	0.99958	0.99837	0.99375
SIG PROC SERIAL	0.99999	0.99999	0.99974	0.99814	0.98754
D.P. COMM EL	0.99999	0.99999	0.99987	0.99906	0.99351
S.P. COMM EL	0.99998	0.99989	0.99742	0.98305	0.90747
PWR DISTR	0.99820	0.99640	0.98925	0.97863	0.95771
BITE + INTERCONN	0.99964	0.99928	0.99784	0.99568	0.99139
IFF	0.99784	0.99568	0.98712	0.97441	0.94948

SYSTEM RELIABILITY   0.99390   0.98766   0.95970   0.90047   0.69097

DATE: 3 25 1977

Table B-13. Configuration 49, 12 Months

VARIANT: 12 MOS OFTM CASE 49

ITEM↓ \ TIME→						360	720	2160	4320	8640
ANT EL/TR SSM	32	6	8.56	1.000	2	1.00000	1.00000	0.99999	0.99987	0.99355
AZ STEER A	2	0	0.78	1.000	1	0.99943	0.99887	0.99663	0.99328	0.98661
B	4	0	0.82	1.000	1	0.99881	0.99764	0.99294	0.98593	0.97205
C	16	1	0.82	1.000	1	0.99998	0.99995	0.99963	0.99854	0.99439
DEF	64	4	1.70	1.000	1	0.99999	1.00000	0.99999	0.99988	0.99753
H	1	0	0.00	1.000	1	1.00000	1.00000	1.00000	1.00000	1.00000
BEAM SW	2	1	7.96	0.000	3	0.99998	0.99993	0.99942	0.99774	0.99136
RCVR INCL S/H	2	2	23.13	0.000	3	0.99999	0.99999	0.99984	0.99885	0.99209
EXCITER	1	1	13.44	0.000	3	0.99998	0.99995	0.99958	0.99837	0.99375
SIG PROC SERIAL	1	3	54.80	0.000	3	0.99999	0.99999	0.99999	0.99989	0.99856
D.P. COMM EL	2	2	21.50	0.000	3	0.99999	0.99999	0.99987	0.99906	0.99351
S.P. COMM EL	4	4	30.80	0.000	3	0.99999	0.99999	0.99999	0.99977	0.99525
PWR DISTR	1	1	5.00	0.000	3	0.99999	0.99999	0.99994	0.99977	0.99909
BITE + INTERCONN	1	0	1.00	1.000	1	0.99964	0.99928	0.99784	0.99568	0.99139
IFF	1	0	3.00	1.000	1	0.99892	0.99784	0.99354	0.98712	0.97441
SYSTEM RELIABILITY						0.99678	0.99348	0.97940	0.95465	0.88037

DATE: 3 25 1977

Table B-14. Configuration 62, 3 Months

VARIANT: 3 MOS OPTM CASE 62

ANT EL/TR SSM	32	0	4	5.86	1
AZ STEER A	1	0	0	0.78	1
B	2	0	0	0.82	1
C	8	0	0	0.82	1
DEF	32	0	2	1.70	1
H	1	0	0	0.00	1
BEAM SW	1	0	0	5.26	1
RCVR INCL S/H	1	1	1	23.13	3
EXCITER	1	0	0	13.44	1
SIG PROC SERIAL	1	1	1	54.80	3
D.P. COMM EL	2	1	1	21.50	3
S.P. COMM EL	2	1	1	30.80	3
PWR DISTR	1	0	0	5.00	1
BITE + INTERCONN	1	0	0	1.00	1
IFF	1	0	0	6.00	1

ITEM↓ \ TIME→	360	720	2160	4320	8640
ANT EL/TR SSM	0.99999	0.99999	0.99995	0.99888	0.93062
AZ STEER A	0.99971	0.99943	0.99831	0.99663	0.99328
B	0.99940	0.99881	0.99646	0.99294	0.98593
C	0.99764	0.99528	0.98593	0.97205	0.94489
DEF	0.99999	0.99999	0.99977	0.99834	0.98878
H	1.00000	1.00000	1.00000	1.00000	1.00000
BEAM SW	0.99810	0.99621	0.98870	0.97753	0.95557
RCVR INCL S/H	0.99996	0.99786	0.99879	0.99532	0.98250
EXCITER	0.99517	0.99036	0.97138	0.94359	0.89036
SIG PROC SERIAL	0.99980	0.99924	0.99352	0.97603	0.91773
D.P. COMM EL	0.99988	0.99953	0.99594	0.98474	0.94591
S.P. COMM EL	0.99975	0.99904	0.99189	0.97028	0.89987
PWR DISTR	0.99820	0.99640	0.98925	0.97863	0.95771
BITE + INTERCONN	0.99964	0.99928	0.99784	0.99568	0.99139
IFF	0.99784	0.99568	0.98712	0.97441	0.94948
SYSTEM RELIABILITY	0.98523	0.96957	0.89952	0.77983	0.52819

DATE: 3 25 1977

Table B-15. Configuration 62, 6 Months

VARIANT: 6 MOS OPTM CASE 62

ANT EL/TR SSM	32	0	4	5.86	1.000	1
AZ STEER A	1	0	0	0.78	1.000	1
B	2	0	0	0.82	1.000	1
C	8	0	1	0.82	1.000	1
DEF	32	0	2	1.70	1.000	1
H	1	0	0	0.00	1.000	1
BEAM SW	1	1	1	5.26	0.001	1
RCVR INCL S/H	1	1	1	23.13	0.000	3
EXCITER	1	1	1	13.44	0.000	3
SIG PROC SERIAL	1	1	1	54.80	0.000	3
D.P. COMM EL	2	2	2	21.50	0.000	3
S.F. COMM EL	2	2	2	30.80	0.000	3
PWR DISTR	1	0	0	5.00	1.000	1
BITE + INTERCONN	1	0	0	1.00	1.000	1
IFF	1	0	0	6.00	1.000	1

ITEM↓ \ TIME→	360	720	2160	4320	8640
ANT EL/TR SSM	0.99999	0.99999	0.99995	0.99888	0.98062
AZ STEER A	0.99971	0.99943	0.99831	0.99663	0.99328
B	0.99940	0.99881	0.99646	0.99294	0.98593
C	0.99999	0.99999	0.99991	0.99965	0.99864
DEF	0.99999	0.99999	0.99977	0.99834	0.98878
H	1.00000	1.00000	1.00000	1.00000	1.00000
BEAM SW	0.99999	0.99999	0.99993	0.99974	0.99899
RCVR INCL S/H	0.99996	0.99986	0.99879	0.99532	0.98250
EXCITER	0.99998	0.99995	0.99958	0.99837	0.99375
SIG PROC SERIAL	0.99980	0.99924	0.99352	0.97603	0.91773
D.P. COMM EL	0.99999	0.99999	0.99987	0.99906	0.99351
S.F. COMM EL	0.99999	0.99998	0.99964	0.99742	0.98305
PWR DISTR	0.99820	0.99640	0.98925	0.97863	0.95771
BITE + INTERCONN	0.99964	0.99928	0.99784	0.99568	0.99139
IFF	0.99784	0.99568	0.98712	0.97441	0.74948
SYSTEM RELIABILITY	0.99457	0.98869	0.96062	0.90506	0.74739

DATE: 3 25 1977

Table B-16. Configuration 62, 12 Months

VARIANT: 12 MOS OPTM CASE 62

Item						
ANT EL/TR SSM	32	0	5.86	4	1.000	1
AZ STEER A	1	0	0.78	0	1.000	1
B	2	0	0.82	0	1.000	1
C	8	0	0.82	1	1.000	1
DEF	32	0	1.70	3	1.000	1
H	1	1	0.00	0	1.000	1
BEAM SW	1	1	5.26	1	0.001	1
RCVR INCL S/H	1	2	23.13	2	0.000	3
EXCITER	1	1	13.44	1	0.000	3
SIG PROC SERIAL	1	2	54.80	2	0.000	3
D.F. COMM EL	2	2	21.50	2	0.000	3
S.F. COMM EL	2	3	30.80	3	0.000	3
PWR DISTR	1	1	5.00	1	0.000	3
BITE + INTERCONN	1	0	1.00	0	1.000	1
IFF	1	0	3.00	0	0.000	1

ITEM↓ \ TIME→	360	720	2160	4320	8640
ANT EL/TR SSM	0.99999	0.99999	0.99995	0.99888	0.98062
AZ STEER A	0.99971	0.99943	0.99831	0.99663	0.99328
B	0.99940	0.99881	0.99646	0.99294	0.98593
C	0.99999	0.99999	0.99991	0.99965	0.99864
DEF	0.99999	0.99999	0.99999	0.99991	0.99882
H	1.00000	1.00000	1.00000	1.00000	1.00000
BEAM SW	0.99999	0.99999	0.99993	0.99974	0.99899
RCVR INCL S/H	0.99998	0.99999	0.99997	0.99984	0.99885
EXCITER	0.99998	0.99995	0.99958	0.99837	0.99375
SIG PROC SERIAL	0.99999	0.99999	0.99974	0.99814	0.98754
D.F. COMM EL	0.99999	0.99999	0.99987	0.99906	0.99351
S.F. COMM EL	0.99999	0.99999	0.99998	0.99983	0.99780
PWR DISTR	0.99999	0.99999	0.99994	0.99977	0.99909
BITE + INTERCONN	0.99964	0.99928	0.99784	0.99568	0.99139
IFF	0.99892	0.99784	0.99354	0.98712	0.97441
SYSTEM RELIABILITY	0.99767	0.99530	0.98515	0.96608	0.89751

DATE: 3 25 1977

APPENDIX C-1

TRACK INITIATION CRITERIA

C.1.1 SINGLE FRAME TRACK INITIATION

The track initiation criterion assumed for the single frame scan type is that the target be detected on three out of four contiguous scans. The same false alarm threshold is used on all scans. These track initiation assumption also apply to the fence/tracker scan type.

The track initiation criterion is that the target be detected on m out of n (m/n) scans, where n scans is a scan-set.

f_{ss} = number of scan-sets per second

N_E = number of elevation cells

N_A = number of azimuth cells

N_R = number of range cells

N_D = number of doppler cells

f_{dt} = track-initiation decision rate

$\quad = f_{ss} N_A N_E N_R N_D$

f_{ft} = false track-initiation rate

P_{fa} = false alarm probability

P_{ft} = probability of false track-initiation

$$= \frac{f_{ft}}{f_{dt}} \tag{2}$$

For the same false alarm probability on each scan,

$$P_{ft} = \sum_{i=m}^{n} \binom{n}{i} P_{fa}^{i} (1 - P_{fa})^{n-i} \tag{3}$$

f_{fa} = false alarm rate

f_r =   pulse repetition rate

N =   number of pulse groups integrated non-coherently

N_C =   number of pulses integrated coherently in each group

f_{da} =   alarm decision rate

$$= \frac{f_{fa}}{P_{fa}}$$

$$= \frac{f_r N_R N_D N_E}{N N_C} \tag{4}$$

For the L-band baseline system,

$$f_{ss} = \frac{1}{16} \text{ Hz} \qquad\qquad f_r = 1150 \text{ Hz}$$

$$N_A = 256 \qquad\qquad\qquad N_C = 8$$

$$N_E = 3 \qquad\qquad\qquad\quad N = 2$$

$$N_R = 150$$

$$N_D = 8$$

Hence:

$$f_{dt} = f_{ss} N_A N_E N_R N_D$$

$$= (\frac{1}{16})(256)(3)(150)(8)$$

$$= 57600$$

The requirement for false track initiation rate is,

$$f_{ft} = \frac{1}{3600} \text{ Hz} = 1 \text{ per hour}$$

Hence,

$$P_{ft} = \frac{f_{ft}}{f_{dt}} = \frac{1}{(3600)(57600)} = 4.82 \times 10^{-9}$$

With m = 3 and n = 4, we have

$$P_{ft} = P_{fa}^4 + 4P_{fa}^3 (1 - P_{fa}) \qquad (5)$$

and,

$$P_{fa} = 1.0645 \times 10^{-3}$$

Also,

$$f_{da} = \frac{f_r N_R N_D N_E}{N N_C}$$

$$= \frac{(1150)(150)(8)(3)}{(2)(8)}$$

$$= 258750 \text{ Hz}$$

The false alarm rate is therefore

$$f_{fa} = P_{fa} f_{da} = (1.0645 \times 10^{-3})(258750)$$

$$= 275.44 \text{ Hz}$$

Now let

$$P_{TI} = \text{probability of track-initiation}$$

$$P_{di} = \text{probability of detection on } i^{th} \text{ scan}$$

If $P_{di} = P_d$ for i = 1, 2, 3 and 4, then

$$P_{TI} = P_d^4 + 4P_d^3 (1 - P_d)$$

For $P_{TI} = .95$ we find that $P_d = .9024$.

For a Swerling II target with N = 2, $P_{fa} = 1.0645 \times 10^{-3}$ and $P_d = .9024$ the detectability factor χ is

$$\chi = 12.2 \text{ dB}$$

The UHF single frame configuration has the same parameter definitions but many of the numerical values are different, namely:

$$f_{ss} = \frac{1}{16} \text{ Hz} \qquad\qquad f_r = 1150$$

$$N_A = 128 \qquad\qquad N_C = 8$$

$$N_E = 2 \qquad\qquad N = 5*$$

$$N_R = 150 \qquad\qquad *\text{Within } 3.5^\circ \text{ beamwidth}$$

$$N_D = 8$$

$$f_{dt} = f_{ss} N_A N_E N_R N_D$$

$$= (\frac{1}{16})(128)(2)(150)(8)$$

$$= 19200$$

$$f_{ft} = \frac{1}{3600}$$

$$P_{ft} = \frac{f_{ft}}{f_{dt}} = \frac{1}{(3600)(19200)} = 1.44 \times 10^{-8}$$

Hence,

$$f_{da} = \frac{f_r N_R N_D N_E}{N N_C}$$

$$= \frac{(1150)(150)(8)(2)}{(5)(8)}$$

$$= 69000 \text{ Hz}$$

$$P_{ft} = P_{fa}^4 + 4P_{fa}^3 (1 - P_{fa}) = 1.44 \times 10^{-8}$$

Solving for P_{fa},

$$P_{fa} = 1.534 \times 10^{-3}$$

$$f_{fa} = P_{fa} f_{da}$$

$$= (1.534 \times 10^{-3})(69000)$$

$$= 105.8 \text{ Hz}$$

For $P_d = 0.9024$, $P_{fa} = 1.534 \times 10^{-3}$, $N = 5$ and Swerling Case 2 the detectability factor is

$$\chi = 6.8 \text{ dB}$$

C.1.2 TRACK INITIATION FOR SPLIT FRAME

The split frame system scans half of the volume on each scan. If a detection is made on one scan, then the same elevation region is revisited on the following three scans in the same azimuth region. The false alarm threshold is required to be higher on the first scan to reduce the number of the times that the scan pattern is changed; however the threshold can be to reduced after the first scan provided that the one per hour false track initiation rate is not exceeded. In general if the false alarm probabilities are different on each scan, then the probability of false track initiation is given by

$$
\begin{aligned}
P_{ft} &= P_{fa1} P_{fa2} P_{fa3} P_{fa4} \\
&+ P_{fa1} P_{fa2} P_{fa3} (1 - P_{fa4}) \\
&+ P_{fa1} P_{fa2} (1 - P_{fa3}) P_{fa4} \\
&+ P_{fa1} (1 - P_{fa2}) P_{fa3} P_{fa4} \\
&+ (1 - P_{fa1}) P_{fa2} P_{fa3} P_{fa4}
\end{aligned}
\tag{6}
$$

Assume $P_{fa1} = P_1$; $P_{fa2} = P_{fa3} = P_{fa4} = P_2$

Then

$$
\begin{aligned}
P_{ft} &= P_1 P_2^3 + 3P_1 P_2^2 (1 - P_2) = (1 - P_1) P_2^3 \\
&= 3P_1 P_2^2 (1 - P_2) + P_2^3
\end{aligned}
\tag{7}
$$

For a false alarm constraint of ten per scan (2.5 Hz), $P_1 = 9.66 \times 10^{-6}$ and, $P_{ft} = 4.82 \times 10^{-9}$ for a false track initiation rate of 1 per hour.

Solving for P_2,

$$P_2 = 1.68 \times 10^{-3}$$

The track initiation probability is given by

$$P_{TI} = 3P_{d1} P_{d2}^2 (1 - P_{d2}) + P_{d2}^3 \qquad (8)$$

where

P_{d1} = detection probability on scan 1 ($P_{fa} = 9.66 \times 10^{-6}$)

P_{d2} = detection probability on scans 2, 3, and 4 ($P_{fa} = 1.68 \times 10^{-3}$)

For P_{TI} = .95 the detectability factor χ is calculated:

χ = 12.6 dB

C.1.3 RANGE WALK LOSS

A range walk loss is encountered when scan-to-scan correlation is employed due to the necessity to examine additional resolution cells. More cells must be compared because the target moves between scans and the target position uncertainty dictates the number of cells which must be examined. A greater chance of false alarms and false alarm correlation then exists and the thresholds must generally be raised. This results in an additional loss referred to as the "range-walk" loss.

Using the general equation (6) for the probability of false track (P_{ft}), the individual false alarm rates per scan can be estimated,

P_{fa1} = P_{a1} = probability of either a false alarm or true alarm in cell

= $P_{fa} + P_{ta}$

where

P_{ta} = target detection rate = $\dfrac{N_T}{N_A N_E N_R N_D}$

N_T = number of targets

Also,

$P_{fa2} = K_1 P_{fa}$

C-1-6

where

K_1 =   number of cells which must be examined given detection on first scan.

$$P_{fa3} \left\{ \begin{array}{l} P_{fa}^* \text{ given detection of scans 1 and 2} \\ = \ K_2 P_{fa} \text{ given detection on scan 1 and no detection on scan 2} \\ K_1 P_{fa} \text{ given no detection on scan 1 and detection on scan 2} \end{array} \right.$$

$$P_{fa4} \ = \ P_{fa}^*$$

*Assumes only one cell needs to be examined for correlation given two prior detection.

Then,

$$P_{ft}' \ = \ P_{a1} P_{fa2} P_{fa}^2 + 2 P_{a1} P_{fa2} P_{fa} (1 - P_{fa})$$

$$P_{a1} (1 - P_{fa2}) P_{fa3} P_{fa4} + (1 - P_{a1}) P_{fa2} P_{fa3} P_{fa4}$$

$$\cong P_{a1} P_{fa}^2 (3 K_1 + K_2), \ P_{fa} \ll 1$$

Also,

$$P_{ta} \ = \ \frac{40}{(256)(3)(150)(8)} \ = \ 4.3 \times 10^{-5}$$

and thus, $P_{a1} = P_{fa} + 4.3 \times 10^{-5} \cong P_{fa}$, and

$$P_{ft}' \ = \ P_{fa}^3 (3 K_1 + K_2)$$

The net difference between this expression and equation (5) is approximately,

$$\frac{P_{ft}'}{P_{ft}} \ = \ \frac{3 K_1 + K_2}{4}$$

The walk extent parameters, K_1 and K_2, are determined by the velocity of the intruder. For a typical intruder of about 1200 knot velocity at 45 degrees aspect angle. The number of range azimuth cells which must be searched is

about 7 after a previous detection and about 24 after a missed detection. Assuming at least 4g acceleration capability in the target aircraft, all doppler bins must be searched; thus

$$K_1 = (7)(8) = 56$$

$$K_2 = (24)(8) = 192$$

Then,

$$\frac{P'_{ft}}{P_{ft}} = \frac{3 (56) + 192}{4} = 90$$

The relationship between P_{ft} and P_{fa} is approximately,

$$\frac{P'_{fa}}{P_{fa}} = \sqrt[3]{\frac{P^1_{ft}}{P_{ft}}} = 3\sqrt{90} = 4.48$$

which corresponds to an additional loss of approximately,

$$\delta\chi = 0.5 \text{ dB}$$

C.1.4 CLUTTER NOTCH LOSS

A loss in detectability also occurs where substantial clutter exists as one or more detections may fall within the regions about the blind speed where insufficient clutter improvement exists. Referring to the clutter improvement results shown in Section 2.7.3, the spectrum lost for an FFT/combination at UHF is that corresponding to filters 0 and 1. Thus the probability of a detection on a single batch is

$$P_v(1/1) = 3/4$$

The visibility on two batches is either,

$$P_v(1/2) = 2 P_v(1/1) (1 - P_v(1/1)) = 0.38$$

$$P_v(2/2) = \left[P_v(1/1) \right]^2 = 0.56$$

where P_{v_1} = probability of target visibility on a single batch.

The probability of detection on the first scan is then,

$$P_d = P_v(1/2) \, P_{d_1}(1/2) + P_v(2/2) \, P_{d_1}(2/2)$$

Letting $P_{d_1} = .92$

Then,

$$P_{d_1}(1/2) = \,\cong 0.7$$

and

$$P_d = 0.38 \, (0.7) + 0.56 \, (0.92)$$
$$= 0.78$$

The probability of detection on the second scan is,

$$P_{d_2} = P_d(2/2), \text{ given detection on scan 1}$$
$$= P_{d_1}, \text{ given no detection}$$

as, if detection occurs on the first scan, it is assumed that the blind speed can then be adjusted to uncover the target.

Also,

$$P_{d_3} = P_{d_1}(2/2) = P_{d_4} = 0.9$$

The probability of track initiation is then computed, in a manner similar to equation (6) and,

$$P_{TI} = (0.78) \, (0.92)^3 + 3 \, (0.78) \, (0.92)^2 \, (0.1)$$
$$+ \, 0.22 \, (0.78) \, (0.92)^2 = 0.951$$

The difference between a per scan detection requirement of 0.92 and 0.90 (derived in Section C.1.1) for $P_{fa} = 1.5 \times 10^{-3}$ and $N = 5$, is approximately 0.4 dB. This is the additional loss which occurs in those cells with severe clutter.

APPENDIX C-2
SUB-CLUTTER VISIBILITY REQUIREMENTS

C.2.1 LAND CLUTTER

Land clutter is assumed to follow a dB-normal distribution. A dB-normally distributed random variable is one whose dB-value has a normal distribution. That is, the clutter back-scatter coefficient, σ^o, has a dB-normal distribution if the related variable w given by

$$w = 10 \log \sigma^o \tag{1}$$

has a probability density function (pdf) given by

$$p(w) = \frac{1}{\sigma_{wdB} \sqrt{2\pi}} \, e^{-\frac{1}{2} \left(\frac{w - \overline{w}}{\sigma_{wdB}} \right)^2} \tag{2}$$

The 84th percentile corresponds to one σ_{wdB} of the normal distribution of the dB value of the reflectivity. Since this is 10 dB higher than the median value given in the Statement of Work, $\sigma_{wdB} = 10$ dB.

The target cross section for a Swerling I target is

$$p(\sigma_T) = \frac{1}{\overline{\sigma}_T} \exp\left(-\frac{\sigma_T}{\overline{\sigma}_T} \right)$$

where

$\overline{\sigma}_T$ = average cross section

The distribution of signal to clutter ratio is a combination of the individual distributions. These factors have been combined in a small Monte Carlo program. The program was used to determine the distribution of required SCV using the above distributions of clutter and signal as inputs. The requirement for detection per scan is about 0.9 or greater (Appendix C-1). It is conservatively assumed that the SCV should be cancelled to the 95 percentile level. This corresponds to about 1.25 clutter standard deviations or 12.5 dB above the median value. Hence the land clutter reflectivity design points (σ^o in dB) are as follows:

AD-A049 777   RAYTHEON CO WAYLAND MASS   F/G 17/9
                UNATTENDED/MINIMALLY ATTENDED RADAR STUDY. VOLUME II.(U)
                DEC 77   A W FRENCH, J L BERUBE   F30602-76-C-0389
UNCLASSIFIED   ER77-4109-VOL-2   RADC-TR-77-401-VOL-2   NL

5 OF 5
AD
A049777

END
DATE
FILMED

3 -78

DDC

	UHF	L-band
	-26.5	-21.5

The clutter radar cross-section is given by

$$\sigma_c = \sigma^o \, R \, \theta_B \, r \, \sec \phi$$

where

σ^o = land clutter reflectivity design point

R = slant range to clutter

θ_B = azimuth beamwidth

r = range resolution

ϕ = slope angle

The calculation for L-band is given below

	dB	
	+	-
σ^o		21.5
$R = 30$ n. mi. $= 55560$ m	47.45	
$\theta_B = 1.4^\circ = 0.0244$ rad		16.12
$r = \dfrac{c\tau}{2}$ ($\tau = 6$ μs) $= 899.4$ m	29.54	
$\sec \phi; \ \phi = 10^\circ$	0.07	
	77.06	37.62
	-37.62	
	39.44	

$$\sigma_c = 39.44 \text{ dBsm}$$

The target radar cross-section @ 30 n. mi. is 0 dBsm. It is also assumed that the antenna gain to the target is 3 dB (one-way) higher than the antenna gain to the clutter. Hence at L-band the SCV requirement is 39.44 - 0 - 6 = 33.44 dB per pulse.

The calculation for UHF-band is shown below.

	dB +	dB -
σ°		26.5
R = 30 n. mi.	47.45	
θ_B = 3.5°		12.14
r = $\frac{c\tau}{2}$ (τ = 6 μs) = 899.4 m	29.54	
sec ϕ; ϕ = 10°	0.07	
	77.06	38.64
	-38.64	
	38.42	

σ_c = 38.42

SCV = 38.42 - 0 - 6 = $\underline{32.42}$ dB per pulse.

C.2.2 SEA CLUTTER

The radar polarization is vertical. The sea clutter reflectivity design points (σ° in dB) from Table 1 at one degree depression angle is as follows:

UHF	L-band
-53	-48

Comparing these values to the land clutter calculations we see that the SCV requirement in dB for sea clutter is as follows:

SCV @ UHF	SCV @ L-band
5.92	6.94

C.2.3 WEATHER CLUTTER

The clutter cross-section per unit volume, η, is given by

$$\eta = 6 \times 10^{-14} r^{1.6} \lambda^{-4} \quad \text{meters}^{-1}$$

where

   r = the rain rate in mm/hr.

   λ = electromagnetic wavelength in meters.

For $r = 14$ mm/hr, $\lambda = 0.23$ m (L-band) we find

$$\eta_L = 1.462 \times 10^{-9} \text{ meters}^{-1}$$

At UHF band, $\lambda = 0.666$ m, we find

$$\eta_{UHF} = 2.077 \times 10^{-11} \text{ meters}^{-1}$$

The volume occupied by a radar beam of vertical beamwidth ϕ_B, horizontal beamwidth θ_B, and a pulse duration of τ is approximately

$$V_m \approx \frac{\pi}{4} R^2 \theta_B \phi_B \frac{c\tau}{2}$$

The clutter radar cross-section is

$$\sigma_c = \eta V_m$$

The L-band calculation is shown below

	dB	
	+	−
$\eta = 1.462 \times 10^{-7}$		88.35
$\pi/4$		1.05
$(R = 30 \text{ n. mi. })^2$	94.90	
$\theta_B = 1.4° = 0.0244$ rad		16.12
$\phi_B = 6°$		9.80
$c\tau/2 =$	29.54	
	124.44	115.32
	−115.32	
$\sigma_c =$	9.32 dBsm.	

C-2-4

The UHF-band calculation is shown below

dB

	+	−
$\eta = 2.077 \times 10^{-11}$		106.83
$\pi/4$		1.05
$(R = 30 \text{ n. mi.})^2$	94.90	
$\theta_B = 3.5°$		12.14
$\phi_B = 18°$		5.03
$c\tau/2$	29.54	
	124.44	125.05
	125.05	

$$\sigma_c = -0.61$$

Since the target radar cross-section is 0 dBdm and the antenna gain to the rain clutter is assumed to be the same as that to the target, we find that the subclutter visibility factors in dB for weather clutter is as follows:

SCV @ UHF	SCV @ L-band
9.32	−0.61

C.2.4 CLUTTER IMPROVEMENT REQUIREMENTS

The clutter improvement factor (I) is related to SCV by

$$I = SCV + X$$

where X is the additional amount that the clutter must be suppressed below the signal to satisfy threshold requirements for a specified P_d and P_{fa}. These requirements must, in general, be satisfied in the presence of the sum of all interference. The value X is therefore predicated on the performance degradation acceptable in clutter plus noise environment as compared to a noise-only situation. The noise-only case has been analyzed in Appendix C-1.

A typical average improvement factor (I) available from an MTI/FFT spectral filter is about 50 dB within the doppler pass-band. Typical improvement envelops are shown in Section 2.7.2. Using 50 dB for I, the allowable value for X is,

	L-Band	UHF
I	50	50
SCV	33.4	32.4
X	16.6	17.6

The parameter X is related to the output S/C as follows. The signal is enhanced with respect to the clutter residue by effective signal processor gain of 5.6 dB (See Appendix C-1). This is equal to the FFT signal gain less the signal losses due to the A/D, weighting, CFAR, etc. This gain is allowable if the clutter residue is uncorrelated which is generally true away from the peak clutter response.

The output S/C is then

$$\frac{S}{C} = X + 5.6 = 22.2 \text{ dB (L-Band)}$$
$$= 23.2 \text{ dB (UHF)}$$

The relationship between signal-to-interference ratio (S/I), S/N and S/C is given by:

$$\frac{S}{I} = \frac{S}{N+C} + \frac{1}{\frac{1}{\left(\frac{S}{N}\right)} + \frac{1}{\left(\frac{S}{C}\right)}}$$

The required S/I for the baseline configuration (L-Band) and the equivalent UHF configuration is (Appendix C-1).

$$\frac{S}{I} = 13.1 \text{ dB (L-Band)}$$
$$7.7 \text{ dB (UHF)}$$

C-2-6

Note that the above values also assume that the clutter is uncorrelated from batch-to-batch. As frequency agility is employed between batches, this is a reasonable assumption.

Solving for the S/N required to achieve the stated S/I,

$$\frac{S}{N} = \frac{1}{\left(\frac{1}{\frac{S}{I}}\right) - \left(\frac{1}{\frac{S}{C}}\right)}$$

$$= 13.7 \text{ dB (L-Band)}$$
$$= 7.8 \text{ dB}$$

These values include an additional loss when compared to the requirement for noise alone of:

$$\text{Clutter Loss} = 0.6 \text{ dB (L-Band)}$$
$$= 0.1 \text{ dB (UHF)}$$

IMPROVEMENT FACTOR FOR MTI & FFT

The calculation of the improvement factor for an MTI canceller in cascade with an FFT filter is described in this appendix. The improvement factor I is defined as

$$I = \frac{X_o}{X_i} \tag{1}$$

where

$$X_i = \frac{|V_i|^2}{C_i} = \text{input signal-to-interference ratio} \tag{2}$$

V_i = input signal voltage

C_i = input interference power

$$X_o = \frac{|V_o|^2}{C_o} = \text{output signal-to-interference ratio} \tag{3}$$

V_o = output signal voltage

C_o = output interference power

We may write equation (1) as

$$I = \left|\frac{V_o}{V_i}\right|^2 \frac{C_i}{C_o} = |H(f)|^2 C_R \tag{4}$$

where $H(f) = \dfrac{V_o}{V_i}$ = voltage transfer function $\tag{5}$

and $C_R = \dfrac{C_i}{C_o}$ = interference attenuation ratio $\tag{6}$

If the input interference power spectrum is $W_i(f)$, then

$$C_i = \int_{-\infty}^{\infty} W_i(f)\, df \tag{7}$$

and

$$C_o = \int_{-\infty}^{\infty} |H(f)|^2 W_i(f)\, df \tag{8}$$

Thus equation (4) becomes

$$I = \frac{|H(f)|^2 \int_{-\infty}^{\infty} W_i(f)\, df}{\int_{-\infty}^{\infty} |H(f)|^2 W_i(f)\, df} \tag{9}$$

If H_{max} is the maximum value[*] of $H(f)$ we can define a normalized response $V_N(f)$ as

$$V_N(f) = \frac{H(f)}{H_{max}} \tag{10}$$

This response function was calculated in reference memo (1) for the MTI + FFT configuration. In terms of $V_N(f)$ equation (9) may be written

$$I = \frac{|V_N(f)|^2 \int_{-\infty}^{\infty} W_i(f)\, df}{\int_{-\infty}^{\infty} |V_N(f)|^2 W_i(f)\, df} \tag{11}$$

---

[*] H_{max} is the value of $H(f)$ in filter number $\frac{N}{2}$ at $f = f_r/2$ where f_r is the prf.

If the radar samples are at a pulse repetition frequency f_r, then the spectrum $W_i(f)$ and the response $V_N(f)$ are both periodic in frequency with period f_r. Hence equation (11) can be written

$$I = \frac{|V_N(f)|^2 \int_0^{f_r} W_i(f)\, df}{\int_0^{f_r} |V_N(f)|^2 W_i(f)\, df} , \quad (0 \le f \le f_r) \tag{12}$$

We shall assume that the interference power spectrum $W_i(f)$ is given by

$$W_i(f) = W_N(f) + W_L(f) + W_R(f) \tag{13}$$

where

$W_N(f)$ is the noise power spectrum,

$W_L(f)$ is the land clutter power spectrum,

and

$W_R(f)$ is the rain clutter power spectrum.

Let the total noise power be denoted by P_N. Then

$$P_N = \int_0^{f_r} W_N(f)\, df \tag{14}$$

We shall assume that the noise power spectrum is constant at a level of M watts per Hertz.

$$W_N(f) = M \tag{15}$$

Then from equation (14),

$$P_N = M f_r \tag{16}$$

Let the total land clutter power be deonted by P_L. Then

$$P_L = \int_0^{f_r} W_L(f) \, df \tag{17}$$

We shall assume that the land clutter power spectrum is given by the gaussian shape

$$W_L(f) = \frac{P_L}{\sigma_L \sqrt{2\pi}} \left[e^{-\frac{1}{2} \left(\frac{f}{\sigma_L} \right)^2} + e^{-\frac{1}{2} \left(\frac{f - f_r}{\sigma_L} \right)^2} \right] \tag{18}$$

where

σ_L = standard deviation of land clutter in Hertz
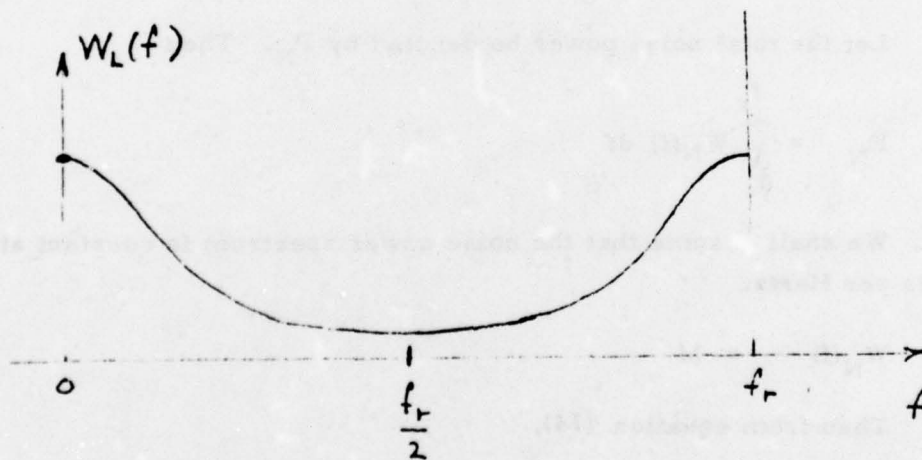
A sketch of the land clutter power spectrum is shown in Figure 1.

Figure 1. Land Clutter Power Spectrum

Let the total rain clutter power be denoted by P_R. Than

$$P_R = \int_0^{f_r} W_R(f) \, df \tag{19}$$

We shall assume that the rain clutter power spectrum is also given by a gaussian shape except that it is offset in doppler frequency by the mean wind radial velocity.

$$W_R(f) = \frac{P_R}{\sigma_R \sqrt{2\pi}} \left[e^{-\frac{1}{2} \left(\frac{f - f_o}{\sigma_R} \right)^2} + e^{-\frac{1}{2} \left(\frac{f - f_o - f_r}{\sigma_R} \right)^2} \right] \tag{20}$$

where

f_o = the doppler offset frequency

and

A sketch of the rain clutter power spectrum is shown in Figure 2.
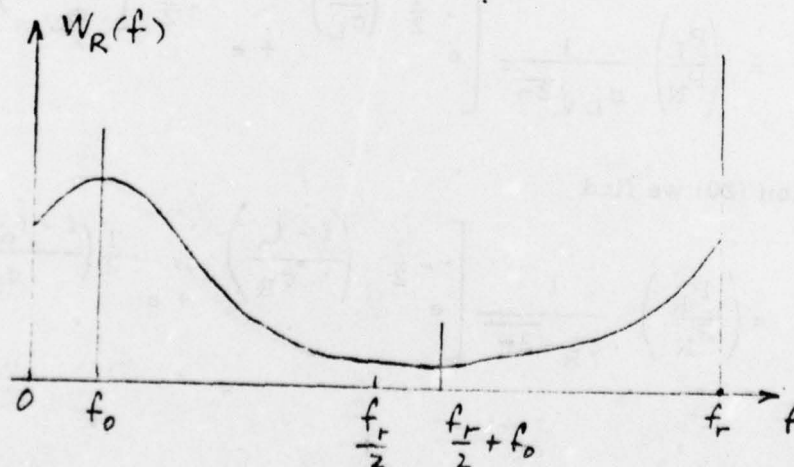

Figure 2. Rain Clutter Power Spectrum

It is easily verified that the total input interference power is

$$C_i = \int_0^{f_r} W_i(f) \, df = P_N + P_L + P_R \tag{21}$$

Now returning to equation (12), divide numerator and denominator by P_N, yielding

$$I = \frac{|V_N(f)|^2 \int_0^{f_r} \dfrac{W_i(f)}{P_N} \, df}{\int_0^{f_r} |V_N(f)|^2 \dfrac{W_i(f)}{P_N} \, df} \tag{22}$$

From equation (13) we have

$$\frac{W_i(f)}{P_N} = \frac{W_N(f)}{P_N} + \frac{W_L(f)}{P_N} + \frac{W_R(f)}{P_N} \tag{23}$$

From equations (15) and (16) we find

$$\frac{W_N(f)}{P_N} = \frac{M}{M f_r} = \frac{1}{f_r} \tag{24}$$

From equation (18) we find

$$\frac{W_L(f)}{P_N} = \left(\frac{P_L}{P_N}\right) \frac{1}{\sigma_L \sqrt{2\pi}} \left[e^{-\frac{1}{2}\left(\frac{f}{\sigma_L}\right)^2} + e^{-\frac{1}{2}\left(\frac{f - f_r}{\sigma_L}\right)^2} \right]. \tag{25}$$

From equation (20) we find

$$\frac{W_R(f)}{P_N} = \left(\frac{P_R}{P_N}\right) \frac{1}{\sigma_R \sqrt{2\pi}} \left[e^{-\frac{1}{2}\left(\frac{f - f_o}{\sigma_R}\right)^2} + e^{-\frac{1}{2}\left(\frac{f - f_o - f_r}{\sigma_R}\right)^2} \right] \tag{26}$$

Now let

$$X_N = \frac{|V_i|^2}{P_N} = \text{signal-to-noise ratio} \tag{27}$$

$$X_L = \frac{|V_i|^2}{P_L} = \text{signal-to-land clutter ratio} \tag{28}$$

$$X_R = \frac{|V_i|^2}{P_R} = \text{signal-to-rain clutter ratio} \tag{29}$$

Then

$$\frac{P_R}{P_N} = \frac{X_N}{X_R} \tag{30}$$

$$\frac{P_L}{P_N} = \frac{X_N}{X_L} \tag{31}$$

Thus we can write

$$\frac{W_i(f)}{P_N} = \frac{1}{f_r} + \left(\frac{X_N}{X_L}\right) \frac{1}{\sigma_L \sqrt{2\pi}} \left[e^{-\frac{1}{2}\left(\frac{f}{\sigma_L}\right)^2} + e^{-\frac{1}{2}\left(\frac{f - f_r}{\sigma_L}\right)^2} \right] \tag{32}$$

$$+ \left(\frac{X_N}{X_R}\right) \frac{1}{\sigma_R \sqrt{2\pi}} \left[e^{-\frac{1}{2}\left(\frac{f - f_o}{\sigma_R}\right)^2} + e^{-\frac{1}{2}\left(\frac{f - f_o - f_r}{\sigma_R}\right)^2} \right]$$

Note that

$$\int_0^{f_r} \frac{W_i(f)}{P_N} \, df = 1 + \frac{X_N}{X_L} + \frac{X_N}{X_R} \tag{33}$$

We are now in a position to calculate the improvement factor from equation (22). A computer program was written for the HP 9820A to plot the improvement factor as a function of doppler frequency. To simplify the plots the improvement factor was plotted in each filter only over the main response lobe.

The results of the computer program are presented in Section 2.7.2.

APPENDIX C-4

IMPROVEMENT FACTOR FOR TRANSVERSAL FILTER

The transversal filter consists of a tapped delay line and a weighted summer as shown in Figure 1. The taps are spaced at delay times equal to the repetition period. The signal and the weights are complex.

Let $\quad V = \{v_k\} \quad (k = 1, 2, \ldots, N)$ (1)

represent the input voltages of N pulses.

Let $\quad W = \{w_k\} \quad (k = 1, 2, \ldots, N)$ (2)

represent the complex weights.

Then the output voltage of the transversal filter is given by

$$r = \sum_{k=1}^{N} w_k v_k = W^T V = V^T W$$ (3)

where the superscript T represents the transpose.

The output complex power in a one ohm impedance is given by

$$P_o = \overline{|r|^2} = \overline{r r^*} = W^T \overline{V V^{*T}} W^*$$ (4)

where the superscript * represents the complex conjugate and the bar represents the ensemble average.

We shall now compute the input and output powers and the filter gain for both the signal and the interference.

Let $\quad P_{is} \quad = \quad$ input signal power

$\qquad P_{os} \quad = \quad$ output signal power

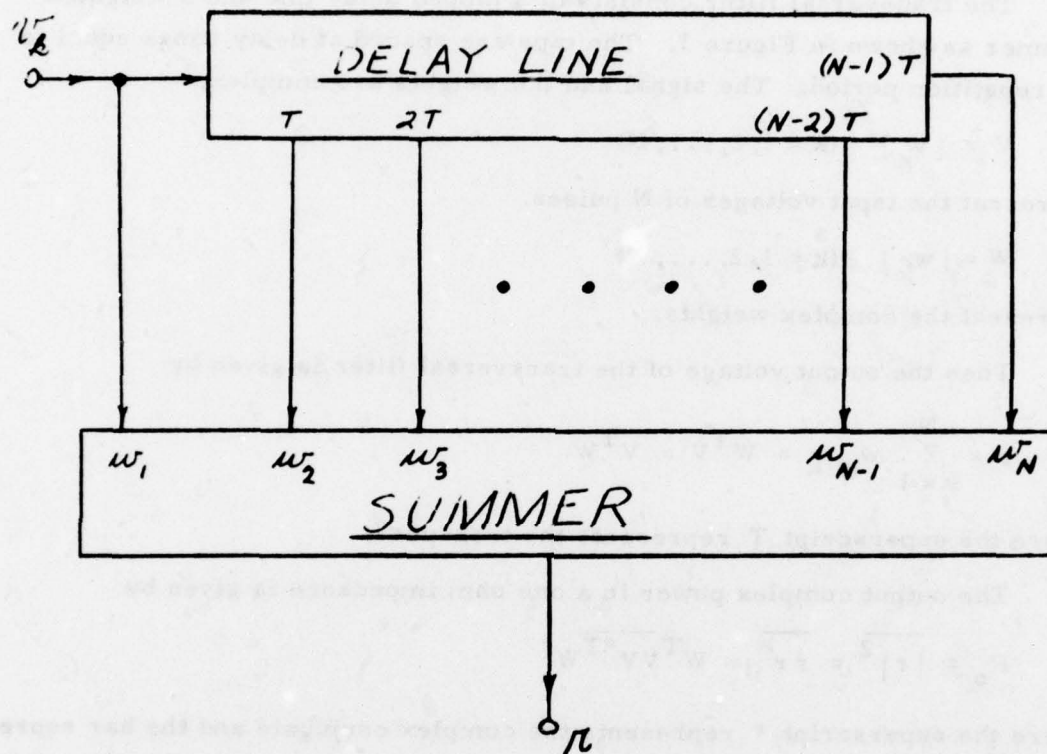$\qquad G_s \quad = \quad \dfrac{P_{os}}{P_{is}} \quad = \quad$ signal gain

Figure 1. Transversal Filter

P_{in} = input interference power

P_{on} = output interference power

$G_n = \dfrac{P_{on}}{P_{in}}$ = interference gain

Then the improvement factor is

$$I_f = \frac{P_{os}/P_{on}}{P_{is}/P_{in}} = \frac{G_s}{G_n} \tag{5}$$

When V consists entirely of interference, we have from Equation (4),

$$G_n = W^T \left(\overline{\frac{VV^{*T}}{P_n}} \right) W^* \tag{6}$$

$$G_n = W^T C W^* \tag{7}$$

where

$$C = \overline{\frac{VV^{*T}}{P_n}} \tag{8}$$

is the covariance matrix of the interference.

Now when V consists entirely of signal, we have

$$v_k = A e^{j([k-1]\omega T + \varphi)} \tag{9}$$

$$= A e^{j\varphi} e^{j[k-1]\omega T} \tag{10}$$

where

A = peak voltage amplitude

φ = phase angle in radians at some reference range

T = pulse period

k = pulse number

ω = radian doppler frequency

Let

$$\alpha = A e^{j\varphi} \tag{11}$$

$$\theta_k = e^{j[k-1]\omega T} \tag{12}$$

$$\Theta = \{\theta_k\} \tag{13}$$

Then

$$V = \{v_k\} = \alpha \Theta \tag{14}$$

The input signal complex power is

$$P_{is} = |v_k|^2 = v_k v_k^* = A^2 \tag{15}$$

The output signal complex power is from Equation (4) and (14)

$$P_{os} = W^T \overline{\alpha \Theta \alpha^* \Theta^{*T}} W^* \tag{16}$$

$$= \alpha \alpha^* W^T \overline{\Theta \Theta^{*T}} W^* \tag{17}$$

$$= A^2 W^T \overline{\Theta \Theta^{*T}} W^* \tag{18}$$

Hence the signal gain is

$$G_s = W^T \overline{\Theta \Theta^{*T}} W^* \tag{19}$$

Let

$$B = \overline{\Theta \Theta^{*T}} \tag{20}$$

Then

$$B = \begin{bmatrix} \overline{\Theta_1 \Theta_1^*} & \overline{\Theta_1 \Theta_2}^* & \cdots & \overline{\Theta_1 \Theta_N}^* \\ \overline{\Theta_2 \Theta_1}^* & & & \\ \cdot & & & \\ \cdot & & & \\ \cdot & & & \\ \overline{\Theta_N \Theta_1}^* & & \cdots & \overline{\Theta_N \Theta_N}^* \end{bmatrix} \tag{21}$$

Using Equations (12) and (13) in (21) yields the Hermitian matrix

$$B = \begin{bmatrix} 1 & & e^{-j\omega T} & \cdots & e^{-j\omega NT} \\ e^{j\omega T} & & & & \\ \cdot & & & & \\ \cdot & & & & \\ \cdot & & & & \\ e^{j\omega NT} & & & & 1 \end{bmatrix} \tag{22}$$

Note that all the rows and columns of B are proportional; hence, it is a singular matrix of rank 1.

C-4-4

From Equations (19) and (20), we have

$$G_s = W^T B W^*$$ (23)

Now from Equations (5), (7), and (23), we find

$$I_f = \frac{W^T B W^*}{W^T C W^*}$$ (24)

We seek the W which will make I_f a maximum. Since the derivative of I_f should vanish at this point, we seek to make I_f stationary. I_f will become stationary if we choose to make $C W^*$ proportional to $B W^*$, i. e.

$$C W^* = \lambda B W^*$$ (25)

where λ is a proportionality constant. For in that case, we would have

$$I_f = \frac{W^T B W^*}{W^T \lambda B W^*} = \frac{W^T B W^*}{\lambda W^T B W^*} = \frac{1}{\lambda}$$ (26)

which is a constant.

Hence, we have the set of equations

$$C W^* = \lambda B W^*$$ (27)

Premultiplying both sides by C^{-1} yields

$$W^* = \lambda C^{-1} B W^*$$ (28)

Transposing

$$\lambda C^{-1} B W^* - W^* = 0$$ (29)

or

$$(C^{-1} B - I_f I) W^* = 0$$ (30)

where I is the identity matrix.

Equation (30) will have non-trivial solutions if and only if

$$|C^{-1} B - I_f I| = 0$$ (31)

The solutions to the polynomial Equation (31) are the eigenvalues of the matrix $C^{-1}B$. Since, as noted before, the rank of B is 1, the matrix $C^{-1}B$ must also be of rank 1. (The rank of a product of two matrices is not greater than the rank of either factor.) This means that all of its eigenvalues are zero except one. Since the trace of a matrix is equal to the sum of its eigenvalues, we have that the eigenvalue of $C^{-1}B$ is given by

$$I_f = tr \ (C^{-1}B) = tr \ (C^{-1}\Theta\Theta^{*T}) = \Theta^{*T}C^{-1}\Theta \tag{32}$$

Since B is a function of the doppler frequency, both I_f and the associated eigenvector W^*_{opt} will vary with frequency.

A computer program for plotting I_f as a function of target doppler frequency was written. The results are shown in Figures 2.7.2- and 2.7.2- . The covariance matrix of the interference is derived below.

Interference Covariance Matrix

The interference is composed of receiver noise, land clutter, and rain clutter. The total interference power spectrum $W_i(f)$ is given by

$$W_i(f) = W_N(f) + W_L(f) + W_R(f) \tag{1}$$

where

$W_N(f)$ is the noise power spectrum,

$W_L(f)$ is the land clutter power spectrum,

and

$W_R(f)$ is the rain clutter power spectrum.

The autocorrelation function of the interference is given by the inverse Fourier transform of its power spectrum, i.e.

$$R_i(t) = \int_{-\infty}^{\infty} W_i(f) \, e^{j2\pi ft} \, df \tag{2}$$

The normalized autocorrelation function is defined as

$$\rho_i(t) = \frac{R_i(t)}{R_i(o)} \tag{3}$$

From Equation (2), we find that this becomes

$$\rho_i(t) = \frac{\int_{-\infty}^{\infty} W_i(f) e^{j 2\pi f t} df}{\int_{-\infty}^{\infty} W_i(f) df} \tag{4}$$

The denominator represents the total interference power C_i,

$$C_i = \int_{-\infty}^{\infty} W_i(f) df = P_N + P_L + P_R \tag{5}$$

where

P_N is the noise power,

P_L is the land clutter power,

and

P_R is the rain clutter power.

The noise power spectrum is assumed to be constant at M watts per Hz. Hence, the autocorrelation function of the noise is

$$R_N(t) = \int_{-\infty}^{\infty} W_N(f) e^{j 2\pi f t} df \tag{6}$$

$$= M \int_{-\infty}^{\infty} e^{j 2\pi f t} df \tag{7}$$

$$= M \delta(t) \tag{8}$$

Note that from Equation (6),

$$R_N(o) = \int_{-\infty}^{\infty} W_N(f) \, df = P_N \tag{9}$$

Let

$$\rho_N(t) = \frac{R_N(t)}{R_N(o)} = \frac{M}{P_N} \delta(t) \tag{10}$$

We shall assume that the land clutter spectrum is given by

$$W_L(f) = \frac{P_L}{\sigma_L \sqrt{2\pi}} e^{-\frac{1}{2}\left(\frac{f}{\sigma_L}\right)^2} \tag{11}$$

where

σ_L is the standard deviation of the land clutter spectrum in Hertz.

Hence the autocorrelation function of the land clutter is given by

$$R_L(t) = \int_{-\infty}^{\infty} W_L(f) \, e^{j2\pi ft} \, df \tag{12}$$

$$= P_L \, e^{-2(\pi\sigma_L t)^2} \tag{13}$$

At t = o,

$$R_L(o) = \int_{-\infty}^{\infty} W_L(f) \, df = P_L \tag{14}$$

Let

$$\rho_L(t) = \frac{R_L(t)}{R_L(o)} = e^{-2(\pi\sigma_L t)^2} \tag{15}$$

The rain clutter power spectrum is assumed to be gaussian with mean doppler f_o, i.e.

$$W_R(f) = \frac{P_R}{\sigma_R \sqrt{2\pi}} \, e^{-\frac{1}{2}\left(\frac{f - f_o}{\sigma}\right)^2} \tag{16}$$

Hence the autocorrelation function of the rain clutter is given by

$$R_R(t) = \int_{-\infty}^{\infty} W_R(f) \, e^{j 2\pi f t} \, df \tag{17}$$

$$= P_R \, e^{-2(\pi \sigma_R t)^2 + j 2\pi f_o t} \tag{18}$$

at $t = o$,

$$R_R(o) = \int_{-\infty}^{\infty} W_R(f) \, df = P_R \tag{19}$$

Let

$$\rho_R(t) = \frac{R_R(t)}{R_R(o)} = e^{-2(\pi \sigma_R t)^2 + j 2\pi f_o t} \tag{20}$$

The autocorrelation function of the interference is

$$R_i(t) = R_N(t) + R_L(t) + R_R(t) \tag{21}$$

At $t = o$,

$$R_i(o) = R_N(o) + R_L(o) + R_R(o) \tag{22}$$

$$= P_N + P_L + P_R \tag{23}$$

Hence

$$\rho_i(t) = \frac{R_i(t)}{R_i(o)} = \frac{R_N(t) + R_L(t) + R_R(t)}{P_N + P_L + P_R} \tag{24}$$

C-4-9

Dividing numerator and denominator of Equation (20) by the signal power P_S yields

$$\rho_i(t) = \frac{\dfrac{R_N(t)}{P_S} + \dfrac{R_L(t)}{P_S} + \dfrac{R_R(t)}{P_S}}{\dfrac{P_N}{P_S} + \dfrac{P_L}{P_S} + \dfrac{P_R}{P_S}} \tag{25}$$

$$= \frac{\dfrac{P_N}{P_S}\, \rho_N(t) + \dfrac{P_L}{P_S}\, \rho_L(t) + \dfrac{P_R}{P_S}\, \rho_R(t)}{\dfrac{P_N}{P_S} + \dfrac{P_L}{P_S} + \dfrac{P_R}{P_S}} \tag{26}$$

$$= \frac{\dfrac{1}{X_N}\, \rho_N(t) + \dfrac{1}{X_L}\, \rho_L(t) + \dfrac{1}{X_R}\, \rho_R(t)}{\dfrac{1}{X_N} + \dfrac{1}{X_L} + \dfrac{1}{X_R}} \tag{27}$$

where

X_N = signal to noise power ratio

X_L = land clutter to noise power ratio

X_R = rain clutter to noise power ratio

Equation (27) can be written

$$\rho_i(t) = K_N\, \rho_N(t) + K_L\, \rho_L(t) + K_R\, \rho_R(t) \tag{28}$$

where

$$K_N = \frac{\dfrac{1}{X_N}}{\dfrac{1}{X_N} + \dfrac{1}{X_L} + \dfrac{1}{X_R}} = \frac{1}{1 + \dfrac{X_N}{X_L} + \dfrac{X_N}{X_R}} \tag{29}$$

$$K_L = \cfrac{\cfrac{1}{X_L}}{\cfrac{1}{X_N} + \cfrac{1}{X_L} + \cfrac{1}{X_R}} = \cfrac{1}{\cfrac{X_L}{X_N} + 1 + \cfrac{X_L}{X_R}} \qquad (30)$$

and

$$K_R = \cfrac{\cfrac{1}{X_R}}{\cfrac{1}{X_N} + \cfrac{1}{X_L} + \cfrac{1}{X_R}} = \cfrac{1}{\cfrac{X_R}{X_N} + \cfrac{X_R}{X_L} + 1} \qquad (31)$$

Since

$$\rho_i(o) = \rho_N(o) = \rho_L(o) = \rho_R(o) = 1 \qquad (32)$$

We have from Equation (28),

$$1 = K_N + K_L + K_R \qquad (33)$$

which can be verified as true by adding Equations (29), (30), and (31).

Since $\rho_N(t) = 0$ for $t \neq 0$, we have

$$\rho_i(t) = \begin{cases} K_L \, \rho_L(t) + K_R \, \rho_R(t) & (t \neq 0) \\ \\ 1 & (t = 0) \end{cases} \qquad (34)$$

The covariance matrix will then be given by

$$C = \begin{bmatrix} 1 & \rho_i(T) & \rho_i(2T) \, . \, . \, . \, . \, . \, \rho_i(NT) \\ \rho_i^*(T) & 1 & \\ \rho_i^*(2T) & & \\ \rho_i^*(NT) \, . \, . \, . \, . \, . \, . \, . \, . \, . \, . \, . \, . \, . \, . \, 1 \end{bmatrix} \qquad (35)$$

where T is the repetition period and N is the number of pulses processed by the transversal filter.

APPENDIX D
MULTIPATH MODEL

D-1 MULTIPATH MODEL

The analytical model used in the multipath analysis leading to curves
2.7.4-1 through 2.7.4-16 is according to classical specular reflection theory
which is discussed in detail in Kerr (2), Beckmann and Spizzichino (3), Barton (4),
Barton and Ward (5), etc. A smooth curved earth is assumed and the sum pat-
tern voltage signal e_Σ is a combination of the direct signal return from the tar-
get and the specular multipath return. Specifically,

$$e_\Sigma \quad C \left\{ \frac{\Sigma(\theta_t)}{R} + \frac{\Sigma(\theta_r)}{R_1 + R_2} \exp(-i\varphi) \right\}^2 \tag{1}$$

where

ρ = amplitude of the reflection coefficient

φ = phase shift = $\frac{2\pi}{\lambda} \Delta R + \alpha$

ΔR = path difference between direct and specular components

$\alpha \simeq 180^\circ$ = phase of the reflection coefficient

θ_t = off-boresight angle to the target

θ_r = off-boresight angle to the specular point

$\Sigma(\theta)$ = normalized antenna pattern

R = direct path distance between target and radar

R_1, R_2 = slant ranges to specular point from radar and target,
respectively

and C is a constant calculated from the expression

$$C^2 = P_t G_t G_r \lambda^2 \sigma/(4\pi)^3 L \tag{2}$$

where

P_t = peak transmitter power

G_t, G_r = peak transmitter and receiver gains, respectively

λ = wavelength

σ = target cross section

L = system losses

Modeling noise N by

$$N = kT\, B_m \tag{3}$$

where

k = 1.38×10^{-23} joule/deg. = Boltzmann's constant

B_m = noise bandwidth

T = receiver temperature

The signal-to-signal noise power (S/N) is given by

$$S/N = |e_\Sigma|^2/N. \tag{4}$$

The heavy lobing structure shown in each of the S/N plots is a result of strong multipath signals adding to and subtracting from the direct signal as the relative phase shift φ changes from 0 to π radians. The upward swing in the curves at the furthest target ranges is also characteristic of expression (1), although as discussed in the next section, this simplistic model needs refinement at these largest target ranges in order to accurately describe signal response from regions in the immediate vicinity of the horizon.

The reflection coefficient, ρ, is given by:

$$\rho = D\rho_o \tag{5}$$

D-2

where ρ_o is the flat earth Fresnel reflection coefficient and D is a divergence factor to modify ρ_o for the effect of the earth's curvature at large target ranges. ρ_o tends to unity as the specular grazing angle tends to zero, or equivalently, when the target approaches the interference/diffraction boundary at the local horizon. The divergence factor

$$D = \left[1 + \frac{2 R_1 R_2}{a_e (R_1 + R_2) \sin \varphi} \right]^{-1/2}$$ (6)

where

a_e = 4/3 earth's radius

φ = specular grazing angle

tends to zero abruptly, however, as the target approaches this boundary so that the total reflection coefficient ρ tends to zero and the S/N curves have positive slope at these ranges.

D-2 VALIDITY OF THE MULTIPATH MODEL

The field integral leading to (1) is evaluated using an asymptotic expansion that excludes values of φ extremely close to zero so that there is a transition region in the vicinity of the horizon where Equation (1) needs modification to continuously pass to the diffraction region. The width of this transition region is not precisely know, however, it is believed (Ref. 2) that expression (1) is always valid for $\Delta R \geq \lambda/4$ and may be extended to target ranges where $360 \frac{\Delta R}{\lambda} \sim 1$ deg in the case of low sighted radar. Translating this last condition to the geometries considered in reference (1) (using curved earth calculations for ΔR) the S/N curves may be considered valid to within 2 - 3 nm of the interference/diffraction boundary

1. Raytheon Company, Technical Report, "A New Generation of Radar Systems", prepared for Rome Air Development Center, Griffis AFB, New York 13441, 22 March 1977.

2. Kerr, D. E., "Propagation of Short Radio Waves", Dover Pub., Inc., New York, 1951.

3. Beckmann, P., and Spizzichino, A., "The Scattering of Electromagnetic Waves from Rough Surfaces", Pergamon Press, 1963.

4. Barton, D.K., "Radar System Analysis", Prentice-Hall, 1964.

5. Barton, D.K., Ward, H.R., "Handbook of Radar Measurement", Prentice-Hall, 1969.

REFERENCES

2-1 RADC Document F30602-76-C-0389, Attachment 1; Statement of Work For An Unattended/Minimally Attended Radar Study, PR No. A-6-1367, 18 May 1976.

2.4.1 O'Donnell, R. M., Digital Moving Target Detector For Use With The FPS-20 Class of Radar, MIT Lincoln Laboratory Technical Note 1973-38, 4 November 1975.

2.4.2 Muehe, C. E., Moving Target Detector, An Improved Signal Processor, Paper Preprint No. 197, AGARD Conference, Neuilly Sur Seine, France.

2.4.3 Barton and Ward, Handbook of Radar Measurement, Prentice-Hall, 1969.